Simulation of Aluminium Extrusion Process

ISAAC FLITTA

A thesis submitted in partial fulfilment of the requirements of Bournemouth University for the degree of Doctor of Philosophy

JANUARY 2004

Bournemouth University

This work is dedicated to my dear wife Angela, without her love and support I could not have attempted this thesis.
To my mother and the memory of my father.
To Mike Azira, Sheila Jarvis and all the family and friends.

ABSTRACT

The aim of this thesis is to model the extrusion process conditions for some aluminium alloys using Finite Element Modelling (FEM) program.

All the simulations were performed with the implicit finite element code FORGE2® (2-D) and FORGE3® (3-D). In this work only the alloys AA2024, AA2014, Al-1%Cu and AA6063 where experimental work is available were considered.

The FORGE2® program was used to investigate and select an appropriate flow stress constitutive equation to describe the material behaviour to model the process conditions. The extrusion pressure and the temperature rise were predicted and the pressure-displacement trace and the events which take place in the deformed material during the extrusion process were also simulated. The effect of the initial billet temperature on friction, and the extent of the surface zone affected by surface friction and the consequence changes in material flow were investigated. The changes in the subgrain size during quasi-static deformation were predicted. This allows a construction of velocity-displacement profiles which would ensure consistent properties over the length of the extrudate.

The FORGE3® program was used to simulate the effect of changing the die geometry on material flow during extrusion for rod, shapes and tube extrusion and the effect of the initial temperature on the deformation zone. The load required, temperature evolution, surface formation of the extrudate and material flow during the process, were also predicted. These included solid sections and the production of tubes using bridge die.

Two most commonly used constitutive flow stress equations, the Zener-Hollomon and the Norton-Hoff were analysed and compared with experimental results. It was found that the Zener-Hollomon relationship provided a better representation of the experimental flow stress under high working conditions than the Norton-

Hoff relationship. FEM has been successfully applied to model the deformation patterns in the load/displacement traces and temperature evolution during the extrusion cycle. The effect of the initial billet temperature on the deformation zone pattern and its consequent effect on friction using both numerical simulation and experimental work are presented. A specific function relationship to measure directly interfacial friction under conditions approaching those encountered in the quasi-static deformation process is described. The results revealed that the friction factor increases with increase in initial billet temperature and varies during the extrusion cycle. The dead metal zone (DMZ) is observed to vary in form and has a greater volume at high temperatures. FEM proved to be a very effective and efficient way to design the ram speed profile to control the extrudate properties. The control of the properties of the extrudate under a constant (Z) parameter resulted in a more uniform distribution of the subgrain size across and along the extrudate cross-section. Furthermore, the speed profile under constant Z conditions resulted in an improved extrusion speed and hence greater productivity coupled with better control of the subgrain size and the exit temperature. This new extrusion process is termed iso-Z Extrusion, and is considered an improvement on Iso-Thermal extrusion.

The usefulness and the limitation of FEM when modelling complex shapes are discussed. Methods to assess the difficulty of hollow and section shapes are presented. The work also illustrates the essentials of numerical analysis in the comprehension of the thermo-mechanical events occurring during extrusion through bridge and shape dies. Results are presented for velocity distribution in the extrusion chamber, Iso-temperature contours and pressure/displacement traces. It is shown that for most of the shapes investigated, the material making up the extrudate cross-sections originated from virgin material within the billet. The outside surface of the extrudate originates from the material moving along the DMZ and the core of the extrudate from the central deformation zone. When simulating tube extrusion, it is shown that the FE program is able to predict the pressure requirements: the pressure/displacement trace showing a double peak for tube extrusion which is discussed in some detail. The FE program appears to predict all the major characteristics of the flow observed macroscopically.

ACKNOWLEDGEMENTS

The author would like to thank and express his gratitude to the many who have supported and helped during the production of this thesis, especially the following:

Prof. Terry Sheppard :

I would like to thank my supervisor, Prof. Terry Sheppard for his encouragement and guidance throughout the research for which I will always be grateful. I could not have imagined having a better advisor and mentor for my PhD.

Dr. Kamran Tabeshfar:

For his help and support in my professional development.

Mr. Xavier Velay:

For his help and support throughout various stages.

School of Design Engineering and Computing

For the provision of the facilities and support throughout the research. I would also like to thank all the rest of the academic and support staff from the Design Group

Dr. J. Subramaniyan, Dr. M. P. Clode, Dr. M. G. Tutcher Dr. E. Nisaratanaporn and R. P. Vierod.

For their excellent contribution of the experimental work and the permission to use it.

CONTENTS

LIST OF FIGURES

LIST OF TABLES

CHAPTER 1: INTRODUCTION

1.1 Aluminium alloys

Aluminium alloys represent some of the most versatile engineering materials due to their unique combination of properties. They have low density, high conductivity, low toxicity, and good electrical and thermal conductivity.

Wrought aluminium alloys are divided into seven major classes, agreed by international nomenclature, according to their principal alloy elements. Each alloy is described by a four digit number plus a further letter and number indicating the temper or condition of the alloy as shown in Table 1.1.

These alloys fall into two main groups as shown in Table1.2: the work hardening alloys, where strength is achieved by the extent of 'cold work' applied by rolling or forming and heat-treatable or precipitation hardening alloys in which the properties are enhanced by heat treatment of various kinds.

Table1.1: Designation of aluminium alloys [1].

Designation	Major alloying element	Characteristic	Typical Alloys
1XXX	99% Al	Excellent corrosion High electrical and thermal conductivity	AA1100 AA1050
2XXX	Al-Cu-Si	High strength-to-weight ratio	AA2014 AA 2024
3XXX	Al-Mn	Medium strength	AA3003 AA3104
4XXX	Al-Si	Lower melting point, Good melting characteristics. This series in wrought form is almost exclusively used for welding rod and wire.	AA4032
5XXX	Al-Mg	Good corrosion resistance, high strength	AA5083 AA 5052
6XXX	Al-Mg-Si	Good formability, machinabilty, weldability	AA6061 AA 6063
7XXX	Al-Zn -Mg	Moderate to very high strength	AA7075 AA 7005

Table1.2: Wrought Aluminium Alloys by Group [1]

WORK HARDENING	HEAT-TREATABLE
1XXX (Al)	2XXX (Al/Cu)
3XXX (Al/Mn)	6XXX (Al/Mg/Si)
5XXX (Al/Mg)	7XXX (Al/Zn/Mg)

Properties such as stress corrosion resistance, machinability, toughness and fatigue strength can be enhanced by careful control of alloying elements as well as careful control of the thermal mechanical process. Copper (Cu) is one of the most important alloying elements in aluminium because of its appreciable solubility and strengthening effect. The addition of Si to Al improves the response to artificial ageing and influences the microstructure through its strong tendency to form intermetallic-compounds with Al, Fe, Mg. and Mn. Magnesium (Mg) has a marked strength effect, due to both its solubility and formation of intermetallic compounds. Zinc (Zn) improves general corrosion behaviour and produces an acceptable compromise between good workability and required strength. In this work

only the alloys AA2024, AA2014 and AA6063 where experimental work is available are considered.

1.2 Extrusion Process

The extrusion process is among the most utilised methods of material processing in the aluminium industry, both for the production of semi-finished products as well as for the manufacturing of net-shaped consumer goods, aerospace applications and military hardware. Since these operations occur within a high-volume industry, even small improvements or optimisation in material properties and manufacturing could translate into substantial savings. The optimisation and modelling criteria may vary, depending on the product requirements, but establishing an appropriate criterion requires a thorough understanding of manufacturing processes.

The extrusion process cycle consists of converting a cast and homogenised billet into a continuous length of generally uniform cross-section through a die with an orifice of a particular design and size to meet product requirement. The great advantage of the extrusion process lies in the relative ease and efficiency with which complex sections, including hollows, can be produced in one operation.

A typical arrangement for the production of rods and shaped sections is shown in the diagram in Figure 1.1. It comprises of container (1), which needs to be constructed from three shrink fit steel tubes, the extrusion ram (2), in front of which is placed a pressure disc, or follower pad (3), fitting the container more closely than the ram; the die assembly (4), locked against the container during working by a die backer (5).

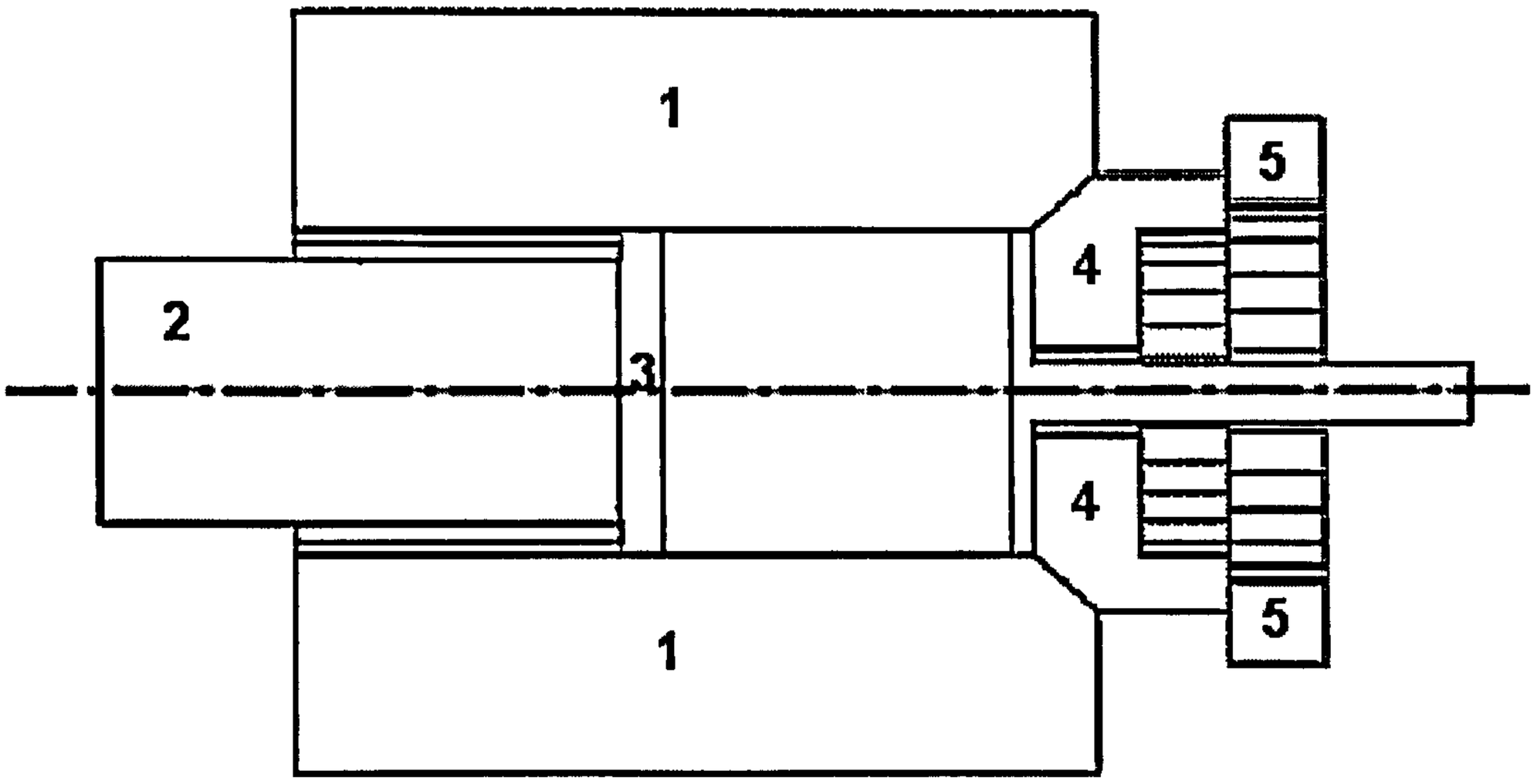

Figure 1.1: Direct Extrusion Layouts

A basic principle of extrusion consists of forcing a heated billet in a container by a ram through a shaped die to obtain the desired final configuration. The billet is never completely extruded, even when it is desirable to do this, it is impossible to exert sufficient pressure to eliminate the thin final disc. The press is stopped when a short stub of the billet, referred to as a discard, remains in the container.

1.3 Extrusion parameters

The necessary force needed to be applied to cause metal breakthrough in extrusion is obviously affected by a variety of circumstances. Predominantly, it is affected by the nature of the material and the manner in which its properties are affected by the temperature and the speed at which the extrusion is carried out [1]. In addition, the amount of deformation

involved must be considered, i.e. the dimensions of the billet in relation to those of the section being produced [2-3]. Additional factors are the shape of the section and the design of the die used [1-7].

For pure aluminium and the softer alloys, reduction ratios of up to 100:1 are not uncommon, while for the hard alloys the ratio is usually between 8:1 and 40:1 [1].

The speed of extrusion depends upon the available pressure and thus on the alloy temperature and reduction ratio. It is also limited by the onset of hot shortness or surface defects in the product [1]. For pure aluminium, exit speeds of up to 75 mm/s are not uncommon whereas the harder alloys must be extruded at speeds as low as 3 to 5 mm/s. Obviously, any improvement to the extrusion process which will enable higher speeds will be very beneficial to commercial production rates.

The complex interaction of structure, strain-rate and temperature during extrusion which defines the working area for a satisfactory extrusion product is usually represented graphically by limit diagrams. The use of such diagrams can provide a practical tool for process control interpretation.

The temperature of extrusion, like speed, has implications in the process other than its effect on the pressure. The forces in extrusion are predominantly compressive, thus permitting high homologous working temperatures. Thus, the extrusion process for aluminium alloys can be regarded as lying between limits set by inherent stiffness (growing stiffness), even at some elevated temperatures, on the one hand, and the maximum temperature that can be tolerated during the process on the other [8]. Hirst and Ursell [9], first proposed a diagram representing these two factors. Assuming adiabatic conditions and relating temperature rise to

extrusion reduction ratio, they concluded that the load limitation could be represented by a specific pressure line and the temperature limitation by an incipient melting line. Further investigations by Sheppard and Raybould. [8, 10-12], led to a development of the most useful format of such diagrams and is schematically shown in Figure 1.2. The format utilised constant strain-rate curves and showed that limits diagrams could provide specific metallurgical data upon the structure of the final extrude, thus providing engineers with the tools for metallurgical process control.

The limit diagrams consist of plotting the extrusion speed against the billet temperature as illustrated in Figure 1.2. The line on the left represents the press capacity; the line on the right represents incipient melting or unacceptable surface. The operating condition for satisfactory extrusion must lie within the region beneath these limiting lines. These lines are dependent upon maximum pressure available for the press and the speed at which extrusion is carried out. The extrusion process offers the possibility of producing a variety of simple and complicated aluminium alloy sections in long lengths, and the extrusion conditions will vary according to the material and its application.

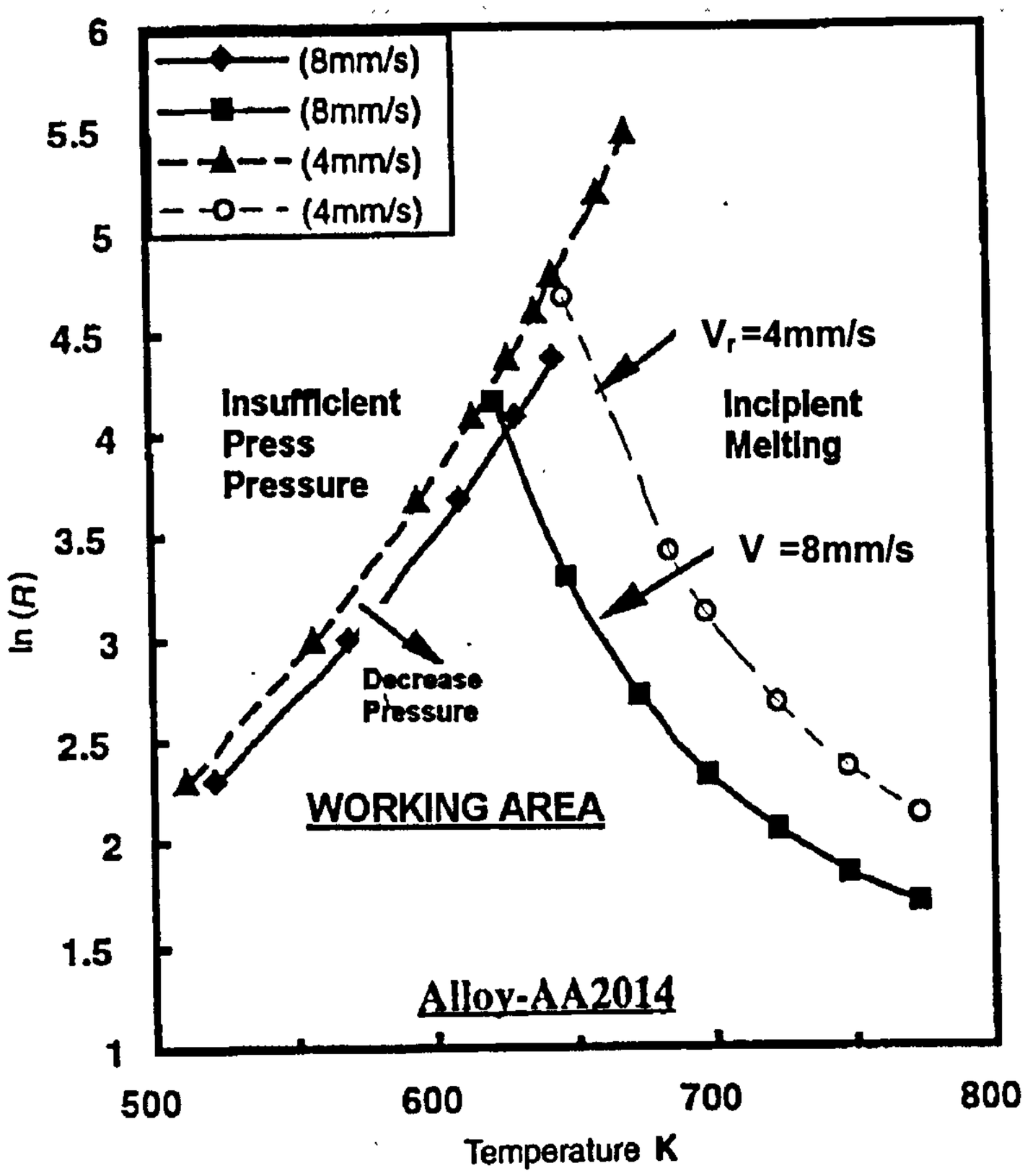

Figure 1.2: Limit diagrams for AA2014 constructed from theory (Courtesy of Sheppard T. [1]).

1.4 Finite element method in extrusion process

Modelling is a consequence of the trend followed by industry in the past few decades towards an improvement of the process and the use of total quality programmes. The task today is to produce more output with better quality and lower costs. Consequently, the use of computer modelling has become increasingly appealing to industry. Its application provides important design information on the shape and integrity of the part, the required force, wear on tools and an understanding of the metal working

process, where conventional analytical methods are restricted to the steady-state stage of the process. Thus, they cannot provide an insight into the dynamic changes occurring during the initial stage of the process.

In extrusion, correct design and control requires, among other things, the determination of the deformation mechanics involved in the process. Without the knowledge of the influence of variables such as friction process conditions, material properties and workpiece geometry on the process mechanics, it would not be possible to design the dies and the equipment adequately, or to predict and prevent the occurrence of defects. Thus, process modelling for computer simulation has been a major concern in modern metal-forming technology.

One of the most powerful potential techniques [ref. 1, page 53] that have been developed in the realm of metal-forming is the non-linear finite element method (FEM) which is now widely recognized as an efficient tool for designing actual processes in industry. Its use can be attributed to the characteristics of metal-forming processes: large deformation, thermo-mechanical events, non-linear boundary conditions and non-linear material behaviour. Also because of its flexibility in reproducing almost any required geometry, FEM is regarded as *potentially* the most practical tool presently available.

In addition [ref. 1, pages 143-170], the simulations are advantageous for the easy variation of geometry and boundary conditions, consequently facilitating detailed studies of deformation patterns. Moreover, the process (billet, tools), once modelled, can be used for a large variety of investigations by simply changing the boundary conditions in the model. Thus, the use of FEM in the extrusion process provides an excellent means of obtaining information on how the material flows, how the desired geometry can be achieved, and what the expected mechanical properties

in the extrudate may be. Such objectives essentially consist of *a)* establishing the kinematic relationships (velocities, strain-rates) between the deformed and undeformed part, i.e. predicting metal flow; *b)* establishing the limits of formability, i.e., establishing, whether it is possible to form the extrudate without surface and\or internal defects; and *c)* predicting the forces and stresses necessary to execute the process so that tooling and equipment can be designed or selected accordingly.

The basic mathematical descriptions of the FEM models, as well as the solutions techniques, are given in several books [13-15] and a brief description is also given in Chapter 3.

1.5 Layout of the thesis

The present work has focused on using the FEM to simulate the extrusion process. The main objectives involve validating the FEM code; choosing appropriate constitutive equations; predicting extrusion pressure, temperature rise and temperature evolution during the process; modelling the variation of coefficient of friction with initial billet temperature; simulating material flow during extrusion for rod, shapes and tube extrusion and effect of the initial temperature on deformation zone; controlling extrudate properties by varying ram speed. Although no experimental work has been attempted, suitable data has been extracted from external PhD theses and literature. A comparison with experiments is made to assess the relative importance of some extrusion parameters in the extrusion process and to ensure that the numerical discretisation provided a true simulation of the process.

Basic concepts on aluminium alloys and the extrusion process are briefly introduced in Chapter 1.

Detailed research history and critical reviews are given in Chapter 2. Principal formulation and analysis techniques of the FEM programs FORGE2® and FORGE3® are recalled in Chapter 3

Code validation, constitutive equations and the effect of some extrusion parameters, such as friction, on the extrusion pressure are first investigated and are given in Chapter 4.

Material flow, surface generation, Extrusion of shapes and hollow sections are given in Chapter 5.

In Chapter 6, the exit temperature for rod extrusion is investigated with reference to isothermal extrusion. The changes of microstructure under both normal and iso-extrusion conditions are investigated. Finally, a modified form of isothermal extrusion process, Iso-subgrain size and Iso-extrusion, are proposed to control the microstructure.

Chapter 7 presents conclusions drawn from the work carried out in the present thesis and indicates further work required in the modelling of the extrusion process.

CHAPTER 2: LITERATURE REVIEW

2.1 Introduction

The modelling of aluminium extrusion must be based on a fundamental understanding of the thermo-mechanical phenomena occurring during the process. While the problem is thus one of broader complexity, the derivation of systematic data from which it can be studied is rendered very difficult under industrial conditions. It is also difficult to quantify by experimental techniques.

The possession of an FEM code and the skill to use it are not sufficient to simulate a metal-forming problem accurately. One of the vital prerequisites is the ability to feed the program with the basic physical data of the process prior to simulation. Apart from the geometrical variables of the die and workpiece and the process kinematics, these consist primarily of physical parameters and boundary conditions prevailing under the given conditions (material, temperature, etc.). Other physical values are needed for purely mechanical simulation. These are the flow stress which must consider the rate and temperature-dependence, together with the description of the frictional relationships between contacting surfaces of the workpiece and the tools. Accurate thermal and microstructural data of materials and, in particular, the interface data such as friction must be available. The accuracy of the results are not only sensitive to the geometric definition of the tooling and the input of the material rheological data under investigation, but they are also highly sensitive to the data input for the boundary conditions between the billet and the tooling. These parameters

are clearly extremely sensitive when attempting to simulate the extrusion process. If incorrect data are entered, substantial errors in result variables may ensue. In early software development, requirements were only confined to a graphical illustration of the change in geometrical shape of the workpiece [16-19] and an approximate value of pressure to undertake the process. In such cases, the accuracy of the data input i.e. friction, heat transfer, etc., was not necessarily high and consisted of an approximation to the flow stress and a global, averaged friction factor. Eulerian description was also permissible. With the ever-increasing use of FEM techniques to the extrusion process in the past decade, the necessity for accurate input data becomes increasingly crucial. The analytical abilities of current FEM codes enable the continuum parameters of the extrusion process, stress and strain histories and metal flow to be predicted in detail as deformation continues. In order to enable full advantage to be taken of the use of FE programs available to simulate manufacturing processes, not only are detailed mechanical, thermal and microstructural constitutive descriptions of materials required but mechanical and thermal properties of workpiece/tool interfaces and the tools also must be available.

2.2 Main Parameters and their Effects

The basic process of extrusion is well described as a thermo-mechanical event in a recent text by Sheppard [1] which indicates that the mathematical description of the process is still largely semi-empirical. The extrusion process is complex, involving interaction between the process variables and the material's high-temperature properties and is typically conducted at relatively high temperatures because the lower flow stress of the material permits larger section reductions to be achieved, lowering the power requirements and processing times. Furthermore, the process variables

have a large effect on the mechanical properties and surface quality of the extrudate. Theoretically [1], the process variables which may be controlled are the extrusion ratio R, the ram speed V, and the initial extrusion temperature T. The possible range of all these parameters is determined by alloy composition and the homogenisation treatment. Customer specification and press capacity, generally fix the extrusion ratio so that the temperature and speed become the only controllable parameters. However, events on the micro-mechanical scale are still not adequately described. The most important of these is possibly the mechanics at the interface between tooling and material i.e. the friction. This influences the analyses of the temperature changes occurring during the process, the final temperature and the temperature history determining the structure of the extrudate and hence, to a large extent, its properties.

Comprehension of the material flow during the hot extrusion of aluminium alloys is also of significant importance for complicated sections and also for better control of the process.

2.2.1 Flow stress

A true stress-strain curve is frequently called a flow curve because it gives the stress required to cause the material to flow plastically at any given strain. The mean equivalent flow stress, $\bar{\sigma}$, is the most important variable used in predicting forming process, because in plastic deformation process, such as extrusion, the load or stress is a function of the extrudate geometry, friction and the flow stress of the deforming material. It also has a significant effect on the temperature field within the deforming body. The flow stress is influenced mainly by two factors: factors unrelated to the deformation process, such as chemical composition, structure, phases and grain size, and prior strain history, and factors explicitly related to the

deformation process, such as temperature, the amount of deformation or strain and the rate of deformation or strain-rate. Thus the mean equivalent flow stress $\bar{\sigma}$ can be expressed as a function of temperature, *T;* strain, $\bar{\varepsilon}$; strain-rate, $\dot{\bar{\varepsilon}}$; and *S*. S, consists of internal variables characterising the resistance to plastic flow caused by the internal microstructure state of the material [9, 20]. The following two equations must be satisfied:

$$\left.\begin{aligned} \bar{\sigma} &= f\left(T, \bar{\varepsilon}, \dot{\bar{\varepsilon}}, S\right) \\ \frac{\partial \bar{\sigma}}{\partial \bar{\varepsilon}} &= \left[T, \bar{\varepsilon}, \dot{\bar{\varepsilon}}, S\right] \end{aligned}\right\} \qquad (2.1)$$

The flow stress of metals must be obtained experimentally for given strain, strain-rate and temperature conditions. The decrease in flow stress with increasing temperature and the increase at higher strain-rate have been measured in several studies [1, 20-21]. The high-temperature flow stress plays a dominant role in determining structure and is the primary factor determining the extrusion pressure. The most commonly used methods for obtaining the flow stress data are, uniform compression [22-23] and torsion tests [20-21]. The flow stresses of nearly all metals are critically strain-rate dependent. Therefore, at high temperatures the tests are conducted at a constant strain-rate condition and maintained throughout the tests. The value is a fixed function of the material and varies with the temperature-compensated strain-rate and with the temperature [20].

In hot extrusion, the influence of the strain on the flow stress may be considered insignificant and makes such a small contribution to deformation that the material is assumed to obey a plastic law [24]. Theories

of metal working operations generally assume that under hot working conditions a metal behaves as an ideal rigid-plastic solid [25]. However, at higher temperature, the influence of the strain-rate (i.e. rate of deformation) becomes increasingly important. Hence the material flow behaviour is rate-dependent, which leads to the theory of visco-plasticity [24, 26].

The Norton-Hoff [27-28] and the Zener-Hollomon [21] relationships are the two constitutive equations most adopted to relate the viscoplastic material behaviour for aluminium alloys under hot working conditions.

The Norton-Hoff law was introduced for uniaxial creep analysis by Norton F. [27], and then extended to three dimensional analysis by Hoff N.J. [28]. The exponential form of the Norton-Hoff law used in FORGE2® is written as follow:

$$\bar{\sigma} = K_0 \cdot (\sqrt{3})^{m+1} \exp\left(\frac{\beta}{T}\right) \cdot \dot{\bar{\varepsilon}}^{m} \cdot (\bar{\varepsilon} + \varepsilon_0)^{n} \qquad (2.2)$$

where K_0, β are material constants, m is the strain-rate sensitivity index, n is the strain-hardening index, $\bar{\varepsilon}$ is the equivalent strain, $\dot{\bar{\varepsilon}}$ is the equivalent strain-rate, ε_0 is a constant (0.001).

There is another viscoplastic flow equation which was originally proposed for creep analysis and has been rearranged to describe the flow stress behaviour at elevated temperatures: the hyperbolic-sine function. The most widely used is that proposed by Sellars and Tegart [29] and subsequently modified by Sheppard and Wright [21] to yield the steady-state flow stress $\bar{\sigma}$ from the equation:

$$Z = A[\sinh(\alpha\bar{\sigma})]^n = \dot{\bar{\varepsilon}} \exp\left(\frac{\Delta H}{GT}\right) \qquad (2.3)$$

from which:

$$\bar{\sigma} = \frac{1}{\alpha} Ln\left\{\left(\frac{Z}{A}\right)^{1/n} + \sqrt{\left(\frac{Z}{A}\right)^{2/n} + 1}\right\}$$

in which Z (s^{-1}) is termed the temperature-compensated strain-rate. The Arhenius term indicates that hot working is a thermally activated process [20] with ΔH ($kJ.mol^{-1}$) as the activation energy for deformation, $\dot{\bar{\varepsilon}}$ (s^{-1}) is the mean-equivalent strain-rate and G ($8.314J\ mol^{-1}K^{-1}$) is the universal gas constant. A (s^{-1}), α ($m^2.MN^{-1}$) and n are constants within the extrudable temperature range; n is generally assumed to be a measure of the strain-rate sensitivity and α appears to be constant to the transition from power to exponential relationships for the flow stress. The remaining terms in the equation require definition because the strain-rate is specific to extrusion geometry and the temperature T (°K) varies throughout the extrusion ram stroke. The activation (ΔH) energy is considered as a material constant in the hot-deformation range and is usually close to the value for self diffusion of the alloy.

Dashwood *et al.* [30] investigated the differences between the Norton-Hoff and the Zener-Hollomon relationships during the extrusion of AA7075 alloy. However, their investigation was not conclusive as they simply mentioned the difference between these two flow stress functions. Therefore, it is still necessary to give more details about their difference under different temperature and strain-rate conditions, especially their influence on the computed FEA results.

Some researchers have adopted more complex and advanced constitutive equations in recent years [25, 31-32]. The major aluminium alloys investigated in the present work have not been represented by these models. In contrast, the hyperbolic-sine function has been applied to describe the behaviour of a number of aluminium alloys in extrusion [1, 2-4, 8, 10-12, 30, 33-35].

2.2.2 Temperature evolution during extrusion process

Extrusion is commonly classified as a hot-working process. Hot working is defined as deformation under conditions of temperature and strain-rate such that recovery processes take place simultaneously with deformation [1].

The critical parameters for the extrusion process are that the work should be carried out in a range of temperatures, in which the metal has adequate plasticity to allow for the desired shape change, usually severe, to be carried out and also to reduce the forces required for extrusion.

As shown in Figure 1.2, the temperature is one of the most important parameters in extrusion. The flow stress is reduced if the temperature is increased and deformation is, therefore, easier, but at the same time, the maximum extrusion speed is reduced because localized temperature must be well below the incipient melting temperature.

During the process cycle most of the work done is converted into heat. This energy will be stored in the deformed structure. Temperature rise and temperature distribution during extrusion have been investigated by many researchers [12, 33-43]. The temperature rise during extrusion depends on many parameters and consists of the following individual processes as outlined by Sheppard [1] and shown in Figure 2.1.

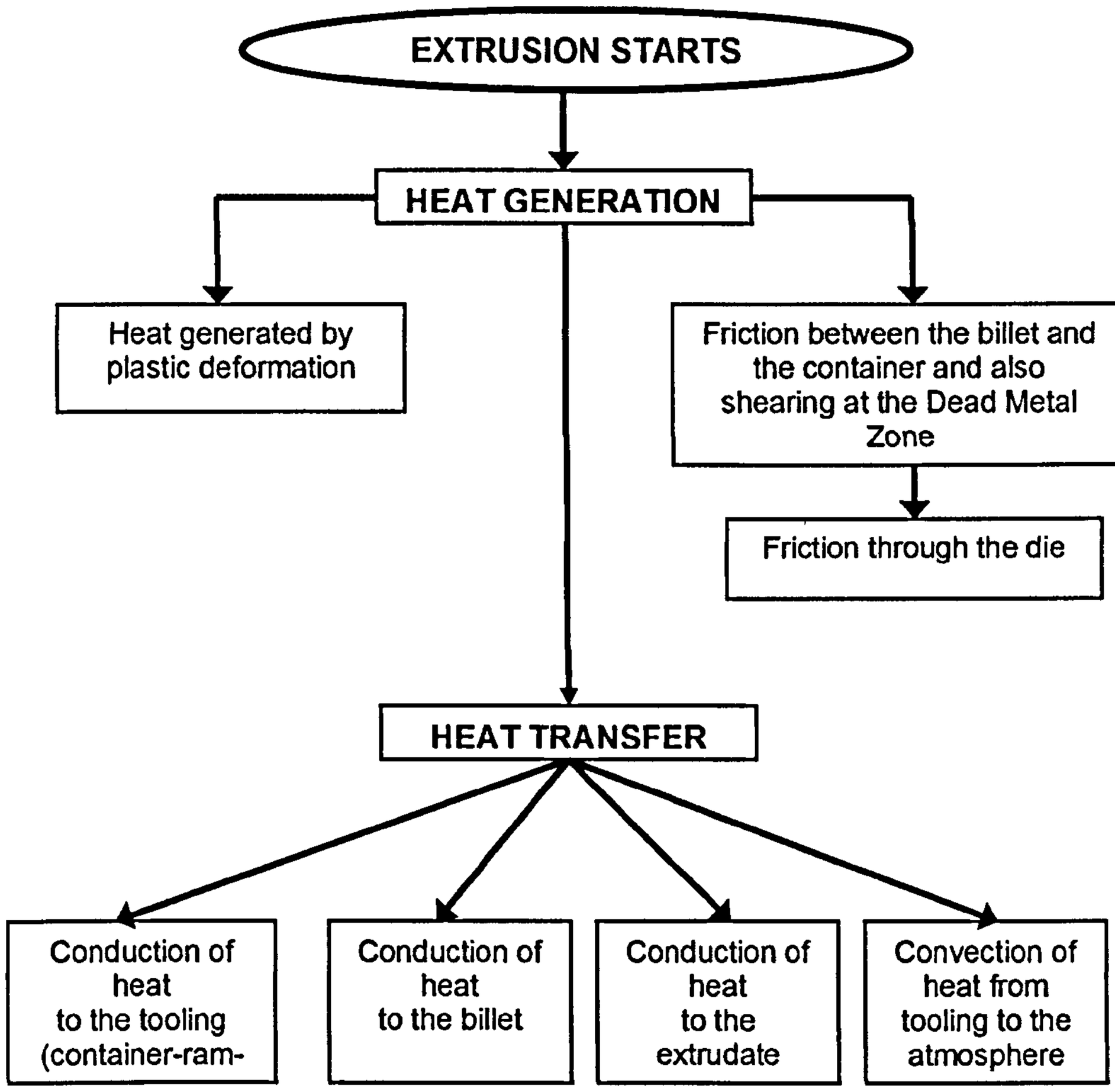

Figure 2.1: Heat balance during the extrusion process.

The temperature rise within the shear zone is a function of the heat generation due to deformation, heat conduction to the cooler material on either side of the deformation zone and convective heat transfer by material elements leaving the deformation zone. Because of the occurrence of the conductive and convective heat transfer, the deformation is not adiabatic. Estimation of the temperature increase is alloy dependent.

Pure aluminium alloy with the lowest flow stress has the lowest temperature rise and the hard aluminium alloys with the highest flow stress have the highest temperature rise.

Bishop [44] first proposed a rigorous mathematical analysis. However, the analysis was only limited to plane strain conditions and assumed that heat loss to the container did not occur. Akeret [39] following a similar approach developed an approximate numerical method in which the temperatures were calculated point by point or cell by cell. The billet was assumed to be divided into a number of uniform discs and the work done and heat transferred was calculated as each disc was extruded. Partial numerical solutions for the heat produced and the heat lost could be combined linearly and the temperature profile along the billet in the container and the extrusion obtained. The method did not appear to function well unless the container was hotter than the billet [1]; a condition seldom encountered in practice.

Although the FEM technique offers great potential, care must be taken when applying the analysis to the hot extrusion of rate sensitive alloys. The accuracy of the results depends on the geometric definition of the tooling, real material data and the governing boundary conditions between the billet and the tooling. These parameters are clearly extremely sensitive when attempting to simulate the extrusion process [33-35]. The extrusion parameters (friction, heat transfer, etc.) are significantly influenced by the temperature gradients produced in the billet during transfer to the container and after upsetting in the container. Previous researchers in simulating the extrusion process have ignored the meshing of the tooling (container and die) [30, 45-48], although the heat transfer at the tool/billet interface governs the temperature profile throughout the billet and tools during extrusion and, consequently, has a critical influence on the results. The most useful approach for an FEM simulation would thus be to include both the tooling

and the billet in the calculation as discretised meshes. This would both provide a more exact description of the thermal conditions and take elastic properties of the tools into account. The disadvantage of this approach is the substantially higher computation time required to solve the numerical equation systems.

Numerous temperature-linked FEM models have been proposed. However, few give any experimental verification. Generic deformation models are available and a number of publications have used the French developed FORGE2® software. In general the authors have not presented details of the temperature changes occurring which arguably are the most important feature of the extrusion process. However, Dashwood and McShane [30] have presented details of temperature rises during the extrusion of 7075 alloy and compared them with experimental data. The temperature was not measured but the results agree with observations made on the onset of cracking and the incipient melting point. Another two-dimensional model by Grasmo *et al* [37] considering only the steady-state presented much experimental evidence to justify their model. These results will be used as a comparison with FEM results in this thesis.

2.2.3 Friction

The most significant parameter to define when modelling extrusion processes is the friction coefficient [34-35, 49-52]. The mechanism of interfacial friction in aluminium extrusion is very complex and is not a well-understood phenomenon. Due to the high pressures and temperatures that are necessary features of the process, experimentation is difficult and this combined with only a rough estimation of the relevant parameters indicates that an accurate simulation might be of some use.

In the industrial context, assumptions are made that sticking friction prevails at the interface between the billet and the tools, and its value is a constant for all extrusion temperatures. Various studies and analytical methods have been used to establish the complex relationship between the extrusion parameters, friction, temperature, stress, strain, strain-rate, etc. Some of these studies [50, 53-57] provided some understanding into the mechanisms that govern friction but fall short in supplying sufficient information to identify the mechanisms that can be applied quantitatively to model friction for the extrusion process.

Other researchers [1, 30, 55-56, 58-64] have expressed the friction coefficient to be constant and to range between 0.8 and 1 based on experimental observations, using either varying billet lengths or by measurement of the slope of the pressure/displacement locus. Variations of pressure with billet lengths have been investigated for 1100 and 2014 alloys by Sheppard [1] and Sheppard and Patterson [64] by extruding billets of varying lengths under identical extrusion conditions. It was observed that the peak pressure/billet length relationship in each case was linear, and the friction coefficient value determined from the data was 0.88 for AA1100 alloy and 0.8 for the AA2014 alloy. The work indicated that the friction coefficient has an approximately constant value during the extrusion process regardless of the initial extrusion temperature.

Clearly neither of these methods of establishing the value of friction is satisfactory and for design purposes, the friction is usually assumed to be 0.85. However, such measurements fail to take into account the differences in temperature at differing locations during the ram stroke and the consequent deviation in the flow stress. The extrusion pressure is significantly influenced by the temperature gradients modified in the billet during deformation. Metal flow in the extrusion process is an important

factor controlling the mechanical and structural properties of the extruded product.

The coefficient of friction at the metal/billet interface contributes significantly to the complexity of extruding, and it is a point where the friction resistance approaches the shear resistance of the hot material during deformation. Furthermore, it is a point where a fraction or all of the displacement of the billet at the interface occurs by shear in its surface layers leaving a fragment of the billet deposited on the wall of the container. In practice, aluminium alloys are extruded without any lubricant or with only a small amount of graphite applied to the die face. Finding a suitable lubricant would be a difficult task and in any case unlubricated aluminium extrusion is desirable in order to prevent impurities being picked up from the tools and to ensure that all the material making up the extrudate surfaces originates from virgin material within the billet. Hence, the interfacial conditions at the billet-container interface during extrusion have a direct effect on metal flow, the stresses acting upon both the tools and within the material, and hence load and energy requirements and extrudate temperature.

During the extrusion process, the force necessary to overcome the friction between the billet and the container results in an increase in overall pressure to extrude. At the extreme condition between the billet and the container, friction at the interface cannot exceed the shear strength of the material. This extreme condition is termed sticking friction, and may be represented generally as:

$$\tau_F = \tau_{\max} \tag{2.4}$$

where τ_F is the interfacial friction, and τ_{max} is the shear yield stress of the billet material. The shear stress may be defined either by the Tresca yield criterion:

$$\tau_{\max} = \frac{\bar{\sigma}}{2} \tag{2.5}$$

where $\bar{\sigma}$ is the mean equivalent yield stress.

or by a Von Mises criterion when the shear strength can be expressed as:

$$\tau_{\max} = \frac{\bar{\sigma}}{\sqrt{3}} \tag{2.6}$$

where $\bar{\sigma}/\sqrt{3}$ is the mean equivalent shear flow stress. A modification to sticking friction is often introduced to account for the fact that friction forces are seldom as high as the shear strength of a material. The friction may be defined using what is sometimes referred to as the Tresca friction law, which assumes proportionality between the friction and the current shear flow stress of the material and may be written as follow:

$$\tau_F = m\,\tau_{\max} \tag{2.7}$$

where $\bar{m}$ is the factor of proportionality and is commonly referred to as a friction factor and varies between $\bar{m}$ = 0 for perfect lubrication and $\bar{m}$ = 1

for sticking friction. The Tresca law treats the interface friction as pressure independent and relates the friction stress directly to the shear flow stress of the deformed material. τ_{max} can be determined from either Tresca or Von Mises yield functions, or from other descriptions of the plastic flow stress in shear.

For the convenience of simulation and modelling purposes, friction is considered in terms of the relative velocity between two surfaces, i.e. billet and tooling. The friction law may be considered by assuming the Tresca friction law criteria described in Equation 2.7 and is written;

$$\tau = -\overline{m}\frac{\sigma_s}{\sqrt{3}} \tag{2.8}$$

At the limit when $\overline{m}$ is of unit value, all deformation will be in the form of shear in the subcutaneous regions of the billet rather than sliding against the tools. However, this simple representation is not able to include the contribution of local conditions such as temperature, pressure, surface quality and geometry. Otherwise, with the description and the inclusion of heat transfer, the value of $\overline{m}$ is defined with the same value as a constant, and it would be more realistic to specify this constant as a function of process variables. Although $\overline{m}$ should be assumed as a constant value, this formulation can be more useful and more sophisticated by allowing the friction coefficient or the friction factor to be functions of several variables.

2.3. Shape Extrusion

Several types of non-symmetric shapes with various cross-sections such as "T", "U" , "Square" and other extremely complex shapes, are produced by the extrusion process. It is generally known that a large increase in the extrusion load is required to extrude a section of these types of complexities containing re-entrant corners or thin fin sections, over that of simple circular cross-sections.

Sheppard [1] and Sheppard and Wood [2] reported in more detail the parameter that can represent the degree of difficulty of extrusion of complex shapes by the use of a shape factor or peripheral ratio λ. λ is defined as the ratio of the periphery Ω_S of the section to the periphery Ω_R of a rod of equivalent cross-sectional area and is defined in the equation below:

$$\lambda = \frac{\text{the periphery of the section}(\Omega_S)}{\text{the periphery of a rod equivalent cross - sectional area}(\Omega_R)} \qquad 2.9)$$

For a normal rod extrusion, λ is equal to 1.

It is shown [1-2] that the temperature-compensated strain-rate can be related to the incremental pressure through the following equation:

$$P = \frac{1}{\alpha n}\left\{a + b\ln\lambda R + c\left[\ln\lambda^2\left(\frac{Z}{A}\right)\right] + d\left(\frac{L_B}{D_B}\right)\left[\ln\lambda^2\left(\frac{Z}{A}\right)\right]\right\} \qquad (2.10)$$

where a, b, c and d are constants and are defined using multi regression technique.

The difficulty of extrusion was thus defined by the λ^2 parameter, since it can be seen from equation 2.9 that λ is proportional to the length while the extrusion ratio is proportional to the area (i.e. D^2/d^2). It was found that equation 2.9 was valid over a wide range of extrusion temperatures and the sections investigated [1, 62].

The material flow is also of particular importance when extruding complicated sections. The occurrences of material flow during the extrusion process has been the focus of much interest in aluminium alloys in general [4, 17, 33-34, 60, 65-71] but has been most often limited to rod extrusions. The influence of section geometry on the deformation zone is difficult to establish, unlike in axisymmetric rod extrusion where the circumferential strain is essentially zero, the introduction of a third dimensional strain requires more careful interpretation. This is especially so near the die throat where the extrudate surface and structural features are being generated. Studies of the material flow during extrusion are well-documented in literature. They range from the most commonly used technique such as the gridded billet [65-68], introducing pins of an aluminium alloy into the as-cast-billet and then grinding and etching the surface after the end of the extrusion [37, 60, 62, 70], to marking grids within the initial billet [33-34, 72]. However, the gridded billet technique relies on planar flow, and is not suitable to study material flow for complex cross-sections. The pins or volume element technique is more successful than the gridded billet technique. The advantage of this technique is the ability of the created pattern not to be erased in regions of heavy shear. However, the process itself is difficult to analyse due to many re-entrant corners and the rotational component of velocity that can cause unpredictable behaviour of

the metal flow during extrusion and may require more that one section-plane to represent the true material flow. Therefore, numerical simulations are necessary to gain more insight during the extrusion process cycle because of the ease with which FEM is able to predict the material flow from the beginning to the end of the extrusion. However, a false assumption of the extrusion being a steady-state deformation is usually applied and Eulerian formulation based FEM codes are used [37,50, 73-77]. Therefore, in order to investigate the microstructural evolution and predict the extrudate properties, material history must be available and traced back and forth during the process cycle, thus, the Lagrangian formulation based FEM has to be adopted.

2.4 Tube extrusion

Aluminium extrusion is the most common method used to produce solid and hollow shapes. Solid profiles are generally produced with a die that consists of only one part, while hollow profiles are produced with at least two parts, a die and a mandrel. The production of tubes represents an important activity in commercial extrusion. In order to extrude hollow sections, the billet has to be pressed through a die that determines the outside diameter, and over a centrally-located mandrel that determines the inside diameter. The metal must, therefore, flow through an annular gap. For the extrusion of hollow aluminium profiles this is achieved by the use of the dies following the principles laid down by Dick [78]. A bridge or porthole dies is usually used to manufacture hollow sections as shown in Figure 2.2. The dies contain a weld chamber in which a solid billet is forced, under pressure, through a composite die tool that first divides the metal into two or more distinct streams. These are then rejoined under the bridge by a pressure weld and emerge as an extruded section, through the orifice formed between the mandrel and the aperture shape. Therefore,

extruded sections produced on such dies have two or more seams or longitudinal weld lines. Because the separate metal streams are joined within the die without atmospheric contamination, a perfectly sound weld is usually obtained.

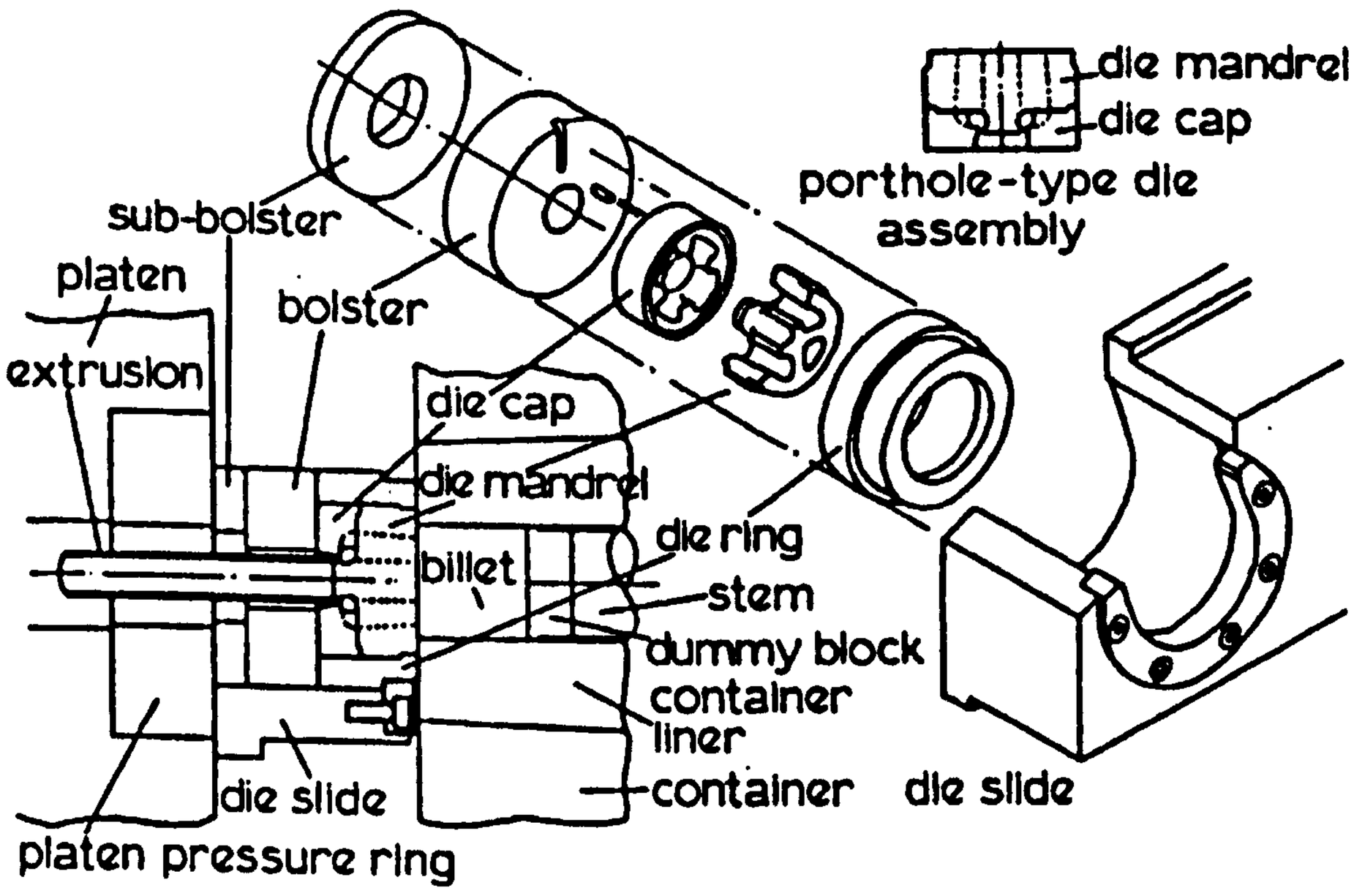

Figure 2.2: A typical porthole tooling arrangement for aluminium hollow sections (Courtesy of Sheppard [1])

Extrusion of the 6XXX alloy series through bridge dies producing hollow shapes is common in the aluminium industry. One of the largest problems in tube extrusion is tube eccentricity reported by Sheppard *et al.* [79] which affects the quality of the product and is generally due to poor design of the welding die. A number of experiments have been conducted into the study and prediction of conditions occurring during the extrusion process in the welding chamber [79-83]. Few of them, however, attempt to quantify the process. The complexity of metal flow calls for simulation of the complete

process in three-dimensions. FEM also gives new and important information, since local values for temperature, stress, and velocity within the deformation zone are not readily accessible by experiments. The research related to metal-forming processes during the last few decades has widely used FEM in investigations. However, it is only during the last decade that useful numerical simulations of aluminium extrusion have been reported. This is partially due to the nature of the process and the excessive time required for computation. Early work was mainly involved with 2D extrusion problems [79, 83-87] or simple 3D geometry with low extrusion ratio [88-91]. Some have been experimentally verified [30, 33, 60, 92-94]. Despite the fact that temperature evolution and distribution are of paramount importance in the extrusion process, very few publications pay attention to this aspect [46, 19-21, 24-25]. During bridge-die extrusion this is an important factor because the quality of the joints along the entire length of the final product is primarily determined by the conditions in the welding chamber [1].

2.5. Subgrain size evolution

To date, a considerable amount of work has been reported on the substructure evolution for aluminium alloys under various hot work conditions: hot torsion, hot rolling and plane strain compression [8, 43, 95-103]. An interesting feature of subgrains is that they are equiaxed and keep equilibrium size and shape in the steady-state regime even at very large strain, whereas the grains are always elongated in the direction of the extension. To date there are two interpretations of this. The first considers that sub-boundaries are constantly migrating in such a way as to keep the substructure equiaxed. The second possible interpretation is by the repeated unravelling of the sub-boundaries and the subsequent

reformation of new sub-boundaries at locations which keep their average spacing and dislocation density constant, termed "repolygonisation" [101].

It is generally accepted that the temperature-compensated strain-rate or Zener-Hollomon parameter (Z), is directly related to the subgrain size δ during steady-state deformation [1] by the flowing equation;

$$\delta_{ss}^{-m} = A + BLnZ \qquad (2.11)$$

where A, B, and *m* are constants.

The subgrain exponent *m* value varies from 0.35 to 1.25. However, most researchers [30, 58, 61-62] have agreed putting *m* = 1, produces an acceptable fit in equation (2.11). This is because the range of subgrain sizes typically obtainable in the hot working range is very small in contrast to the range of Ln(*Z*) values. Constants in equation (2.11) for various alloys are well documented and are listed in Appendix 1. It can be seen in Appendix 1 that *m* equals 1 is widely used. It should be emphasised here that the equation (2.11) is not valid for prediction of subgrain sizes in a transient deformation.

It should be noted that equation (2.11) is not the only form of formula that relates subgrain size with process parameters for steady deformation. Other researchers [101-105] have proposed alternative formulae modified from equation (2.11), however, these equations require too many constants to be statistically defined from experimental data, and hence, they will not be discussed here.

Compared with the work on subgrain size during steady-state deformation, there is still lack of quantitative relationship to relate the subgrain size with the deformation parameters in a transient deformation. During the last few years, Sellars and Zhu [103] and Furu et al [104] have carried out some exploration work in this field. They have performed the transient deformation by altering the strain-rate in plane strain compression tests. Zhu and Sellars [105], have explicitly expressed the evolution of subgrain size in a differential form based on the most classical theories of work hardening and dynamic recovery:

$$d\delta = \frac{\delta}{\varepsilon_\delta \delta_{SS}}(\delta_{SS} - \delta)d\varepsilon \qquad (2.12)$$

where δ_{ss} is the subgrain size at steady-state deformation, δ is the instantaneous subgrain size, $d\varepsilon$ is the increment of strain, $d\delta$ is the increment of subgrain size, ε_δ is characteristic strain, which determine the rates of evolution of subgrain size, δ_{ss} is defined as the same as equation (2.11). ε_δ, is assumed to be in proportion to Z'', which indicates that ε_δ is a function of Z. The specific form relating ε_δ with the Zener-Hollomon parameter may depend upon the deformation conditions and the material. However ambiguity was found about the value of the exponent *n*. Zhu and Sellars [103, 105], assigned different values (-0.5 and ¾) to the exponent *n* in two papers for the same material and experimental conditions.

There is a great lack of research in prediction of subgrain size by FEM in aluminium extrusion. Dashwood *et al* [30], attempted to predict the subgrain size using FEM. They investigated the change in subgrain size for extrusion of AA7075 during rod extrusion. The predicted results fit

reasonably well with the experimental measurements in a small region around the die mouth. The distribution of subgrain size within the container was not given. However, in their investigation, they appear to adjust the value of activation energy ΔH (156 KJ/mol) defined in equation (2.3) as a material constant to nearly twice its value. No justification was given to support their alteration to this value. The activation energy is considered to be a material parameter for nearly all aluminium alloys. It is not a parameter which can be tuned in order to match the predicted result with experimental measurement. Another dubious assumption is the use of the instantaneous nodal strain temperature-compensated strain-rate to predict the change in subgrain sizes. From Equation (2.11) one would expect a decrease in subgrain size from the rear of the billet to the die mouth to the increase in strain-gradient and hence a strain-rate. This will, of course, be influenced greatly by the temperature variation and thus it would appear that the expected decrease in this case is somewhat balanced by a small rise in temperature along the flow line. Although the substructure is continuously undergoing rearrangement, it cannot change instantaneously and must depend on the deformation history.

2.6 Iso-Extrusion

Extrusion parameters (e.g., billet temperature and extrusion speed) are dictated by the chemical composition and homogenisation treatment of each alloy. Harder alloy extrusions used in applications such as the aerospace industry, present challenges to the extruder because they must be defect-free and have a specific final structure yielding the appropriate properties which should be consistent along the length of the extrudate. Harder alloy extrusion is thus rather more complex and demanding than soft and medium-strength alloys. Because the hot-working temperature

range is very narrow, there is, critically, more severe interaction between process variables and material properties at the working temperature.

It is commonly known that the extrusion process must be performed at low lnZ values (i.e. high temperature). However, the process is limited by two factors, as shown in Figure (1.2). The first limiting factor lies in the press capacity (maximum extrusion pressure) and the second limiting factor lies in the maximum temperature that can be tolerated during the process, which is determined by the occurrence of incipient melting.

The occurrence of incipient melting and friction-related tearing depend on the initial billet temperature. If exit temperature is not properly controlled, the extrudability will be reduced drastically.

It is an obvious conclusion that better and more careful control of the extrusion process is mandatory if productivity is to be significantly increased. A more typical plant problem is to determine the optimum speed for some fixed extrusion ratios.

The combination of the extrusion speed and the billet temperature result in the bulk temperature of the deforming billet exceeding a critical value which for AA2024 is about 495°C (511°C incipient melting). However, the most important limitation on the extrusion speed is imposed by the temperature increase in the deforming billet. This increase if not under control may cause the temperature of the extrudate to exceed the critical value, in which either incipient melting or friction-related tearing occurs.

Isothermal extrusion has thus been proposed to control the change of mechanical properties by adjusting the ram speed according to the feedback of the measurement of temperature at the die exit. It was first

proposed in the 1970s [107] and has been studied for many years by the use of various methods [108-113]. However, little work has been done to develop an understanding of the details of the deformation and temperature transients that occur within the shear zone and how they affect substructure evolution.

The substructure experiences a very complicated evolution during the extrusion process. Previous investigations [43, 97, 101] show that a substantial number of the mechanical properties could be directly related to the substructure of the extrudate. Therefore, in order to approach an optimum extrusion condition, it would be more constructive if that included the control of substructure evolution (i.e. subgrain size) in addition to or instead of exit temperature for desired mechanical properties. This can be achieved by controlling both the substructure through the ram speed and the exit temperature. The benefit of iso-subgrain lies in its consistent product quality in terms of surface and dimensional stability, both of which are of particular interest to extruders. It can also result in an increase in mean extrusion speed and thus productivity.

This new extrusion process is termed iso-subgrain size extrusion, differing from what is normally termed isothermal extrusion.

CHAPTER 3: FEM PROGRAMS AND FORMULATION

3.1 FEM programs

In the present thesis all the simulations were conducted using the French developed software FORGE2® and FORGE3® from TRANSVALOR. Only those theories and analysis techniques, which are adopted by FORGE2® and FORGE3® and related to the work in the following chapters, are taken from the literature [114-116] and briefly introduced in this Chapter.

FORGE2® and FORGE3® are dedicated to simulating the hot, warm and cold axisymmetric bulk deformation and plane strain processes, such as forging, rolling and extrusion. Originally this package was developed more than a decade ago at Ecole des Mines de Paris and was successfully applied to 2D and 3D FEM simulation on various forming processes [30, 33-35, 37, 49, 117-118]. In addition to the plastic deformation of the work- piece, FORGE2® software is capable of coupling the temperature calculation of both the work piece and the die(s), and of incorporating the elastic deformation of the die(s). It has three databases: material database, process condition database and press database. Hundreds of alloys have quite recently been added to the material database. The latest version of FORGE2® is V.3.0 (2003-2004).

FORGE3® predicts material flow for 3D bulk metal-forming processes. The automatic remeshing technique enables the simulation of very complex parts. The ability of the solver in using multi-processors significantly cuts the analysis time. The latest version of FORGE3® is V6.2 (2003-2004)

3.2 Finite element approximation

3.2.1 Finite element discretisation

In modelling of the extrusion process, the governing equations are strongly non-linear. These non-linearities are due to complex constitutive equations, non-linear kinematics and contact. The vast majority of approaches for solving systems of non-linear equations are based on the Newton-Raphson iterative scheme or its variants.

Using isotropic elements, the velocity field v, is discretised with the help of the nodal velocity vectors $\mathbf{V}_n$, shape functions N_n and local co-ordinate vector ξ as:

$$\mathbf{v} = \sum_n \mathbf{V}_n \mathrm{N}_n(\xi) \tag{3.1}$$

The mapping with the physical space is defined by:

$$\mathbf{x} = \sum_n \mathbf{X}_n N_n(\xi) \tag{3.2}$$

and the strain-rate tensor is computed with the help of the **B** linear operator:

$$\dot{\varepsilon} = \sum_n \mathbf{V}_n \mathbf{B}_n \tag{3.3}$$

The pressure field is discretised in terms of nodal pressure $\mathbf{P}_m$, with compatible shape functions M_m:

$$p = \sum_m \mathbf{P}_m M_m(\xi) \tag{3.4}$$

The discretised mixed formulation for viscoplastic material gives the set of non-linear equations:

$$\mathbf{R}_n^V = \int_\Omega 2\mathbf{K}\left(\sqrt{3}\dot{\bar{\varepsilon}}\right)^{m-1} \dot{\boldsymbol{\varepsilon}} : \mathbf{B}_n dV + \int_{\partial\Omega_c} \alpha_f K |\mathbf{v}_s|^{p-1} \mathbf{v}_s N_n dS - \int_\Omega p tr(\mathbf{B}_n) dV = 0 \tag{3.5}$$

$$\mathbf{R}_m^p = \int_\Omega \mathbf{M}_m div(\mathbf{v}) dV = 0 \tag{3.6}$$

which takes the symbolic form:

$$\mathbf{R}(\mathbf{X}, \bar{\varepsilon}, \mathbf{V}, \mathbf{P}) = 0 \tag{3.7}$$

where Ω and Ω_c are the part domain and the domain interface between the part and tools respectively. α_f, the friction coefficient and P, the interface sensitivity to sliding velocity.

The time evolution of co-ordinate vectors and equivalent strain is governed by:

$$\frac{d\mathbf{X}}{dt} = \mathbf{V} \tag{3.8}$$

$$\frac{d\bar{\varepsilon}}{dt} = \dot{\bar{\varepsilon}} \tag{3.9}$$

3.2.2 Increment approach

In the numerical simulation of the extrusion process, the displacement finite elements method is often used. For purely viscoplastic materials, the most popular scheme for nodal update can be performed with the Euler explicit scheme. If $\mathbf{X}_n^t$ is the co-ordinate vector of node number n at time t, with velocity vector $\mathbf{V}_n^t$; at time $t + \Delta t$ the new co-ordinate vector will be:

$$\mathbf{X}_n^{t+\Delta t} = \mathbf{X}_n^t + \Delta t \mathbf{V}_n^t \tag{3.10}$$

A second order scheme was shown to improve the accuracy [114], especially regarding the volume conservation of the part material, with a Runge and Kutta method or the semi-implicit scheme:

$$\mathbf{X}_n^{t+\Delta t} = \mathbf{X}_n^t + \tfrac{1}{2}\Delta t\left(\mathbf{V}_n^t + \mathbf{V}_n^{t+\Delta t}\right) \tag{3.11}$$

The efficiency of this scheme strongly depends on the corresponding procedure for the error and step size control.

3.2.3 Lagrangian and Eulerian FEA

There are two modes of description generally used in formulation of finite elements for large plastic strain analysis; Eulerian and Lagrangian technique.

The Lagrangian technique considers all matter consists of single cells that retain their identity and nature as they move through space. This description employs the position coordinates of a typical particle in the reference or undeformed state, and these coordinates are functions of time. In other words, in the Lagrangian technique, the finite element mesh is deformed incrementally over time with the material making it easy to track surfaces and apply boundary conditions. Lagrangian formulations are well suited for the problems concerning path-dependent material properties and free surfaces. However, they suffer from numerical problems when the material sustains significant distortion, the mesh follows suit and may become heavily distorted. As the distortion increases, the quality of the results suffers. Nevertheless, this is not a disadvantage as such if modelling and meshing of the tool/part is planned carefully.

In the Eulerian technique all processes are characterised by field quantities which are defined at every point of space. The finite element mesh remains fixed while the material passes through it. The independent variables are the coordinates of space and time of a material point in the deformed state. This description of the continuum problems allows one to focus attention on one point in the space and then to observe the problem occurring there. Eulerian formulations are able to cope with large material deformation, but surfaces, boundary conditions and material history are impossible to track using this approach. However, mesh distortion is not a problem because the mesh never changes.

In the simulation of the extrusion process, material history and contact phenomena play an important role. Therefore, the best-suited approach for the numerical simulation of extrusion process is the Lagrangian method. The advantage of tracking the history of the material point or a node, for surface formation, microstructure evolution and temperature evolution are of paramount importance to the process optimisation.

In FORGE3, the meshing is based on two concepts: the quality of the elements and the shape preservation (geometry). These two concepts are quantified and controlled by the user. The strategy to obtain the "best" mesh is based on node addition, suppression and regularisation to improve an existing given surface or to rebuild a new surface from an initial one. These should be done without modifying the domain geometry (shape preservation). In order to generate a volume mesh, the program requires an initial triangular surface mesh with three node linear triangles. The quality of this volume mesh depends on the quality of the part's (billet) surface mesh generated in a CAD system (I-DEAS, Pro-Engineer, etc.)

3.2.4 Remeshing and transfer of state variables

The large deformations during the simulation of the extrusion process produce large deformations of the finite element mesh which are badly adapted to the problem. It is very often necessary to regenerate the mesh several times in order to complete the simulation. As soon as one of the following remeshing criteria has been reached, a new mesh has to be automatically generated using an automatic mesh generator. For this reason, and in order to satisfy the compatibility condition between the velocity and pressure, tetrahedral elements seem more convenient for automatic meshing and remeshing. The 5-node tetrahedral mini element for the velocity, with linear continuous pressure is shown in Fig.3-1.

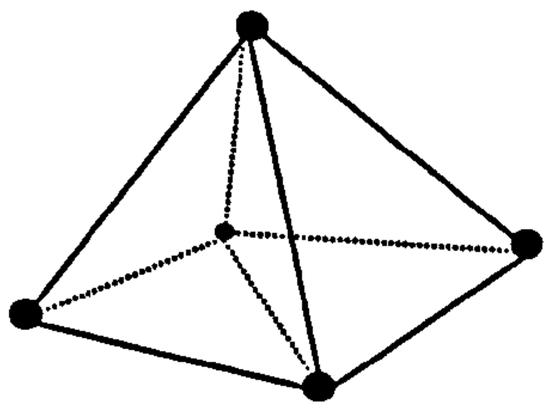

Figure 3.1: Finite element interpolation in a tetrahedron

The remeshing criteria [116] are as follows:

a) distortion of a finite element, due to internal shear.
b) penetration of a part of the mesh inside the tool
c) large curvature of the segments of the free boundary
d) detection of a fold (see Figure 3.2),

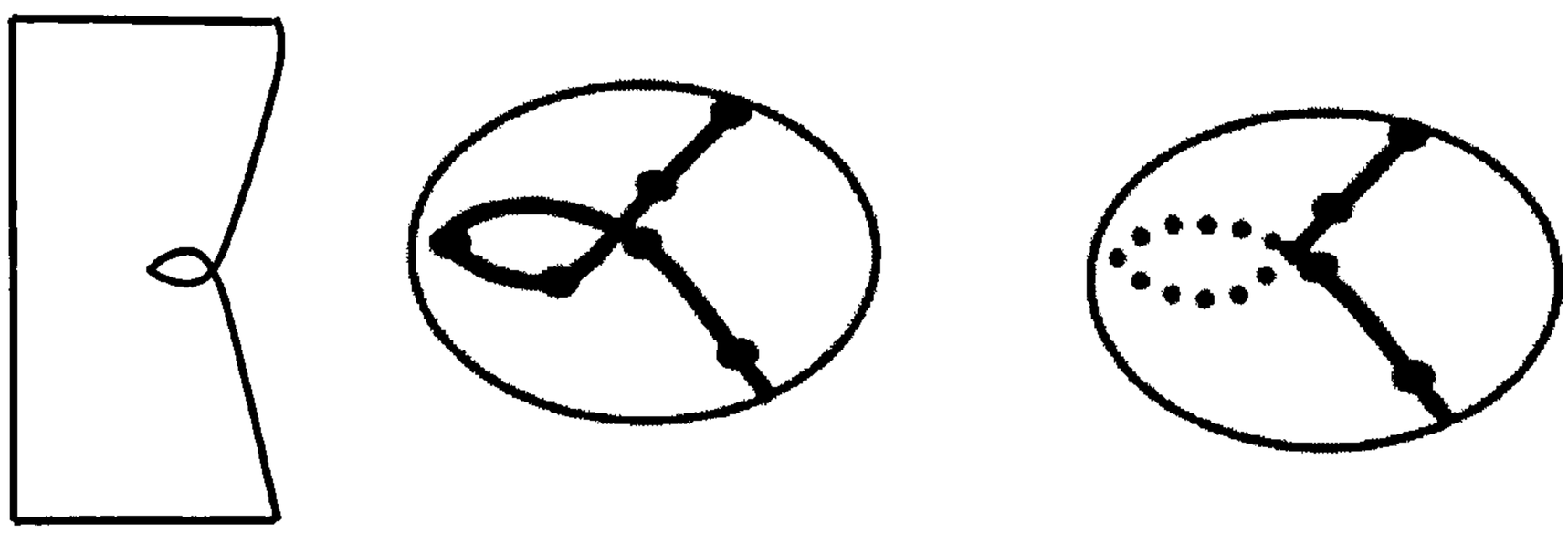

Figure 3.2: Folding defect noticed by the remeshing procedure when two boundary segments cross each other.

3.2.5 Approach of the coupled thermal and mechanical problem

The temperature field is discretised with the same elements as for the velocity field according to:

$$T = \sum_n T_n N_n(\xi) = \mathbf{T} \cdot \mathbf{N} \qquad (3.12)$$

The classical semi-discretised form is easily obtained from equation:

$$\mathbf{C}\cdot\frac{\mathrm{dT}}{\mathrm{dt}}+\mathbf{H}\cdot\mathbf{T}+\mathbf{F}=0 \tag{3.13}$$

where **C**, is capacity matrix, **H**, conductivity matrix and **F**, vector contains the visco-plastic heat dissipation and boundary conditions. **C** and **H** are computed by:

$$\mathrm{C_{ij}}=\int_{\Omega}\rho\mathrm{cN_iN_j}\mathrm{dV} \tag{3.14}$$

and

$$\mathrm{H_{ij}}=\int_{\Omega}\mathrm{k}\mathbf{grad}(\mathrm{N_i})\cdot\mathbf{grad}(\mathrm{N_j})\mathrm{dV} \tag{3.15}$$

The temperature field can be integrated with a second order scheme where:

$$\mathbf{T}=\mathrm{a}\mathbf{T}^{\mathrm{t}-\Delta\mathrm{t}}-(1.5-2\mathrm{a}-\mathrm{g})\mathbf{T}^{\mathrm{t}}+(\mathrm{a}-0.5+\mathrm{g})\mathbf{T}^{\mathrm{t}+\Delta\mathrm{t}} \tag{3.16}$$

$$\frac{\mathrm{dT}}{\mathrm{dt}}=(1-\mathrm{g})\frac{\mathbf{T}^{\mathrm{t}}-\mathbf{T}^{\mathrm{t}-\Delta\mathrm{t}}}{\Delta\mathrm{t}}+\mathrm{g}\frac{\mathbf{T}^{\mathrm{t}+\Delta\mathrm{t}}-\mathbf{T}^{\mathrm{t}}}{\Delta\mathrm{t}} \tag{3.17}$$

$$\mathbf{C}=(0.5-\mathrm{g})\mathbf{C}^{\mathrm{t}-\Delta\mathrm{t}}+(0.5+\mathrm{g})\mathbf{C}^{\mathrm{t}} \tag{3.18}$$

where a and g are constants. In the Dupont scheme, a=0.25 and g=1.

3.3 Constitutive equations

The FEM used in metal-forming can be generally categorised into viscoplastic and elastic-viscoplastic FEM, depending on which material constitutive equations are used. Constitutive equations for plastic deformations are usually based on rate equations. For large deformation

processes, i.e. extrusion, the elastic deformations are totally ignored (the elastic part of the strain-rate can be neglected). That means that a calculated strain increment equals the plastic strain increment. This rigid plastic can be very effective for large strain increments but lacks accuracy for small strain increments. This can be a drawback, because even in simulations with large strain increments there are often areas with almost no deformation i.e. dead zones. One way to overcome this drawback is to include some elasticity into a rigid-plastic or viscoplastic model.

For extrusion of hot aluminium alloys, viscoplastic FEM is adopted to simulate the process because plastic strain dominates the process. The most economical laws are purely viscoplastic approximations. The 3-D isotropic viscoplastic Norton-Hoff law is written [114]:

$$\mathbf{s} = 2K\left(\sqrt{3}\dot{\bar{\varepsilon}}\right)^{m-1}\dot{\boldsymbol{\varepsilon}} \tag{3.19}$$

$\dot{\bar{\varepsilon}}$ is expressed in terms of the strain-rate tensor $\dot{\boldsymbol{\varepsilon}}$:

$$\dot{\bar{\varepsilon}} = \left(2/3\sum_{i,j}\dot{\varepsilon}_{ij}^{2}\right)^{1/2} \tag{3.20}$$

K is the material consistency, function of temperature T, and equivalent strain $\bar{\varepsilon}$. The consistency, K, is a general property used to quantify the resistance of the metal to permanent deformation. The dimensions of K depend on the value of m and are M.L.T, where L represents a length dimension, T a time dimension and M a mass dimension. FORGE2® and FORGE3® model these variations by defining consistency to be an explicit function of temperature, strain-rate and strain.

$$K = K_0\left(\varepsilon_0 + \bar{\varepsilon}\right)^n \exp(\beta'/T) \qquad (3.21)$$

where n and β' are constants. m in equation (3.19) is the strain-rate sensitivity index, which ranges between 0.1 and 0.2 for hot metals (i.e. metal above its recrystallisation temperature), and between 0.5 and 0.7 for superplastic metals. m is a power index with no units.

Dense materials show a negligible volume change, which results in the incompressibility constraint:

$$div(\mathbf{V}) = 0 \qquad (3.22)$$

Another visco-plastic flow stress law exists: hyperbolic-sine function, which is usually used to describe the flow stress behaviour at elevated temperature,

$$\bar{\sigma} = \frac{1}{\alpha} Ln\left\{\left(\frac{Z}{A}\right)^{1/n} + \sqrt{\left(\frac{Z}{A}\right)^{2/n} + 1}\right\} \qquad (3.23)$$

A, α ,n are constants. Their physical interpretations are given in the literature [1] for various alloys, these constants are listed in Appendix 2.

In FORGE2® and FORGE3®, the default constitutive equation is the Norton-Hoff law. The hyperbolic-sine function is incorporated into these two programs by programming the user subroutine.

3.4 Friction model

Three kinds of friction law are available in the FORGE2® and FORGE3® codes; Tresca friction, Viscoplastic friction and Coulomb friction. The Tresca friction law is written in the following form:

$$\tau = -\overline{m}\frac{\sigma_s}{\sqrt{3}}\frac{\Delta \mathbf{V}}{\Delta V} \tag{3.24}$$

where σ_s represents the yield stress, $\sigma_s/\sqrt{3}$ is usually termed shear strength, m is commonly referred to as friction factor, ΔV is the velocity difference at the interface. The Tresca law treats the interface friction as pressure independent and relates the friction stress directly to the yield strength of the deformed material. When m=1, sticking friction occurs. The range of m is $0 \le \overline{m} \le 1$.

The viscoplastic friction law arises from the consideration of a thin interface layer of a viscoplastic lubricant between the workpiece and tool, as shown in Figure 3.3.

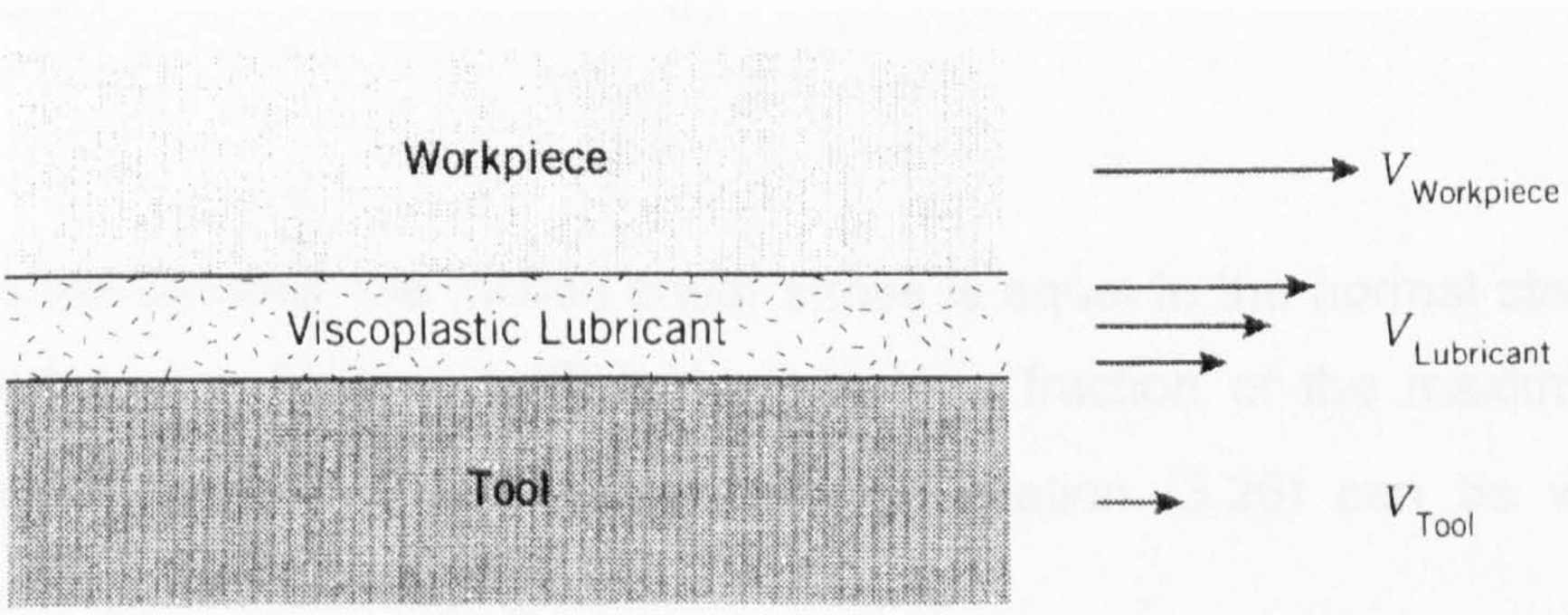

Figure 3.3: Conceptual view of viscoplastic friction condition (Courtesy of Wagoner and Chenot [115])

The Viscoplastic friction law is written in the following form:

$$\tau = -\alpha * K * \Delta V^{p-1} * \Delta \mathbf{V} \tag{3.25}$$

where α is a Viscoplastic friction coefficient and $0 \leq \alpha \leq 1$, which is a function of normal stress. K is the consistency of the material, which is defined in equation (3.21). P is the sensitivity parameter to the sliding velocity. P is usually chosen as the same value as the strain-rate sensitivity index in equation (3.19). When p=0, equation (3.25) turns into equation (3.24).

The modified Coulomb friction law can be written as:

$$\tau = \mu\sigma_n \frac{\Delta \mathbf{V}}{\Delta V} \qquad \text{if } \mu\sigma_n \prec \frac{\sigma_s}{\sqrt{3}}$$

and: (3.26)

$$\tau = m\frac{\sigma_s}{\sqrt{3}}\frac{\Delta \mathbf{V}}{\Delta V} \qquad \text{if } \mu\sigma_n \succ m\frac{\sigma_s}{\sqrt{3}}$$

with this relationship, the friction shear stress is equal to the normal stress multiplied by the friction coefficient μ or to a fraction of the maximum shear stress sustainable by the material. Equation (3.26) can be well illustrated by the following Figure.

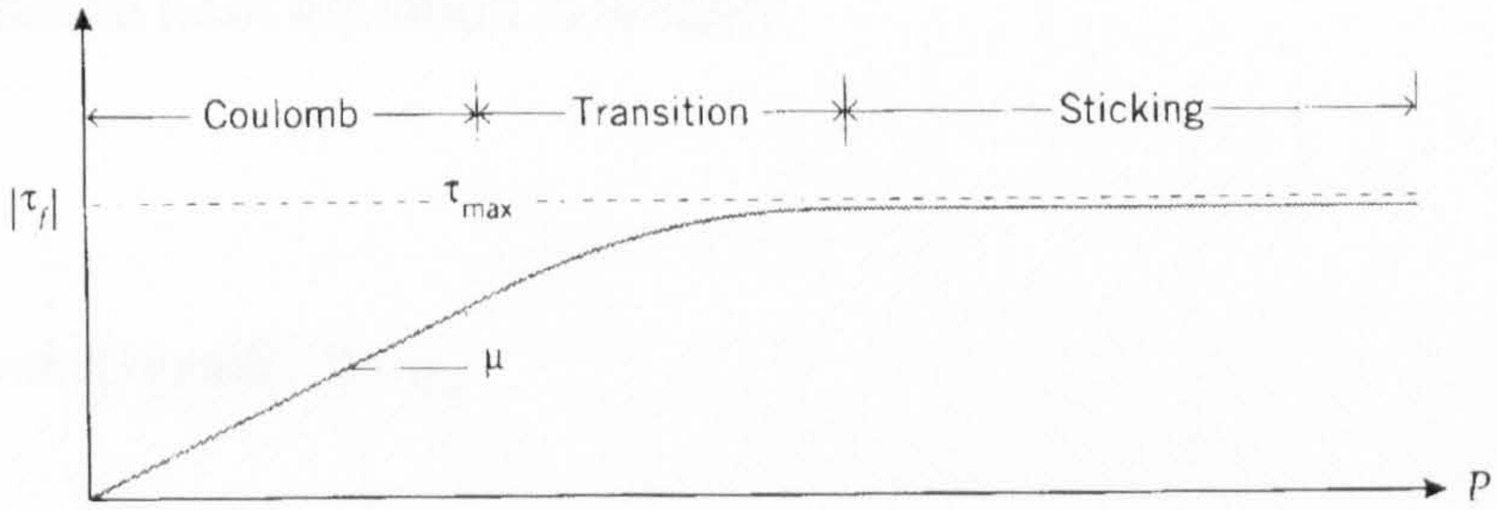

Figure 3.4 :Conceptual view of the modified Coulomb friction law (Courtesy of Wagoner and Chenot [115])

From the above equations, it is clear that each equation includes a term ΔV , the velocity difference between tool and workpiece. When ΔV is close to zero, certain problems occur. To solve these convergence problems in such cases, these friction laws are regularised, i.e. written as follows:

$$\tau = -m\frac{\sigma_0}{\sqrt{3}}\frac{\Delta \mathbf{V}}{\sqrt{\Delta V^2 + \Delta V_0^2}} \qquad (3.27)$$

The regularisation sliding velocity ΔV_0 has a very small value.

3.5 Thermal analysis

The classical heat equation is written:

$$\rho c \frac{dT}{dt} = div\left(k\mathbf{grad}(T)\right) + \dot{q}_v \tag{3.28}$$

where $\rho c \frac{dT}{dt}$ is Temperature evolution, $div\left(k\mathbf{grad}(T)\right)$, internal conduction and $\dot{q}_v$ heat dissipation.

The Norton-Hoff viscoplastic heat dissipation $\dot{q}_v$ is written as:

$$\dot{q}_v = fK(\sqrt{3}\dot{\bar{\varepsilon}})^{m+1} \tag{3.29}$$

The *f* factor takes into account the fraction of energy which is converted into heat, it ranges generally between 0.9 and 1.0. f=0.95 is used throughout the present thesis.

On the free surface, radiation is modelled by:

$$-k\frac{\partial T}{\partial n} = \varepsilon_r \sigma_r \left(T^4 - T_0^4\right) \tag{3.30}$$

where ε_r is emissivity parameter, σ_r, Stephan's constant and T_0, outside temperature.

On the surface of contact with the tools, conduction with the tool and surface dissipation due to friction must be taken into account:

$$-k\frac{\partial T}{\partial n} = h_{cd}\left(T - T_{tool}\right) + \frac{b^*}{b^* + b^*_{tool}}\alpha_f K\left|\Delta \mathbf{V}\right|^{q+1} \tag{3.31}$$

CHAPTER 4: MODELLING THE PARAMETERS WHICH AFFECT EXTRUSION

4.1 Introduction

This chapter uses FORGE 2® and involves validating the FE code to simulate the process condition and selecting an appropriate flow stress describing the material behaviour. The extrusion pressure and the temperature rise were predicted and the pressure-displacement trace and the events which take place in the deformed material during the extrusion process were also simulated. The effect of the initial billet temperature on friction, and the extent of the surface zone affected by surface friction and the consequence changes in material flow were investigated.

The force required for extrusion depends on the flow stress of the billet material, the extrusion ratio, the friction condition at the billet container interface, the friction condition at the die material interface, and the other process variables, such as initial billet temperature and the speed of extrusion. Extrusion can become impossible or can yield an unsatisfactory product when the load required exceeds the capacity of the press available or when the temperature of the extrusion exceeds the solidus temperature of the alloy. Knowledge of the initial billet temperature, the strain-rate, flow stress of the working material, and the extrusion ratio are required if correct and economical use is to be made of expensive extrusion facilities.

4.2 Process conditions

4.2.1 Numerical and experimental models

Numerical models and experimental extrusion have been used to evaluate the extrusion of AA2024 aluminium alloy. The chemical compositions of the alloys used in this investigation are shown in Appendix 3. All the experimental data are extracted from the literature [62-63, 79, 120]. Experiments were performed on a 5 MN vertically mounted press with a heated container. The main ram was driven by a hydraulic pump during the extrusion cycle. The load was measured by a Mayes load cell situated directly above the ram, the output from the cell being recorded on a Labmaster data recorder. Ram displacement and speeds were measured by a rectilinear potentiometer fixed between the moving crossheads and the press bolster.

A comparative experiment was made to assess the relative importance of some extrusion parameters in the extrusion process and to ensure that the numerical discretisation gave a true simulation of the process. The comparisons of major interest are the extrusion pressure and the die exit temperature since if these are coincident then a valid numerical simulation model of the process may be assumed. Pressure values and exit temperatures produced from simulation were compared with experimental values and predicted exit temperature results from Grasmo *et al* [37], Subramaniyan [62] and Vierod [63] theses. This comparison enabled an independent check of the changes in billet temperature and friction conditions during extrusion.

A constant ram speed of v = 3 mm/s was imposed with an extrusion ratio of 20:1 for AA2024 alloy. In the Forge 2 program, only half of the cross-section requires modelling due to the symmetry. A flat-faced die with a 5-

mm die bearing length was used for all simulations unless stated otherwise. The boundary conditions between the billet and the container at the interface were evaluated for the Tresca friction type mechanism and will be discussed in detail later in this Chapter.

The container-die and ram temperatures were 50°C and 100°C below the initial billet temperature respectively for all the analyses (unless stated otherwise) in an attempt to reduce the temperature of the extrudate and, hence, to simulate industrial conditions.

4.2.2 Meshing and remeshing

During the simulation of the extrusion process, large deformations are predominant and if the material history (material flow, temperature, strain-rate, etc) are required, a Lagrangian mesh evolution must be defined. However, the elements become severely distorted during the process and consequently, the need for remeshing is necessary to continue the simulation. The frequency of remeshing is controlled by the degree of deformation and is a user-variable. To improve the accuracy of the results, it is critical to control the degree of remeshing in the areas where high deformation is expected. Refinement mesh boxes of Eulerian type (but maintaining Lagrangian flow) were applied to the billet at die entrance and section re-entrant corners where high deformation is expected to occur. A coarser mesh is used for the remainder of the billet. The mesh for the FEM simulations was generated automatically for a space domain that included billet, container and the ram. To overcome any discrepancies in the results as a consequence of the meshing and remeshing in the billet during extrusion, only one model consisting of the billet and tool set-up was used throughout the simulations. The initial billet and tool temperatures, friction conditions, and constitutive equations were changed accordingly.

The FORGE2's general data-file structure and the detail of the variables used to simulate the extrusion process is shown in Appendix 4. Simulations were conducted on a DELL dual processor workstation.

4.3 Comparison between Norton-Hoff and Hyperbolic-sine functions

Presently there is no accepted procedure for a well-defined material constitutive equation which will result in the accurate prediction of both mechanical and microstructural development over the wide variations in boundary conditions expected in the extrusion process.

This section is focused on the differences of two commonly used constitutive equations in the simulation of metal-forming processes. In FORGE2® and FORGE3® programs, the Norton-Hoff law describes the default rheology of the material. However, it is also possible to define different flow stress behaviour (i.e. Sheppard-Wright law [21]), by coding the law within a user defined subroutine which can then be incorporated into the main program by recompiling the finite element solver with the appropriate modifications. The two flow stress equations are compared with respect to the temperature changes and pressure loci. The discrepancies between these two equations in terms of pressure and temperature under different temperature and strain-rate conditions are analysed and compared with experimental results [62-63].

The flow stress details of most aluminium alloys available to the author were predicted using the hyperbolic-sine function. The data describing the material behaviour for the Zener-Hollomon equation were obtained using

Torque-Twist data from torsion tests and optimised to obtain the form of Equation (4.1)

$$\bar{\sigma} = \frac{1}{\alpha} Ln\left\{\left(\frac{Z}{A}\right)^{1/n} + \sqrt{\left(\frac{Z}{A}\right)^{2/n} + 1}\right\}$$

(4.1)

$$Z = A[\sinh(\alpha\bar{\sigma})]^n = \dot{\bar{\varepsilon}} \exp\left(\frac{\Delta H}{GT}\right)$$

The data for the Zener-Hollomon flow equation are given in Appendix 2 for a wide range of aluminium alloys [1]. However, in order to use the Norton-Hoff equation in FORGE2® and FORGE3®, conversion from the hyperbolic-sine function is inevitable. To verify any loss in accuracy during conversion, a comparison with the experimental flow stress is made. The AA2014 was the only alloy in which the experimental data for the flow stress was available to the author and it was used together with AA2024 in this investigation as an independent check. Therefore, it is still necessary to give more details about variations under different temperature and strain-rate conditions, especially influences on the computed FEA results. Since the only available experimental data for the present author is 4%Cu binary 2014 alloy (see Appendix 5), the comparison is made for this alloy first. The comparison for AA2024 follows.

The Norton-Hoff equation is written as follows,

$$\bar{\sigma} = K_0 \cdot (\sqrt{3})^{m+1} \exp\left(\frac{\beta}{T}\right) \cdot \dot{\bar{\varepsilon}}^m \cdot (\bar{\varepsilon} + \varepsilon_0)^n \qquad (4.2)$$

The constants, *m, β and* K_0 for the Norton-Hoff equation are obtained by regression analysis using the values obtained from the hyperbolic-sine function in Equation (4.1). The flow stress for the sine equation is regressed at differing strain-rates and ranges of temperatures. Using regression of $Ln\bar{\sigma}$ against $Ln\dot{\bar{\varepsilon}}$ and the inverse temperature $\frac{1}{T}$, the constants were obtained such that:

$$Ln\bar{\sigma} = mLn\dot{\bar{\varepsilon}} + X \qquad \Rightarrow \qquad m = \frac{Ln\bar{\sigma} - X}{Ln\dot{\bar{\varepsilon}}}$$
$$Ln\bar{\sigma} = \beta Ln\dot{\bar{\varepsilon}} + Y \qquad \Rightarrow \qquad \beta = \frac{Ln\bar{\sigma} - Y}{Ln\dot{\bar{\varepsilon}}} \tag{4.3}$$

where X and Y are intercepts of $Ln\bar{\sigma}$ versus $Ln\dot{\bar{\varepsilon}}$ and $\frac{1}{T}$ respectively.

Together with the previously calculated constants *m* and *β*, the consistency *K* could be obtained using the Norton-Hoff equation as follows:

$$\bar{\sigma} = K.Exp\left(\frac{\beta}{T}\right)(\bar{\varepsilon} + \bar{\varepsilon}_0)^n \sqrt{3}^{(1+m)} \dot{\bar{\varepsilon}}^m \tag{4.4}$$

and since in the extrusion process, the areas in which small strains occur can be ignored because they do not affect either the pressure or the properties of the material, the strain hardening index, *n* is taken to be close to zero.

$$Ln\bar{\sigma} = LnK + \left(\frac{\beta}{T}\right) + (m+1)Ln\sqrt{3} + mLn\dot{\bar{\varepsilon}} \qquad \text{and}$$

$$K = Exp\left[Ln\bar{\sigma} - \frac{\beta}{T} - mLn\dot{\bar{\varepsilon}} + (m+1)Ln\sqrt{3} \right] \qquad \text{or} \qquad (4.5)$$

$$\mathrm{K} = Exp\left[X^{'} - (m+1)Ln\sqrt{3}\right]$$

where $X^{'}$ is the intercept of $Ln\bar{\sigma}$ against $Ln\dot{\bar{\varepsilon}}$ and $\frac{1}{T}$.

The regressed Norton-Hoff equations for AA2014 for 4% Cu binary and AA2024 are written as follows:

$$\bar{\sigma}_{AA2014} = 0.87571.Exp\left(\frac{2607.937}{T}\right)\sqrt{3}^{(1+0.177206)}\dot{\bar{\varepsilon}}^{0.177206} \qquad (\mathrm{MPa}) \qquad (4.6)$$

$$\bar{\sigma}_{AA2024} = 15.2755.Exp\left(\frac{1154.301}{T}\right)\sqrt{3}^{(1+0.068679)}\dot{\bar{\varepsilon}}^{0.068679} \qquad (\mathrm{MPa})$$

4.3.1 The effect of flow stress function on the peak extrusion load

The effect of the initial temperature on the predicted and experimental peak extrusion loads is shown in Figure 4.1. The Figure shows a good correlation between the experimental and calculated hyperbolic-sine function stresses.

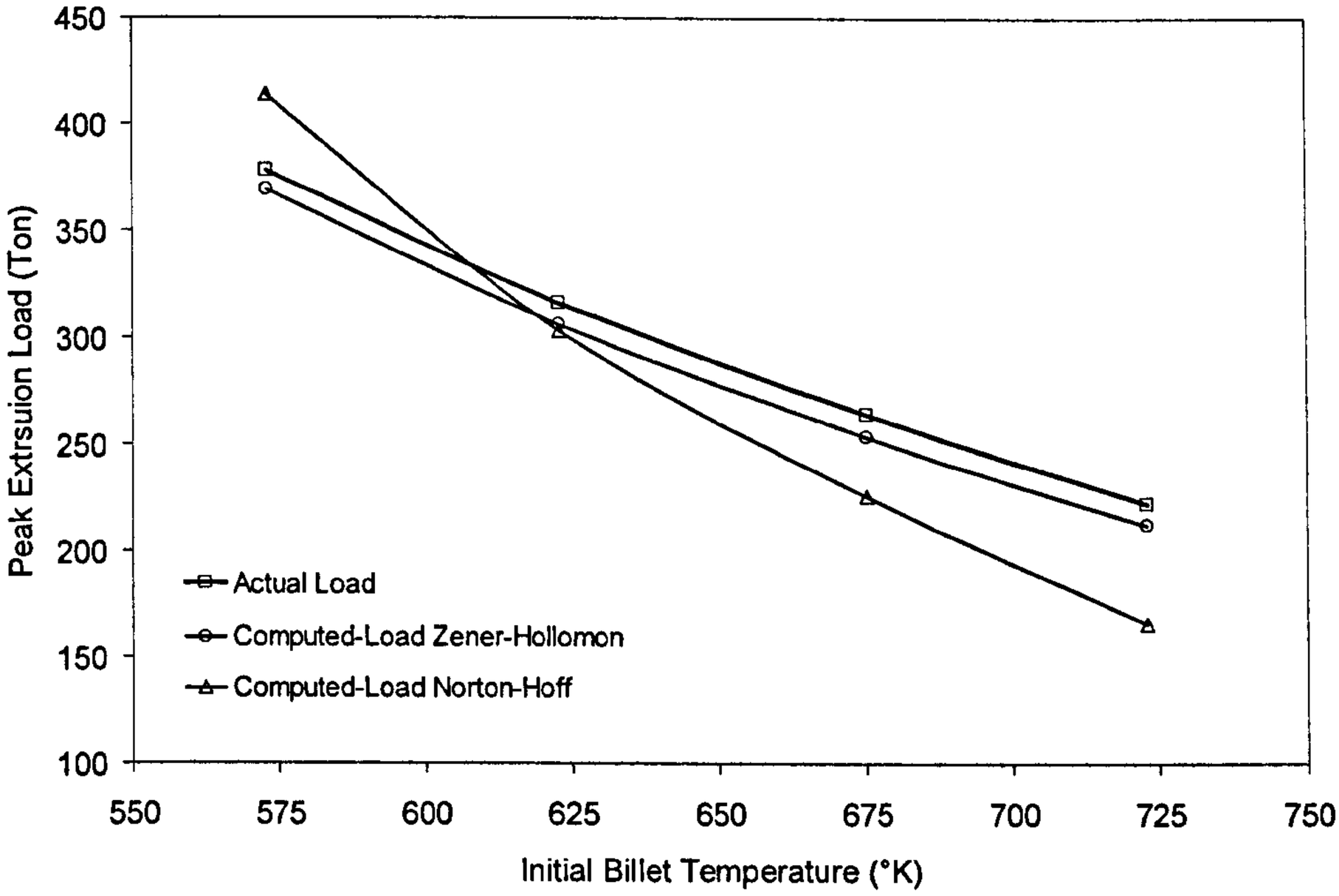

Figure 4. 1: Comparison of computed and actual peak extrusion load as a function of initial billet temperature for AA2024.

The first observation from the figure reveals a slight underprediction of the peak load using the Zener-Hollomon equation. This is because the extrusion pressure is significantly influenced by the temperature gradients produced in the billet during the process. The relative error between the experimental and the predicted peak load by hyperbolic-sine function was between 2.28% and 4.28% at lower and higher temperatures respectively. This is possibly due to the fact that in this investigation, the tools used to represent the container/die were modelled as rigid tools. The drawback to adopting this approach is that the tools are described solely as a line at which motion in relation to the workpiece is governed by simple laws and heat loss via the contact area is unknown because the geometrical conditions beyond the rigid line are unknown. This results in the contour appearing to be of infinite thickness and hence promotes a slightly slower apparent heat exchange rate and therefore results in slightly higher

temperatures being predicted and accounts for the difference observed between the experimental and predicted pressure when using the hyperbolic-sine function.

However, the Norton-Hoff equation portrayed a different behaviour from both the experimental and the hyperbolic-sine results. A significant divergence from the experimental results was observed at both ranges of temperature: an under-prediction at low stress level "high temperature" and a significant over-prediction at higher stress level "low temperature" of the peak load. The relative error between the experimental peak load and the predicted peak load by the Norton-Hoff equation was between 9.4 % and 29.27% at low and higher temperature respectively. Clearly, there is a discrepancy between the Norton-Hoff relationships to predict the peak extrusion load at both stress levels.

To identify the failure of the Norton-Hoff equation in predicting the peak extrusion load, it is necessary to go back to the experimental flow stress data. As previously mentioned, the alloy used in this investigation is AA2014 alloy since it was the only alloy for which the experimental flow stress data were available to the author (see Appendix 5). The experimental flow stress data can be regressed to fit both hyperbolic-sine and Norton-Hoff relationships. The equivalent flow stresses for both equations were calculated over a range of strain-rates and temperatures, 0.5-50s^{-1} and 300-450°C respectively. The regressed Norton-Hoff flow stress from the Zener-Hollomon equation is shown in Figure 4.2.

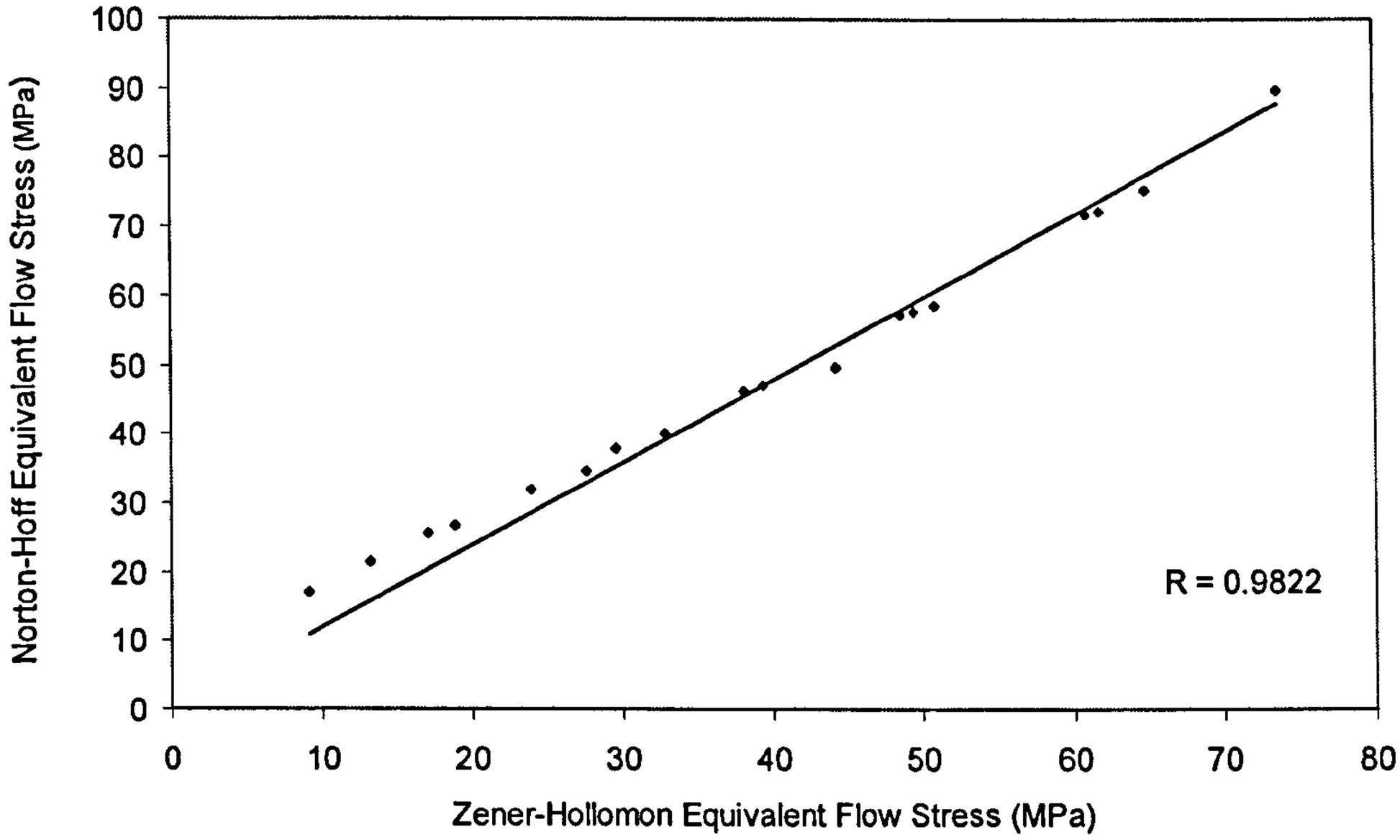

Figure 4.2: The Norton Hoff Law regressed from the hyperbolic-sine equivalent flow stress.

A good correlation coefficient of r = 0.9822 was obtained, indicating that there is no loss in accuracy during conversion from the equivalent hyperbolic-sine to the Norton-Hoff relationship. When the experimental flow stress data were fitted to the hyperbolic-sine and to the Norton-Hoff relationships as shown in Figures 4.3 and 4.4, reasonably good correlations were obtained for both equations. However, the hyperbolic-sine relationship provided a better fit to the experimental flow stress data (r=0.9991) than the Norton-Hoff relationship (r=0.9855). This high correlation coefficient obtained by using the hyperbolic-sine equation indicates that the relationship is applicable to all temperatures and strain-rates considered. The figures also clearly illustrate that the hyperbolic-sine relationship provides a better representation for the experimental flow stress with strain-rate and temperature under hot working conditions than the Norton-Hoff relationship.

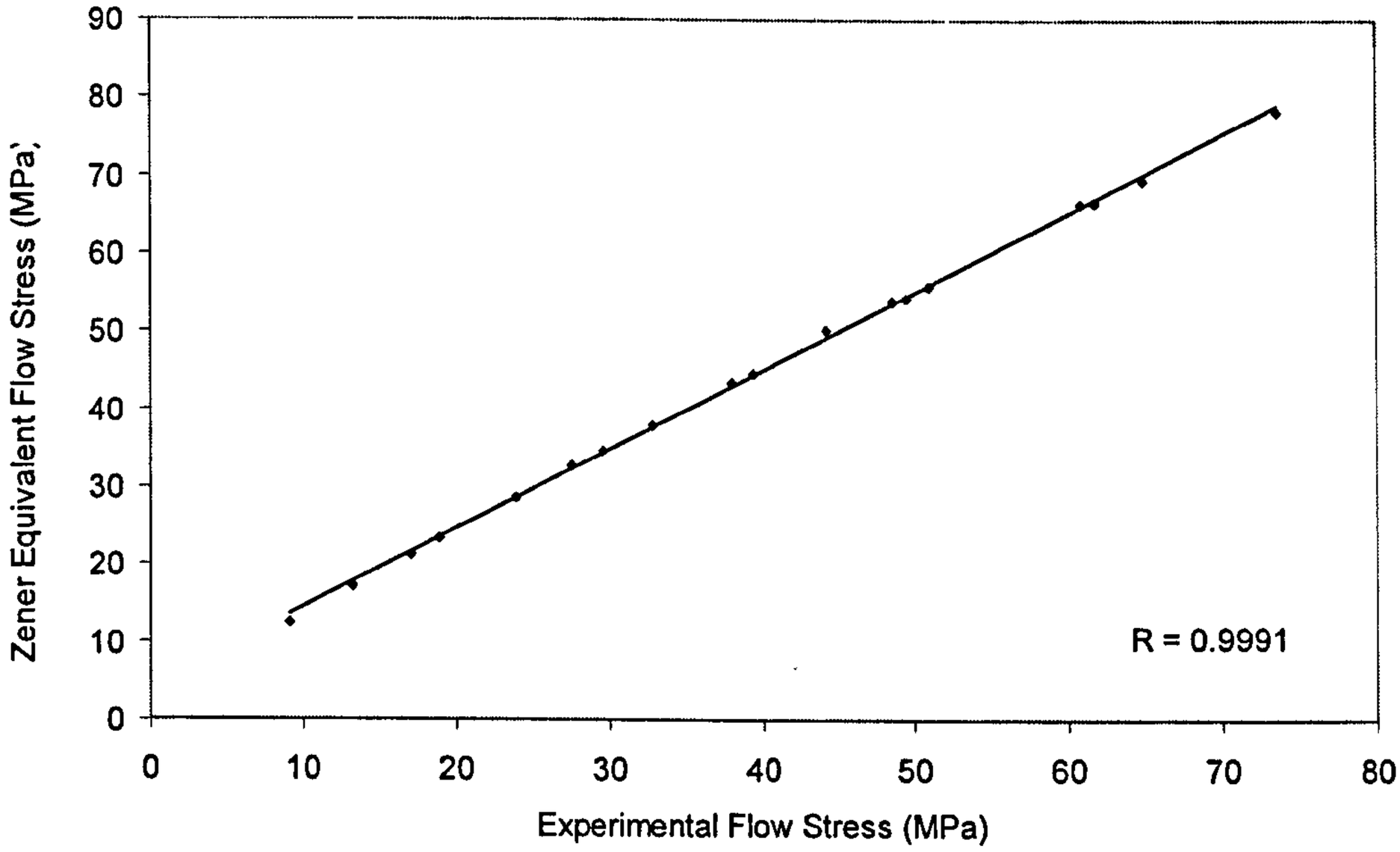

Figure 4 3: Zener Hollomon Law regressed from the experimental data.

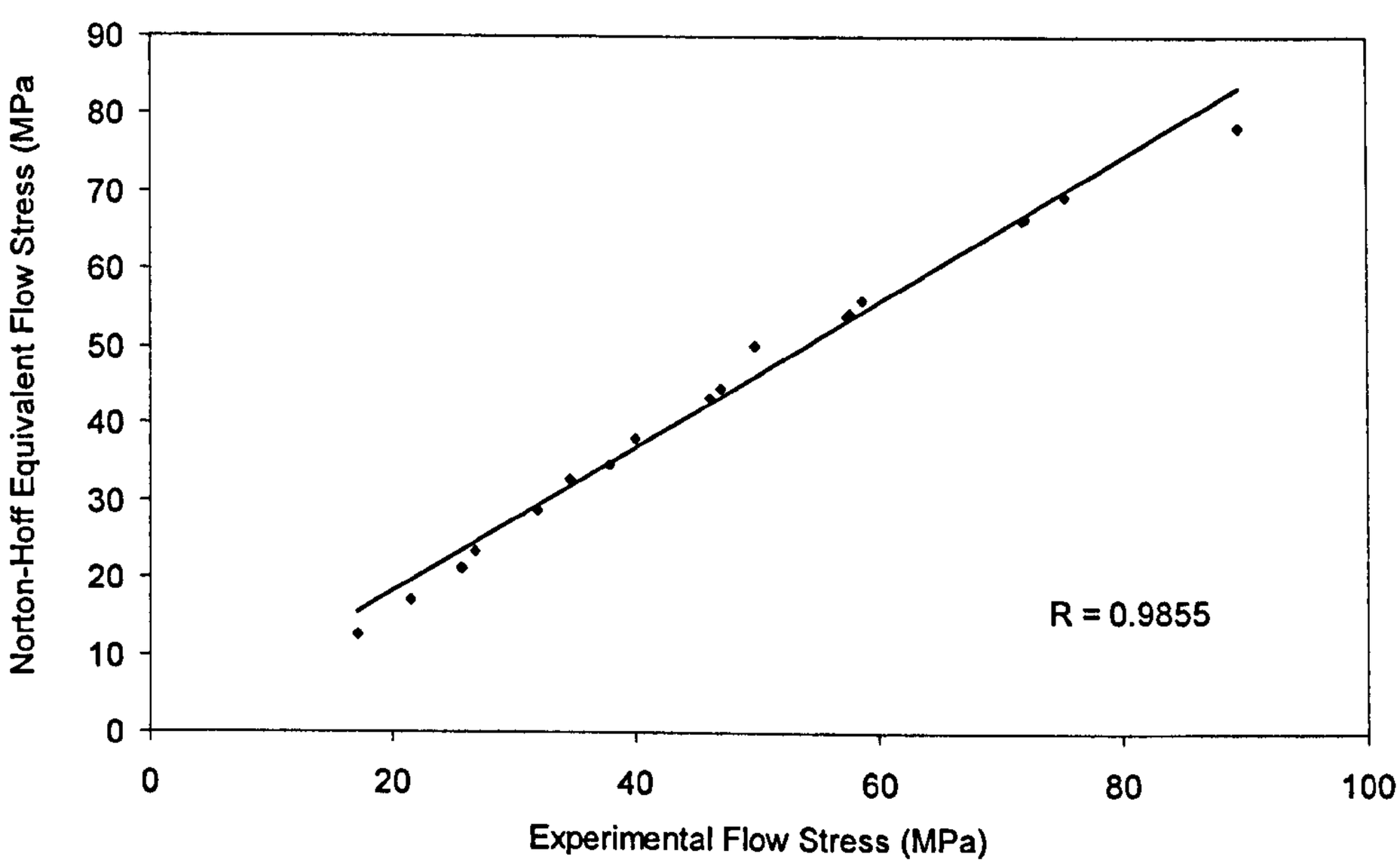

Figure 4.4: Norton Hoff Law regressed from experimental data.

4.3.2 The effect of extrusion temperature and strain-rate on the flow stress functions

The effect of temperature and strain-rate on both flow stress relationships is illustrated in Figure 4.5. To be consistent with the regression and experimental data, the temperature ranges in these figures are within the limits selected to obtain the Norton-Hoff constants (between 300°C and 450°C). No necessary measurements below or above the selected range were made, since it corresponds with the working temperature ranges in extrusion for hard alloys.

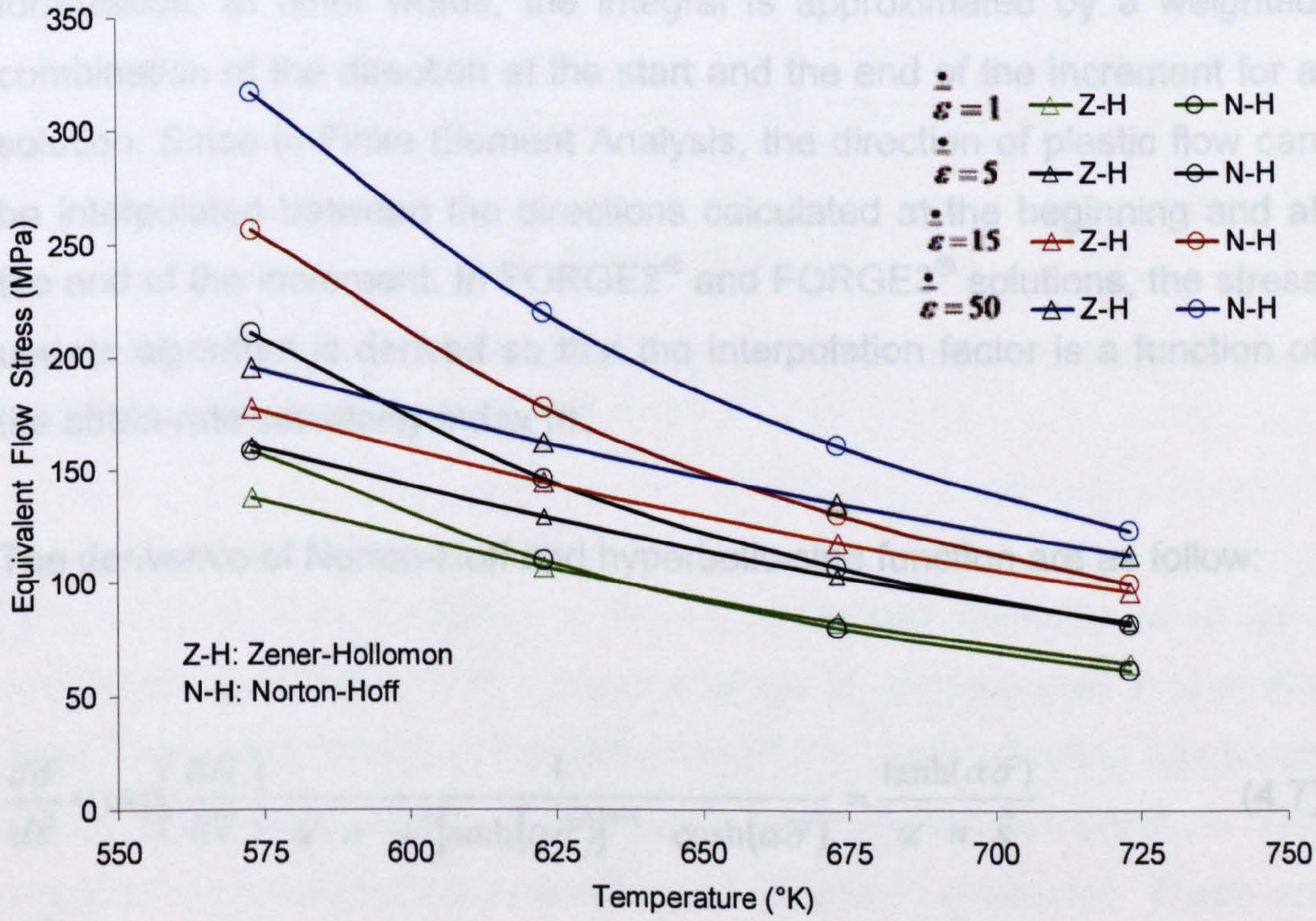

Figure 4.5: Comparison of the flow stress vs. temperature for 4%Cu binary AA2014. at $\dot{\varepsilon}$ =1, $\dot{\varepsilon}$ =5, $\dot{\varepsilon}$ =15 and $\dot{\varepsilon}$ =50 s^{-1}.

The figure reveals significant differences between two flow stress relationships at different strain-rates and temperatures. It is clear from Figure 4.5 that there are significant differences between the two flow stresses at low temperatures. This difference decreases with increase of temperature. At low temperatures, an overprediction of the flow stress is predicted by Norton-Hoff over the range of strain-rates selected, and a slight underprediction of flow stress at lower strain-rate. As the equivalent strain-rate increases, the differences widen as shown in Figure 4.5.

In order to have a clear idea of how the flow stress affects the computed results, it is worth investigating the derivative of flow stress for both relationships, since the constitutive relations for plastic deformations are usually based on rate equations. In a numerical solution it is necessary to integrate the constitutive equations in order to obtain an incremental formulation. In other words, the integral is approximated by a weighted combination of the direction at the start and the end of the increment for a solution. Since in Finite Element Analysis, the direction of plastic flow can be interpolated between the directions calculated at the beginning and at the end of the increment. In FORGE2® and FORGE3® solutions, the stress update algorithm is derived so that the interpolation factor is a function of the strain-rate sensitivity index *m*.

The derivative of Norton-Hoff and hyperbolic-sine function are as follow:

$$\frac{d\bar{\sigma}}{d\dot{\bar{\varepsilon}}} = \exp\left(\frac{\Delta H}{RT}\right) \cdot \frac{1}{\alpha \cdot n \cdot A \cdot \left[\sinh(\alpha\bar{\sigma})\right]^{n-1} \cdot \cosh(\alpha\bar{\sigma})} = \frac{\tanh(\alpha\bar{\sigma})}{\alpha \cdot n \cdot \dot{\bar{\varepsilon}}} \tag{4.7}$$

$$\frac{d\bar{\sigma}}{d\dot{\bar{\varepsilon}}} = \bar{\sigma} \cdot m / \dot{\bar{\varepsilon}} \tag{4.8}$$

The derivatives of the Norton-Hoff and hyperbolic-sine equations are shown in Figure 4.6. The figure reveals that the temperature and the strain-rate affect the derivative of the flow stress in both equations. This indicates that the derivative of the flow stress with strain-rate is sensitive to the material.

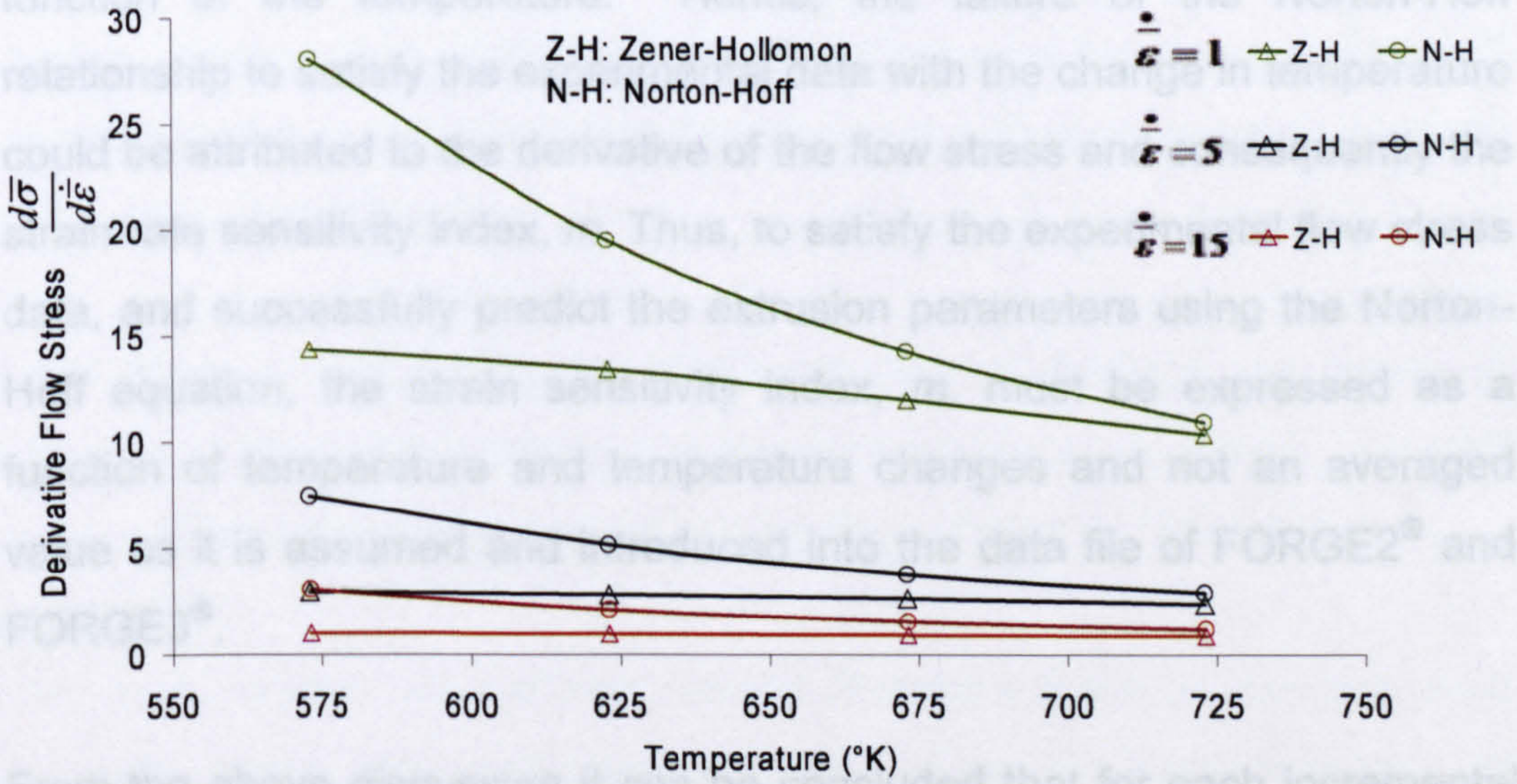

Figure 4.6: Comparison of the derivative of the flow stress vs. temperature for 4%Cu AA2014 at $\dot{\varepsilon}$ =1, $\dot{\varepsilon}$ =5 and $\dot{\varepsilon}$ =15. s^{-1} .

The two equations exhibited a more pronounced disparity when their derivatives were fitted over the same range of temperatures and strain-rates. The characteristic of the derivative of the hyperbolic-sine function in Figure 4.6 reveals small variations with the change in temperature. This variation becomes insignificant with the increase in strain-rate. These are expected since the expression $\tanh(\bar{\sigma}\alpha)$, in equation 4.7, carries the temperature term and changes very little with the temperature and is clearly reflected in derivative flow stress shown in Figure 4.6. However,

the derivative of Norton-Hoff flow stress showed a considerable variation over a range of temperatures and strain-rates, revealing that the relationship is not only affected by strain-rate, but, as expected, is also sensitive to the temperature changes. This behaviour is as anticipated, since equation 4.8 shows that the strain-rate sensitivity index significantly changes with the temperature and the strain-rate, making the relationship very much temperature and strain-rate sensitive which in fact, is not dissimilar to the sine equation. This clearly shows, that *m,* is in fact a function of the temperature. Hence, the failure of the Norton-Hoff relationship to satisfy the experimental data with the change in temperature could be attributed to the derivative of the flow stress and consequently the strain-rate sensitivity index, *m*. Thus, to satisfy the experimental flow stress data, and successfully predict the extrusion parameters using the Norton-Hoff equation, the strain sensitivity index, *m,* must be expressed as a function of temperature and temperature changes and not an averaged value as it is assumed and introduced into the data file of FORGE2® and FORGE3®.

From the above discussion it can be concluded that for each incremental finite interval the stress is updated by consideration of the derivative of the constitutive equation with respect to strain-rate and stress. It is difficult to quantify this adjustment precisely but, if different constitutive equations produce differing derivations, then this would affect the calculated parameters i.e. load, temperature, etc, hence Norton-Hoff and hyperbolic-sine equations. The most important characteristic of the sine relationship is that it could be easily checked through the activation energy which must be close to that of self-diffusion for aluminium alloys.

The hyperbolic-sine relationship was found to provide a better fit to the experimental results (i.e. maximum extrusion load see Figure 4.1) and the experimental flow stress with strain-rate and temperature than the Norton-

Hoff relationship. Therefore, the hyperbolic-sine relationship was adopted to describe the behaviour of the extrusion process in this thesis.

4.4 Load Displacement Diagram.

The pressure required for extrusion is a function of many variables. Lower extrusion temperatures require higher extrusion pressure and the opposite is true. Clearly, the parameter that determines whether the extrusion will succeed or fail to extrude is that the maximum pressure required must be within the press capacity.

Load-displacement curves for direct extrusion of AA2024 are shown in Figure 4.7. The stages preceeding the peak load (i.e. upsetting) and until the so called quasi-static stage is reached are shown in Figure 4.8.

The figure shows the different stages that take place in the deformed material during the extrusion process. The locations selected for examination in Figure 4.8 are shown in Figure 4.9 a to e in the form of a sequence of illustrations of the shear stress.

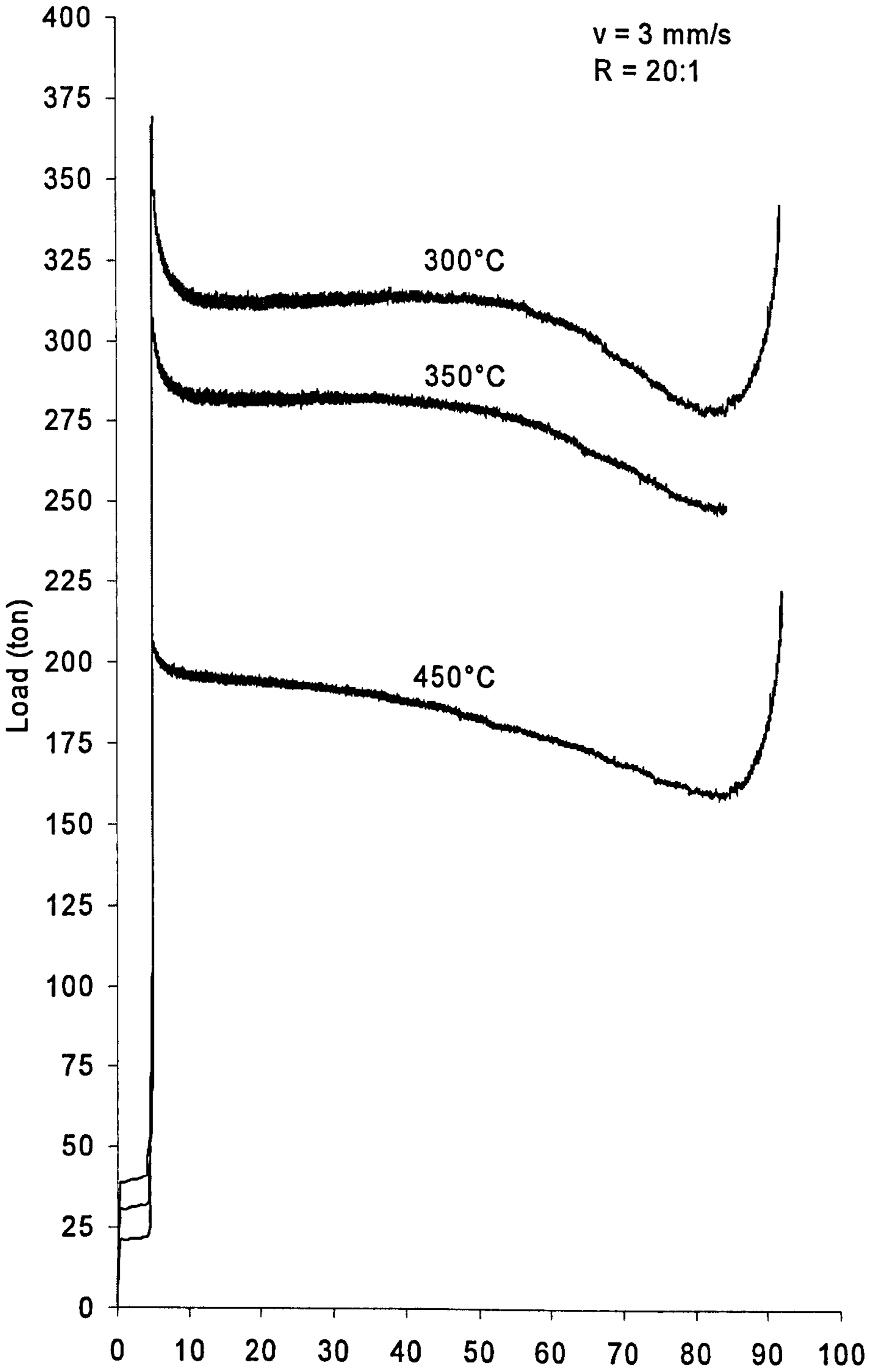

Figure 4.7: Ram load vs. ram displacement (AA2024)

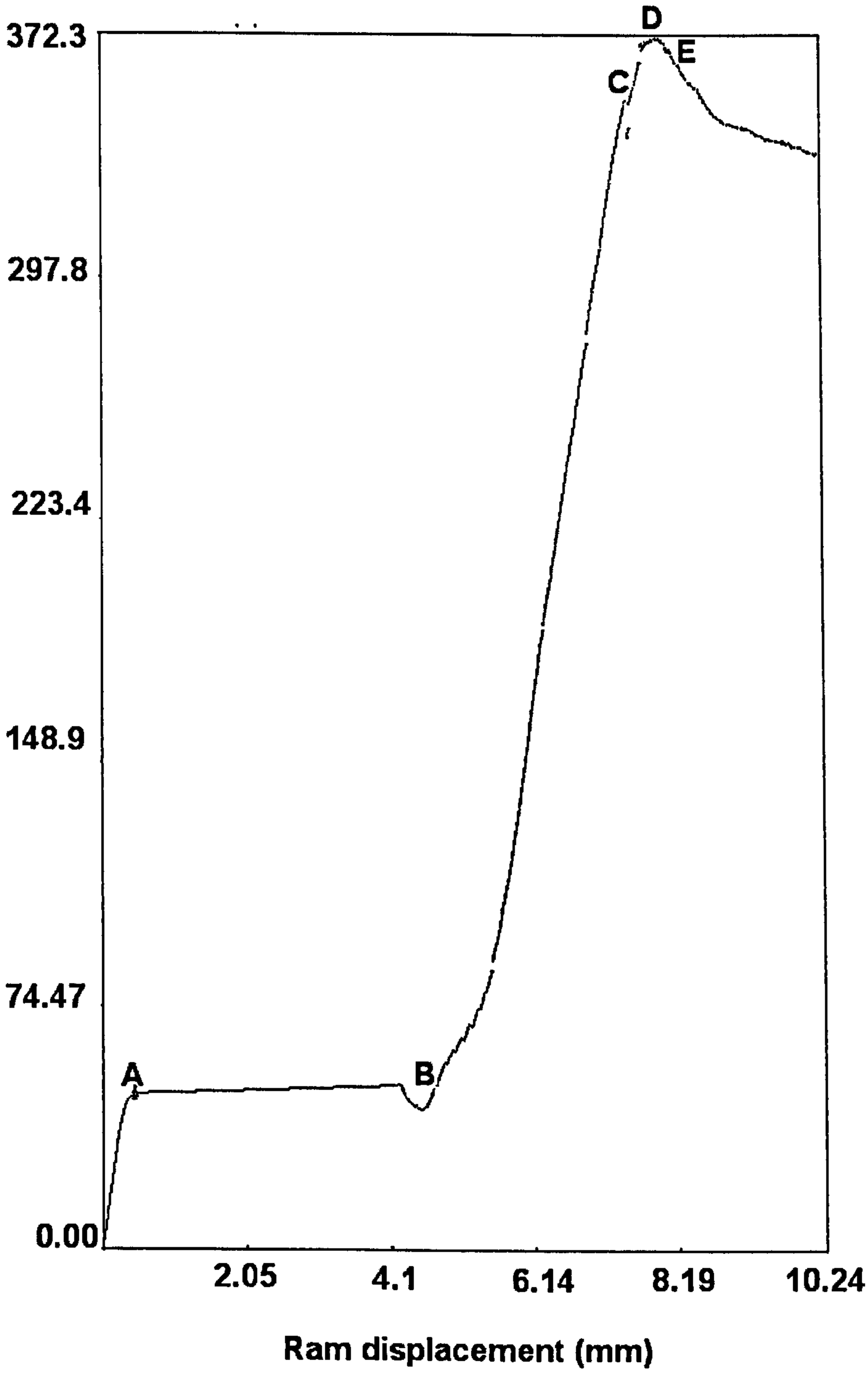

Figure 4.8: The stages preceeding the peak load and until the so-called quasi-static stage selected for examination in Figure 4.7.

Before extrusion can proceed, the billet must be inserted into the container and to facilitate entry there is generally appreciable clearance between the two. At this initial set-up, the only contact of the billet with the tools is at the die face. The necessary force needed to be applied to cause the billet to fill the clearance is affected predominantly by the nature of the material and the manner in which its properties are affected by the temperature i.e. material flow stress and the rate at which the work is carried out. The first effect of pressure at this stage is thus to compress or upset the billet into firm contact with the cylinder wall as shown in Figure 4.9a corresponding to position A in the load-displacement diagram in Figure 4.8. At this stage there are no significant differences in the deformation to the original billet except at the region adjacent to the die entry where some deformation may be detected. Deformation elsewhere in the billet is not apparent at this stage as indicated in Figure 4.9a. When the billet is further compressed into the container localised deformation at the container wall and die entry is observed as shown in Figure 4.9b. The stage B-C in Figure 4.8 is characterised by a rapid increase in pressure and an extension of the main deformation zone into the back of the billet may be observed. At this stage a very small amount of extrusion takes place (Location B-C) as illustrated in Figure 4.9c. At the commencement of the peak pressure region (C-D), a significant amount of extrudate material has already passed through the die land which agrees with the observations made by Sheppard and Tutcher [121]. However, the dead metal zone (DMZ) and main deformation zone are not fully established until the peak load reaches stage D in Figure 4.8 as shown in Figure 10 (DMZ formation). During this stage, the shearing of the billet at the container wall becomes apparent and a full deformation zone is established. The deformation zone is not stationary, the billet is deforming plastically while the shearing forces are operating which promotes the burnishing effect at the DMZ-billet interface necessary to obtain a satisfactory surface.

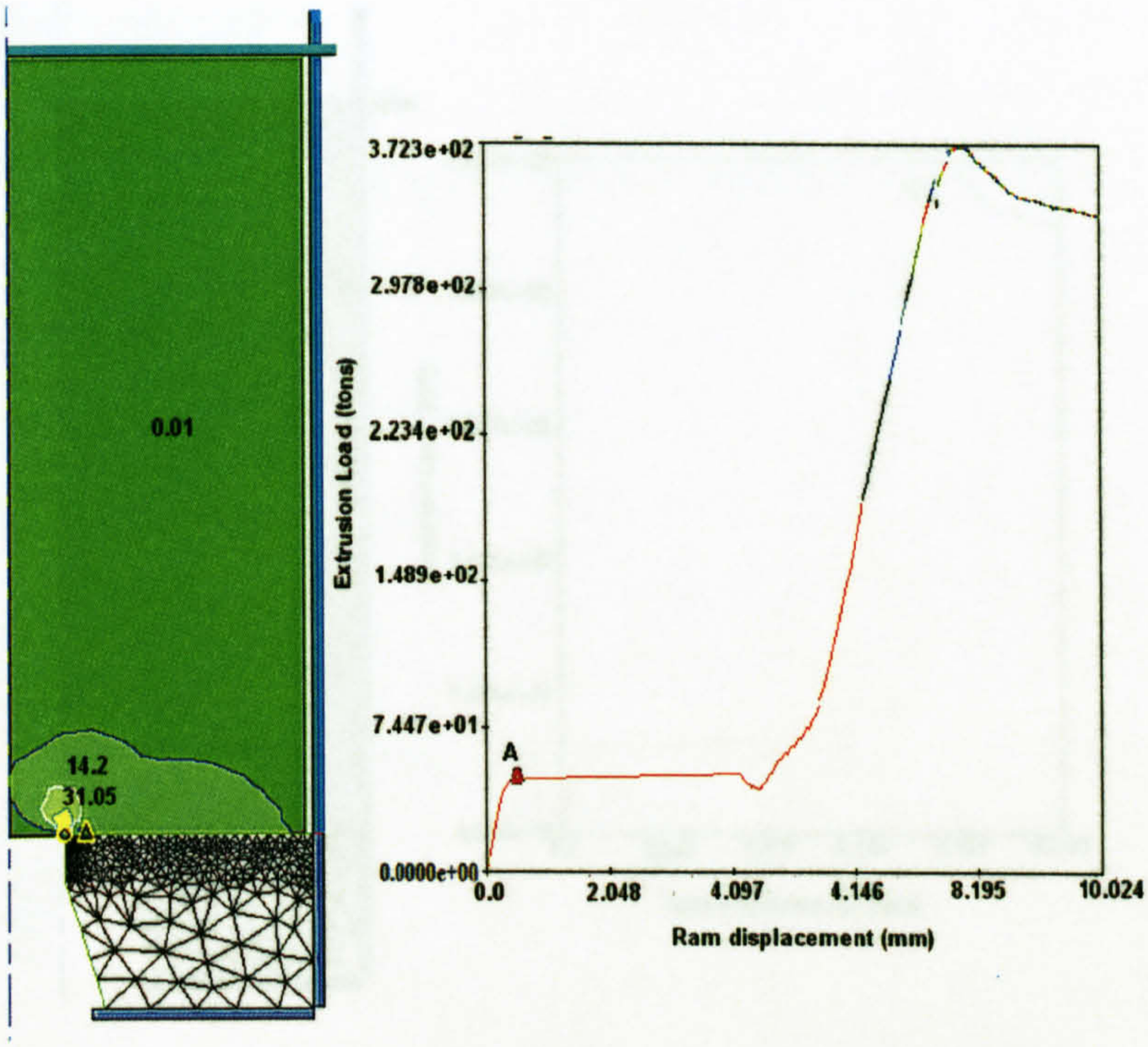

a): Location A in Figure 4.8 illustrated by the shear stress (MPa), showing deformation only at the die entry.

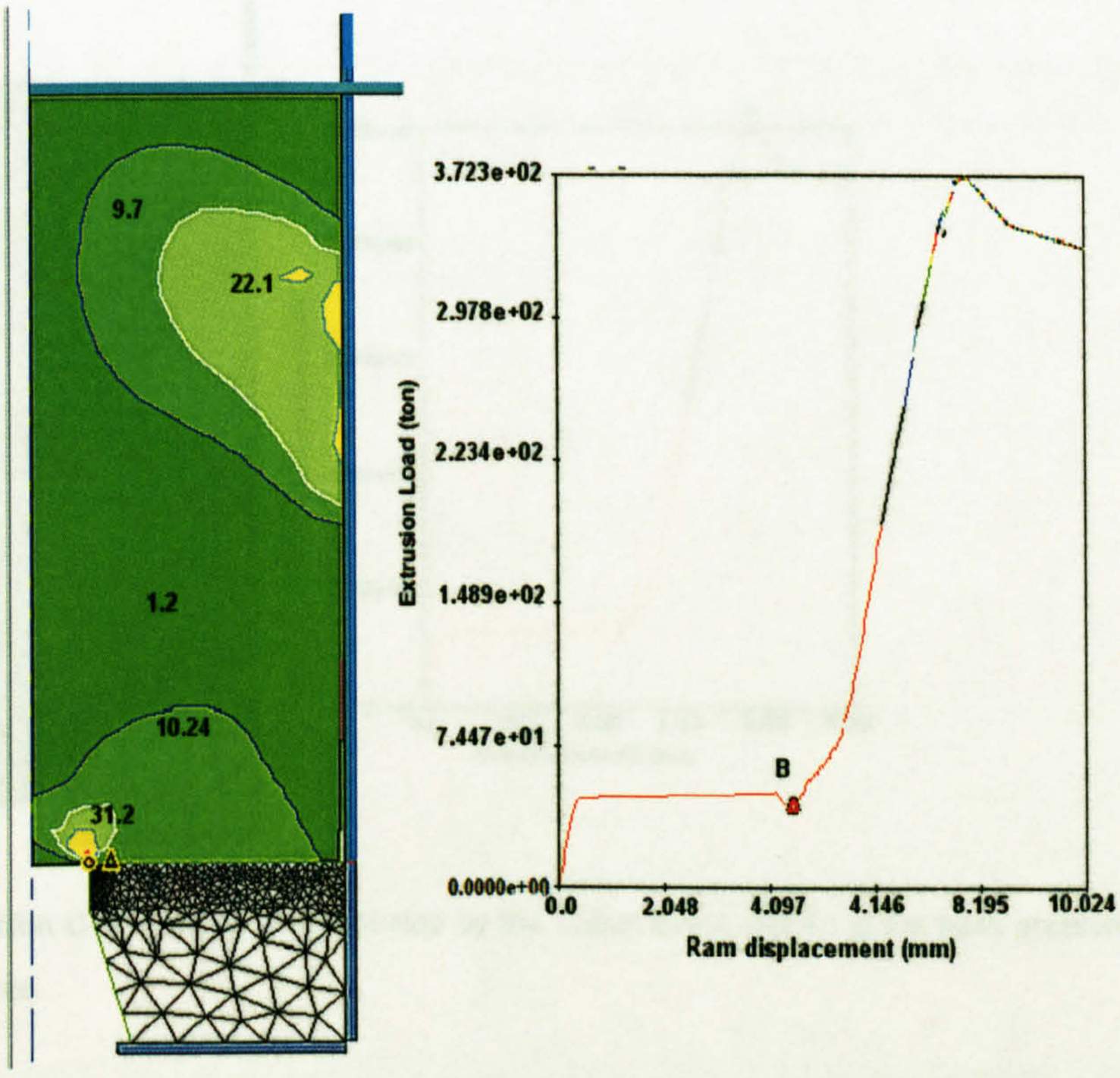

b): Location A-B in Figure 4.8 illustrated by the Shear Stress (MPa) when the billet is further compressed to fill the container, localised deformation at the die entry and the container

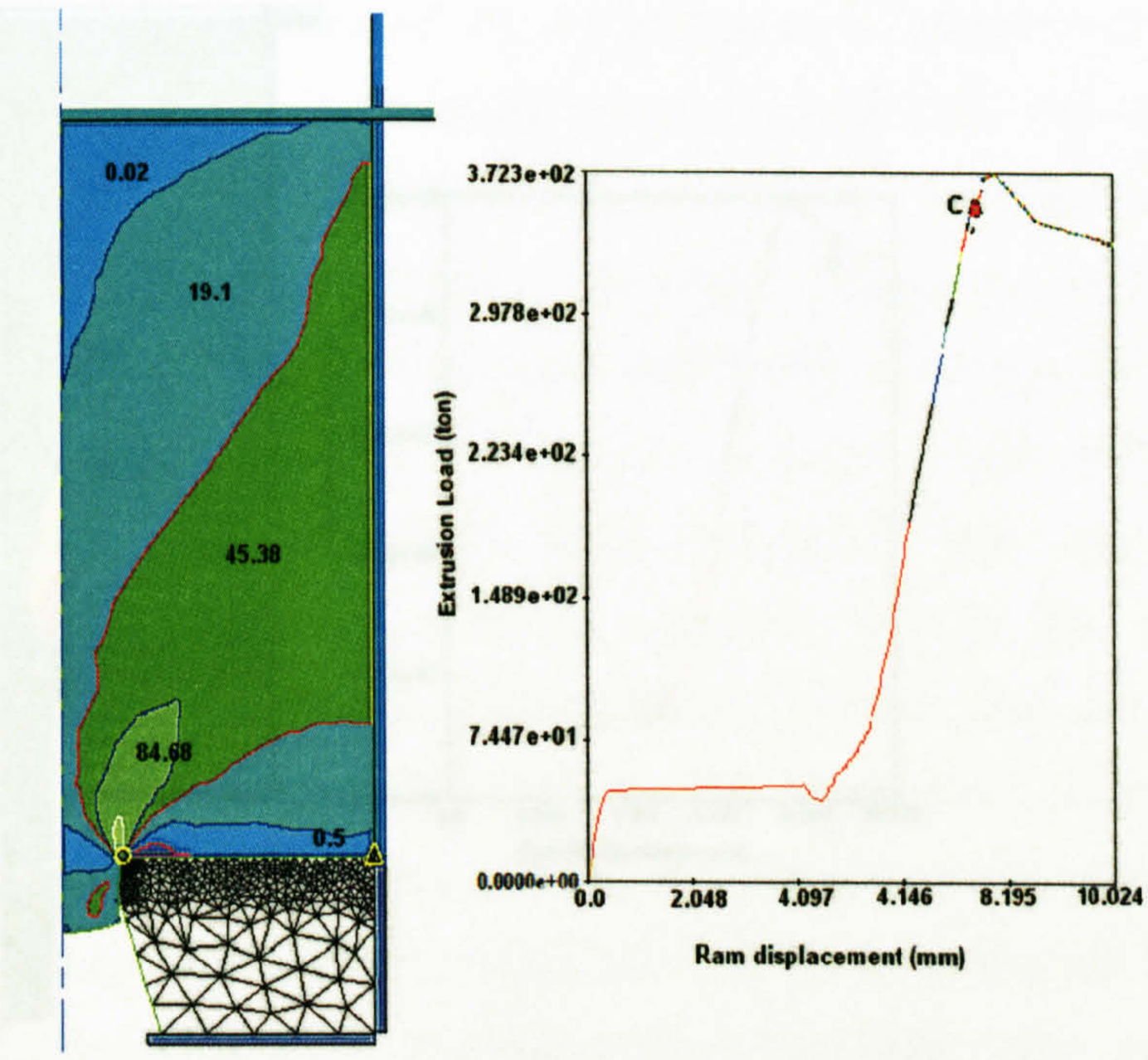

c): Location B-C in Figure 4.8 illustrated by the Shear Stress (MPa); showing extension of the deformation zone into the back of the billet

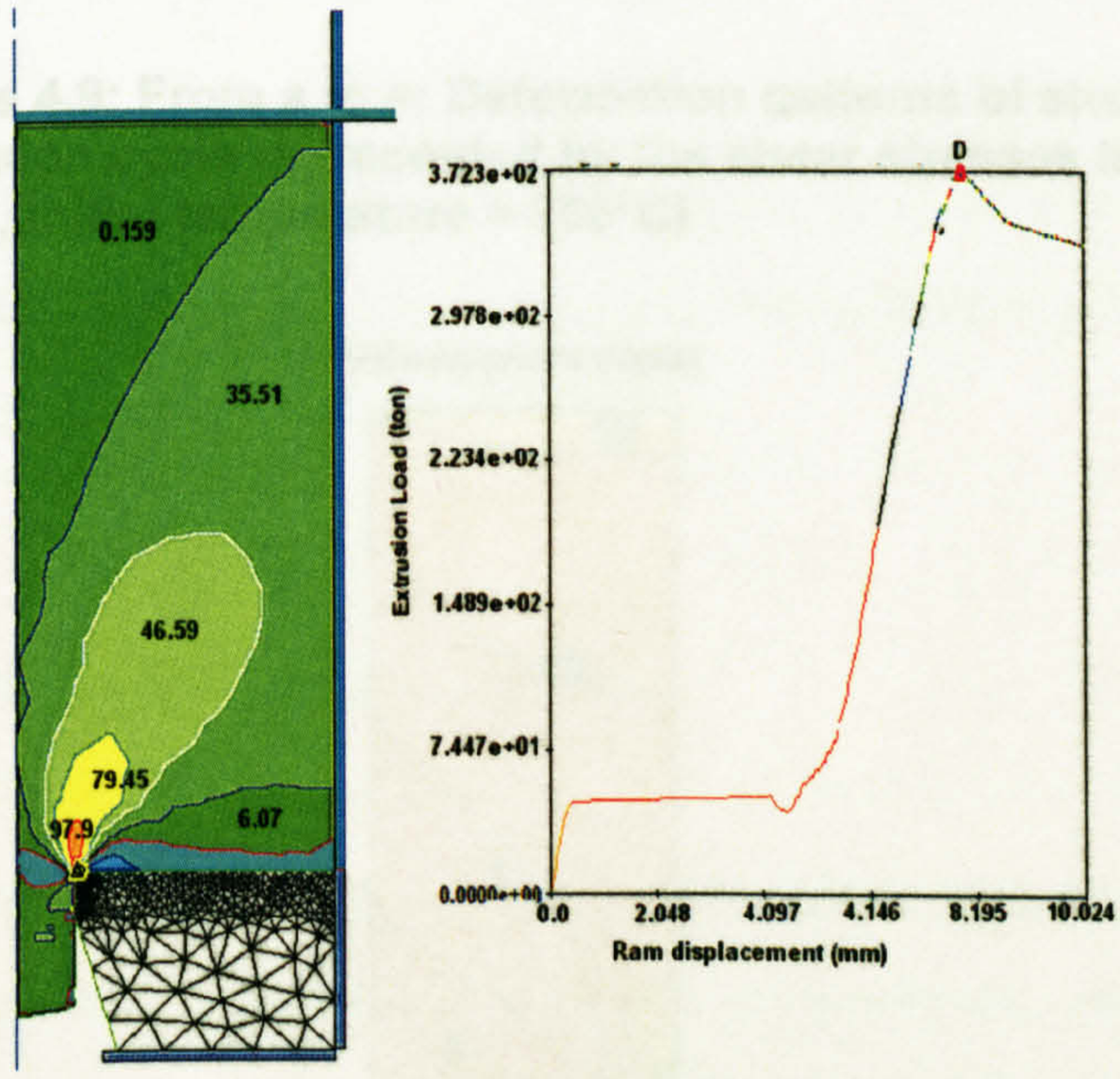

d): Location C-D in Figure 4.8 illustrated by the Shear Stress (MPa); at the peak pressure region. Extrusion commences

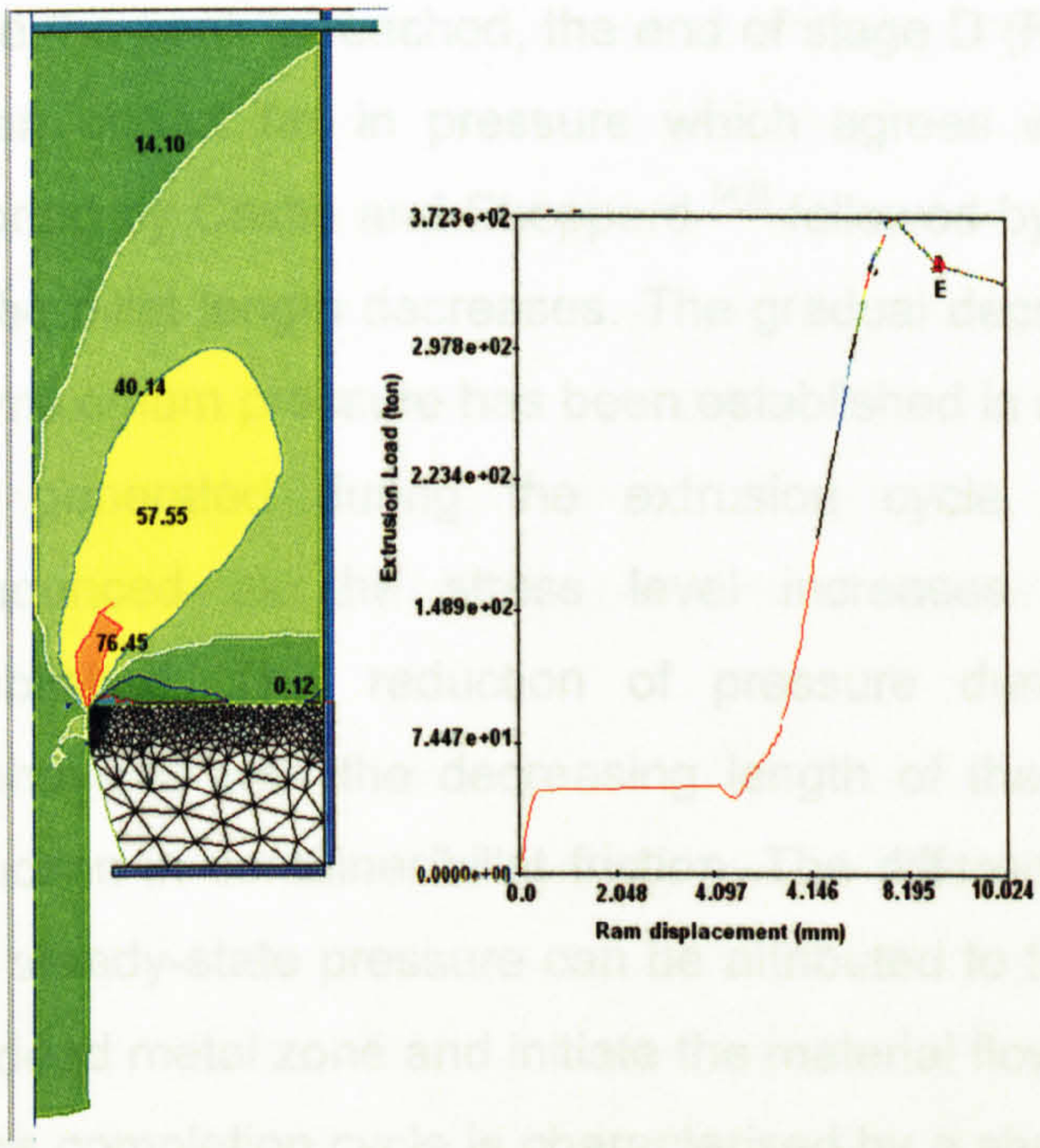

e): Location D-E in Figure 4.8 illustrated by the Shear Stress (MPa), the peak pressure region, the Deformation zone and the DMZ are fully established at the end of this stage.

Figure 4.9: From a to e: Deformation patterns of shear stress during an extrusion cycle represented by the shear stresses in Figure 4.8. (v = 3 mm/s, initial temperature = 300°C)

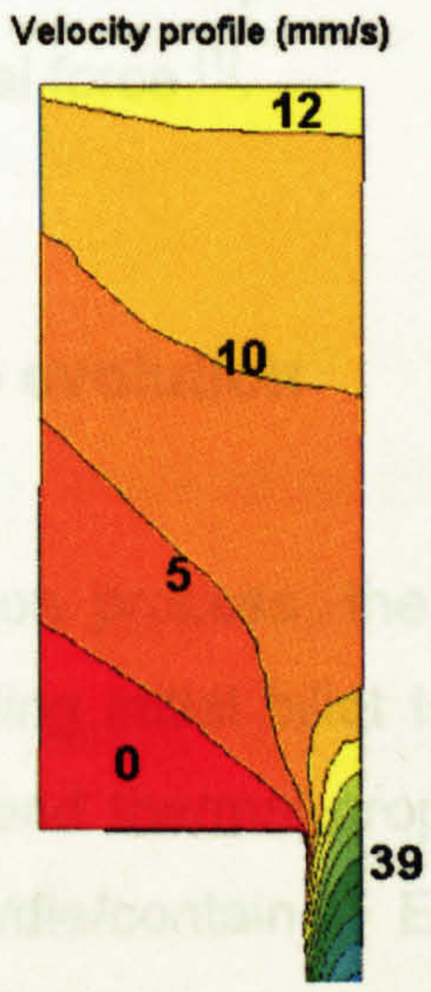

Figure 4.10: Velocity profile illustrating the formation of the DMZ after the peak pressure region.

Once the peak is reached, the end of stage D (Figure 4.8) is characterised by an abrupt fall in pressure which agrees with the observations first reported by Castle and Sheppard [42] followed by a more gradual decrease as the billet length decreases. The gradual decrease in the pressure after the maximum pressure has been established is caused by the temperature rise generated during the extrusion cycle. This decrease is more pronounced as the stress level increases and the steady-state is established. This reduction of pressure during this stage is further emphasised with the decreasing length of the billet and the associated reduction in container/billet friction. The difference between the maximum and steady-state pressure can be attributed to the force required to set up the dead metal zone and initiate the material flow through the die. The end of the completion cycle is characterised by a sharp increase in pressure as shown in Figure 4.7 resulting from the excess pressure required to affect radial flow in the extrusion discard.

The difference between the maximum and steady-state pressure (ΔP) can be attributed to the force required in moving the billet through the container against the frictional force [1].

4.5 Temperature evolution

During the extrusion process, the exit temperature is affected by many parameters, including initial billet temperature, extrusion speed, extrusion ratio, mechanical and thermal properties of the billet material and friction between the billet/die/container. Even the extrusion of simple rods is a complex process involving highly inhomogeneous deformation and high strain-rate. The heat generated by the plastic deformation and friction significantly affects the mechanical properties of the deforming material,

thereby increasing the temperature of the extrudate, and, in turn, affecting its microstructure and mechanical properties. The increase in temperature also affects the surface quality of the extrudate which is of prime importance in many industrial extrusion processes, and is as important as the mechanical properties. Because extrusion is a non-linear process involving high inhomogeneous deformation and high strain-rate, it is difficult to predict the exit temperature analytically.

It is recognised that during extrusion the deformation energy is converted into heat, thereby increasing the temperature of the extrudate and in turn affecting the microstructure and mechanical properties. The increase in temperature also affects the surface quality of the extrudate. The present investigation focuses on the evolution of the temperature in the billet during the extrusion cycle.

The temperature increase in the billet material during the extrusion cycle is the sum of the following components:

$$\Delta T = \Delta T_{def} + \Delta T_{fric} - \Delta T_{loss}$$

where ΔT_{def} is the temperature increase due to deformation, ΔT_{fric} is the temperature increase due to friction between billet/tools and ΔT_{loss} is the temperature loss during the deformation to the tooling and to the environment.

4.5.1 Model validation

The Temperature measurements of Grasmo's [37] model were conducted on AA6060 alloy by inserting eight thermocouples in which one was fitted very close to the die surface (thermocouple 7). The model has been used in this thesis in order to validate the predicted temperature readings from FORGE2®. The experimental details used are summarised in Table 4. 1.

Table 4. 1: Experimental details used in Grasmo's model.

Material	Billet Temp. (°C)	Cont Temp. (°C)	Die Temp (°C)	Ram Temp (°C)	Ram speed (mm/s)	Billet length (mm)	Diameter Billet-Extrudate(mm)
AA6060	473	450	445	50	5	302.5	97-15.8

The results of their temperature readings are shown in Figure 4.11. The figure shows the experimental and predicted temperature evolution at four different locations with ram travel. The experimental measurements are represented by thinner curves while the predicted measurements are illustrated by bolder curves. A similar model has been simulated and applied in FORGE2®. The predicted temperature results at thermocouple 7 are shown in Figure 4.12.

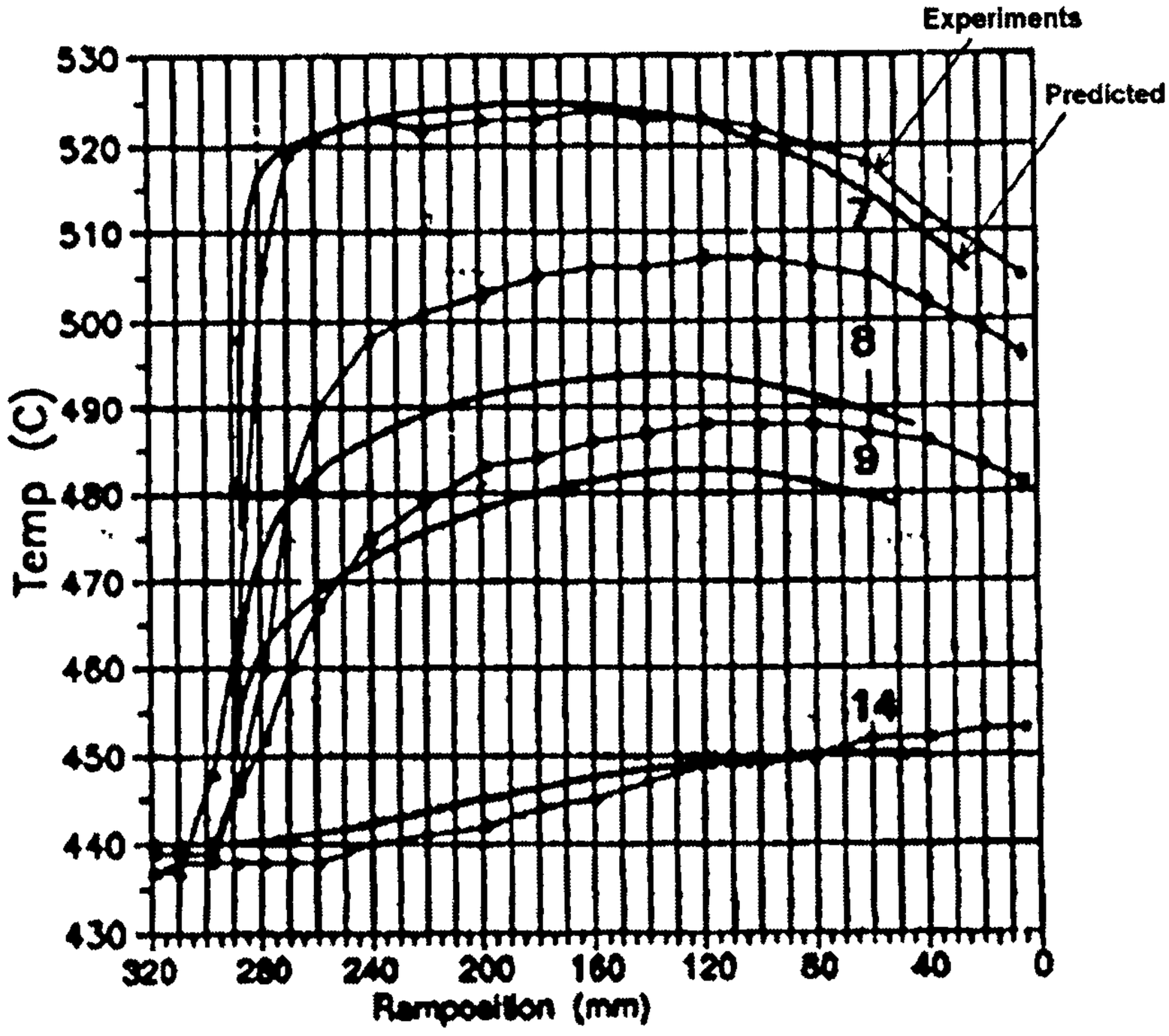

Figure 4.10: Temperature changes according to *Grasmo et al.* [37]

Figure 4.11: FORGE2 temperature prediction vs. Grasmo's experimental measurements at thermocouple 7.

A close agreement was found between the experimental and simulation results. However, small but acceptable deviations from the experimental results can be seen. This small variation between the measured and calculated temperature may be caused by the die bearing length used in the experimental model which appears to have a zero bearing length. This is practically impossible and we must assume that some small land length existed. It is still not desirable to use such a die using the FEA technique to simulate a process such as extrusion, especially, if Lagrangian techniques for meshing and remeshing are adopted in the software logarithm i.e. FORGE2®. To overcome this problem, the model simulation conducted in this investigation has a 1.5 mm bearing length with a 0.5 mm radius at the re-entrant corner. This should have no effect on the predicted temperature evolution. However Grasmo did explain that there may have been some uncertainty in the placement of the thermocouple and of the die and container properties. Nevertheless the agreement between the simulation and the experimental results was satisfactory and demonstrates that the FORGE2® software can predict the temperature changes during the extrusion cycle.

It is appropriate at this point to draw attention to some of the limitations of the simulation in the present model apart from the die bearing length. The major limitation was the amount of computing time necessary for simulation of the model. It required more than 10 days (251 h) on a dual processor (1.7 MHz) workstation to extrude 1/3 of the billet length. A vast number of elements were generated during meshing and re-meshing of the billet and the formation of the extrudate. This of course will have a great effect on the number of equations to be solved and the time to solve them, since small time steps of 0.005 were used during the simulation for accuracy. Consequently, the simulation was stopped just after 1/3 of the billet was extruded and enough data were available for discussion. One can safely conclude that a close agreement between the experimental and

simulation results was found. However, small deviations from the experimental results can be seen.

4.5.2 Temperature evolution during extrusion

The simulation models used for this investigation are similar to the models used to investigate pressure-displacement diagram in Figure 4.8 (AA2024, R=20:1 and v= 3mm/s).

The temperature evolution during a complete extrusion cycle is shown in Figure 4.13. It is worth noting that the figure shows the maximum temperature recorded during the simulation. The starting temperatures shown in the Y-Axis coincided with the initial billet temperatures. Obviously these temperatures were recorded at time t = 0, as maximum temperatures. This would not affect the overall temperature evolution with ram travel except of course at the upsetting stage.

The extrusion pressure is significantly influenced by the temperature gradients produced in the billet after upsetting in the container. Therefore it will be more useful to investigate the temperature evolution during the extrusion process in a similar manner to the pressure-displacement curve.

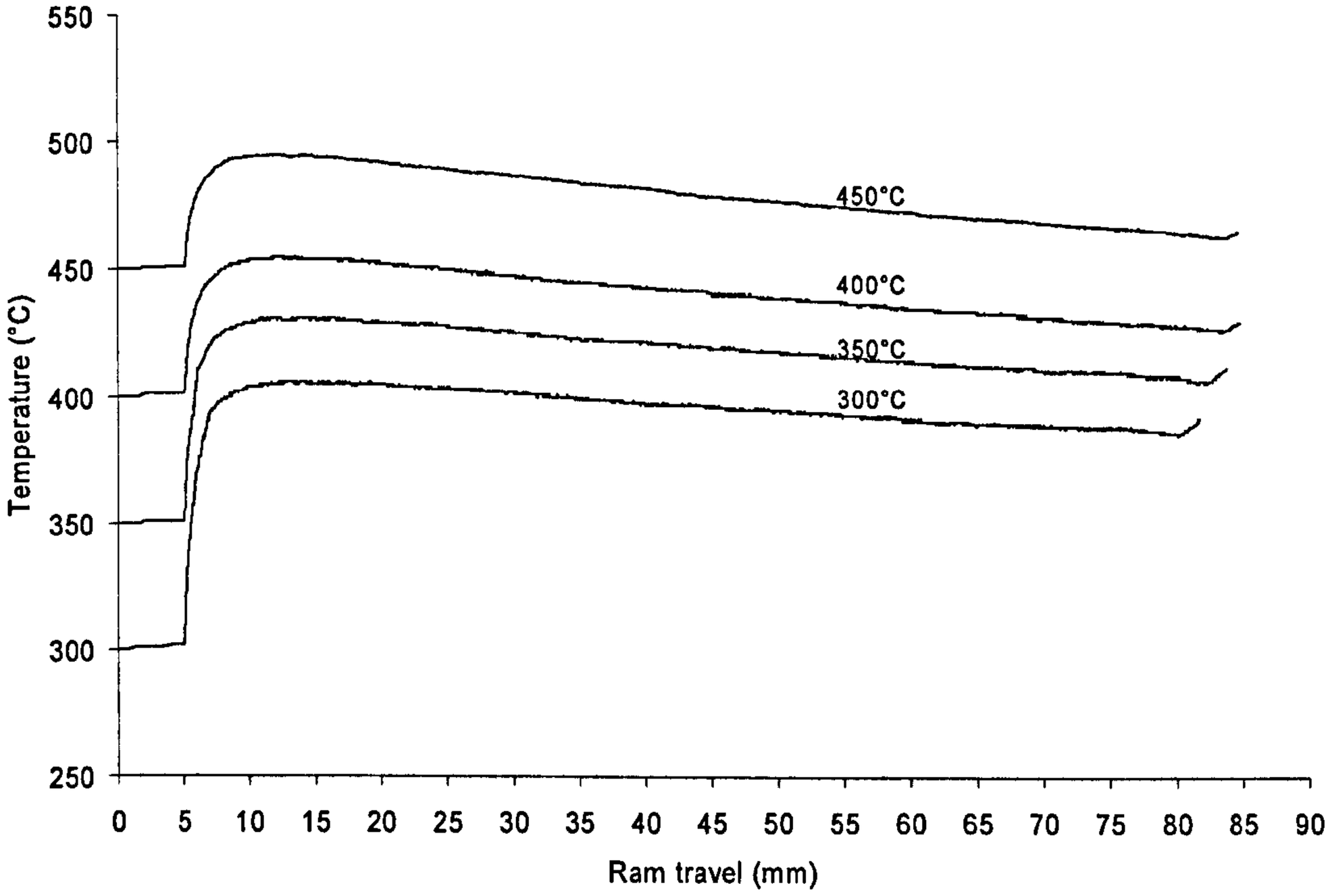

Figure 4.12: Temperature evolution cycle during the extrusion of AA2024 alloy, R20:1 and 3mm/s speed.

The temperature evolution in the billet (initial temperature 300°C) as the extrusion proceeds from the start and until quasi-static steady-state is shown in Figure 4.14. Heat transfer will occur as soon as the billet contacts the tools. As the billet is upset to fill the container, a small loss of temperature from the billet surface to the die face and the container wall is encountered as shown in Figure 4.14a. This stage corresponds to the end of stage A in Figure 4.8 when the billet is fully compressed into the container. Obviously the maximum temperature remained equal to the initial billet temperature and is located at the centre of the billet since no deformation is apparent elsewhere at this stage. It is interesting to note that following the events occurring shown in the pressure displacement diagram in Figure 4.8 at location B when extrusion commences, the tooling continues to act as a heat sink to the billet surface and in particular at the

die front as shown in Figure 4.14b. However, as the figure also illustrates, a small increase in the billet temperature is observed at the die entrance at this stage. This rapid increase in temperature continues throughout the peak pressure region and subsequently as shown in Figure 4.14c at the peak pressure and Figure 4.14d at the end of peak pressure region. This increase in the billet temperature is the consequence of the production of heat by deformation of the billet to breakthrough the die orifice proceeding to the front of the die in the deformation zone. Accordingly heat is conducted from the deformation zone toward the rear of the billet and results in an increase in overall temperature. The steady-state-region is characterised by a slow increase in temperature as shown in Figure 4.14e. This is as a result of less heat being generated from the mechanical work done due to the thermally softened billet and the decrease in billet length.

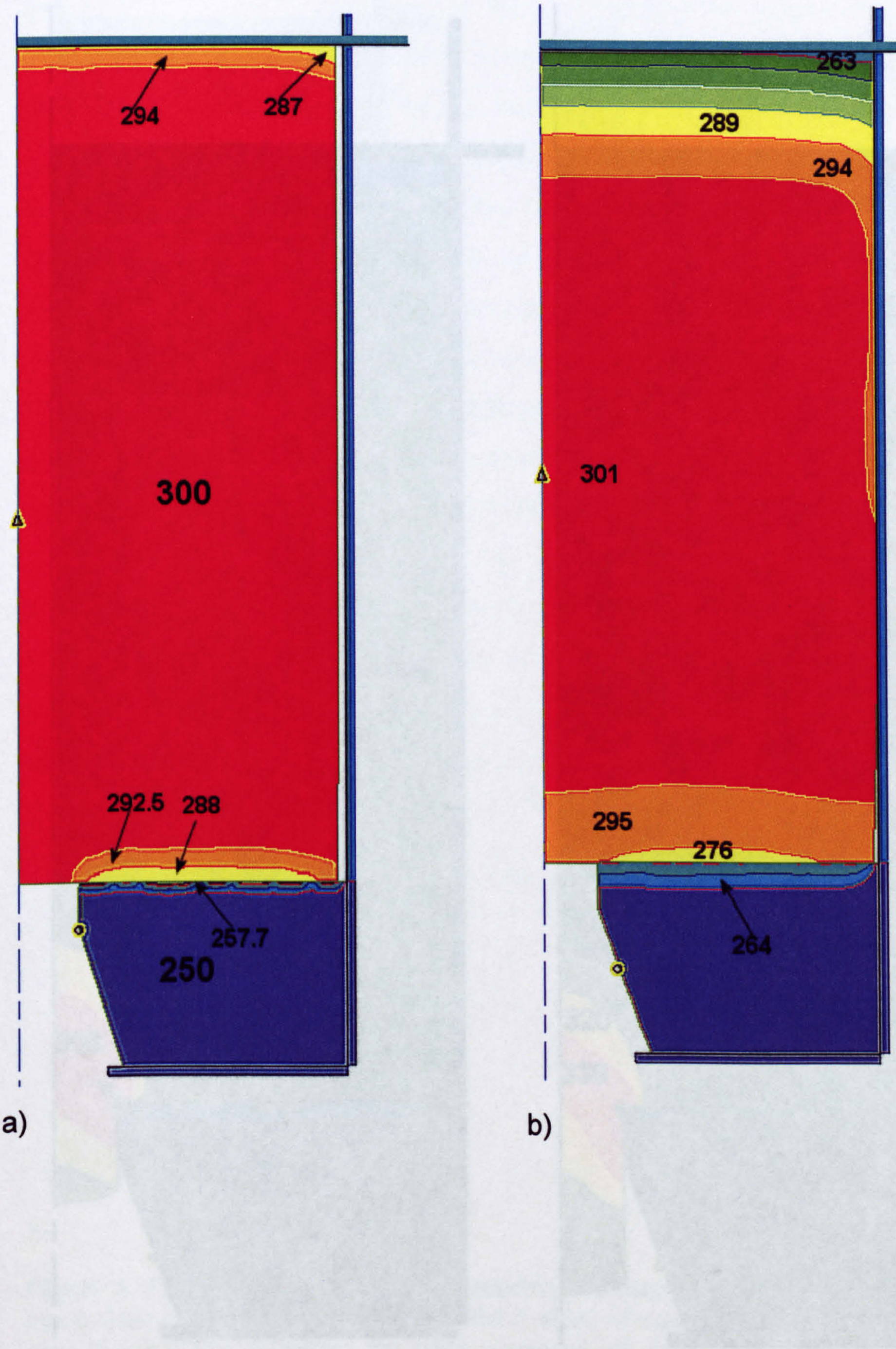

a) b)

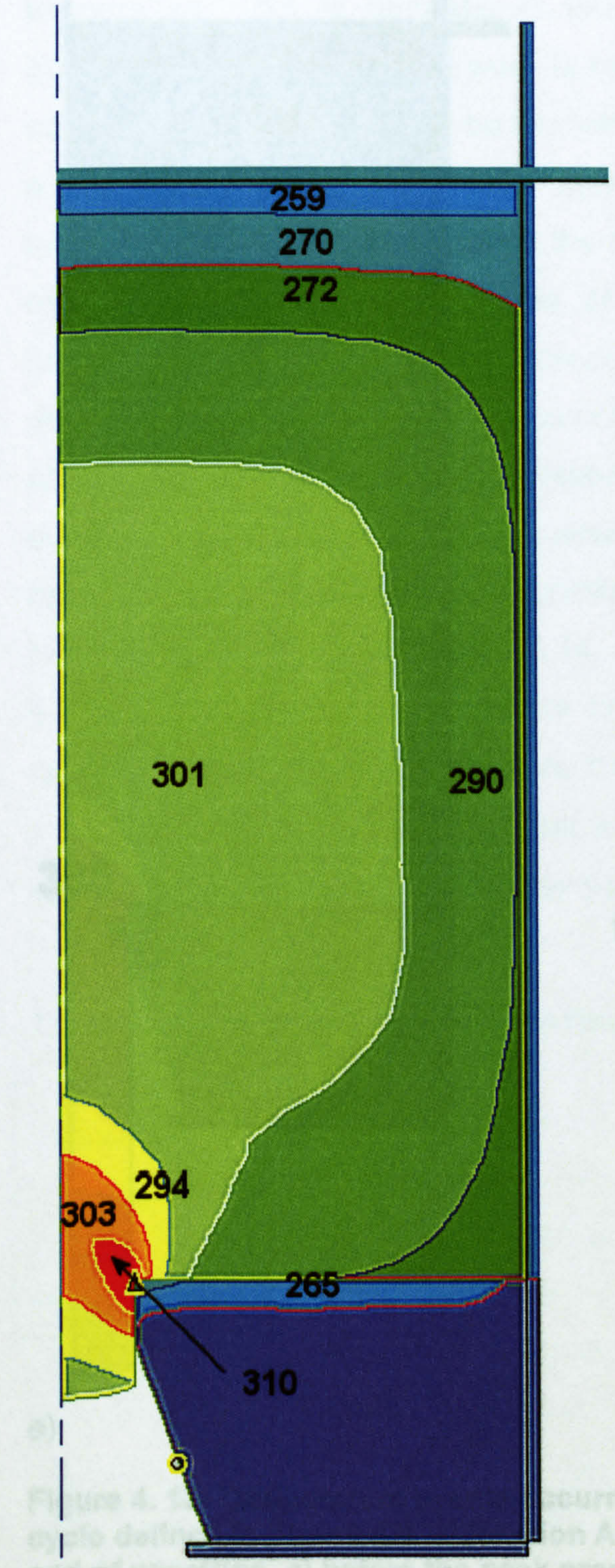
259
270
272
301
290
294
303
265
310

c)

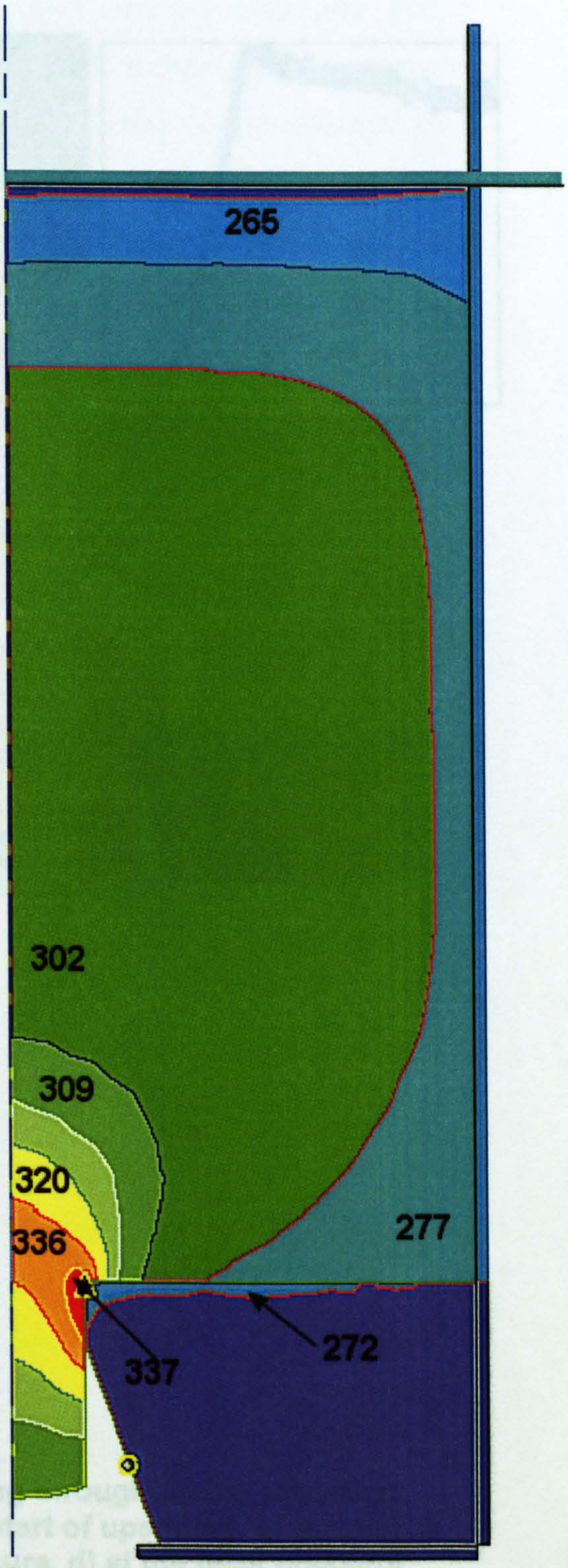
265
302
309
320
336
277
272
337

d)

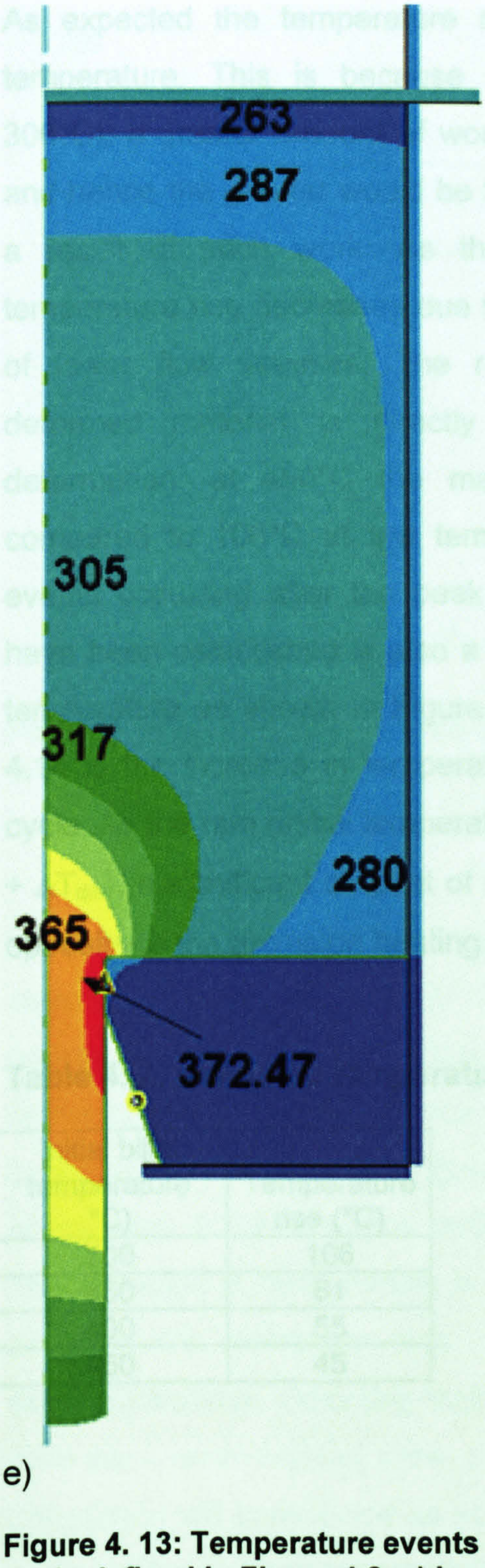

e)

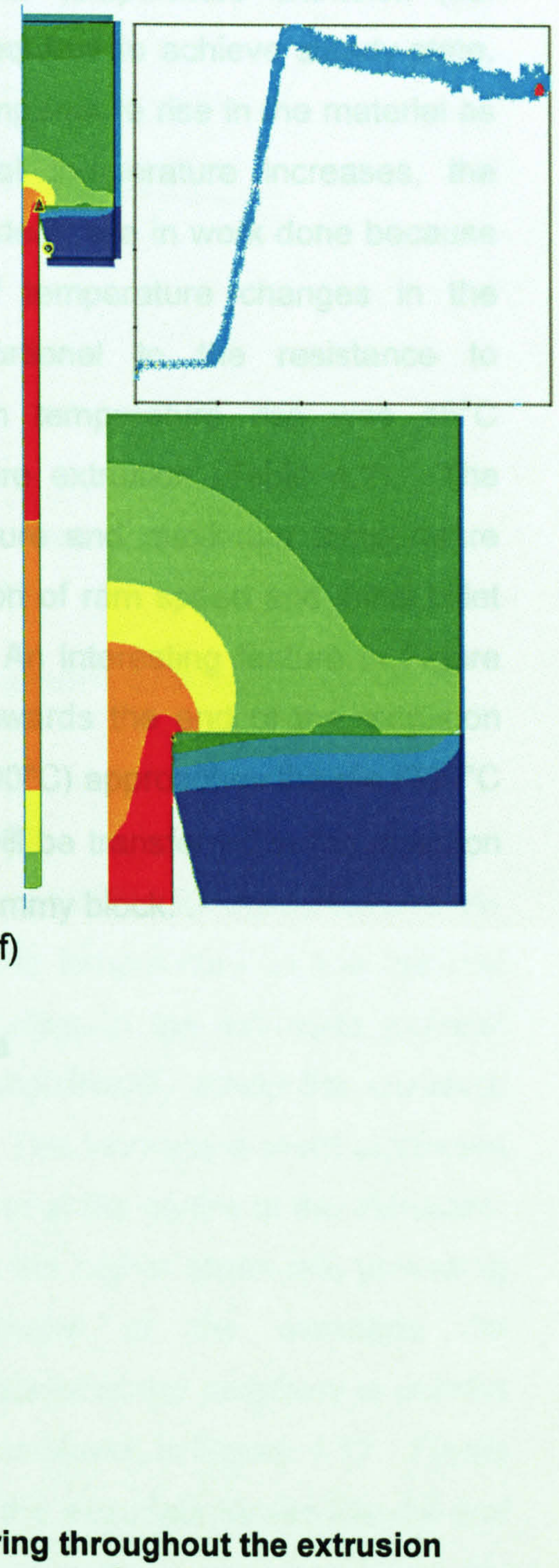

f)

Figure 4. 13: Temperature events occurring throughout the extrusion cycle defined in Figure 4.8. a) location A start of upsetting, b) location B end of upsetting, c) before the peak pressure, d) at the peak pressure and e) quasi-static deformation. Initial billet temperature 300°C.

As expected the temperature rise is significant at low initial billet temperature. This is because at lower temperature extrusion (i.e. 300°C), a greater amount of work is required to achieve steady-state, and hence the greater would be the temperature rise in the material as a result of such work. As the initial temperature increases, the temperature rise decreases due to the decrease in work done because of lower flow stresses. The rate of temperature changes in the deformed material is directly proportional to the resistance to deformation; at 450°C the maximum temperature rise was 45°C compared to 106°C at low temperature extrusion (Table 4.2). The events occurring after the peak pressure and maximum temperature have been established is also a function of ram speed and initial billet temperature as shown in Figure 4.14. An interesting feature in Figure 4.14 is the increase in temperature towards the end of the extrusion cycle. As the ram (initial temperature 200°C) approaches the die (300°C + ΔT_{die}), a significant amount of heat will be transferred in the direction opposite to the extrusion heating the dummy block. .

Table 4. 2: predicted temperature rise

Initial billet temperature °C)	Temperature rise (°C)
300	106
350	81
400	55
450	45

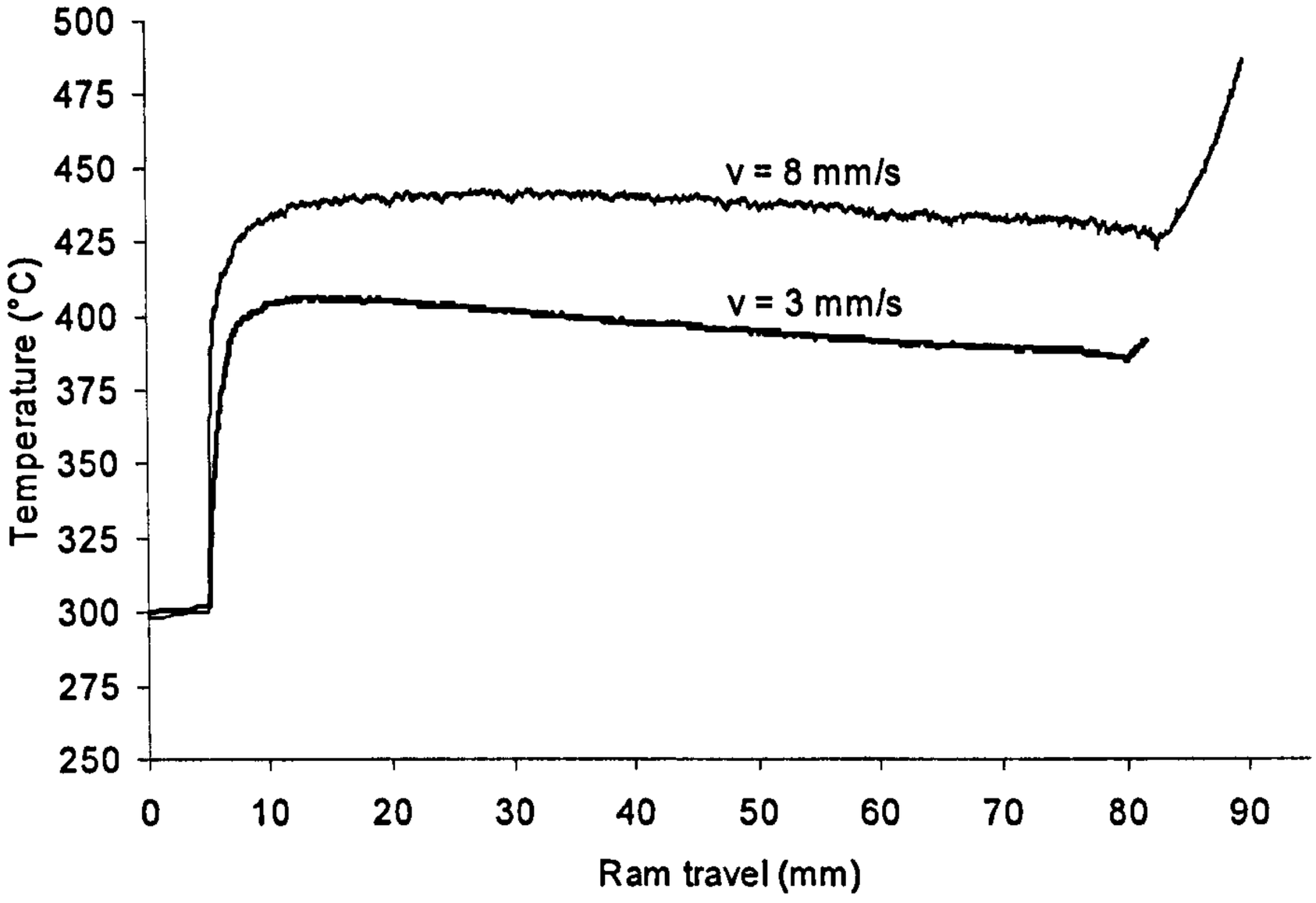

Figure 4.14: Effect of ram speed on temperature evolution during the process.

Much of the heat generation occurs at the DMZ/deformation zone shear region and results in a steep rise in the temperature as the material approaches the die land. The temperature in the extrudate material emerging through the die orifice varies significantly across the extrudate cross-section, as shown in Figure 4.16. This increase is more significant at the edge of the extrudate surface than at the centre of the extrudate. This increase in temperature is due to the higher strain-rate prevailing at the die entrance and the friction at the extrudate die bearing/interface, indicating that the material at the periphery is derived from the heavily-worked shear zones, as shown in Figure 4.17. Finally convection will commence as soon as the extrudate leaves the die and contacts the ambient temperatures.

Throughout the region A-D in Figure 4.8, at 0.5 mm from the interface, the surface temperature at the billet/container interface remained lower than the initial billet temperature (350°C) as shown in Figure 4.17 with a slow increase as the billet is further upset from A-D. Furthermore, it was

not until the steady-state region that a significant increase was observed at the billet/surface-interface which indicates that heat generated by deformation contributes significantly more towards the overall temperature increase than the heat generated at the interface.

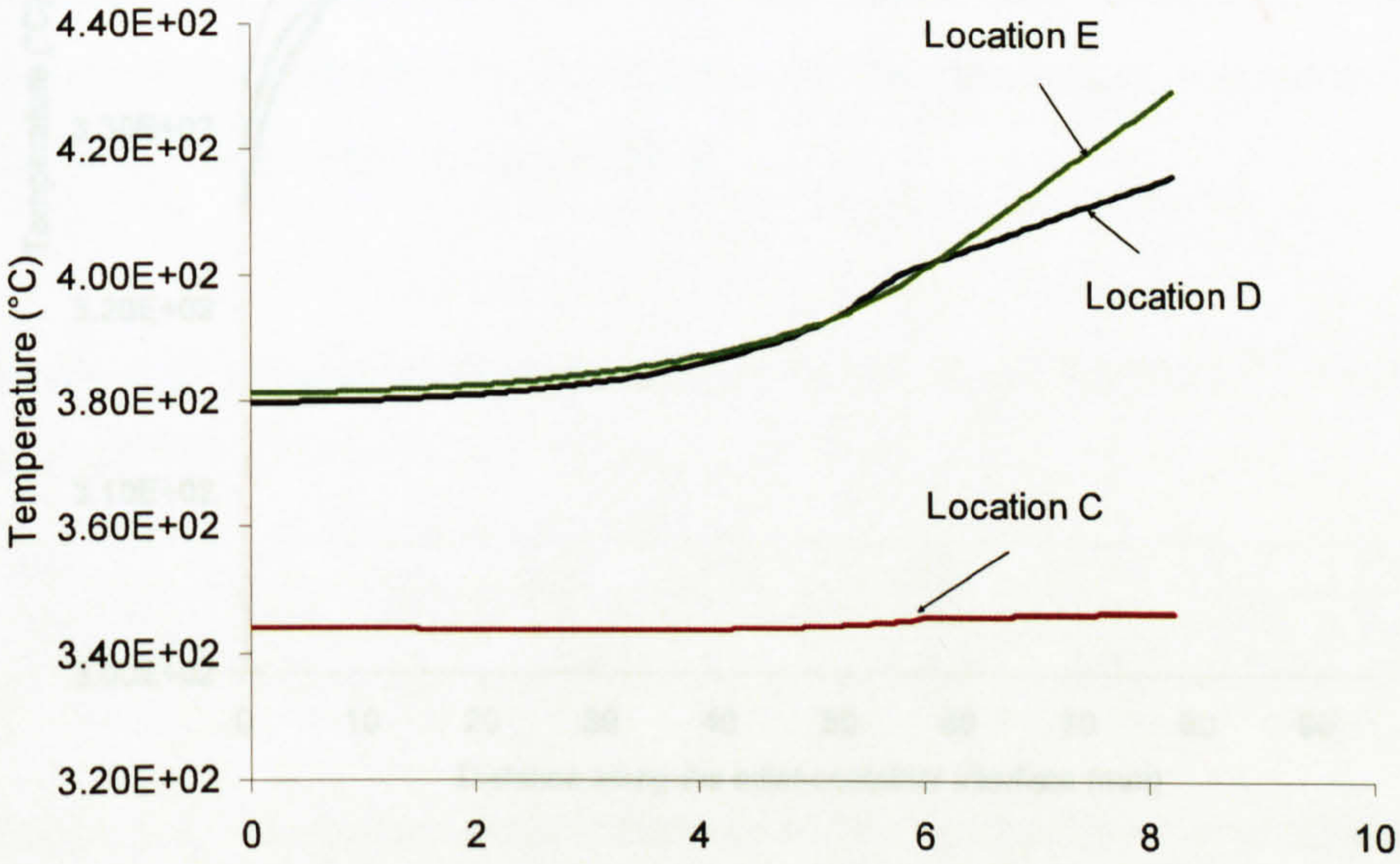

Figure 4.15: Temperature evolution across the extrudate cross-section shown at the location between C and D regions in Figure 4.8.

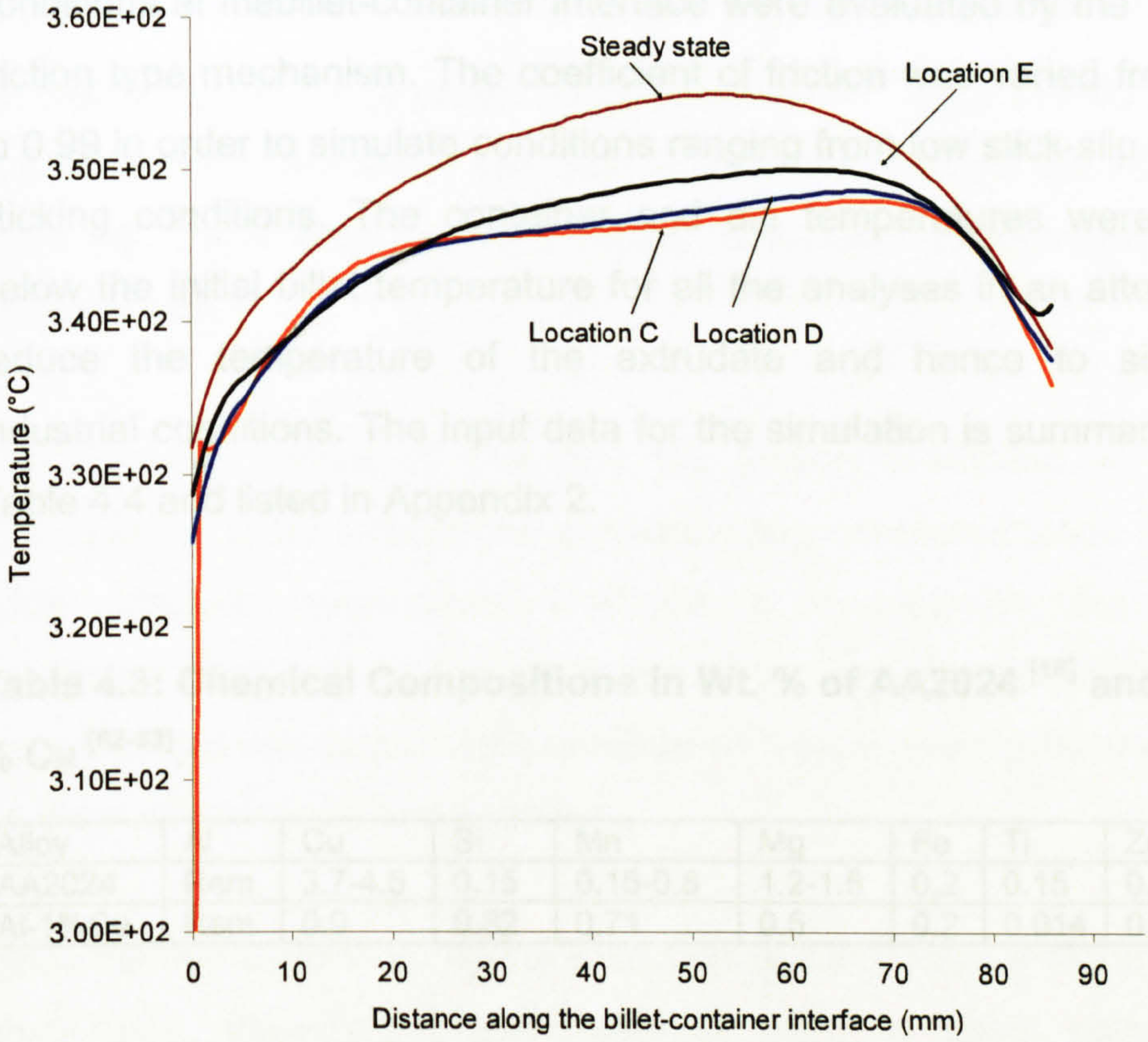

Figure 4.16: Billet surface temperature at 0.5 mm from the interface container wall shown at the location between C and D regions in Figure 4.8 and until the steady state is reached.

4.6 Friction in extrusion process

4.6.1 Process conditions

The chemical compositions of the alloys used in this investigation are shown in Table 4.3 and listed in Appendix 3. All the experimental data are extracted from the literature [62-63]. Constant ram speed of v = 3 and 8 mm/s were imposed with an extrusion ratio of 30:1 for AA2024 and Al-1%Cu respectively. In the FORGE 2 program, only half of the cross-section requires modelling due to the symmetry. A flat-faced die with a

5-mm die bearing length was used for all simulations. The boundary conditions at thebillet-container interface were evaluated by the Tresca friction type mechanism. The coefficient of friction was varied from 0.5 to 0.99 in order to simulate conditions ranging from low stick-slip to fully sticking conditions. The container and die temperatures were 50°C below the initial billet temperature for all the analyses in an attempt to reduce the temperature of the extrudate and hence to simulate industrial conditions. The input data for the simulation is summarised in Table 4.4 and listed in Appendix 2.

Table 4.3: Chemical Compositions in Wt. % of AA2024 [16] and Al-1-% Cu [62-63].

Alloy	Al	Cu	Si	Mn	Mg	Fe	Ti	Zn
AA2024	Rem	3.7-4.5	0.15	0.15-0.8	1.2-1.5	0.2	0.15	0.25
Al-1%Cu	Rem	0.9	0.82	0.71	0.5	0.2	0.014	0.02

Table 4.4: Rheology Data input used for Computer Simulation [62-63]

Alloy	Flow Stress Data				T (°C)
	α	n	ΔH	Ln(A)	
AA2024	0.016	4.25	148880	19.6	300-350-400-450
Al-1%Cu	0.0167	5.65	147950	26.7	300-450

4.6.2 Method of identifying the friction factor

The extrusion process requires large compressive loads and involves a minimal displacement when first upsetting the ram to fill the container. The simulation output ensures that given the correct data, the FEM is able to predict the real material behaviour which is determined in such a way that conditions are identical to those encountered in industrial practice.

The basic experimental principle of the extrusion process consists of applying a velocity v to a billet heated at an initial temperature $T°$ while recording the values of experimental pressure P^{ex} as a function of the displacement of the ram. The data is obtained from the experimental pressure displacement trace curves obtained for different initial temperatures.

The method consists of changing the friction coefficient $\overline{m}$ in the simulation in order to build the corresponding computed loads (P^{C}) for each extrusion temperature. The goal is to determine the friction coefficient which allows the prediction of the experimental data when the computed results are close or agree with experiment measurements for a specific material and conditions.

Since various factors during the extrusion process require experimental procedures, there are many points at which a direct comparison between the experimental work and its analytical counterpart can be compared and the accuracy of the output assessed. To investigate in greater detail the friction phenomena during the extrusion cycle, two locations of interest were selected for examination and are shown in Figure 4.18. The first location identifies the friction at the start of the extrusion after the peak pressure has been established and the second location where the pressure is influenced to a greater extent by the associated temperature rise.

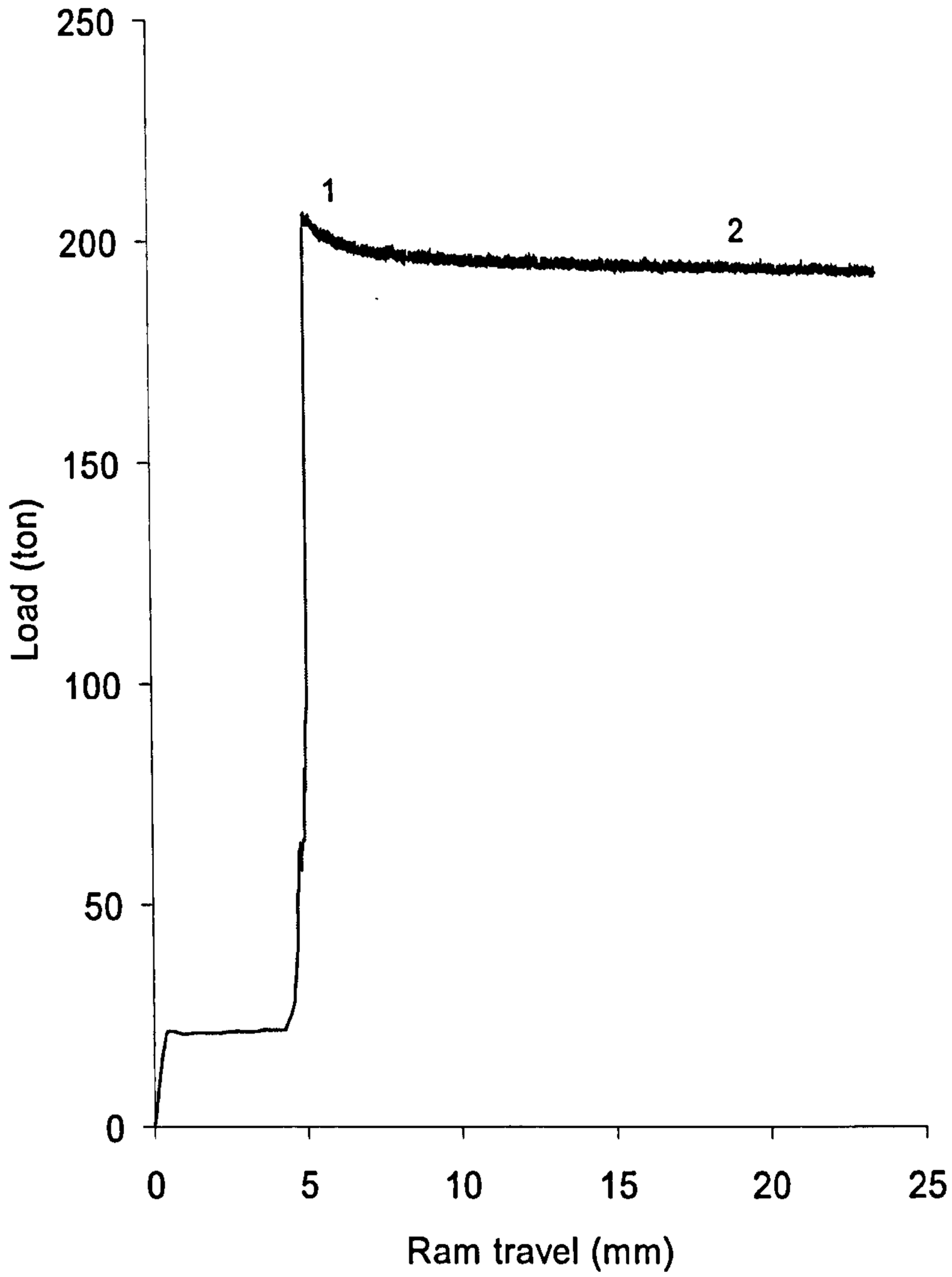

Figure 4.17: Locations where friction is examined.

4.6.3 Computation of the Zener-Hollomon parameter Z and the Strain-rate

In finite element modelling, two approaches are used to calculate the history of the temperature-compensated strain-rate parameter (Z) during deformation. The first is simply substituting the nodal strain-rate and nodal temperature into equation (4.1) to calculate the history of (Z). The Zener-Hollomon parameter calculated by this way is termed "instantaneous Zener-Hollomon parameter" and is calculated either by:

increment of time:

$$(\overline{Z}_{ins})_t = \frac{\sum \overline{Z}_{ins} \Delta t}{t} \tag{4.8}$$

or by increment of strain

$$(\overline{Z}_{ins})_\varepsilon = \frac{\sum \overline{Z}_{ins} \Delta \varepsilon}{\overline{\varepsilon}} \tag{4.9}$$

where Δt and $\Delta \varepsilon$ are time and strain increments respectively, t is the deformation time, $\overline{\varepsilon}$ is the final equivalent strain.

The second method is using the averaged strain-rate and nodal temperature to derive the value of (Z). The averaged strain-rate is obtained by averaging strain-rate over the whole deformation zone in each increment during finite element computation. This mean value of (Z) can be obtained by averaging the history of (Z) on the basis of time or strain. The (Z) calculated in this way is termed "averaged Zener-Hollomon parameter", represented by Z_{ave} and is given by:

$$(\overline{Z}_{ave})_t = \frac{\sum \overline{Z}_{ave} \Delta t}{t} \tag{4.10}$$

$$(\overline{Z}_{ave})_\varepsilon = \frac{\sum \overline{Z}_{ave} \Delta \varepsilon}{\overline{\varepsilon}} \tag{4.11}$$

However, the strain-rate varies from point to point throughout the deformation zone during the extrusion process and varies from the rear of the billet to the die mouth. Therefore, the modelling of temperature-

compensated strain-rate to describe the changes in friction or in structure during deformation should be used with the mean equivalent strain-rate. Thus, the mean equivalent strain-rate used in this investigation is calculated from an average area (A) over the deformation zone where the maximum deformation is expected to occur as illustrated in Figure 4.19. Adopting such an average (Z), is practical because the strain-rate in equation (4.1) is also a mean value over the whole deformation zone.

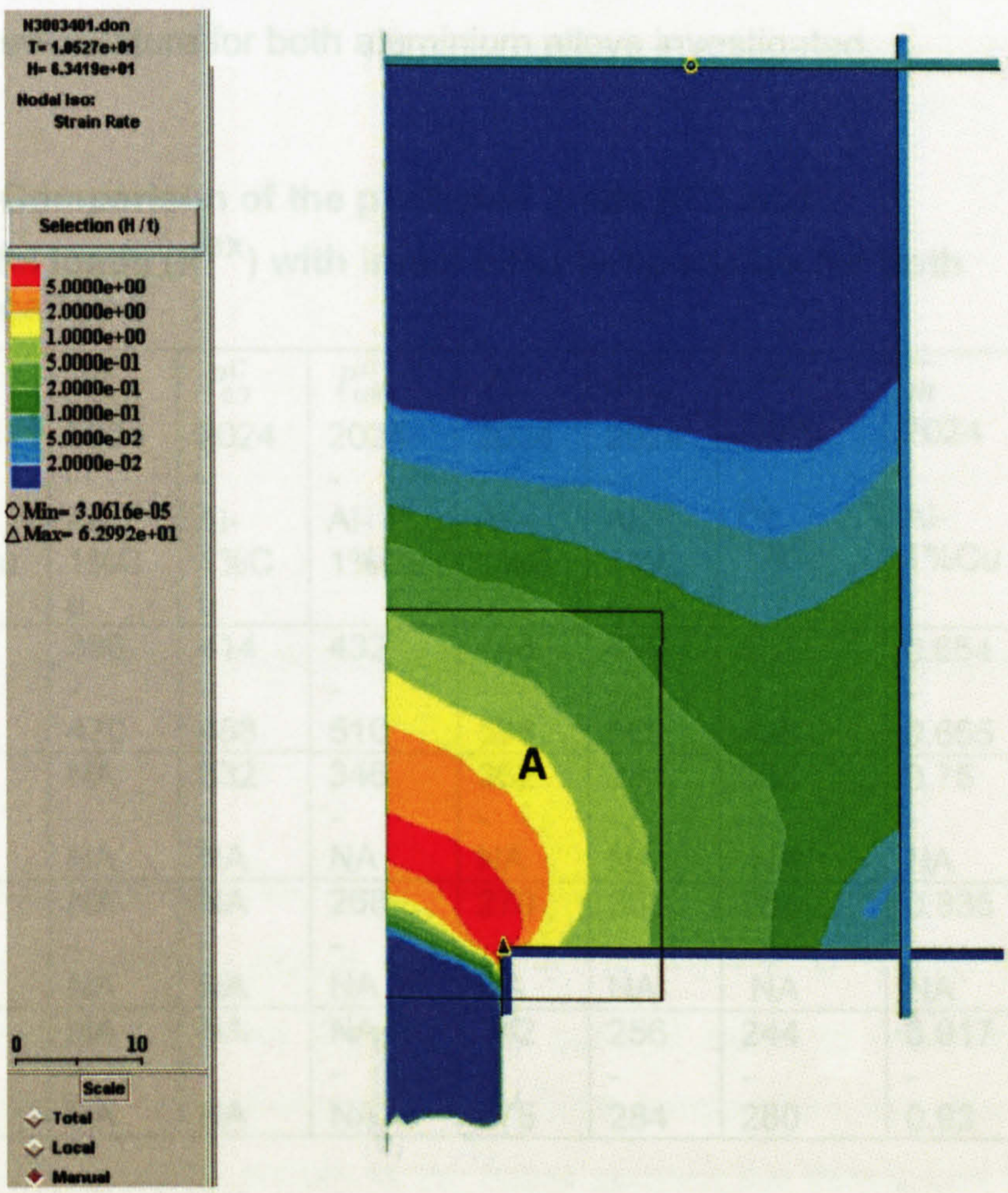

Figure 4.18: Boundary area where the values of Z were averaged

4.6.4 Effect of initial billet temperature on friction

Friction conditions at the billet/tool interface are known to affect the flow paths of the material at the container and through the die by changing the extrusion parameters, loads, stresses and surface quality. Using different friction conditions and various input temperatures permits the experimental pressure to be predicted from the simulation. The predicted loads ($P_{\bar{m}}^{C}$) of the corresponding friction coefficients for each extrusion temperature are shown in Table 4.5. By comparing the predicted loads ($P_{\bar{m}}^{C}$) with the experimental loads (P^{ex}), the results gave a clear indication that the coefficient of friction varies with the initial billet temperature for both aluminium alloys investigated.

Table 4.5: Comparison of the predicted loads (P^{C}) and experimental loads (P^{ex}) with initial billet temperature for both alloys at location 1

T (°C)	$P_{0.5}^{C}$ 2024 - Al-1%Cu	$P_{0.6}^{C}$ 2024 - Al-1%Cu	$P_{0.7}^{C}$ 2024 - Al-1%Cu	$P_{0.8}^{C}$ 2024 - Al-1%Cu	$P_{0.9}^{C}$ 2024 - Al-1%Cu	$P_{0.99}^{C}$ 2024 - Al-1%Cu	P^{ex} 2024 - Al-1%Cu	$\bar{m}$ 2024 - Al-1%Cu
300	385 - 456	396 - 470	414 - 488	432 - 510	448 - 536	469 - 569	401 - 458	0.654 - 0.655
350	NA - NA	NA - NA	332 - NA	346 - NA	362 - NA	381 - NA	338 - NA	0.75 - NA
400	NA - NA	NA - NA	NA - NA	268 - NA	279 - NA	306 - NA	284 - NA	0.835 - NA
450	NA - NA	NA - NA	NA - NA	NA - NA	242 - 275	256 - 284	244 - 280	0.917 - 0.93

The computed results for the variation of the coefficient of friction $\bar{m}$ with temperature are illustrated in Figure 4.20. The figure indicates a linear relationship with a good correlation of the form:

$$\overline{m} = A + B.T \qquad (4.12)$$

The figure also illustrates that the difference in friction coefficient between low and high temperature extrusion increases with increasing temperature.

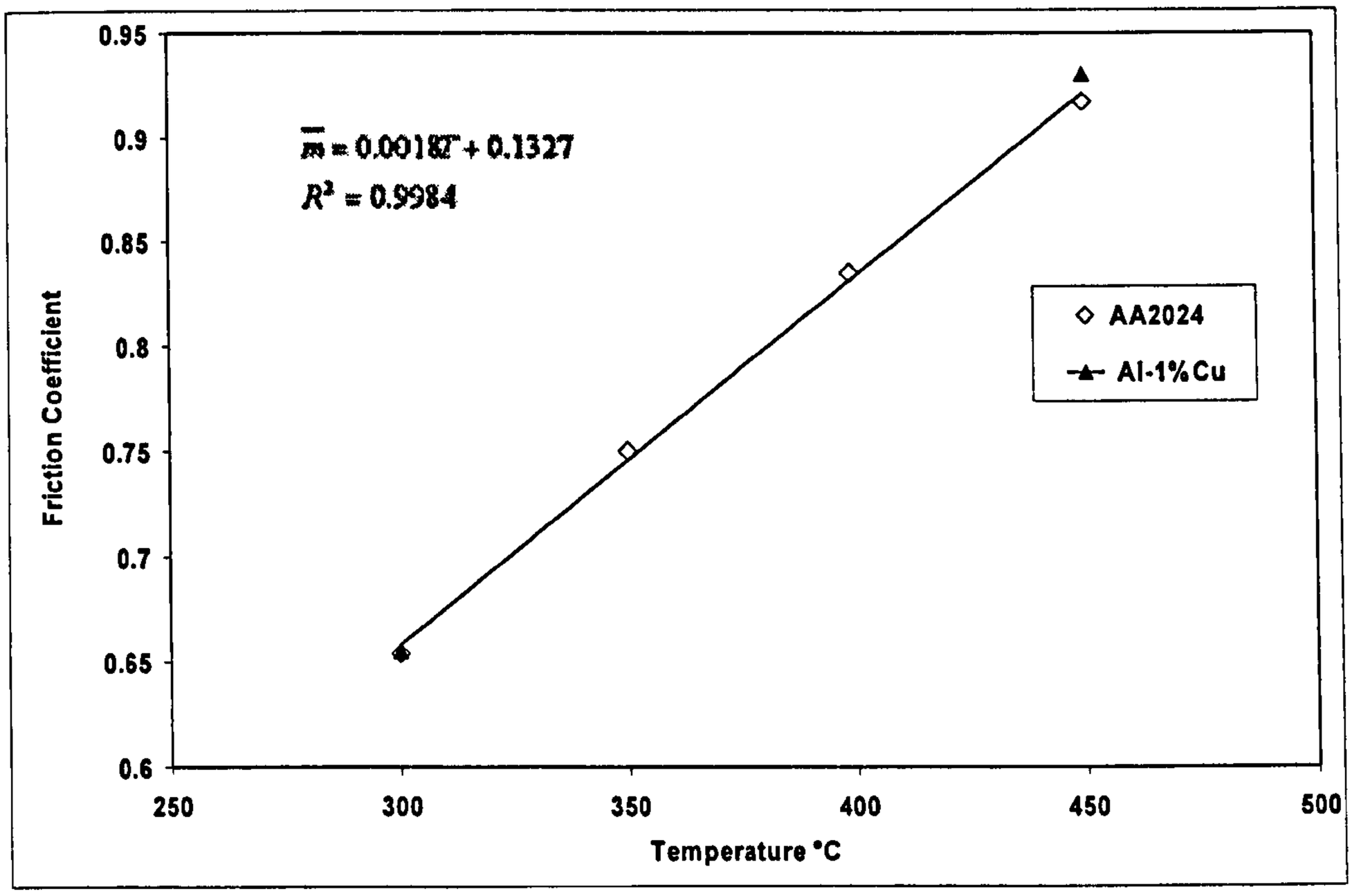

Figure 4.19: Variation of friction coefficient with initial billet temperature

The predicted pressures for input temperatures corresponding to the extremes of frictional conditions, denoted by m = 0.5 to m = 0.99, are shown in Figure 4.21. As expected, a general trend of increasing extrusion pressure with decreasing initial billet temperature was found. The experimental points shown in the figure support the thesis that the friction coefficient varies with temperature and, hence, we may conclude that it will also vary during the ram stroke. The figure also illustrates a greater difference between the experimental and predicted pressure at low and high friction for all extrusion temperatures. The

results show that at 300°C sticking friction overestimates the peak pressure significantly. Hence, the assumption that the friction is a constant value for all extrusion temperatures is incorrect. Moreover, the friction coefficient was found to vary from 0.654 for 300°C to 0.92 for 450°C as shown in Table 4.5 at location 1 (just after the peak pressure has been established).

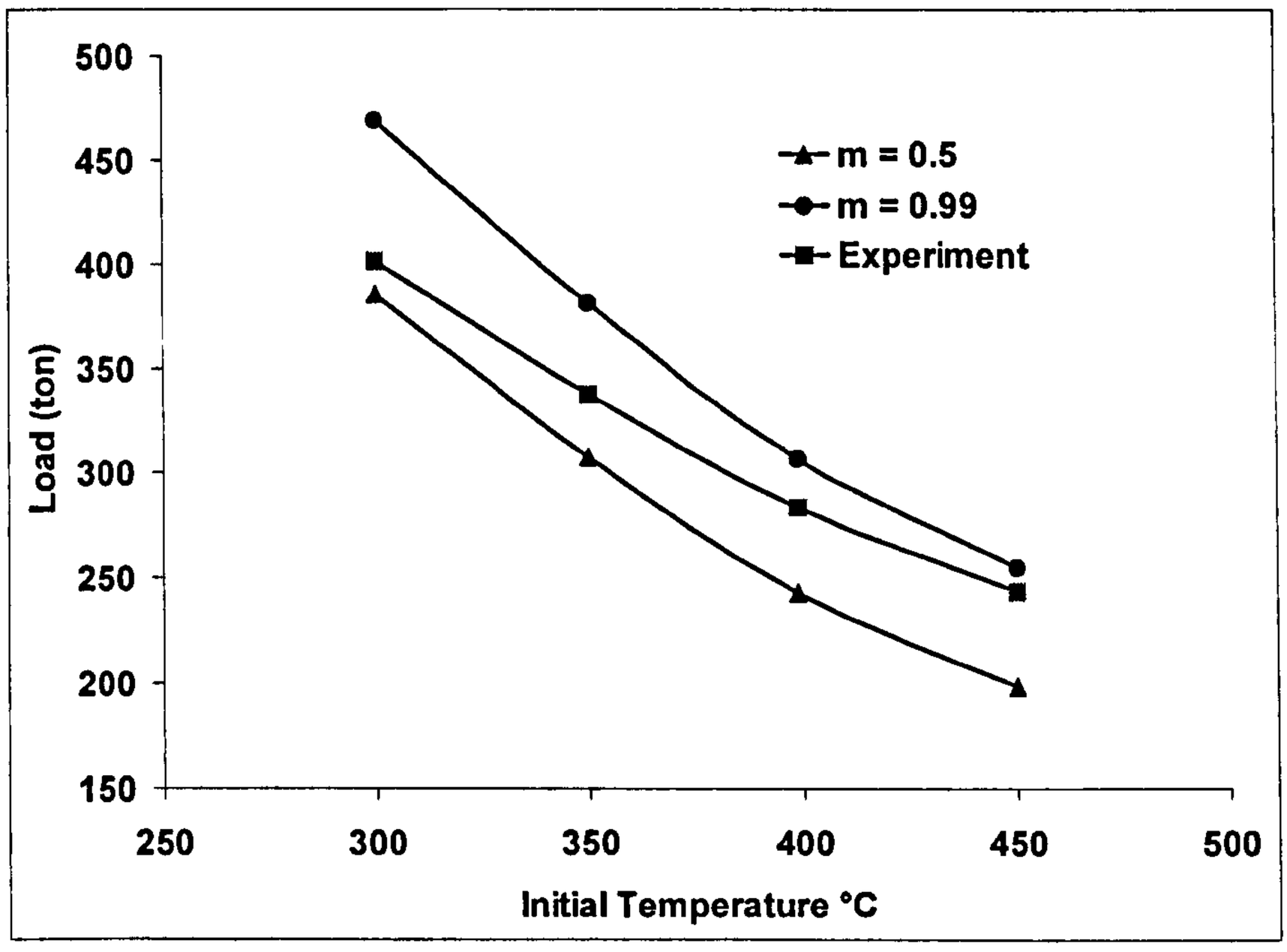

Figure 4.20: Predicted and experimental load variation with initial billet temperature for AA2024.

The upsetting stages, before location 1 has been reached for the billet at high and low temperature extrusions are shown in Figure 4.22 and represented by the prevailing velocity profiles. The pressure at this stage rises sharply while the billet is being compressed to fill the container. As the figures illustrate, at higher temperature extrusion, the deformation is characterised by more rapid flow. The velocity at which the material flows to fill the space of the container proceeding towards

the die opening is significantly greater compared to that at lower temperature. This is evident since the resistance to deformation of the billet material decreases as the temperature increases and reaches its lowest permissible value when the material is close to the melting point of the alloy's lowest melting phase (i.e. 511°C for 2024). However, there are significant differences in the rate at which this change occurs and in the ultimate degree of ductility which is reached. Consequently at higher temperature extrusion, the billet is more ductile and tends, under deformation, to spread more easily to fill the container. The deformation of the billet at this initial stage is characterised by nearly half of its length sticking along the container wall as illustrated in Figure 4.22a. On the other hand, at lower temperature extrusion, the billet is less ductile and acts in a relatively stiffer manner. The upsetting stage at this temperature extrusion is initiated by sliding along most of the container wall and only one-fifth of the billet length is sticking as shown in Figure 4.22b. The shapes of the dead metal zones (DMZ) are also quite different at these varying temperatures. This initial contact and the extent of this contact area along the container wall have a significant effect on the commencement of the deformation path which occurs in localised regions in the billet where the interface results in a sticking, slipping or fully sticking friction situations prior to the quasi-static DMZ formation. Moreover, when the billet has been fully compressed to fill the container, the elastic properties of the container and plastic properties of the materials in contact, have a significant effect on the difficulty of the two materials to slide relative to each other. Similarly, the plastic work dissipated depends on the local temperature at the contact area and the thermal conductivity for the two materials in contact i.e. billet and container. As a result of the extent of the area of contact, at higher temperature and lower flow stress, the force to deform the material increases as the contact pressure at the container increases. In addition, at lower temperature extrusion (i.e. 300°C), the surfaces in contact would produce a greater elastic deformation in the container due to the higher flow stress.

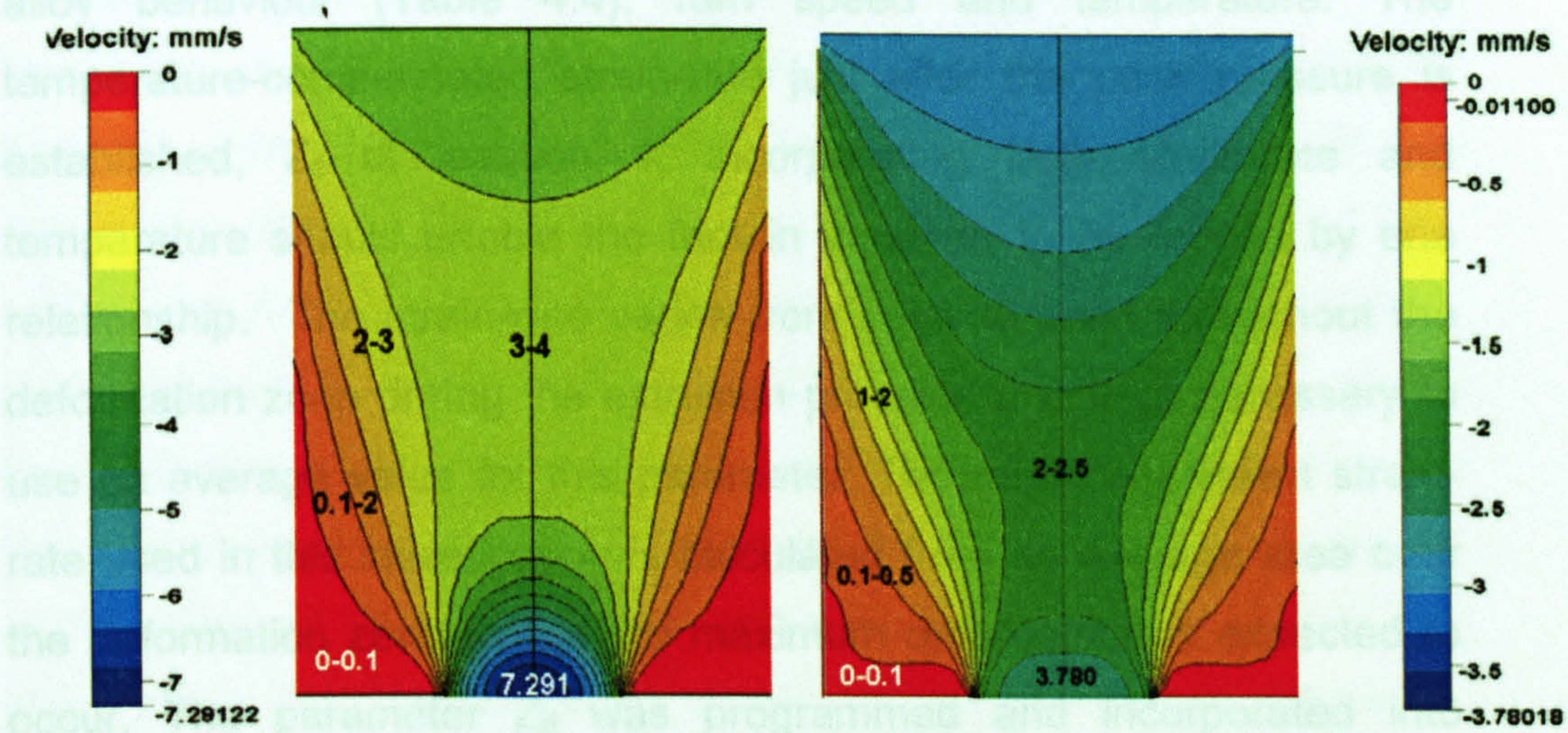

a) b)

Figure 4.21: Initial contact area at a) 450°C and b) 300°C extrusion

After further ram travel, the billet is further compressed and a very small amount of extrusion takes place. The DMZ is fully-established by this time. However, the deformation zone is not clearly-defined at this stage until the peak pressure reaches its maximum. The deformation zone is not stationary, the billet is deforming plastically while the shearing forces are operating which promotes the shearing effect at the DMZ-billet interface. It is at this stage, after the peak pressure has been established, that the friction is of great interest, not only because of press capacity requirement, but also because of its contribution to the temperature changes occurring in the material whilst reaching the peak pressure.

In order to relate the friction factor through a relationship applicable for all extrusion variables and to overcome the separate relationships generated for the variation of friction coefficient with temperatures as given in equation (2.8), it would be more instructive to incorporate the friction factor into a sine relationship by using the Ln Z parameter. The

parameter Z defined in Equation 4.1 contains the data describing the alloy behaviour (Table 4.4), ram speed and temperature. The temperature-compensated strain-rate just after the peak pressure is established, Z_d at location 1, incorporating both strain-rate and temperature should enable the friction variation to be related by one relationship. The strain-rate varies from point to point throughout the deformation zone during the extrusion process. It is thus necessary to use an average value for this parameter. The mean equivalent strain-rate used in this investigation is calculated from an average area over the deformation zone where the maximum deformation is expected to occur. The parameter Z_d was programmed and incorporated into FORGE2® and FORGE3® by the author as one of the outputs of the simulation. The parameter Z_d used in this investigation is calculated in the same manner as the mean equivalent strain-rate at an instantaneous maximum temperature as illustrated in Figure 4.19. To ensure different alloys are represented by the same mathematical expression and to account for the effect of chemical composition of the materials, Ln (Z_d/A) together with the function ($\alpha.n$) was used as proposed by Sheppard [1] for pressure calculations. The constant α is a reciprocal flow stress, and its value has been interpreted as the position where the dependence of flow stress upon strain-rate changes from a power relationship to an exponential one, and is a function of material chemistry. The constant n can be termed the 'inverse of the temperature-compensated strain-rate sensitivity'. The actual value of this constant is strongly dependant upon the value ofα. Both are intimately related to the chemical composition of the material.

When friction coefficients are plotted against $\alpha.n$.Ln (Z_d/A) a linear relationship of the form:

$$\overline{m} = -0.6011.\alpha.nLn(Z_d/A)+1.1261 \qquad (4.13)$$

is apparent and is shown in Figure 4.23. The resistance of the material to withstand the imposed strain gradients at low Z_d conditions, i.e. low flow stress, results in a larger deformation zone extending to the rear of the billet whilst at high Z_d conditions the high flow stress restricts the deformation zone to the die mouth region. As shown in Figures 4.24a and Figures 4.24b, at 5 mm from the ram face, high deformation occurs such that there is a shear zone at the billet/container interface in which the strain-rate and the shear stress vary from a higher value to zero for the strain-rate and to a minimum value for the shear stress at the centre of the billet. At 25 mm distance from the ram, the decay of both the shear stress and the strain-rate when moving from interface to billet centre is much more gradual. This is clearly due to the absence of deformation at the rear of the billet in the first case and the interaction with the dead metal zone and the position of greater deformation as the material approaches the die. When approaching the die, the zone of intense shear increases toward the die opening, separating the deformation zone from the *DMZ*. In this case, the frictional stress is identical to the flow stress of the billet material in pure shear, whereas the relative speed increases from the ram speed at the rear end of the billet to approach the exit speed of the extrudate when approaching the die opening.

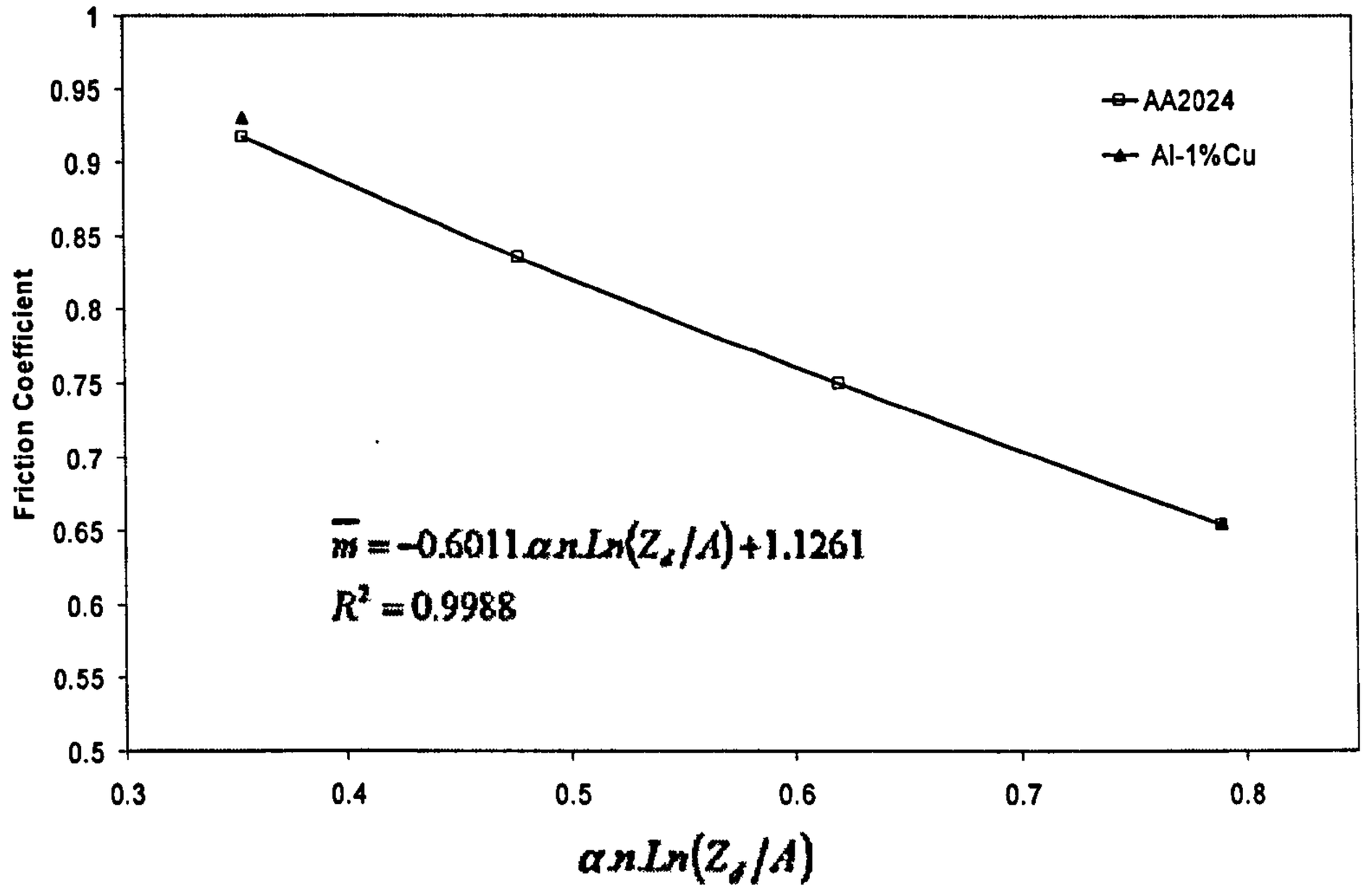

Figure 4.22: Friction variation with $Ln(Z_d/A)$ at location 1.

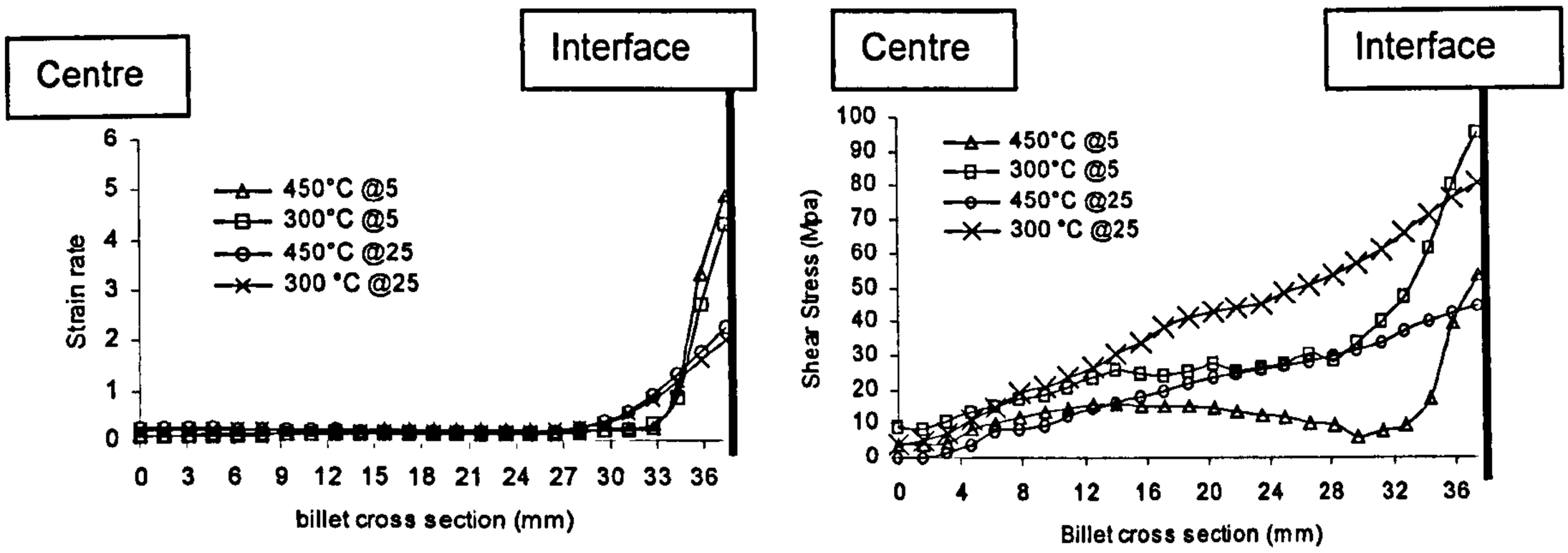

Figure 4.23: a) Strain-rate variation across the billet cross-section. 5 and 25 mm are the distances from the ram position respectively after the peak pressure has been achieved. b) Shear stress variation across the billet cross-section at 5 mm from the ram.

Another factor which must be considered is the strain-rate. Although the total strain is the same for each case, i.e. in terms of the reduction, the time in which the heavy deformation zones form is different. Since the

deformation is initiated nearer the rear of the billet in the high temperature case, over a longer contact area, there will be an associated greater time available for the major deformation to be completed resulting in a lower strain-rate. Thus the friction coefficient is raised and approaches a unit value. In terms of the material plastic flow behaviour, the observations are not unrealistic.

However, these values of friction do not remain constant through the extrusion process. These changes are the consequences of an increase in the overall billet temperature within the deformation zone and the decrease of the area of contact with further ram travel. Complex thermal changes begin as soon as the extrusion commences. The most critical temperature is clearly the die exit temperature of the extrudate, which is related to the heat balance history commencing at the upsetting stage of the operation. It increases if the heat produced by deformation and friction exceeds the heat losses and decreases if the reverse is true. The exit temperature increases sharply as the peak pressure is reached and appears to continue rising after further ram travel as shown in Figure 4.25. The figure illustrates the variation of pressure-displacement with the exit die temperature.

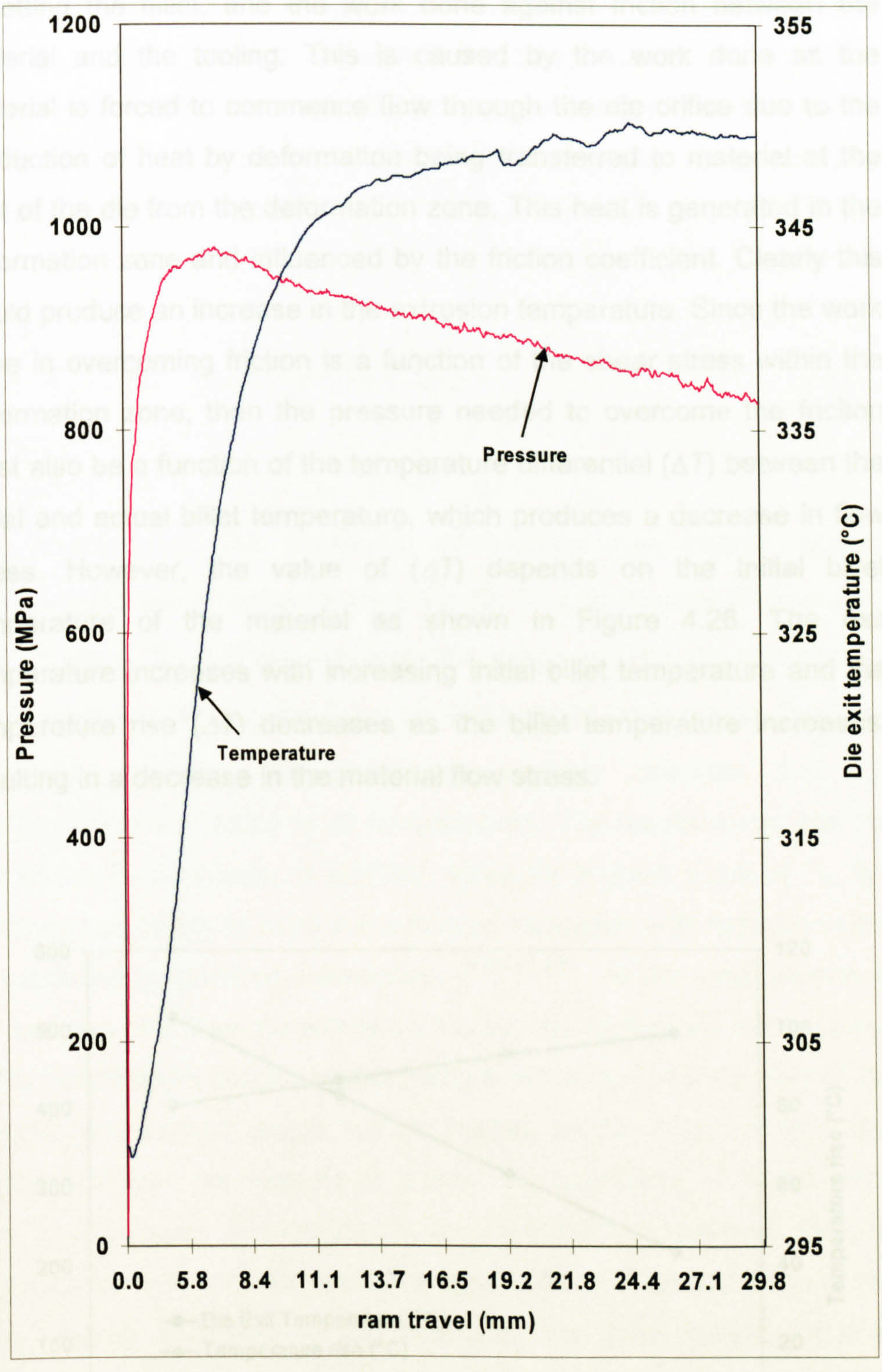

Figure 4.24: Variation of the billet temperature with pressure.

For the initial temperature of 300°C, the temperature of the billet increased sharply by 27°C in reaching the peak pressure. This temperature rise would be expected as a result of the work done in

upsetting the billet, and the work done against friction between the material and the tooling. This is caused by the work done as the material is forced to commence flow through the die orifice due to the production of heat by deformation being transferred to material at the inlet of the die from the deformation zone. This heat is generated in the deformation zone and influenced by the friction coefficient. Clearly this would produce an increase in the extrusion temperature. Since the work done in overcoming friction is a function of the shear stress within the deformation zone, then the pressure needed to overcome the friction must also be a function of the temperature differential (ΔT) between the initial and actual billet temperature, which produces a decrease in flow stress. However, the value of (ΔT) depends on the initial billet temperature of the material as shown in Figure 4.26. The exit temperature increases with increasing initial billet temperature and the temperature rise (ΔT) decreases as the billet temperature increases, resulting in a decrease in the material flow stress.

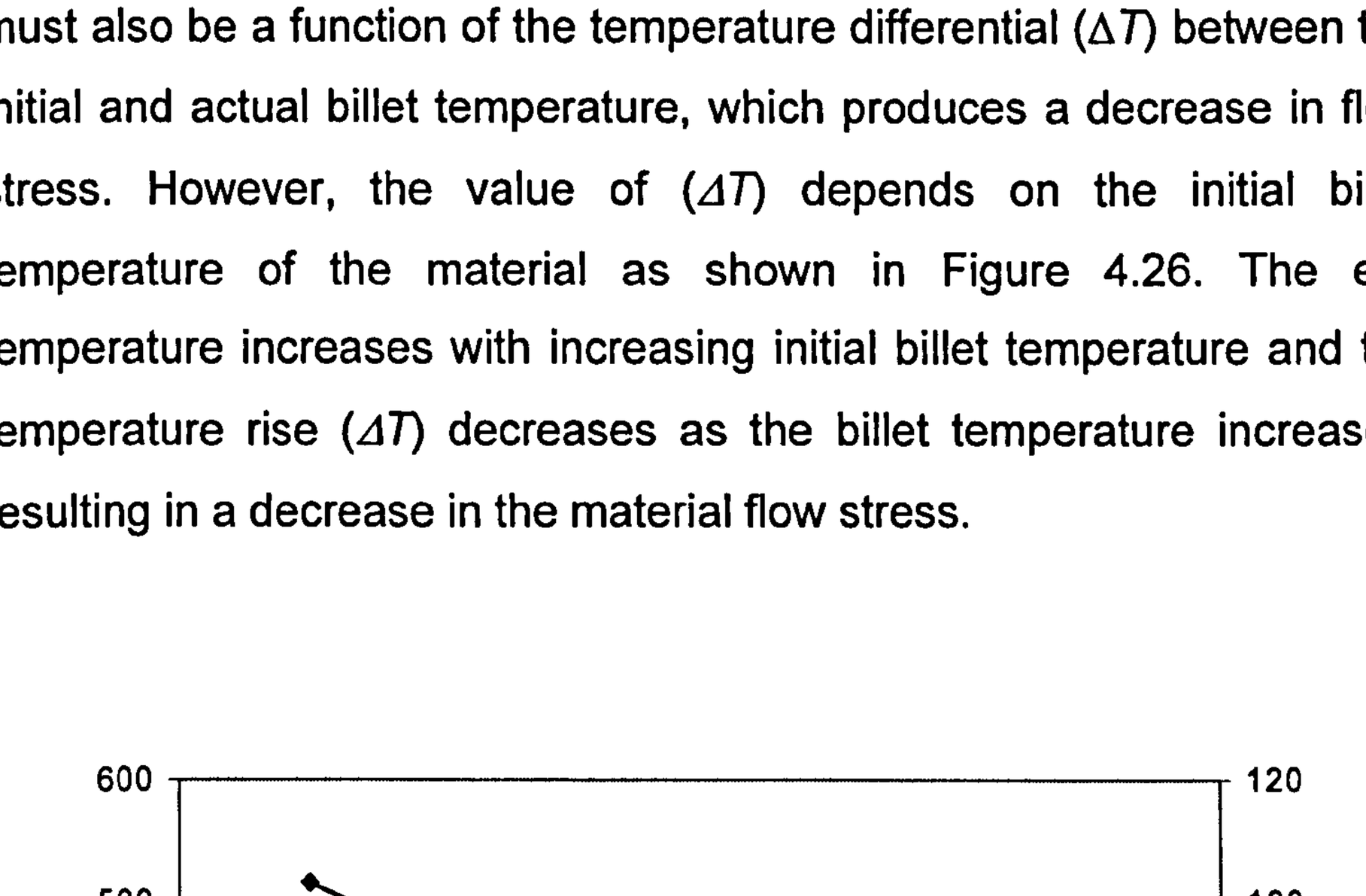

Figure 4. 25: Predicted die exit temperature rise.

Taking into account the temperature rise (ΔT) within the deformation zone at location 2, it was found that the friction coefficient increases from 0.65 to 0.89 for the initial billet temperature of 300°C and from 0.91 to 0.98 for 450°C as shown in Figure 4.27. At location 1, an apparent linear relationship of the form:

$$\overline{m} = -0.4973.\alpha.nLn\left(Z_d / A\right) + 1.1056 \qquad (4.14)$$

was found when the coefficient of frictions was plotted against $\alpha.n.\mathrm{Ln}(Z_d/A)$ and is shown in Figure 4.28. The two figures (Figure 4.23 and Figure 4.27) indicate that over the range of $\mathrm{Ln}(Z_d/A)$ considered, the functions relating $\overline{m}$ and $\alpha.n.\mathrm{Ln}(Z_d/A)$ are of similar form. The high correlation obtained throughout the analysis indicates that the relationship is applicable to all temperatures. The results show that the use of the Z_d parameter is justified, since for a given value of Z_d, the pressure necessary to carry out extrusion increases with reduction ratio as predicted by previous researchers [1,62-63, 95]. At the initial stages of the process, the main parameters affecting the friction are the increase in the temperature and the contact length. However, near the end of the process, the contact length has diminished as the length of the billet shortens. It was not feasible to predict the coefficient of friction after location 2 because of computer time considerations. However, there is no indication that such an operation would alter the interpretation of the data already collected. At all locations, the total friction force is significantly influenced by the billet length remaining in the container, and thus falls as extrusion proceeds.

Hence, the only method of predicting friction could be to program the FEM code to define friction as:

$$\overline{m}_{\Delta L_n} = \left[A + \alpha.n.Ln\left(Z_d/A\right) + B \right]_{\Delta L_{n-1}} \qquad (4.15)$$

where ΔL_n, is incremental ram travel (i.e. each 2.5 mm of ram displacement).

The author realises that programming a boundary condition in this way would not be a trivial task and would increase computing time considerably. Nevertheless, if friction is to be addressed in a scientific manner such an approach will be necessary.

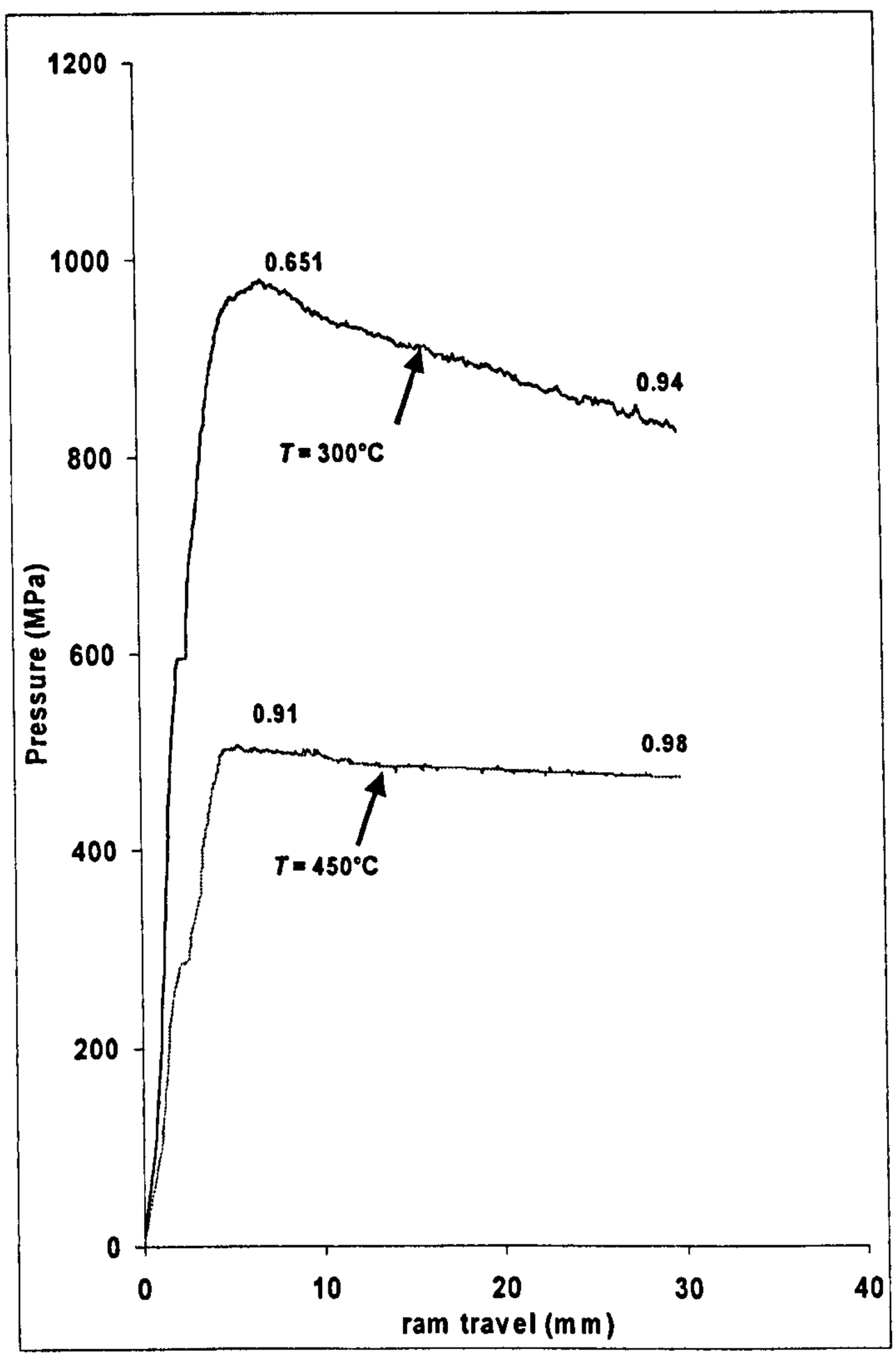

Figure 4.26: Friction variation during the extrusion process for AA2024 at locations 1&2. Temperatures given are initial billet temperatures.

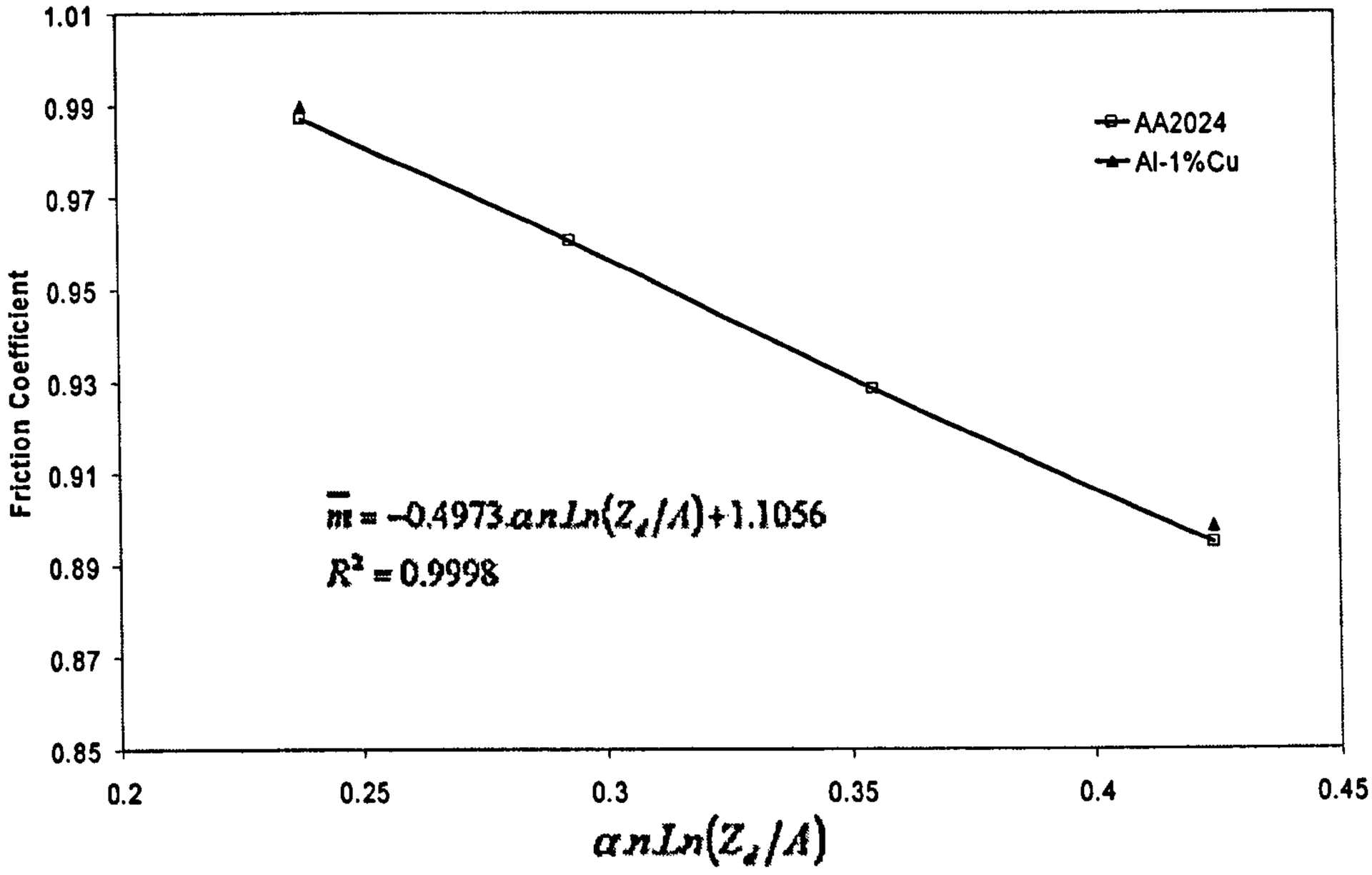

Figure 4.27: Friction variation with α.n. *Ln*(Z_d/A) at location 2.

4.7 Conclusions

1. The failure for the Norton-Hoff relationship to satisfy the experimental data with the change in temperature lies in the derivative of the flow-stress and consequently with the strain-rate sensitivity index, *m*. To satisfy the experimental flow stress data, and successfully predict the extrusion parameters using the Norton-Hoff equation, the strain sensitivity index, *m*, must be expressed as a function of temperature and temperature changes and not an averaged value as it is assumed and introduced into the FORGE's program data file.

2. The hyperbolic-sine relationship provided a better representation for the experimental flow stress with strain-rate and temperature under high working conditions than the Norton-Hoff relationship.

3. The FEM Code Forge 2 with the programmed hyperbolic-sine function provided a suitable model for simulation and successfully predicted the major extrusion parameters.

4. Finite EM has been successfully applied to model the deformation patterns in the load/displacement traces and temperature evolution during an extrusion cycle.

5. The comparison of the experimental and simulated temperature rises are seen to agree substantially and this demonstrates that FORGE2 Software can predict the temperature changes during the extrusion cycle.

6. The initial stages of the deformation, where the billet is primarily affected by the flow stress of the material and the rate at which the work is carried out, proved to be of some significance in

dictating the material flow distribution during the extrusion process.

7. The extrusion pressure is significantly influenced by the temperature gradients modified in the billet during transfer to the container, and after upsetting in the container.

8. The increase in friction results in an increase of initial extrusion load.

9. The assumption that the friction conditions are a constant value for all extrusion temperatures is incorrect. The apparent friction coefficient was found to vary from 0.654 for 300°C to 0.92 for 450°C as shown in Table 4.5.

10. At the initial stages of the extrusion process, the main parameters affecting the friction are the increase in the temperature and the contact length. At all other locations after that, the total friction force is significantly influenced by the billet length remaining in the container, and thus falls as extrusion proceeds.

11. The $\overline{m}$ values do not remain constant throughout the extrusion cycle. The increases in overall temperature of the billet and hence decreases in flow stress, lead to an increase in friction for both alloys and temperatures.

12. The variation of friction conditions during the extrusion cycle for both alloys relating to the process conditions, resulted in relationships of the form:

$$\overline{m} = -0.6011.\alpha.nLn(Z_d/A)+1.1261$$ at location 1 and

$$\overline{m} = -0.4973.\alpha.nLn\left(Z_d / A\right) + 1.1056 \qquad \text{at location 2.}$$

This implies that friction should be introduced into the computer program in the form of:

$$\overline{m}_{\Delta L_n} = \left[A + \alpha.n.Ln\left({}^{Z_d}\!/_{A}\right) + B \right]_{\Delta L_{n-1}}$$

13. For an accurate simulation of extrusion, the friction coefficient must be identified continuously during the process cycle. This is not only required for press capacity, but also the effect on the temperature changes occurring in the material. This subsequently has an effect on the surface quality of the extrudate.

14. During the extrusion process, the billet surface adheres to the container and presents the possibility of surface layer incorporation into the extrudate. Using a constant value for friction for all extrusion temperatures, as many researchers have indicated, would affect the incorporation of the surface layers into the extrudate. This would directly affect the predicted minimum discard.

15. The accuracy of the friction factor $\overline{m}$ is largely dependent upon the flow stress of the material at the billet, container interface.

16. Good agreement between experimental and simulated results was found for high and low temperature extrusion flow. An enlarged DMZ was observed as a result of the increase in the initial billet temperature and in turn yielded an increase in the friction factor.

CHAPTER 5: EXTRUSION SECTION SHAPES

5.1 Introduction

This chapter deals with the extrusion of shape and tube sections and uses a 3-dimensional (FEM) solution to predict the effect of die geometry on maximum extrusion load and temperature of the extrudate during the process. A description of material flow in the container is considered in more detail for rod, shapes and tube sections in order to fully comprehend the transient conditions occurring during the process cycle. A comparison with experiments is made to assess the relative importance of some extrusion parameters in the extrusion process and to ensure that the numerical discretisation yields a realistic simulation of the process. The limitations of FEM when modelling complex shapes is also discussed.

5.2 Simulation Considerations

The simulation approach is based on a viscoplastic constitutive model. This type of model neglects the elastic behaviour of the material, due to the fact that hot aluminium has rate dependent behaviour and that the elastic deformations are small when compared to the large plastic deformations that occur during the process.

The definition of the tooling is one of the essential data inputs that have to be integrated into the simulation calculation. Consequently, both for the geometry (the precision of the boundary) and the kinematics (to follow the mechanical deformation), simulation must be designed

accurately. The accuracy of the results is closely related to the meshing quality.

During the simulation of extrusion, large deformations are predominant which require a Lagrangian mesh to be defined. Thus, complete remeshing which is mandatory in areas of excessive deformation is a source of loss/gain of volume. The elements become severely distorted during the process and consequently, the need for remeshing is necessary to continue the simulation. The frequency of remeshing is controlled by the degree of deformation and is a user variable. Therefore, careful judgement for the mesh refinement is required and the user must be able to identify the locations that need remeshing and call for local remeshing. This is crucial to minimise the computation volume loss.

5.3 Pre-processing

The tooling geometry of the shape dies and the billets were modelled using the I-DEAS Master-Series software. Taking advantage of the symmetry planes in the design and in order to reduce computation time, half of the models were constructed for "T" and "U" shapes. The Square shape and the bridge-die were constructed using only a quarter and sixth of symmetry of the models respectively. A surface mesh (2-dimension) was then generated using three node linear triangles corresponding to the outer surface of the tooling and the billet. Once these models were built and meshed in 2D, the finite element model information was imported by FORGE3^{TM} program algorithm in order to check the surface quality of the tools and to generate the three-dimensional volume mesh for the billet using three node tetrahedral elements as shown in Figure 5.1.

To control the degree of remeshing in the areas where high deformation is expected, fine refinement mesh boxes of an Eulerian type (but

maintaining Lagrangian flow) were applied to the billet. The remeshing values are controlled by an average aimed size of an edge of an element and the distribution is specified by "mesh-boxes", i.e. boxes that define regions of the mesh on which a mesh size is imposed during the computation. Refinement mesh boxes for the "T", "U" and Square shapes were defined and applied at the re-entrant corners where high deformation is expected as illustrated in Figure 5.2. The average initial mesh size in the billet is 4.

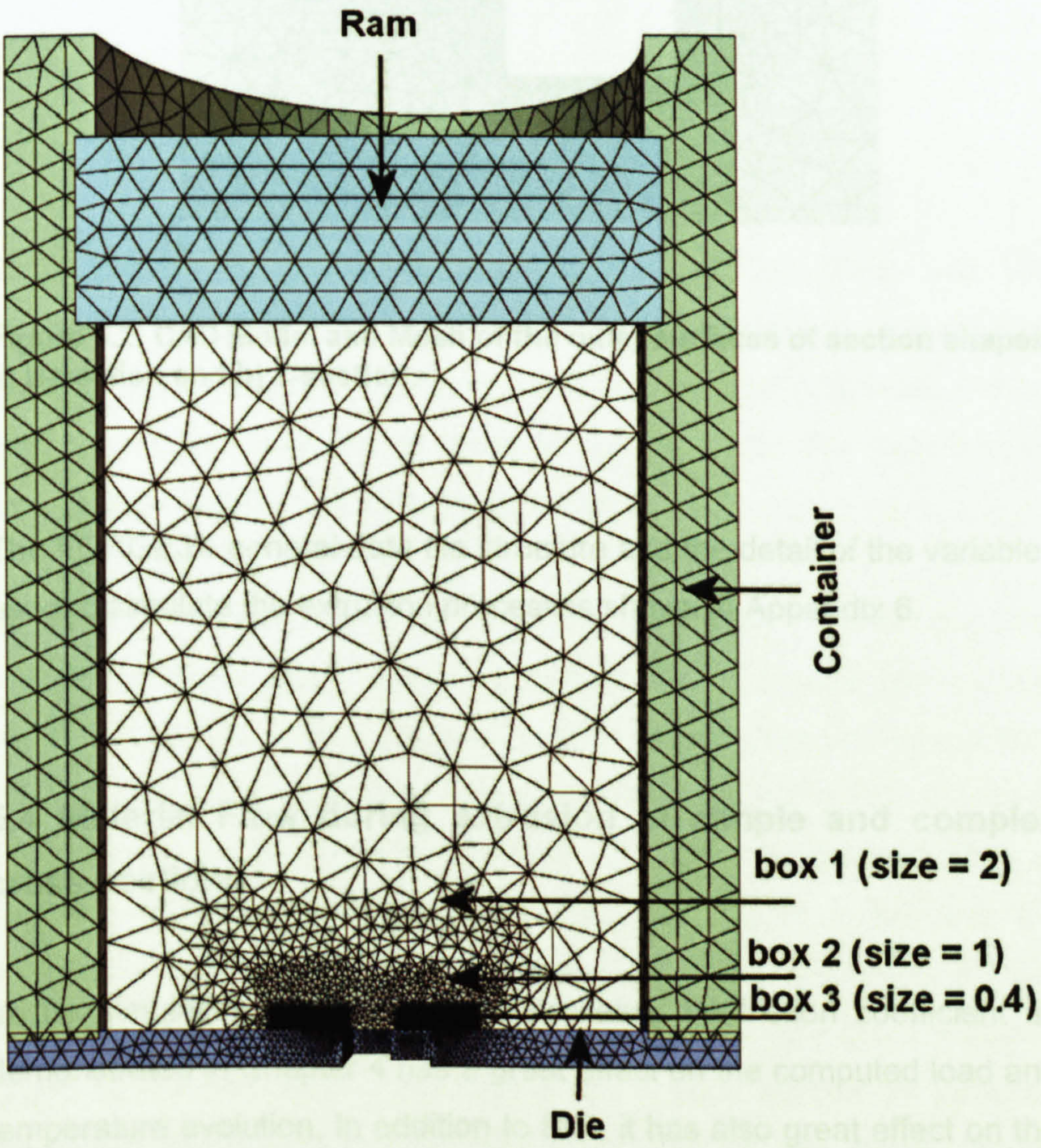

Figure 5.1: Meshing of the billet-tool and setup configuration prior to simulation in FORGE3

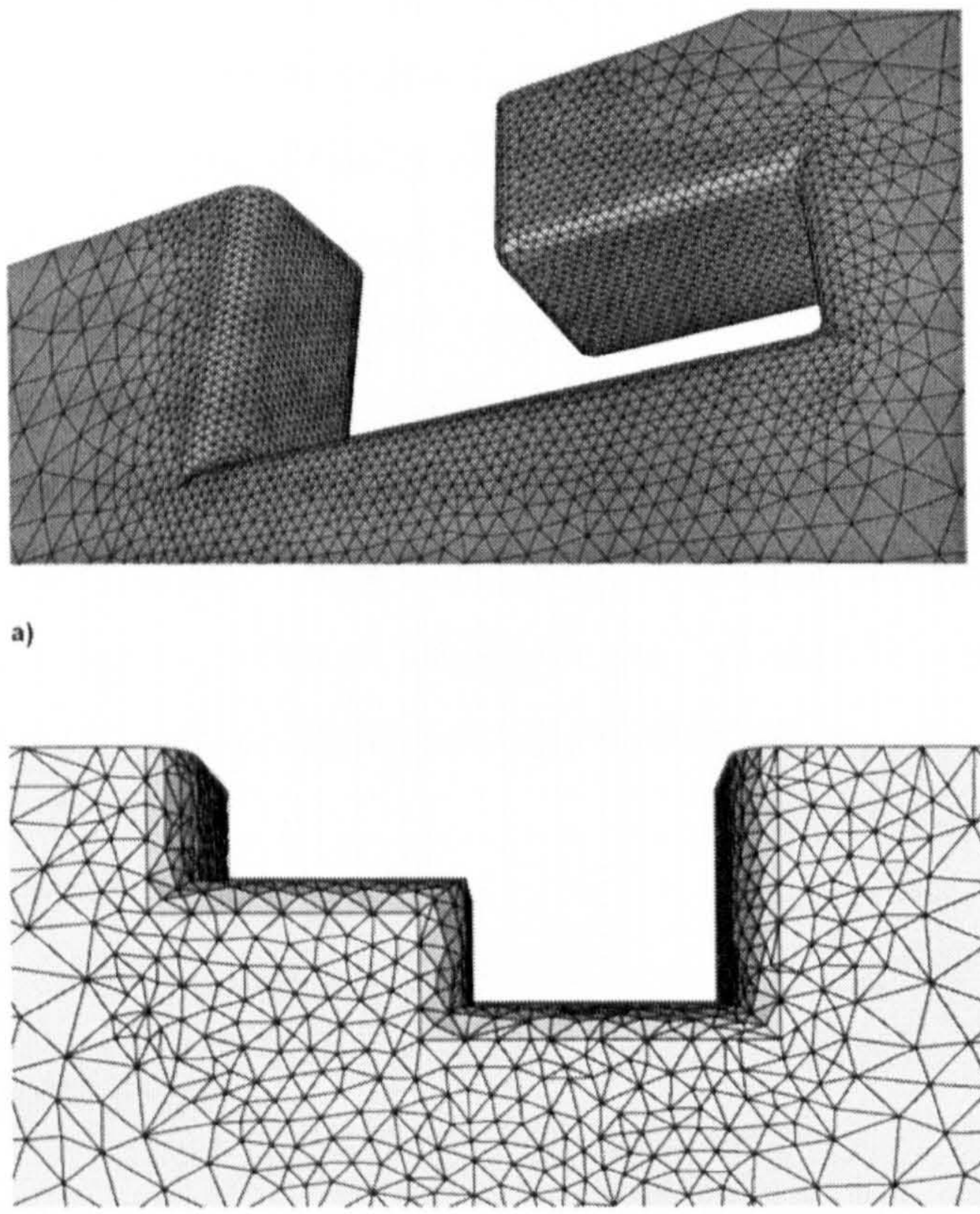

a)

b)

Figure 5.2: CAD Model and Mesh of the outer surfaces of section shapes a) U-section and b) T-section.

The FORGE3's general data-file structure and the detail of the variables used to simulate the extrusion process is shown in Appendix 6.

5.4 Material Flow during extrusion of simple and complex cross-sections

In the simulation of the extrusion process, the friction coefficient as demonstrated in Chapter 4 has a great effect on the computed load and temperature evolution. In addition to that, it has also great effect on the computed results, such as material flow [34-35], microstructural evolution and the product surface quality.

To investigate and illustrate the material flow characteristics in detail during extrusion of complex and simple shapes, both FORGE3 and FORGE2® software (for simple rod) were used at different locations in the pressure-displacement curve. The point at which the "U" shape is illustrated, coincided with the full development of the deformation zone and after the peak pressure was established. The "T" and "S (square)" sections coincided with the quasi-static deformation indicated by the pressure-displacement curves reaching the steady-state region. In addition, at the same location at which the "T" and "S" sections were illustrated the rod section coincided just before the end of the extrusion cycle.

5.4.1 Rod extrusion

To evaluate the effects of material flow at both high and low temperature extrusion i.e. 450°C and 300°C respectively, two billets were sectioned along a meridian plane with square grid lines. Similar grid lines were simulated in order to compare with the experimental results from Tutcher [122] and Subramaniyan [62].

In the direct extrusion process, a relative movement between the billet and the container exists, encouraging the inhomogeneous nature of the material flow. The effects of the initial billet temperature on material flow for high and low temperature extrusion are illustrated in Figure 5.3a-d. The figure shows a comparison between the simulated gridded billets at the end of the extrusion (Figure 5.3a and Figure 5.3b) and the corresponding macrographs taken from Tutcher's experiments (Figure 5.3c and Figure 5.3d). The flow patterns represented by grid lines were originally perpendicular to the billet axis. A good agreement between the experiments and the simulation is obvious. As these figures illustrate, it is clearly evident in both cases that there is a significant change in deformation zone geometry. For high temperature extrusion

(i.e. 450°C), the deformation zone gradually spreads from above the die mouth to the container walls by progressive thickening of the zones of heavy shear. The shearing zone occurs in the subcutaneous regions of the billet in preference to sliding at the container wall interface. On the other hand for lower temperature conditions (i.e. 300°C), the extent of this zone is volumetrically less than that observed with higher temperature conditions, the most severe deformation is limited to a small volume close to the die mouth.

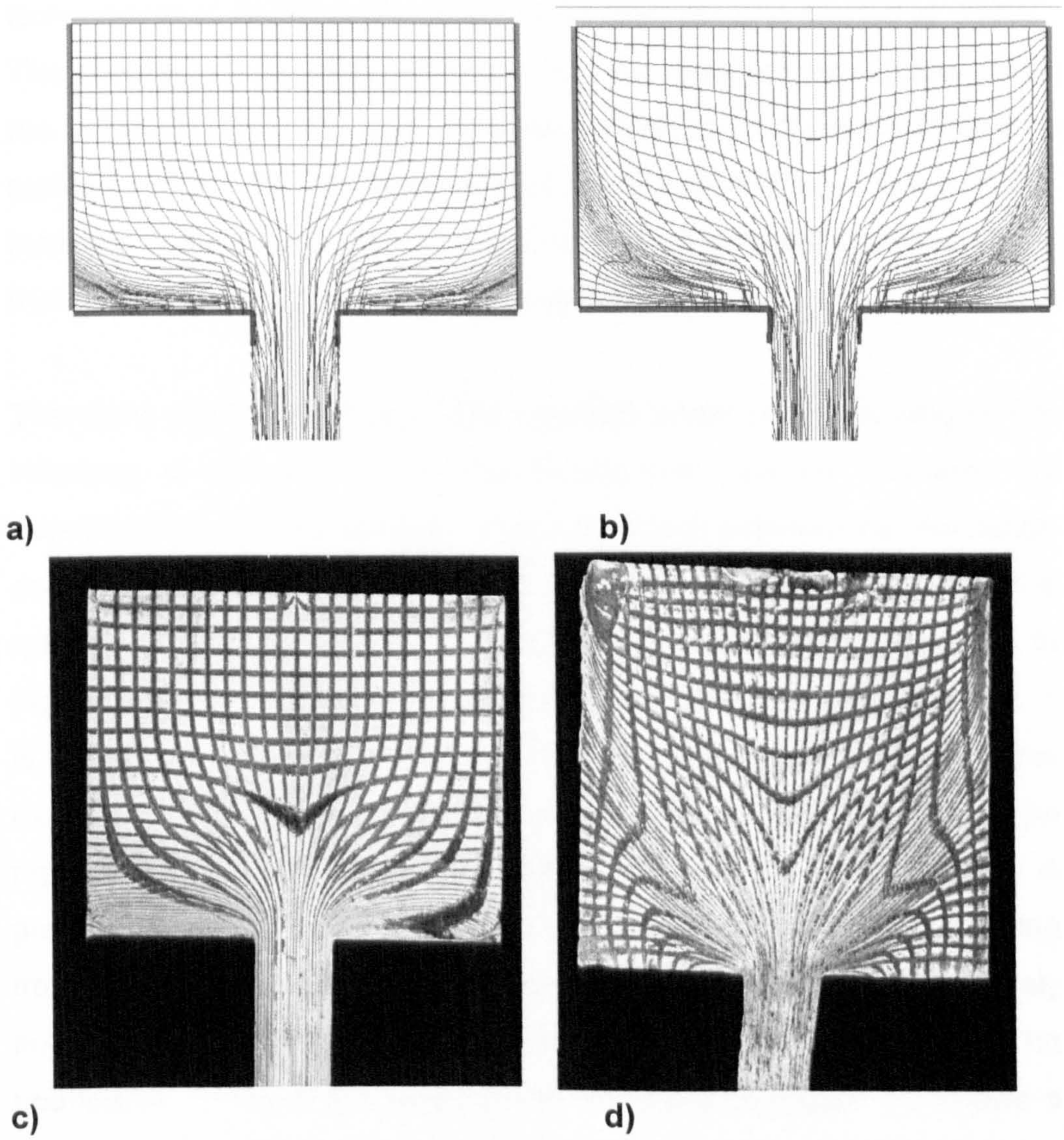

Figure 5.3: Simulated flow patterns a) Flow at 300 °C and b) Flow at 450°C. c) and d) are the corresponding experimental [121] flow patterns at 300°C and 450°C respectively.

The formation of the dead metal zones is evident and over at least 50% of the volume shown there is no evidence of deformation, the grid is regular across the entire width. Comparing this with the result of the high temperature extrusion shows a considerable difference. In this case, the effects of the deformation can be found over the entire surface shown. Considerable amounts of cylinder wall shear may be seen stretching from the rear of the billet up to the dead metal-zone boundary and progressing further back into the billet, leaving the die mouth flow at a more obtuse angle to the DMZ than the one observed at lower temperatures. The zone of shear produced by friction at a temperature of 450°C is greater in depth than the one formed at 300°C. The shearing at the DMZ boundary may be regarded as a measure of the work required to provide the force needed to produce a satisfactory surface. This work increases with an enlarged DMZ as a result of the increase of the initial billet temperature and consequent increase in the friction factor at the billet/container interface.

Therefore, the extent of the DMZ provides some understanding of the influence of temperature on the friction and can be visualised by assessing the velocity profiles. The comparison between the simulation contour lines scalar of material displacement in FORGE3 and the macrograph obtained from Subramaniyan's experiments are shown in Figure 5.4a and Figure 5.4b respectively. As these figures illustrate, it is clearly evident that there is a good agreement between the experiments and the simulation. As illustrated by Figure 5.4a, in the regions of the deformation zone close to the die, the central velocity is greater; the rate of travel of material at the billet centre is increasing from the rear of the billet towards the die throat, progressively augmenting the restrained flow of metal near the container wall. The boundaries of the deformation zones illustrated in Figure 5.3 shows a smaller volume for the lower temperature extrusion. In addition there is a greater amount of material from the billet subcutaneous layers appearing to reach the extrudate in the high temperature case than the

low temperature. This would tend to imply greater diffusion of internal energy dissipation. The temperature gradient between the centre of the billet and the container wall will also cause the shearing layer between the billet and the container to occur at a greater depth below the surface, and so leaves a thicker rim of metal at the billet/container interface. In this connection, the strong adherence of aluminium at lower flow stress to the wall of the container would eventually lead to a very high value of friction.

Thus, the evidence confirms that a lower temperature extrusion increases the resistance to deformation, reduces the volume of DMZ and decreases the proportion of the work required to produce the desired surface. Therefore, the friction factor is associated with the thermally activated events involved. The results found in Figure 4.22 and Figure 4.27 of a decreasing $\bar{m}$ with increasing $\alpha.n.\mathrm{Ln}(Z_d/A)$ term can therefore be attributed to a change in deformation zone geometry caused by a variation in the plastic flow behaviour of the material.

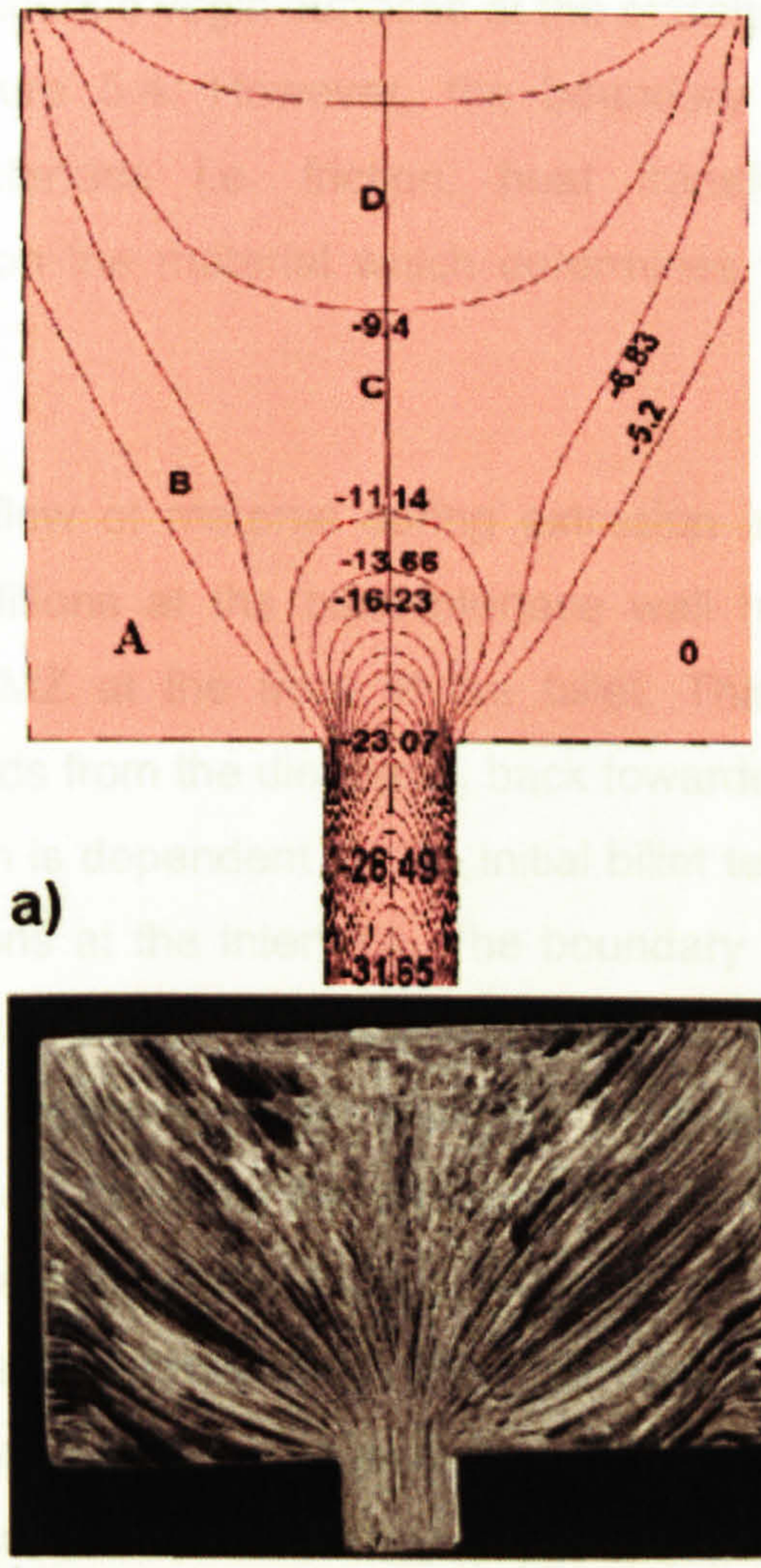

Figure 5. 4: Quasi-static flow of material during extrusion a): Flow velocity (mm/s) of material during extrusion at 450°C. A) DMZ, B) Surface generation zone, C) Main deformation Zone and D) Central deformation zone. (Initial velocity 3 mm/s). b): the corresponding experimental micrograph (After Subramaniyan [62]).

5.4.2 Surface Generation

In order to achieve a sound quality surface during the extrusion process, the surface of the extrudate must be generated from within the billet. The generation of this surface involves the production of a virgin surface by shearing of the DMZ. The nature of shear involves

production of continuous virgin surfaces at the entrance to the die throat as shown in Figure 5.4. However, the boundary conditions at the billet/container interface i.e. friction, heat transfer, etc., have a significant effect on the material which determines the surface of the extrudate.

The quasi-static flow of material during extrusion is shown in Figure 5.5a. The conditions at the billet-interface wall have promoted the formation of a DMZ at the front of the billet. This static volume of material (A) extends from the die throat, back towards the container wall at an angle, which is dependent on the initial billet temperature and the boundary conditions at the interface. The boundary of this Zone (A) is illustrated in Figure 5.5a. Outlining this zone is a region of intense shear. The zone resembles the frustrum of a cone in shape and extends from the die throat to the container wall as illustrated in Figure 5.5b. It can be seen from the Figure 5.4a that the extrudate material originates from various locations in the deforming billet which may be represented by three zones. The surface generation zone (B) outlining the DMZ, the main deformation zone (C) and the central deformation zone (D). The outer surface of the extrudate originates from the surface generation zone (B) as illustrated by Figure 5.4a. It is material from this zone moving along the DMZ boundary that forms the extrudate surface. The figure also suggests that the outside surface of the extrudate originates from the material which is located on the edge of the DMZ and moving more slowly into the extrudate surface promoting a continuous formation of a virgin surface. The material forming the core of the extrudate originates from the central deformation zone (D) of heavy shear feeding into the bulk of the extrudate as illustrated also in Figure 5.5c. This central deformation zone supplements the material feeding the body of the extrudate from within the main deformation zone (C).

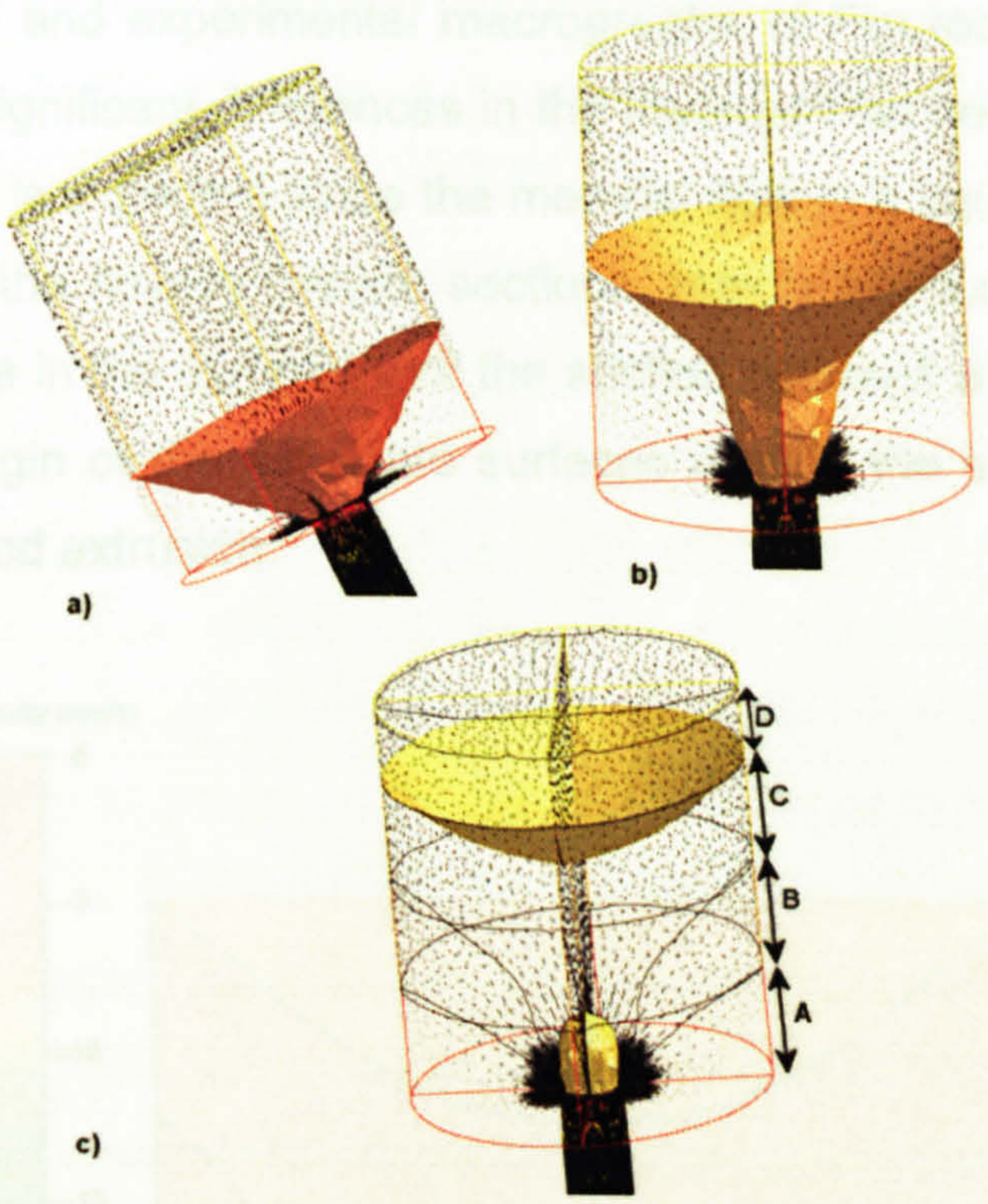

Figure 5.5: Boundary zones in the quasi-static flow a) DMZ, b) Main deformation zone boundary and c) Central deformation zone boundary and the corresponding zones outlined in Figure 5.4.

5.4.3 Section Shapes

The effect on the material flow of changing the section geometry from circular to square is shown in Figures 5.6a and 5.6b. The figure shows a comparison between the predicted contour lines scalar of the shear stress using FORGE3 (Figure 5.6a) and the macrographs of a partially extruded billet of super purity aluminium obtained from experiments [62], (Figure 5.6b) The planar section shown was taken along the diagonal of the square. As these figures illustrate, it is clearly evident that there is a good agreement between the experiments and the simulation. Similar to the material flow in a circular cross-section, the flow patterns resemble a typical direct extrusion flow with the fast moving central zone outlined by a slow-moving restrained periphery. as shown in Figure 5.6a. Both

the simulation and experimental macrographs of Figures 5.4 and 5.6, exhibited no significant differences in the material flow between the two sections. This is expected since the material flow in a square section is analogous to the flow in circular sections, mainly because there is no severe change in the symmetry of the section between a square and a circle. The origin of the extrudate surfaces remain the same as those observed by rod extrusion.

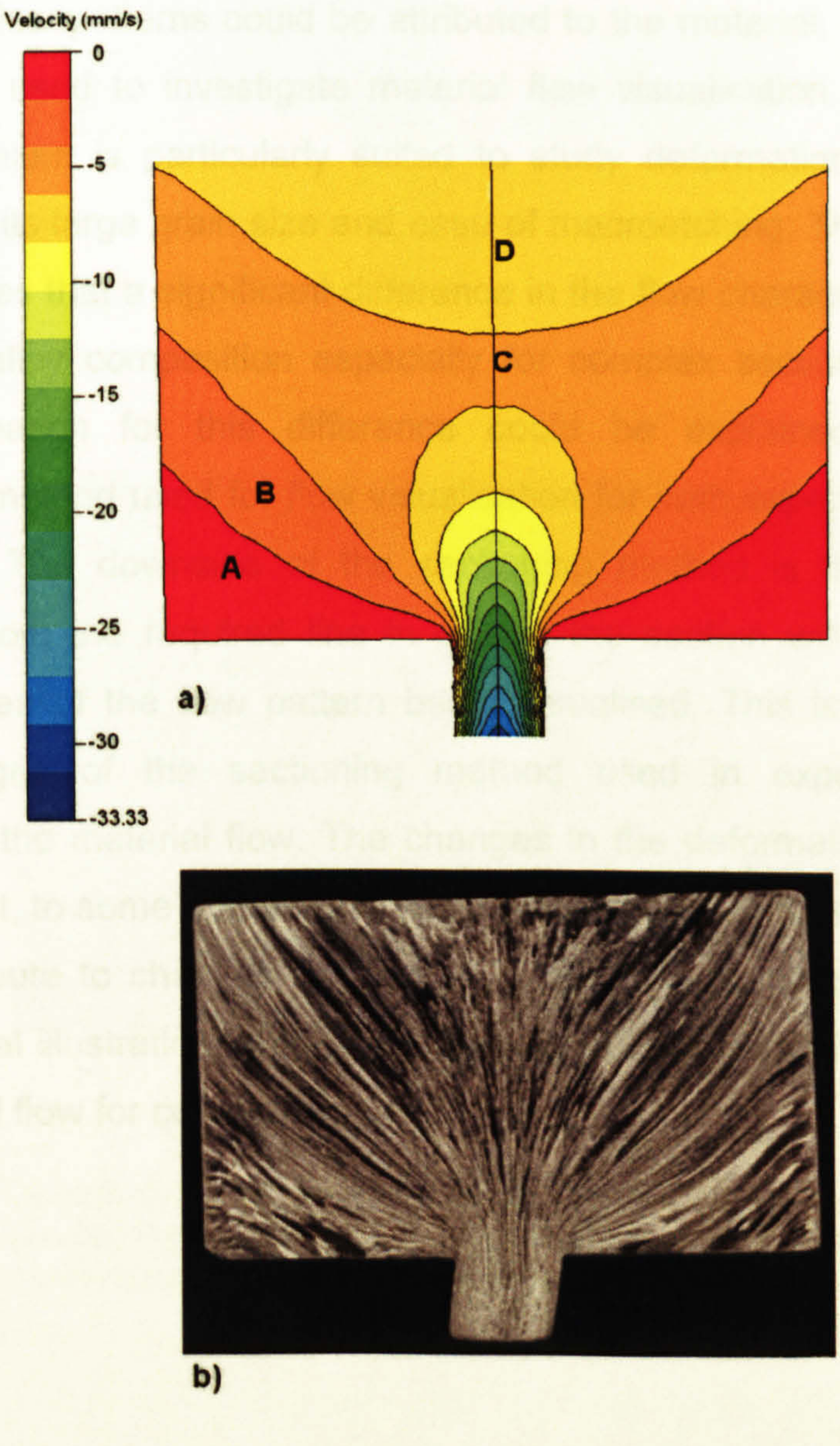

Figure 5.6: Quasi-static flow of material during square section extrusion a): Flow velocity (mm/s) of material during extrusion at 400°C. A) DMZ, B) Surface generation zone, C) Main deformation zone and D) Central deformation zone. (Initial velocity 3 mm/s). b): the corresponding experimental micrograph (After Subramaniyan [62]).

The experimental and simulation of the quasi-static deformation flow corresponding to the extrusion of T sections are shown in Figures 5.7a and 5.7b respectively. The simulation patterns, in Figure 5.7, are presented by the shear stress distribution on the sectioning plane. The plane from which the billet was sectioned is shown in Figure 5.8. It can be seen that the flow patterns are slightly different from the experimental patterns in contrast to those obtained for rod and square sections. This small difference between the experimental and the simulation flow patterns could be attributed to the material, Super Pure Aluminium, used to investigate material flow visualisation. The super pure aluminium is particularly suited to study deformation behaviour because of its large grain size and ease of macroetching. This probably demonstrates that a significant difference in the flow characteristics can exist with alloy composition especially for complex sections. Another possible reason for this difference could be explained from the sectioning method used for flow visualisation for both experimental and simulation. The downside of the sectioning method is that a slight deviation from the required line in cutting the section will result in a different area of the flow pattern being visualised. This is one of the disadvantages of the sectioning method used in experiments to investigate the material flow. The changes in the deformation patterns indicate that, to some degree, the variations in profile across the section may contribute to changes in the flow patterns. It is evident from the experimental illustrations that there is some differences in representing the material flow for complex shapes.

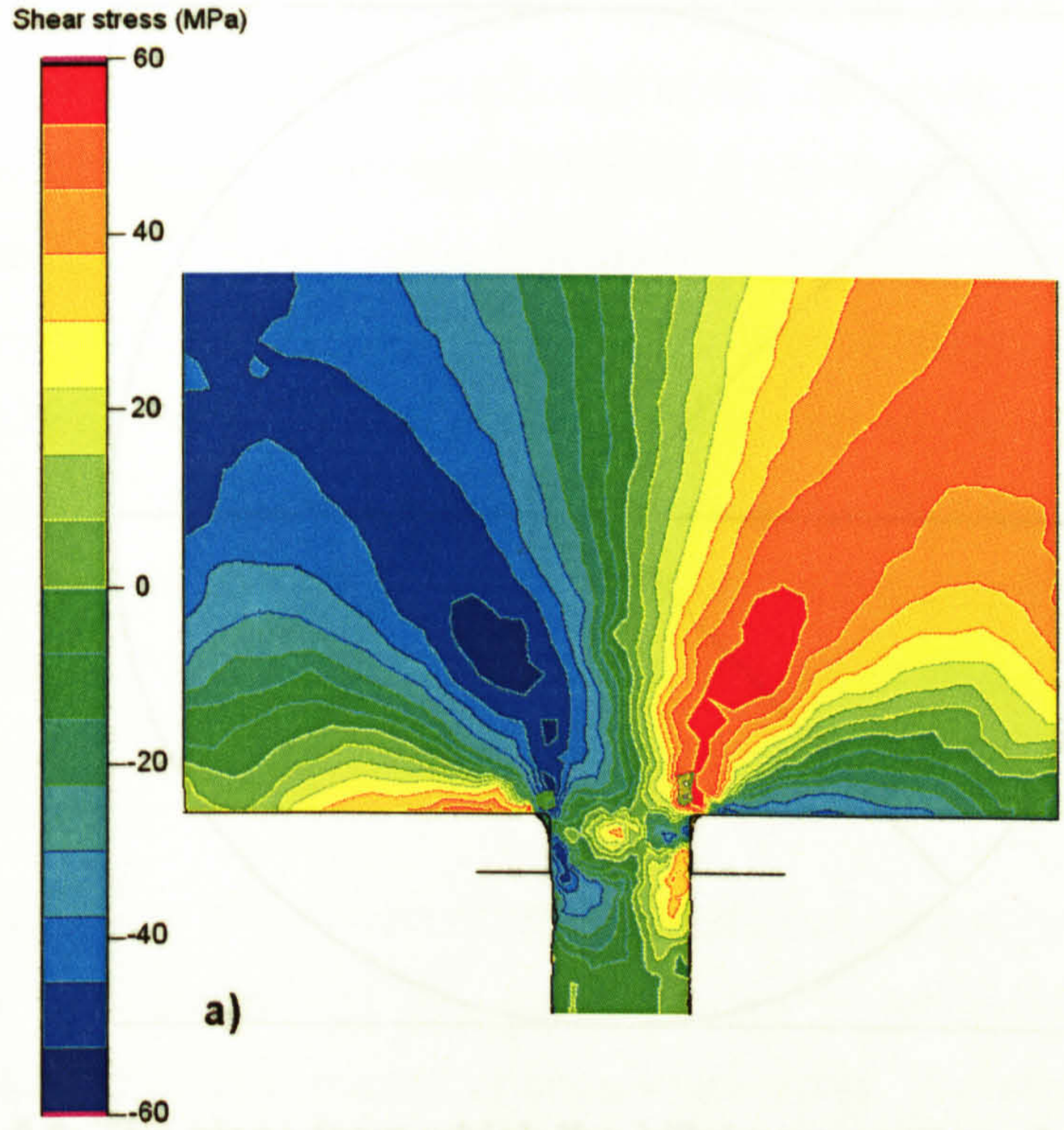

b)

Figure 5.7: T-section extrusion showing the asymmetry of material during quasi-static flow a): Shear stress. b): the corresponding experimental micrograph (After Subramaniyan [62]). (Initial velocity 3 mm/s)

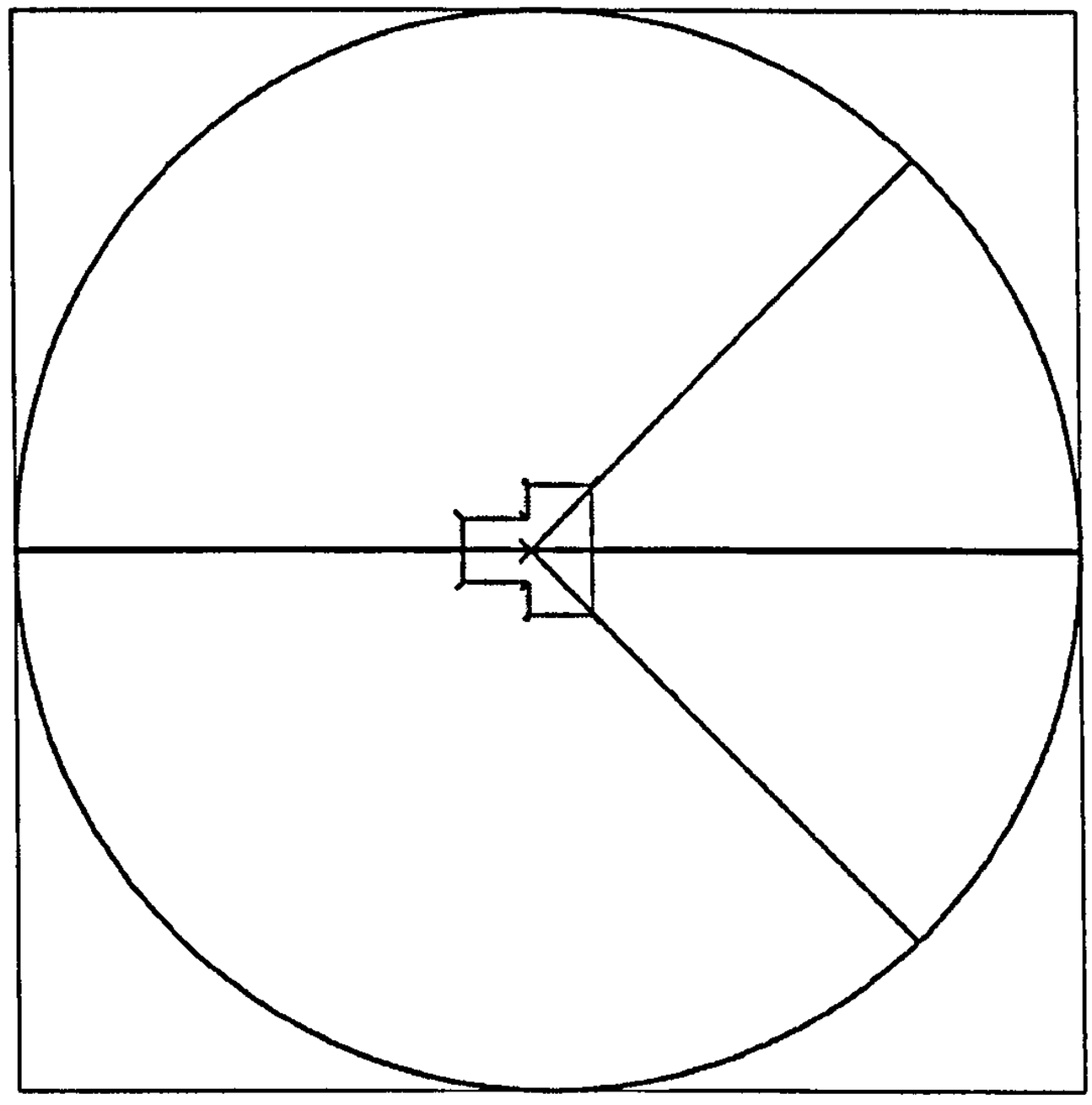

Figure 5.8: The plane from which the billet was sectioned used in the experiments and the simulation.

The material flow in the "T" shape remained slightly similar to that of rod and square extrusion. It can be seen clearly in Figure 5.7 that the region of the intense shear feeding the extrudate surface extends from the die face, adjacent to the die mouth, to the container/billet interface located towards the rear of the billet. However, a certain amount of asymmetry about the billet axis can be seen, especially near the dead metal zone as illustrated by the velocity profile in Figure 5.9. A similar behaviour was observed in the extrusion of the "U" section as shown in Figure 5.10, demonstrating that in terms of complexity of flow both sections "T" and "U" are the same. This irregularity about the billet axis is due to the inhomogeneous nature of the material flow encountered when extruding complex sections. The distance over which the material flows on the transverse and the longitudinal axis on both sides of the section geometry is different causing the asymmetry of the flow patterns. It is not unreasonable to expect a certain amount of asymmetry and complexity as the flow of the extruded sections becomes more and more asymmetric. The material flow does not remain in a radial plane

along the longitudinal axis of the die and this behaviour results in a non-uniform stress and strain distribution in the deforming material resulting in a slightly curved extrudate (Figure 5.11) that may require correct positioning of the exit section in relation to the entry section. In practice, however, even for the centric extrusion, the extruded product may exit bent due to the increased frictional resistance at the die land and the die bearing. Most often a straight product is achieved by adding die lands to correct the die, which in most cases will alter the material flow significantly. This could also explain the small differences observed between the experimental and simulated flow behaviour.

The complexity grows even further in determining the optimum location of the exit section of the extrusion die particularly in the three-dimensional (3-D) extrusion of shaped sections. Therefore investigation of the problems relating to the extrusion of non-symmetric shaped sections and the effect of their positioning in the die land area is of paramount importance as these sections are widely used. The positioning of the exit section not only affects the required extrusion pressure but influences considerably both the curvature of and the soundness of the extruded product. However, die correction is a vast subject and it is not a focus of this investigation and therefore it has not be considered in this thesis.

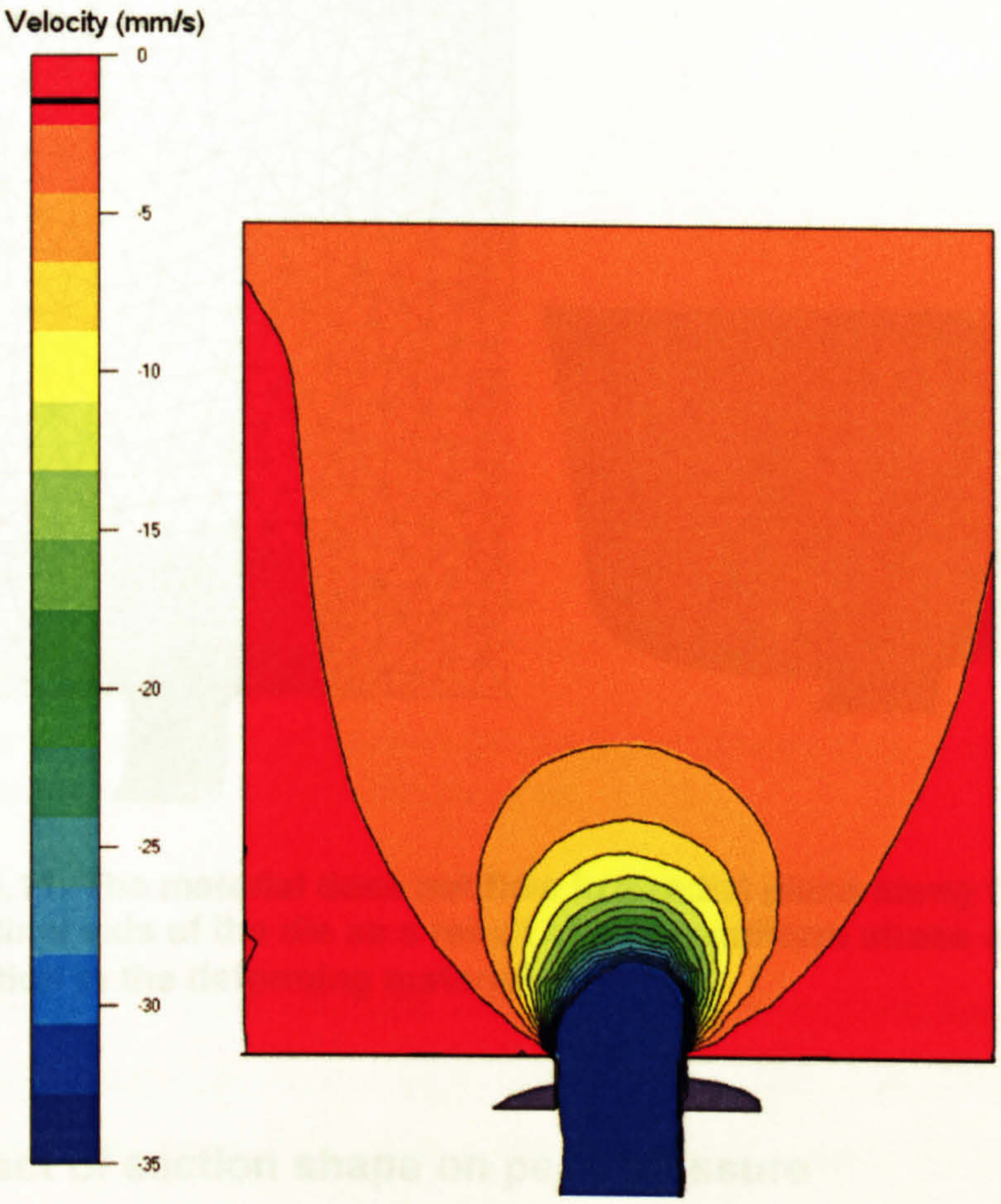

Figure 5.9: Asymmetry in material flow in the T-section represented by the velocity profile. (Initial velocity v=3mm/s).

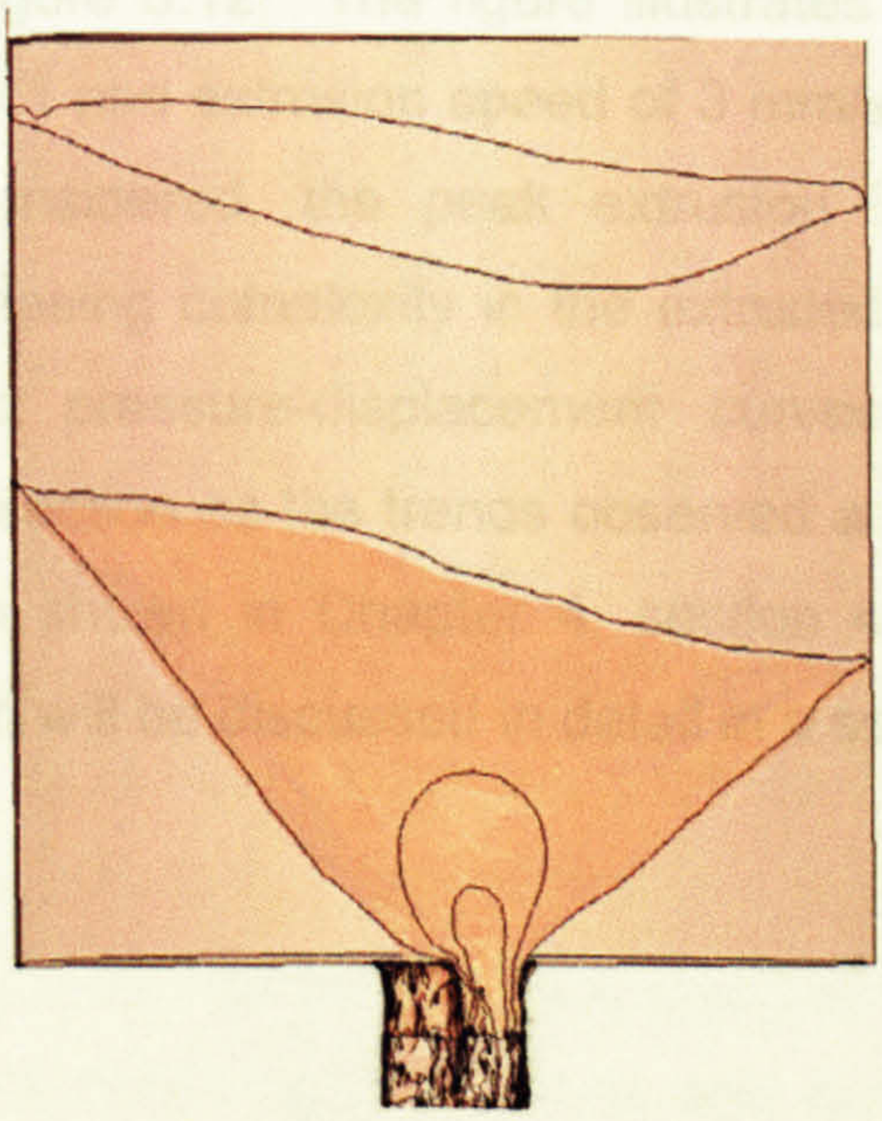

Figure 5.10: U-section extrusion showing the asymmetry flow during quasi-static deformation.

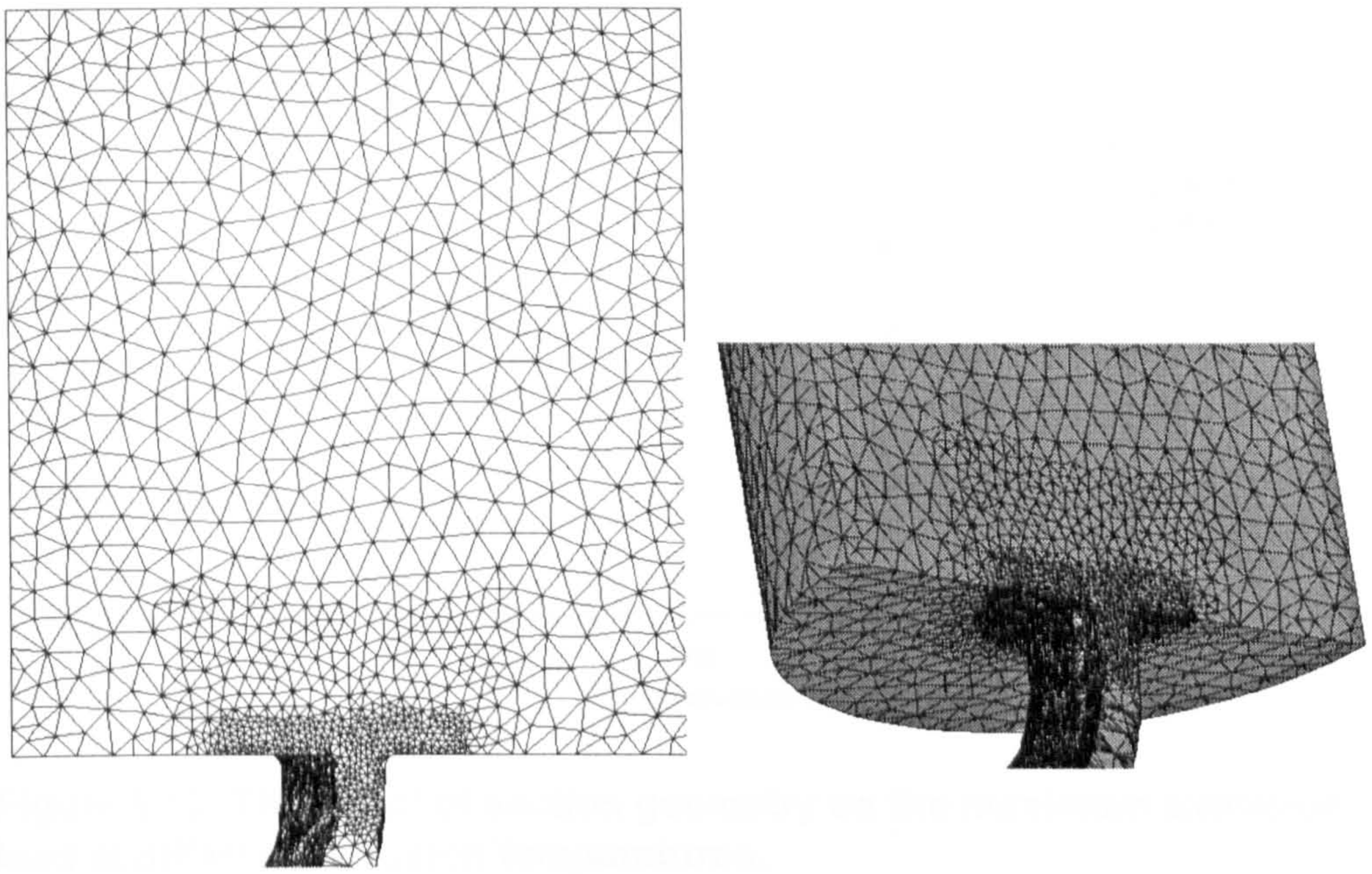

Figure 5.11: The material does not flow in a radial plane along the longitudinal axis of the die as a result of a non-uniform stress and strain distribution in the deforming material.

5.5 Effect of section shape on peak pressure

The effect of the die geometry on the computed maximum extrusion load is shown in Figure 5.12. The figure illustrates that for the same extrusion ratio of 40:1 and extrusion speed of 3 mm/s and over a range of temperatures considered, the peak extrusion load increment is increased with increasing complexity in the extruded section. It should be noted that the pressure-displacement curves have not been represented in this section as the trends observed are similar to that of round cross-section shown in Chapter 4, section 4.4, except for the tube-extrusion which will be discussed in detail in a separate section.

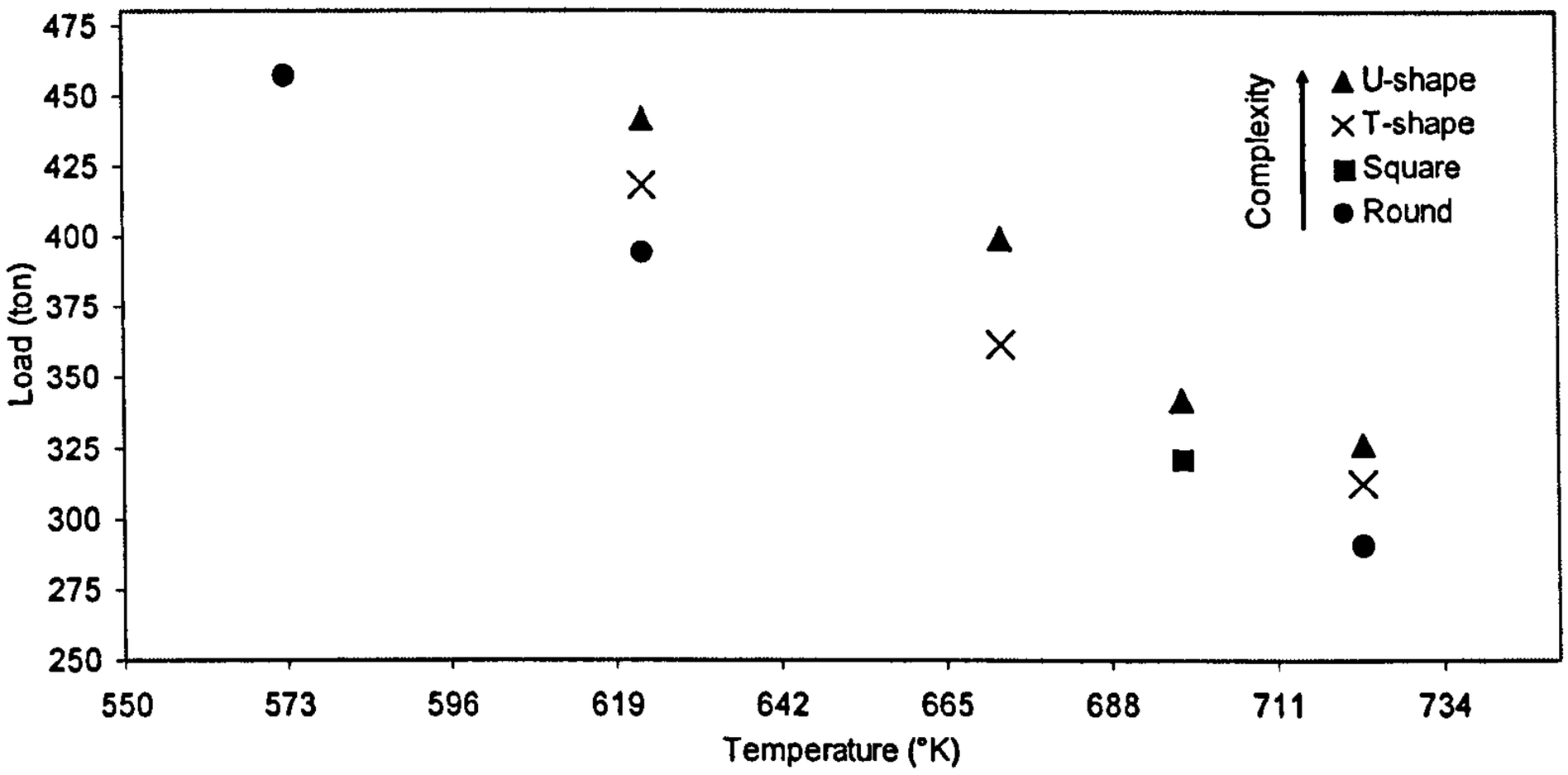

Figure 5.12: The effect of section geometry on the maximum extrusion load at different extrusion temperatures.

This increase in load with the increase in section complexity can be attributed to several interrelated reasons in which the complexity of extrusion increases the resistance to deformation. Primarily, the increase in load is required to overcome the increase in frictional resistance associated with the increase in the contact area in the die land regions. Secondly, after the peak pressure is reached, the deformation zone is established and an increase in complexity of the deformation zone is observed as shown in Figure 5.4, 5.6, 5.9 and 5.10. This becomes more intricate and larger in shape as the section geometry diverges from simple rounds to complex shapes. This is due to the inhomogeneous nature of the material flow encountered when extruding complex sections. The material approaching the die corners is divided, forming regions of divergent flow and as a consequence, promoting localised distortions at the die entry as illustrated in Figure 5.13 (for example "T" section). This material flow is associated with the bending of the flow lines into the die as a result of re-entrant corners similar to the events occurring at the inlet and outlet regions of the deformation zone. The extrudate surfaces also suffer a higher degree of deformation with the increase in section complexity, and as a

consequence a further load is required to overcome the region of intense shear feeding the extrudate surfaces and in particular at the narrow sides of a flat section.

Irrespective of the section geometry, as shown in Figure 5.14, the material forming the extrudate, originates from various locations in the deforming billet similar to those observed during the rod extrusion.

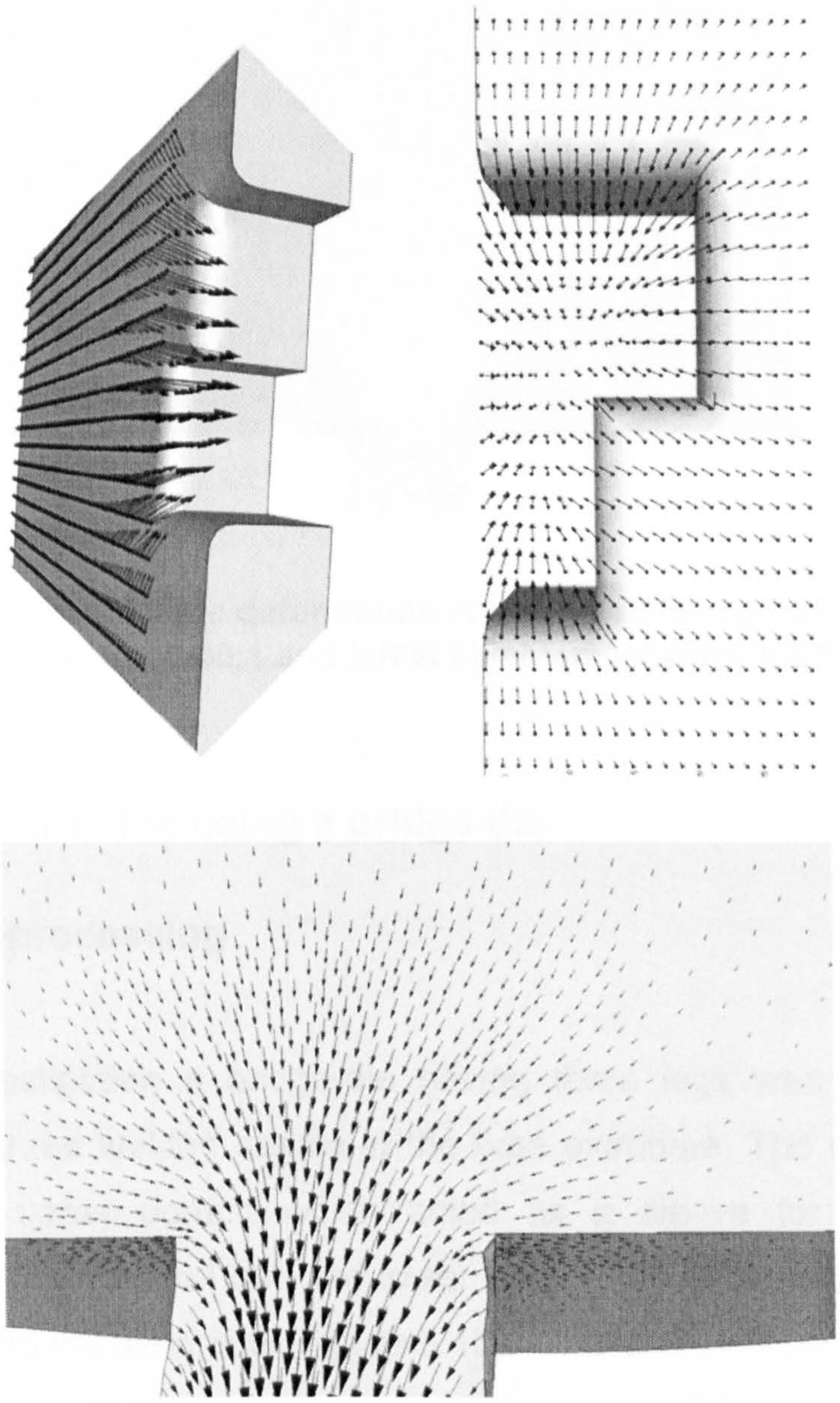

Figure 5.13: T- Section. Different views illustrating the bending of the material flow-lines at the die entrance.

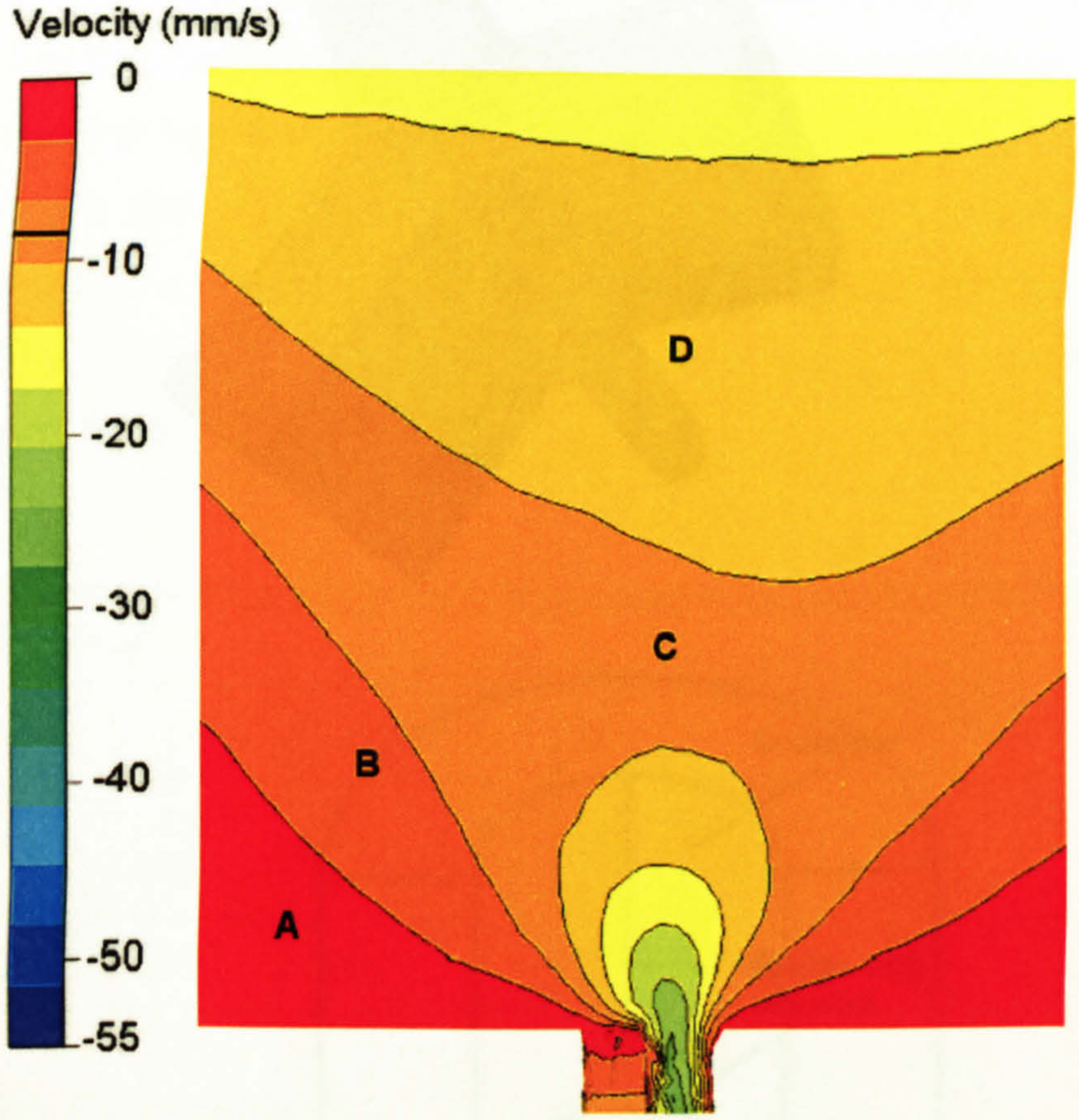

Figure 5. 14: Quasi-static deformation represented by the velocity profile U-shape. V= 3mm/s, R=40:1 and initial billet temperature 300°C.

5.6 Tube Extrusion using a bridge die

5.6.1 Pre-processing

In this investigation a bridge-die having three legs was used, thus producing three welded seams in the tube extrudate. The die had two parts; the upper portion which acted as a sleeve for the bridge supporting the mandrel and the lower portion which formed a welding chamber and the die orifice (Figure 5.15).

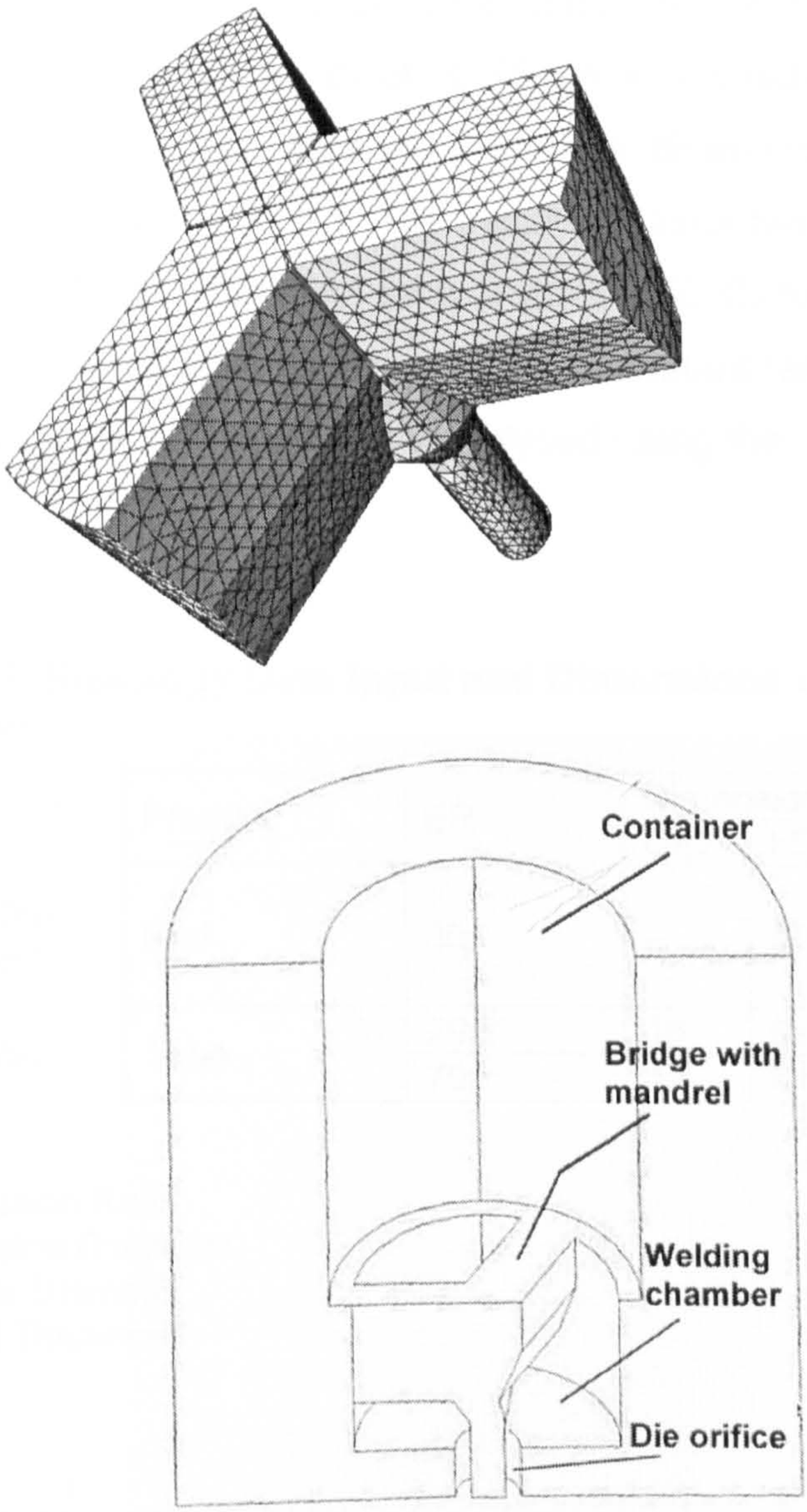

Figure 5.15. Bridge-Die and Bridge-die Mandrel Assembly.

5.6.2 FEM Models and Source of Experimental Data

The chemical compositions of the alloys AA2024 and AA6063 used in this investigation are shown in Appendix 3. All the experimental data are extracted from the literature [79,123]. Experiments were performed on a similar press as in the previous experiments.

The input data for the bridge-die simulation is summarised in Appendix 2. The dimension of the billet is 75mm in diameter and 100 mm in length. The rheological data input and the dimensions of the extruded tubes are given in Table 5.1. The initial container temperature was 50°C below that of the initial billet temperature (450°C) to simulate industrial conditions. The billet was extruded at a constant ram speed of 3mm/s. The mathematical models were analysed using the viscoplastic solution algorithm of FORGE3™.

Table 5.1: Rheology Data input and Dimensions used for Computer Simulation

Mat	T (°C)	Product	ER	Dimensions (mm)		
				O/D	I/D	WT
2024	300-450	Rod	30	-	0	-
6063	450	Tube	29.2	16	8	4
			70	12	8	2

ER: Extrusion Ratio
O/D: Outside Diameter
I/O: Inside Diameter
WT: Wall Thickness

In the bridge-die analysis, three boxes were defined in what is considered the most important areas in the billet during the deformation as shown in Figure 5.16. The first refinement was applied just before the material started to flow around the core support (mesh-box1). The second refinement was applied just before the material started to weld in the welding chamber (mesh-box2). The final refinement was applied just before the material started to flow through the die orifice (mesh-box3). The aimed mesh size refinement value of 1.5 mm was imposed for mesh-box 1&2 and a value of 1mm for mesh-box3. The average initial mesh size in the billet is 4 mm.

Notes:

Although some of the figures presented in the next section show illustration greater than 1/6 of symmetry, the analyses, in all cases, were conducted only for 1/6 of the model.

Most of the figures are more or less carefully defined in the discussion. In order assist the reader some of the terminology used more frequently to describe the features of the figures are;

Step: is used to describe the succession of metal flow in **Figure 5.17**

DMZ: is used to describe the location of dead metal zones in **Figure 5.18**.

Zone: is used to describe the heavy shear zones in **Figure 5.18**

Region: is used to describe the Pressure/displacement curve in **Figure 5.19**.

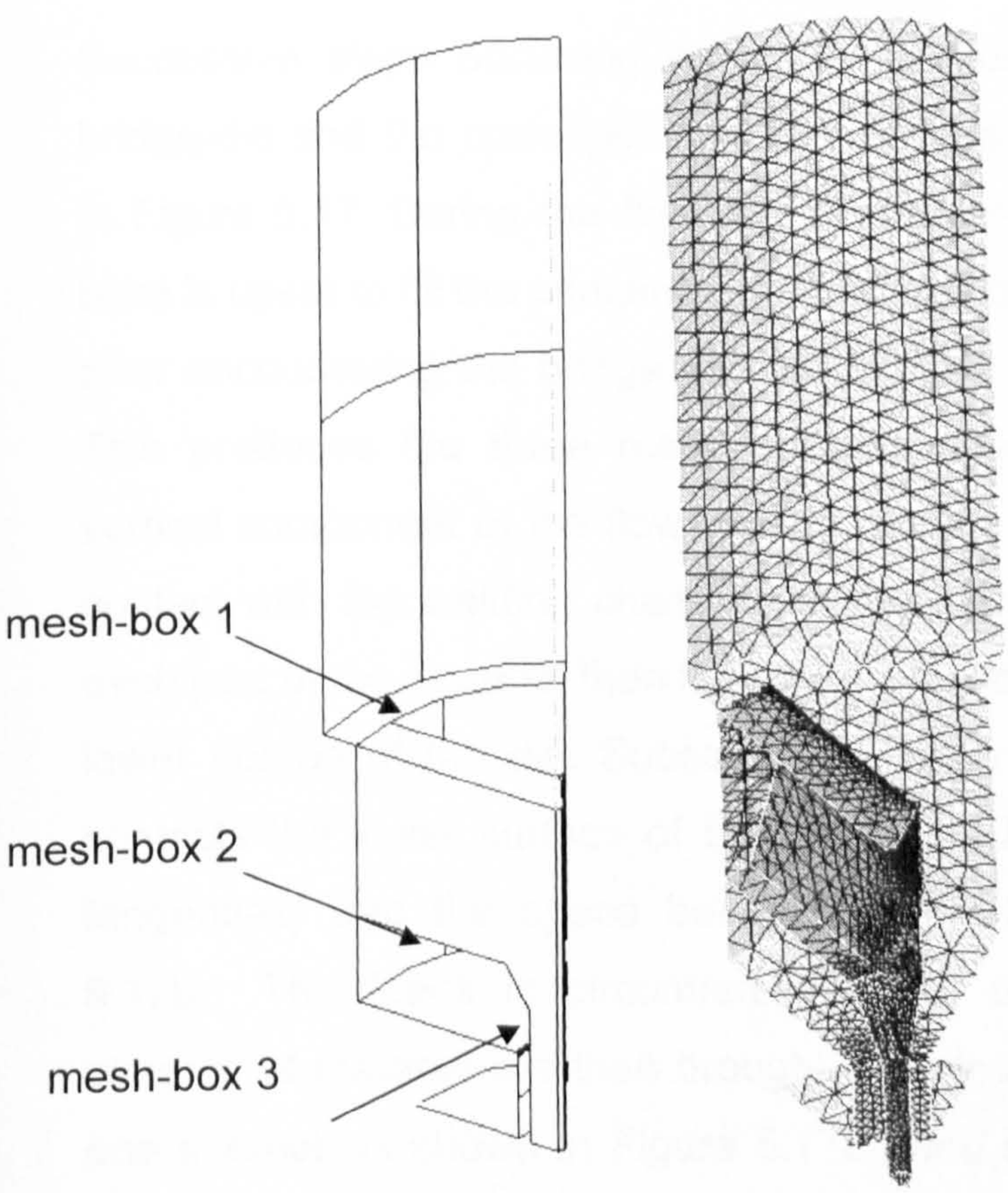

Figure 5.16: CAD Model and Mesh of the outer surfaces of Bridge-die

5.6.3 Metal Flow in Tube Extrusion

When extruding with a bridge die, there are many surfaces in contact with the material. The die has two parts, the upper portion which forms a welding chamber and the lower portion which consists of the die orifice. The metal during the extrusion process undergoes severe deformation to adapt to the new shapes following the streamline course of flow determined by the geometrical dimensions of the die. Therefore, the flow patterns during the extrusion process are very complex compared to a normal extrusion. There are three material flow streams of which each stream flows around the central axis. Hence, metal flow through a bridge-die can be described as a succession of four steps: division of the metal, circumferential extrusion, joining of the metal and formation of the tube.

Successive steps occurring during the extrusion of tubes using the bridge-die and the corresponding flow vectors at each step are shown in Figure 5.17. During the *first step* as illustrated in Figure 5.17a, the billet is upset to fill the container, the material divides into three sections after encountering the bridge and the surface of the upper die portion. This produces the three metal streams which initially show only a vertical component of the flow vectors. At this stage the metal is not in contact with the welding chamber. In the *second step* of the process, each part of the material then flows along the bridge before entering the lower portion of the die. Subsequently, each stream approaches and contacts the lower surface of the die i.e. welding chamber and flows tangentially into the space beneath the bridge as shown in Figure 5.17b. This leads to circumferential flow of the extrusion. These streams of material are then brought into close contact and bonded to one another as shown in Figure 5.17c (*third step*). Excessive shear is induced causing a large component of the velocity vector to become circumferential, thus permitting individual streams to bond. This solid-

state bonding produces seam welds in the extrudate. The formation of the weld lines is the results of solid state welding involving circumferential extrusion in which metal flow has been distorted severely beneath the bridge legs. The final stage is shown in Figure 5.17d (*fourth step*), the material in the welding chamber is extruded to form the tube effected by the mandrel attached beneath the centre of the bridge and suspended in the centre of the die orifice. It is clear that the flow through the bridge and over the mandrel is in very close agreement with experimental findings of Sheppard et *al.* [79].

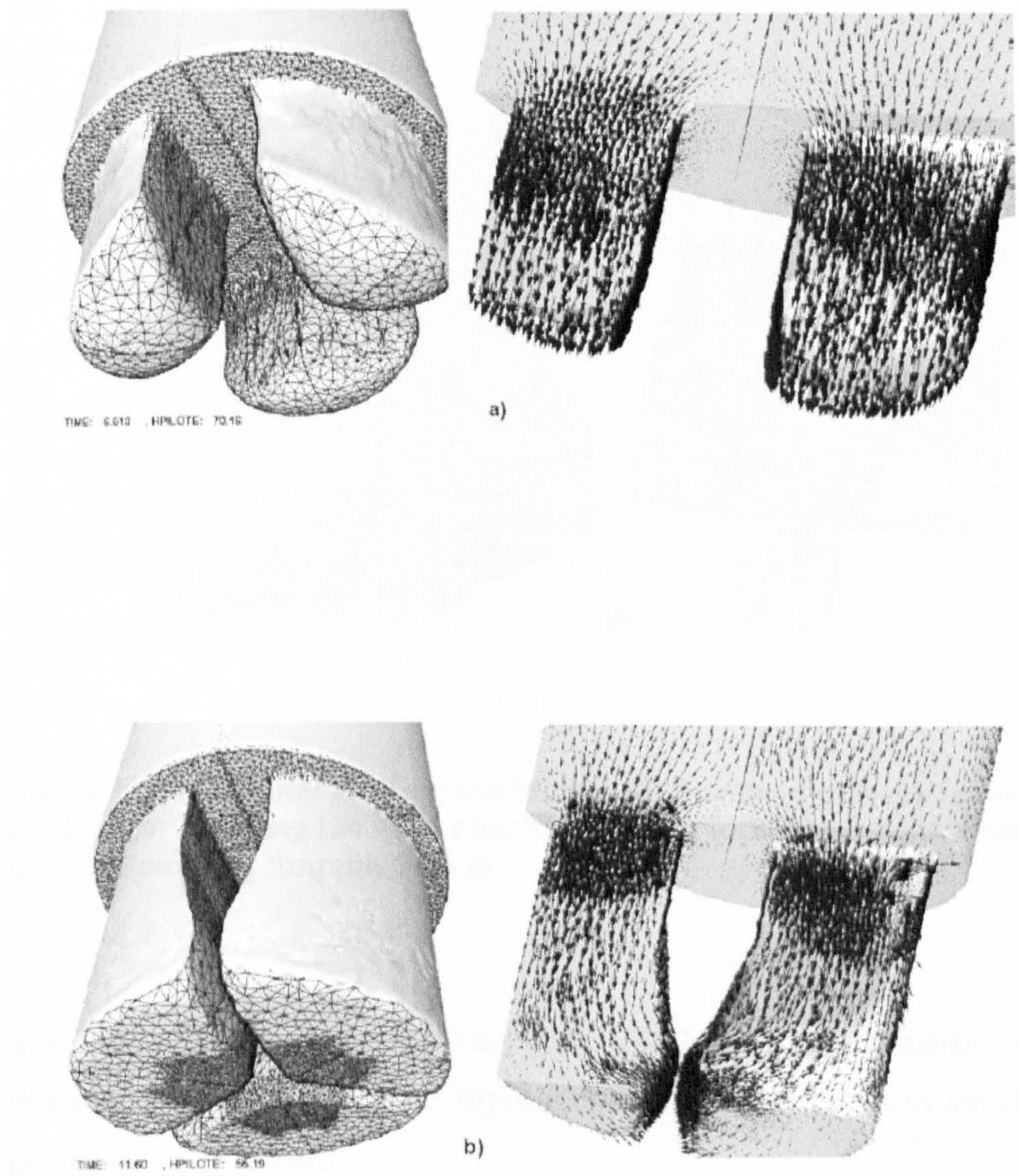

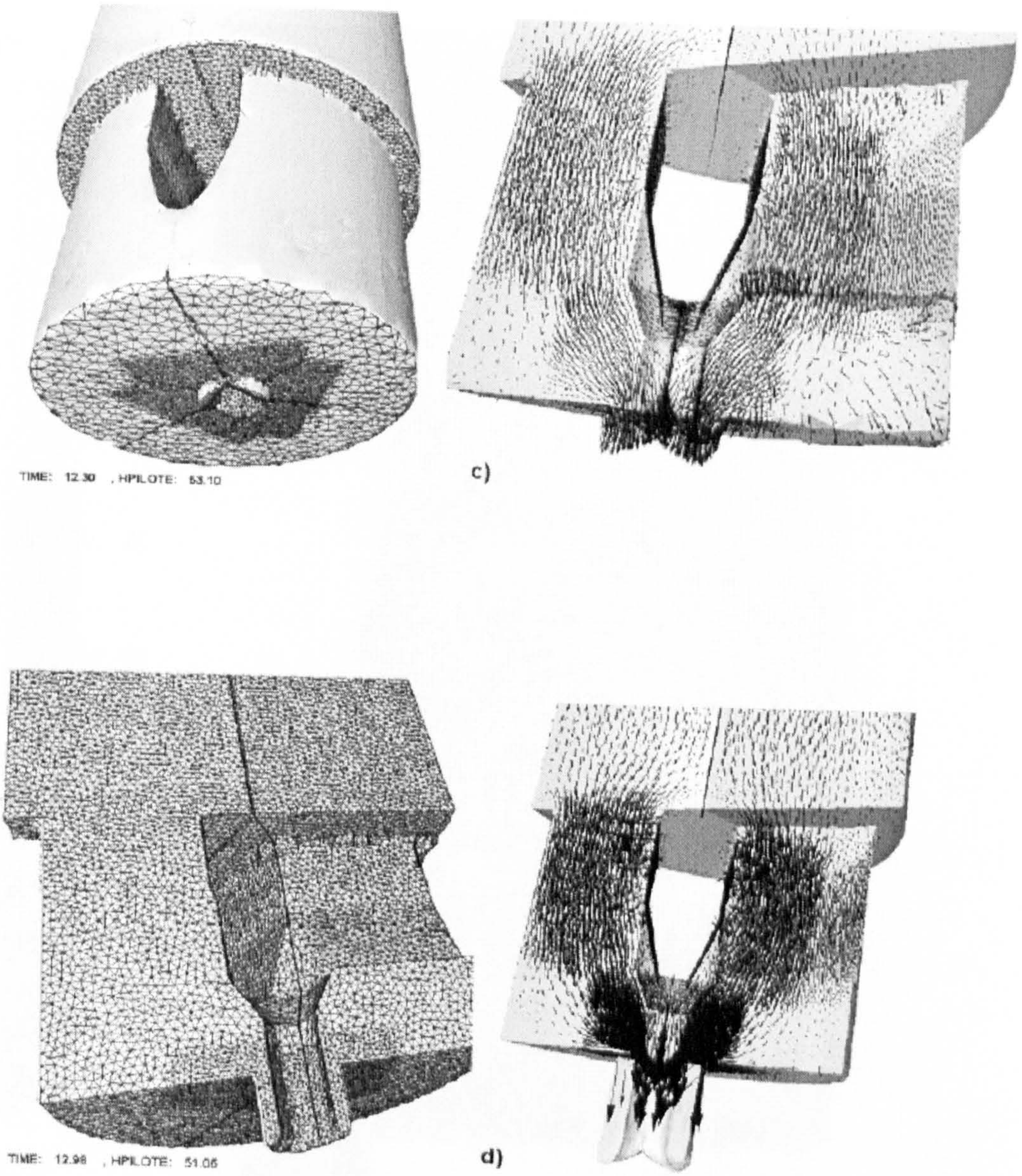

Figure 5.17: (a) Metal passing the bridge; (b) flowing sideways beneath the bridge; (c) filling the weld chamber and the formation of the weld line; (d) passing through the die.

The remaining dead metal zones (DMZ) in the die during extrusion are depicted in Figure 5.18 and represented by those zones in which the profile velocity is zero.

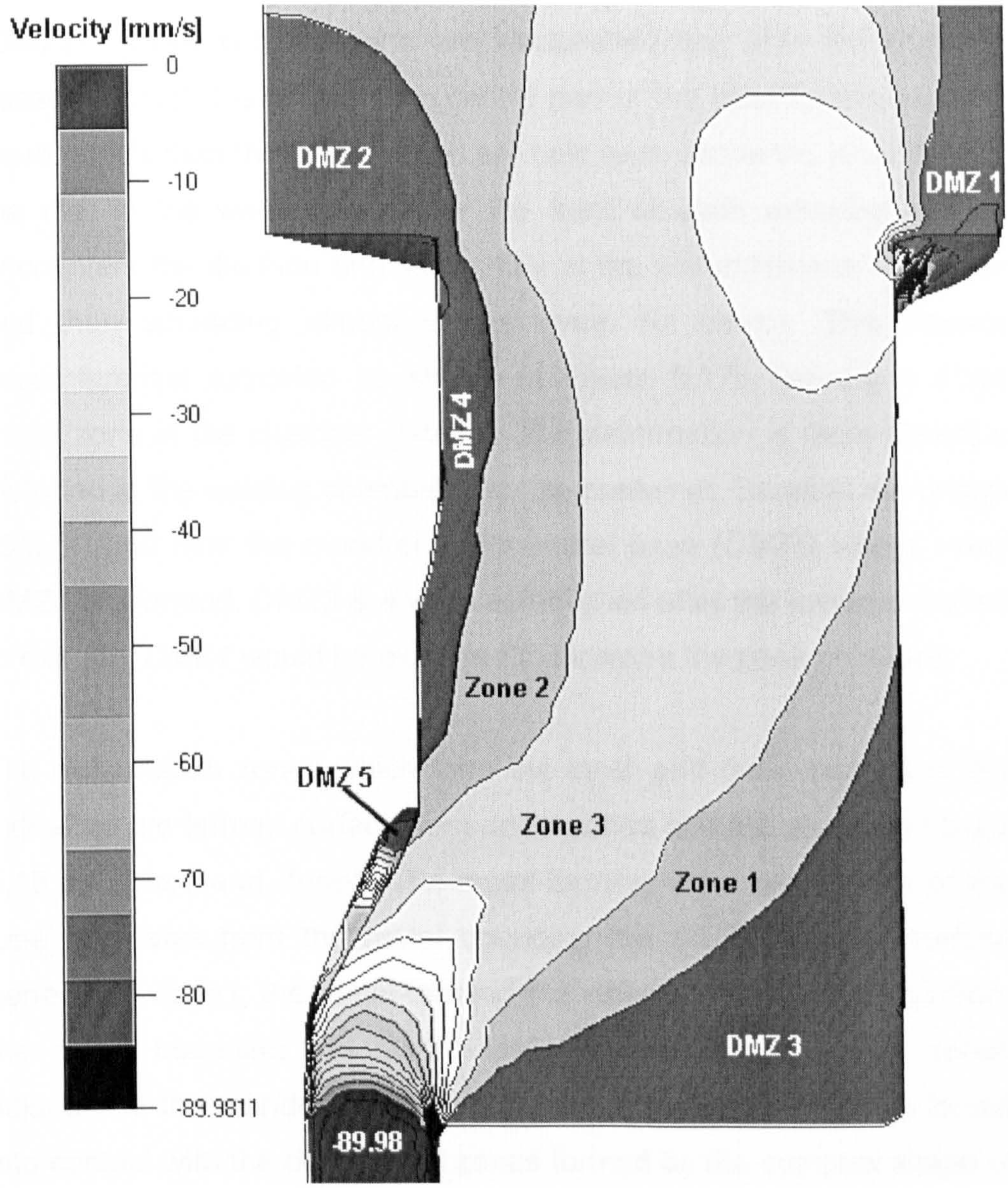

Figure 5.18: Dead Metal Zones formation represented by the velocity field.

This figure shows the dead metal zones in the die during extrusion. As the extrusion proceeds, there is a tendency for relative motion between the billet and the interfaces (container/bridge/welding-chamber). Because of high shearing forces generated at these interfaces, dead metal zones are formed during extrusion. This material remains sensibly stationary throughout the process. It can be seen that the

dead metal zones form in the container adjacent to the surface of the upper portion of the bridge-die (*DMZ*1) and the area above the bridge (*DMZ2*). These two locations are established just after the material passes through the bridge. The centre part of the billet travels forward more rapidly than the sides, which are held back above the shoulders of the die. In the welding chamber the front of each extruded stream encounters the die face and sticks, first at the circumference of the die and then spreading almost to the inner die corner. This causes circumferential extrusion as shown in Figure 5.17b, leaving a dead metal zone in the chamber (*DMZ3*). The deformation is more severely distorted in the welding chamber than the container. Beneath the bridge (*DMZ4*) and near the mandrel and mandrel base (*DMZ5*) where small DMZs are formed. *DMZ3* & *4* were established after the material started to extrude. *DMZ4* would be expected to increase the peak pressure.

The deformation zones which form the inner and outer surface of the extrudate are termed surface generation zones and are shown in Figure 5.18 as *Zone1* and *Zone2*. The metal-forming the outer surface of the tube originates from the metal bounding the *DMZ3 and* the surface generation *Zone1*; the metal-forming the inner surfaces originates from the metal bounding the *DMZ4* and the surface generation zones adjacent to the mandrel *Zone2.* At these locations, the metal is forced into contact with the dead metal zones formed by the complex shape of the die and the bridge. The metal-forming the centre of the tube originates from the metal of heavy shear in *Zone3*. Reference to Figure 5.18 also indicates that these zones originate from the interior of the billet in the intense shear zones. This is due to the interaction of *DMZ 3&4* with the *Zones 1&2* respectively and the position of greater deformation as the material approaches the die in *Zone3*.

5.6.4 Pressure Prediction Curve and Temperature Profile for Tube Extrusion

There is little in the literature concerning the pressure required for the extrusion of multi-holes or extrusion using bridge or porthole-dies. The prediction of peak pressure is critical because it determines the pressure capacity required to extrude the billet under extrusion conditions. An estimate of the pressure required to extrude through a bridge die may be produced by considering the operation as two separate extrusions. The pressure required to force the metal into the weld-die and the pressure required to extrude the tube from the weld-chamber.

The Pressure/Displacement curve is shown in Figure 5.19. The locus for the bridge extrusion is considerably more complex than normal rod extrusion, this is logical since there are four separate extrusion stages as shown in Figure 5.17, compared with the almost single operation required for rod extrusion. The curve can conveniently be divided into six regions.

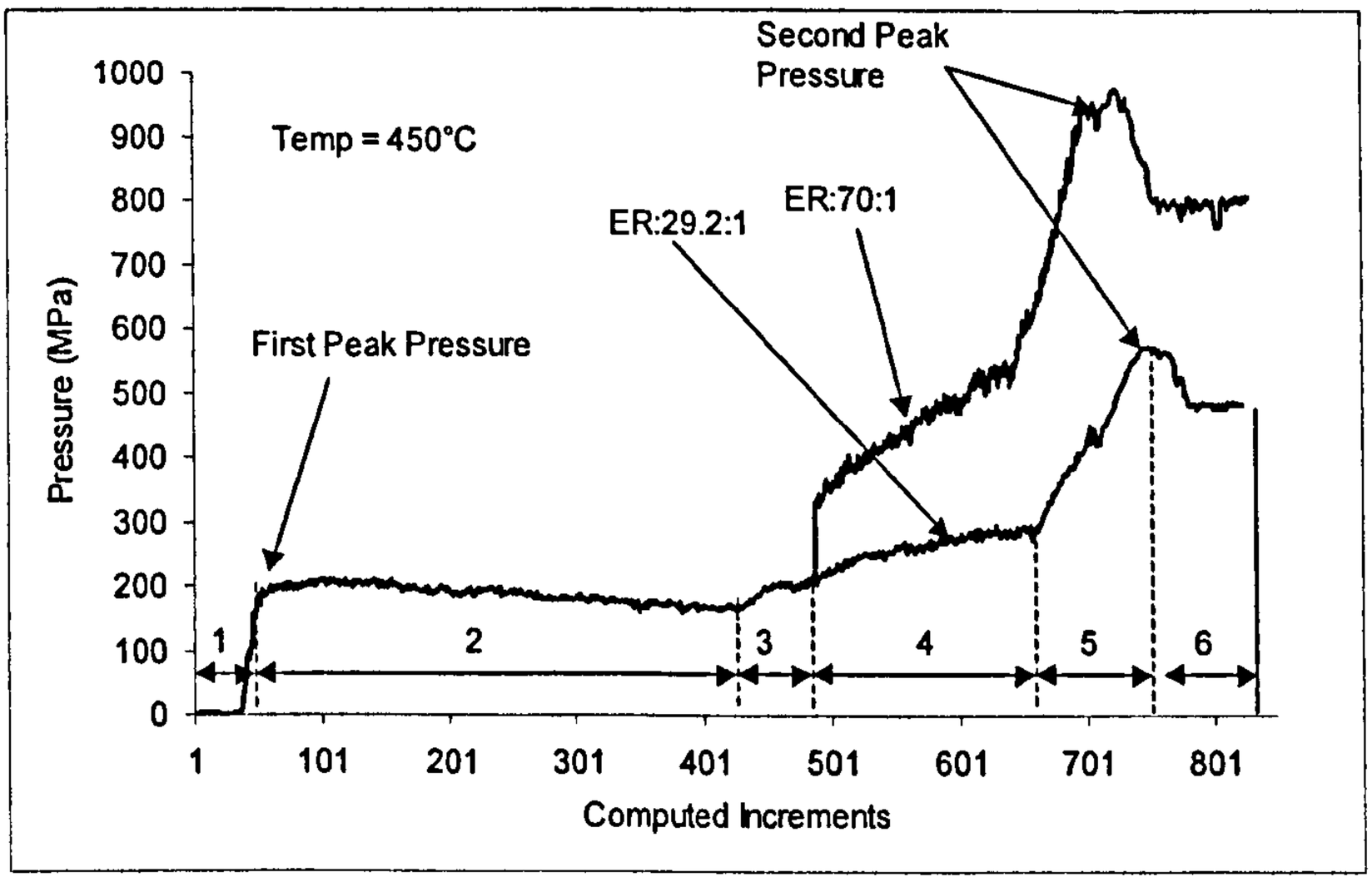

Figure 5.19: Pressure prediction curves

The billet is upset to fill the container and the pressure rises rapidly to the first peak value (first breakthrough pressure) after encountering the bridge and the surface of the upper die portion. Some material has already been extruded past the bridge. When the pressure has reached the first peak value, the dead metal zones in the billet (*DMZ 1&2* in Figure 5.18) have been established where the material is held back by the shoulders of the container and above the bridge (*region 1*, Figure 5.19). Pressure then decreases slightly from the first peak pressure as the material continues to pass the bridge and fill the die chamber. This is due to the slight rise in temperature in the billet caused by the work done when the material passes through the upper portion of the bridge (*region 2* Figure 5.19). As soon as the metal streams contact the welding chamber as shown in Figure 5.17b, a small incremental rise in pressure can be discerned followed by a steep rise in pressure when the metal fills the chamber. This pressure rise is needed to overcome the increase of frictional resistance associated with the increase in the contact surface area of the welding die to produce sufficient energy for the bonding process (*stage 3&4* in Figure 5.19). Subsequently, the pressure rapidly rises to the second peak value allowing extrusion to commence and to force the material through the mandrel/die gap. Some material has already been extruded through the die orifice and when the pressure reaches its peak value, the *DMZ 3, 4 & 5* are completely formed in the die chamber (*region 5* in Figure 5.19). The pressure falls from the second peak value and so-called quasi-static extrusion will be established. A gradual fall in pressure can be seen in this region which can be attributed to the decreasing billet length and hence decreasing friction and the decrease in flow stress due to the temperature rise. When the back of the billet approaches the bridge apex the metal ideally is cropped, allowing the introduction of a further billet. Therefore very little scrap is formed. This concurred with experimental observations by Sheppard *et al.* [76, 120].

The occurrence of the peak in the pressure displacement curve is the result of the combined effect of the "three maxima" flow formed from the three streams in the die chamber and the friction of the mandrel which produces the effective strain for the extrusion.

Sheppard and Wood [1, 3] and Sheppard [1], presented formulae for pressure prediction and is as shown below:

$$P = \bar{\sigma}\left\{0.17 + 1.86Ln\left[\lambda^2 R\right] + \left(\frac{4L_B}{D_B\sqrt{3}}\right)\right\} + \Delta p \qquad (5.4)$$

L_B represent the billet length, Z is the Zener-Hollomon constant and is the same as in equation (2.3). λ, is the shape factor, R, is the modified extrusion ratio. Δp being the additional pressure to initiate extrusion and for aluminium 6063 is equal to:

$$\Delta p = 6.62 + 0.921\frac{\left(Ln\,Z/A\right)}{\alpha n} \qquad (5.5)$$

It was found that equation (5.4) gives a good correlation between the predicted and experimental extrusion pressure data in aluminium alloys [1]. However, this has been proved true only over a limited range of extrusion conditions. There is no evidence to show the equation (5.4) can deal with, for example, a tube incorporating thin fins at internal or external surfaces. The pressure required for the *stage1, 2* & *3* in Figure 5.19 is dependent upon the extrusion temperature and the extrusion ratio of the metal passing the bridge. Furthermore, the pressure required for the *stages 4, 5* & *6* also in Figure 5.19, is dependent upon the rise in temperature from the previous stages in the welding chamber and the extrusion ratio of the metal leaving the chamber and passing through the mandrel/die gap. The rise in temperature is due to the heat

generated by the work done as the metal passes the upper portion of the bridge, the friction in overcoming the surface contact area inside the welding chamber and in the metal passing through the die to produce the tube.

Consequently, the variation in the pressure for the first three steps at different temperatures affects the total pressure required to extrude the tube. Equation (5.4) does not take into account the temperature rise during the first three stages and is based on initial billet temperature. Equation (5.4) is derived from an axi-symmetric upper bound solution and thus cannot be as accurate as the FEM solution (which is a refined upper bound). Furthermore, in equation (5.4) and in general all empirical formulae, it may not be possible to account for the geometrical complexity of the dies other than simple tubes and the intricacy of the consequent flow could present a problem. Hence, FEM codes which by definition are analytical have great advantage over semi-empirical formulae in predicting the main parameters before and after the so-called steady-state is achieved.

In this investigation, the value of the peak pressures, 623 MPa and 975 MPa for the two extrusion ratios 29.2:1 and 70:1 respectively agreed with those observed experimentally predicting a 5% and 4% difference respectively (593 MPa and 937MPa). The multi-step extrusion distorts the metal flow more severely and increases the friction due to an increase in the area of billet/tool interface. Therefore, the complex shear leads to an increase in the pressure; particularly for the high extrusion ratio.

Complex thermal exchanges begin as soon as the extrusion commences. The most critical temperature is clearly the die exit temperature of the extrudate, which depends on heat balance history commencing at the upsetting stage of the operation. The temperature evolution simulated in the tube extrusion is shown in Figure 5.20.

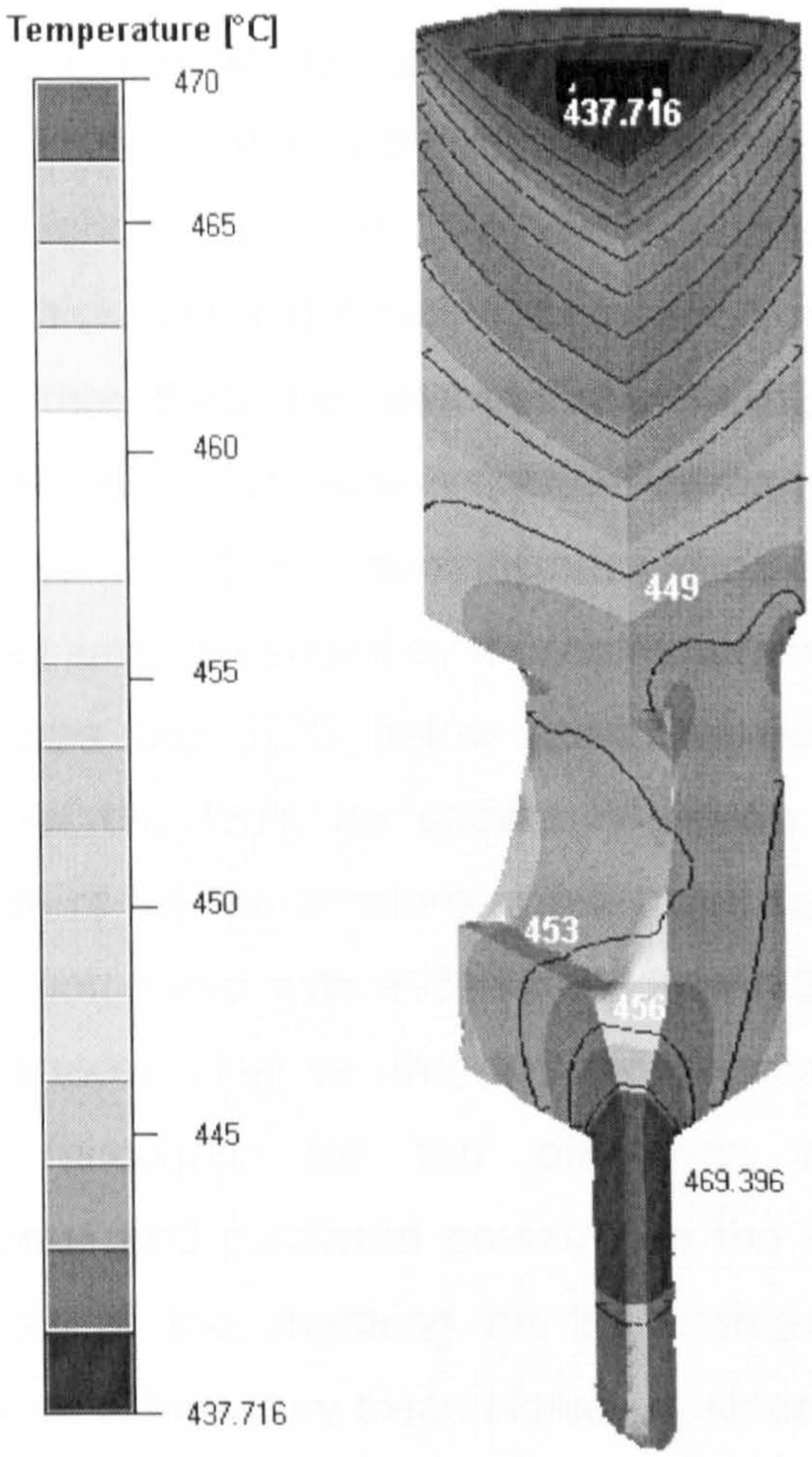

Figure 5.20:Temperature evolution ER 29.2:1.

The figure shows that there is a small increase in temperature of the billet after encountering the bridge and the upper die (453°C for both extrusion ratios). The maximum temperature occurs at the die exit and it is 470°C and 493°C for the extrusion ratios 29.2:1 and 70:1 respectively. This is caused by the work done as the material flows through the die orifice and by the friction which is converted into heat at the die exit during extrusion and consequently results in an increase in the extrusion temperature. The heat generated near the die exit increases the local temperature. However, the temperature in the billet at the container surface thus appears lower than the actual temperature

(449°C). Unlike the FORGE2® program, where the meshing of the tooling through the thickness is possible for coupled thermo-analysis as illustrated in Figure 9, in the FORGE3® program, the tooling can only be surface meshed (rigid die). This results in the contour appearing to be of infinite thickness and hence promotes a slightly slower apparent heat exchange rate. It can be seen from Figure 5.21a for the 2-D simulation using FORGE2®, that there is thermal exchange between the billet and the container wall. It also demonstrates, there is a temperature increase at the billet surface caused by friction at the container wall (initial tooling temperatures are 50°C below the billet temperature). Ignoring the meshing of the tools as shown in Figure 5.21b gives a differing distribution of the temperature at the interface and an exit temperature of 485°C compared with 495°C in Figure 5.21a when we are able to mesh the tools. Hence, the 10°C difference in the exit temperature probably accounts for the difference observed between the experimental and predicted pressure in the 3-D tube extrusion. The critical role of tool meshing on the temperature evolution and exit temperature is thus very clear. However, since the container and the die were at 50°C below the initial billet temperature (450°C) for the tube extrusion, they acted as a heat sink to the metal. Consequently the boundary conditions for heat flow in the tooling might have a significant effect on the cooling of the billet. Although we might expect a higher temperature rise than observed, the reader should recall that the velocity of the ram was just 3mm/s, which is slow for this alloy.

The bridge-die would, however, be better modelled by assigning to it a higher temperature than 50°C below the initial billet temperature. There is, however, no doubt that the assumed temperature of the tooling resulted in a lower final material temperature. Hence, a slightly greater force was needed to extrude the material. The temperature rise was expected as a result of the work done in upsetting the billet, and the work done against friction between the material and the tooling during extrusion. These contribute only relatively small changes to the mean

temperature due to the heat flow to the container, but the effect of friction on the surface temperature is more significant. Despite these minor errors in boundary conditions the results are very close to the experimental data. However, this might be the subject of further research.

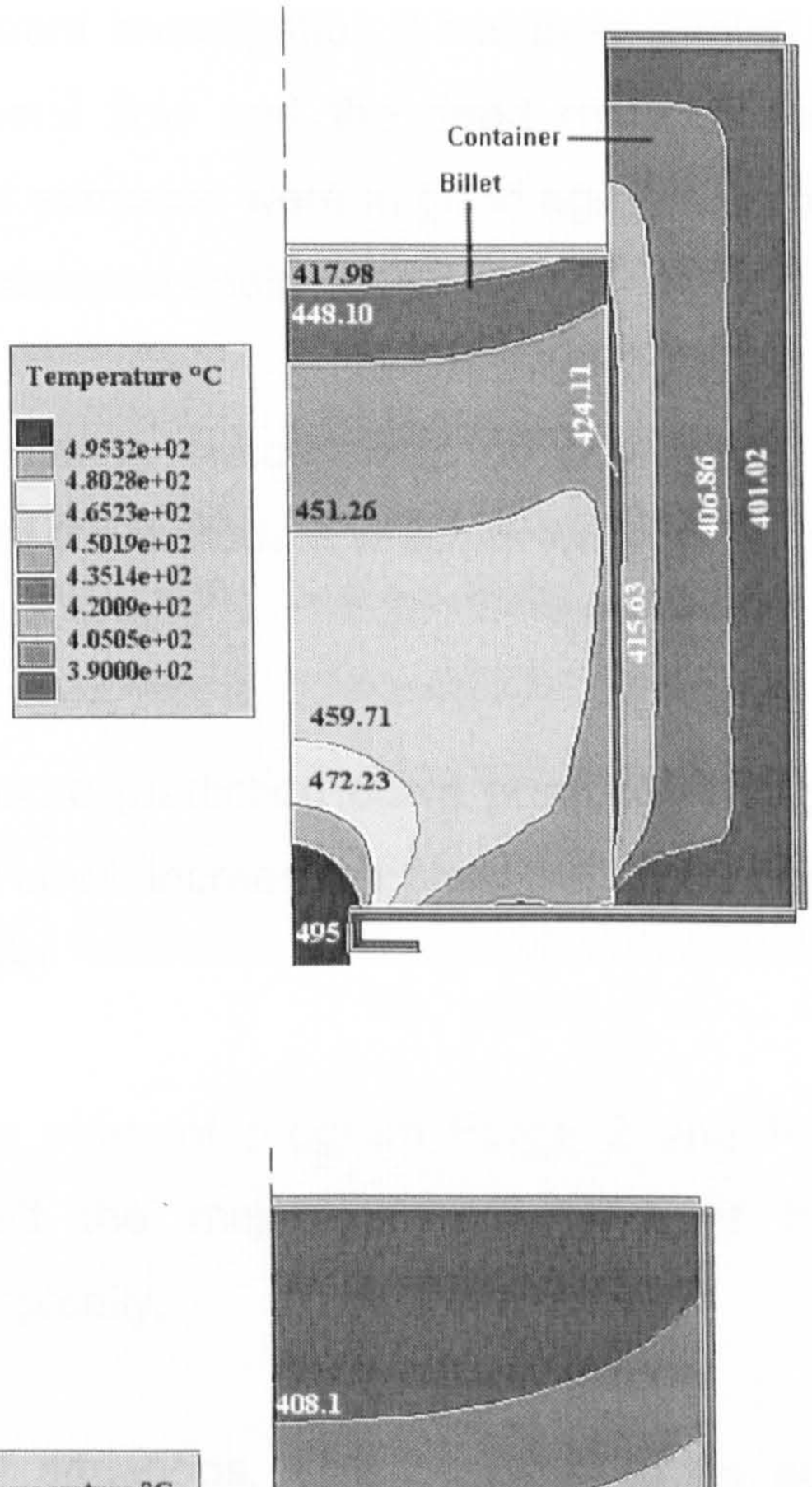

Figure 5.21: Temperature evolution for rod extrusion (450^{O}C initial billet temperature, ER. 30:1) a) meshed tools b) rigid tools.

5.7 Conclusions

1. The FEM Code Forge 2 & 3 with the programmed hyperbolic-sine function provided a suitable model for simulation for simple rod extrusion and complex tube profile.

2. In the current investigation it has been shown that the prediction of the metal flow and the dead metal zone formation of the bridge-die extrusion were in good agreement between simulation and experimental findings.

3. FEM simulation successfully predicted the origin of differing sections of the extrudate which flows from varying portions of the deformation zones.

4. The pressure prediction curve produces two peak pressures as well as a small increase in pressure rise when the metal fills the welding die.

5. The finite element program Forge 2 and Forge 3 appears to predict all the major characteristics of the flow observed macroscopically.

6. Empirical equations, which appear to be adequate to predict pressure requirements, will not predict either metal flow or final temperatures. There is therefore the requirement to refine the FEM approach by further research.

CHAPTER 6: SIMULATION AND CONTROL OF MICROSTRUCTURE EVOLUTION

6.1 Introduction

It is accepted that the process variables, temperature and speed (strain-rate), determine the acceptability of surface quality in the extrudate and the productivity of the extrusion process. It is these two variables (exit temperature and ram speed) that are considered the most crucial and decisive factors in producing the extruded product. Acceptable surface quality is only obtained if the exit temperature lies within close limits specified for each alloy and depends upon stress conditions obtaining near the die land regions. If the tensile friction force exceeds the fracture stress of the material, then some tearing is encountered. Additionally if the heat generation near the die land area increases the local temperature in excess of the solidus point, localised melting can occur which is referred to as hot shortness and produces severe cracking of the surface. This is a specific problem during extrusion of hard aluminium alloys, which have to be extruded at relatively slower speeds (i.e. ram speeds of 3-7 mm/s). The safe hot-working temperature range of any hard alloy is comparatively narrow and it is important to control the variables such that the final temperature of the extrusion does not exceed the incipient melting temperature of that particular alloy or result in excessive surface cracking. Hence, correlation between surface quality and temperature-compensated strain-rate or (Z) parameter should be the focus for an optimum extrusion condition.

One should note that unacceptable surfaces may be produced at temperatures below that of incipient melting because areas surrounding a particular phase will fracture before that temperature is reached.

The objective of this investigation is two-fold, firstly is to validate a model for the subgrain evolution during the process and secondly, to use the understanding of such a model for the control and interpretation of the effects of strain-rate and temperature on subgrain evolution. The calculated histories of temperature and subgrain size during deformation are presented. Finally a modified form of the isothermal extrusion process is proposed to control the extrudate properties.

Controlling the substructure distribution in the final product is a challenging and demanding task for the aluminium extrusion industry. This can only be achieved when the microstructure evolution during the process is fundamentally understood.

6.2 Modelling of subgrain size

The microstructure of aluminium alloys during hot deformation consists of subgrains within the original grain formed by a dynamic recovery process. Dynamic recrystalisation (i.e. during the process) is limited to just a few high Magnesium (Mg) containing alloys. In extrusion, the final substructure in the extrudate material has a significant influence on mechanical properties i.e. the strength, ductility, texture, etc. Thus, knowledge of the evolution and the distribution across and along the extrudate section of subgrain size during the extrusion process are critical for quality control.

6.2.1 Experimental data and finite element analysis model

In this section, simulation has been carried out to study the final substructure distribution in two dimensions in a 1%Cu alloy. The alloy's constitutive equation constants is given in Appendix 2. The predicted results are compared with observations on substructural measurements taken from Vierod's [63] experiments on a partially extruded billet.

The chemical composition of the alloy used in this investigation is shown in Appendix 3. All billets were extruded from a 75mm diameter container using flat faced dies having a die land length of 5mm. The billet length is 95mm. The ram speed and the initial billet temperature were 6.7mm/s and 325°C, respectively. All subgrain sizes were measured by using a Phillips EM301 microscope at 100 kV. The averaged subgrain size was evaluated by measuring the long and short dimensions of a subgrain. At least 100 subgrains were measured from each specimen. The process conditions applied in this investigation are summarised in Table 6.1.

Table 6.1: Process conditions

Billet Size (mm)	R	v (mm/s)	BT (°C)	CT (°C)	DT (°C)	RT (°C)
Ø73.5x95	40:1	6.7	325	275	225	225

R: Extrusion ratio
v: Ram Velocity
BT: Initial Billet Temperature
CT: Initial Container Temperature
DT: Initial Die Temperature
RT: Initial Ram Temperature

6.2.2 Subgrain size evolution

The relationship between the subgrain size and the deformation parameters in the steady-state regime for direct extrusion was given by [63].

$$\delta_{ss}^{-1} = -1.747 + 0.096 * LnZ \qquad (6.1)$$

where δ_{ss} is the steady-state subgrain size, and (Z), is the Zener-Hollomon parameter. In order to restrict the computation of the subgrain size to the steady-state regime, equation 6.1 is initiated just immediately after the peak pressure is established.

The approach in which the Zener-Hollomon parameter, Z, was calculated to predict the change in structure during deformation in Equation (6.1), is similar to that in Chapter 4, section 4.6.3. The use of the instantaneous strain-rate cannot describe accurately the changes in structure during deformation, because the nodal strain-rate varies considerably from node to node during discretisation. Besides, the major point here is that we are forced to use an average value of (Z) because the specific nodal strain-rates do not, over much of the volume, include i.e. the presence of subgrain and are outside the experimental values from which the constitutive equation was computed. It is thus necessary that if equation (6.1) is to be used to describe the change in subgrain size, an average value of strain-rate of carefully selected areas must be used.

The computed histories of temperature and subgrain size are shown in Figure 6.1. The billet temperature increases rapidly at the beginning of the extrusion. As previously stated in Chapter 4, this increase in the billet temperature is the consequence of the production of heat

generated by the deforming material to enable breakthrough at the die orifice, and to generate the dislocation density necessary to form the deformation zone and the shear deformation of the billet at the interface. Therefore heat is conducted from the deformation zone toward the rear of the billet and results in an increase in overall temperature. Subsequently, this is followed by a slow decrease for the remainder of the ram stroke. This is due to less heat being generated from the mechanical work done and the decrease in billet length. A total temperature rise of 142°C is observed for an initial extrusion temperature of 325°C with an extrusion ration of 40:1. The two curves, temperature and subgrain size in Figure 6.1, exhibit a similar behaviour during the deformation. The change in the subgrain size evolution during the process cycle is attributed to the temperature changes during the process and subsequently the changes in the (Z) parameter (Temperature-compensated strain-rate).

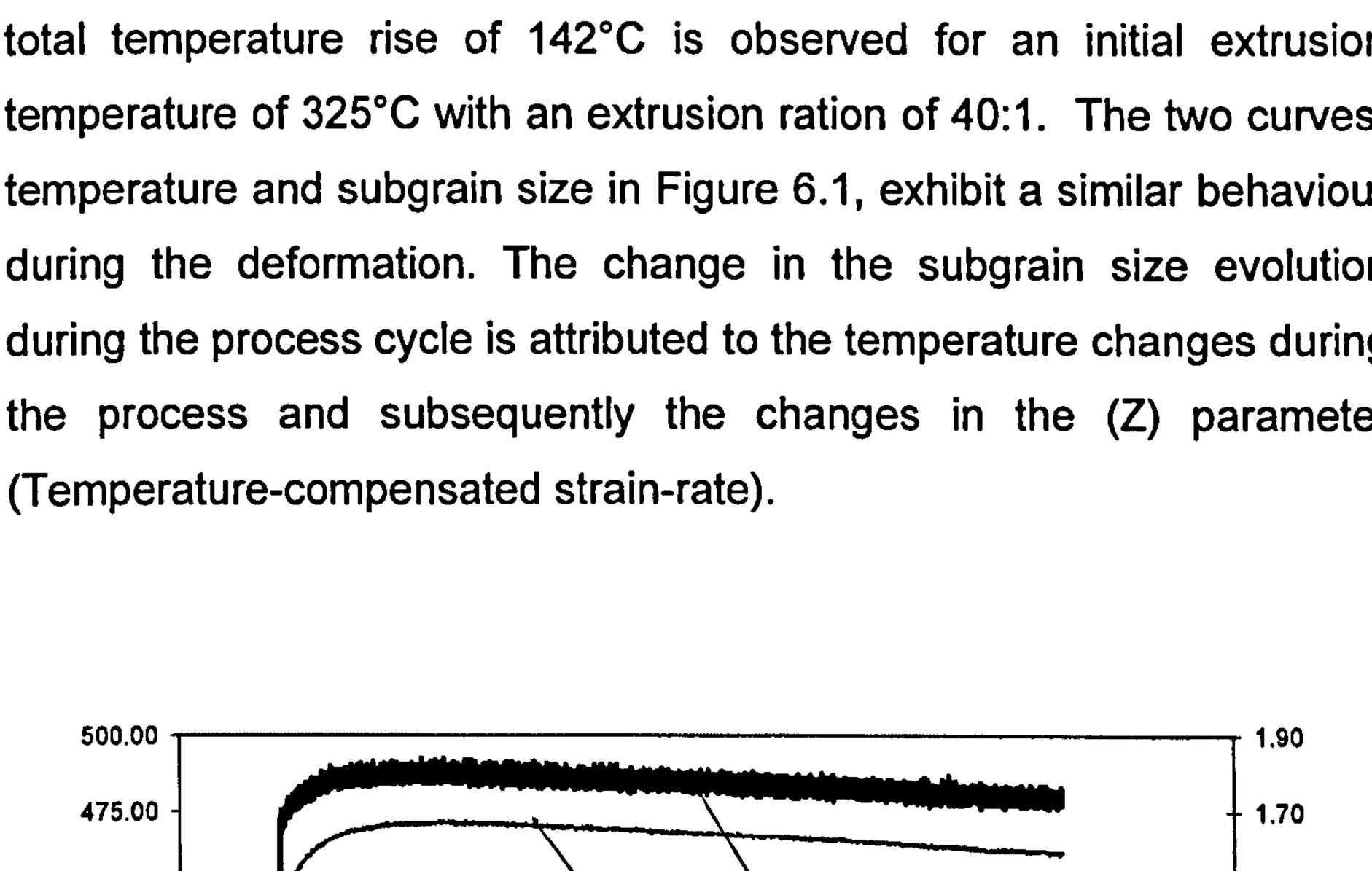

Figure 6. 1: Computed histories of subgrain size and temperature evolution during the process cycle

In order to examine the flow patterns and determine the flow lines during steady-state extrusion, billets were extruded to half their length. The flow lines were determined by Vierod [63] from consideration of the upper bound technique. The measured and the predicted subgrain size were taken along the flow line at different positions in the container as shown in Figure 6.2 and listed in Table 6.2. The approximate measurement corresponding to the steady-state subgrain size taken along the flow line is also illustrated in Figure 6.3.

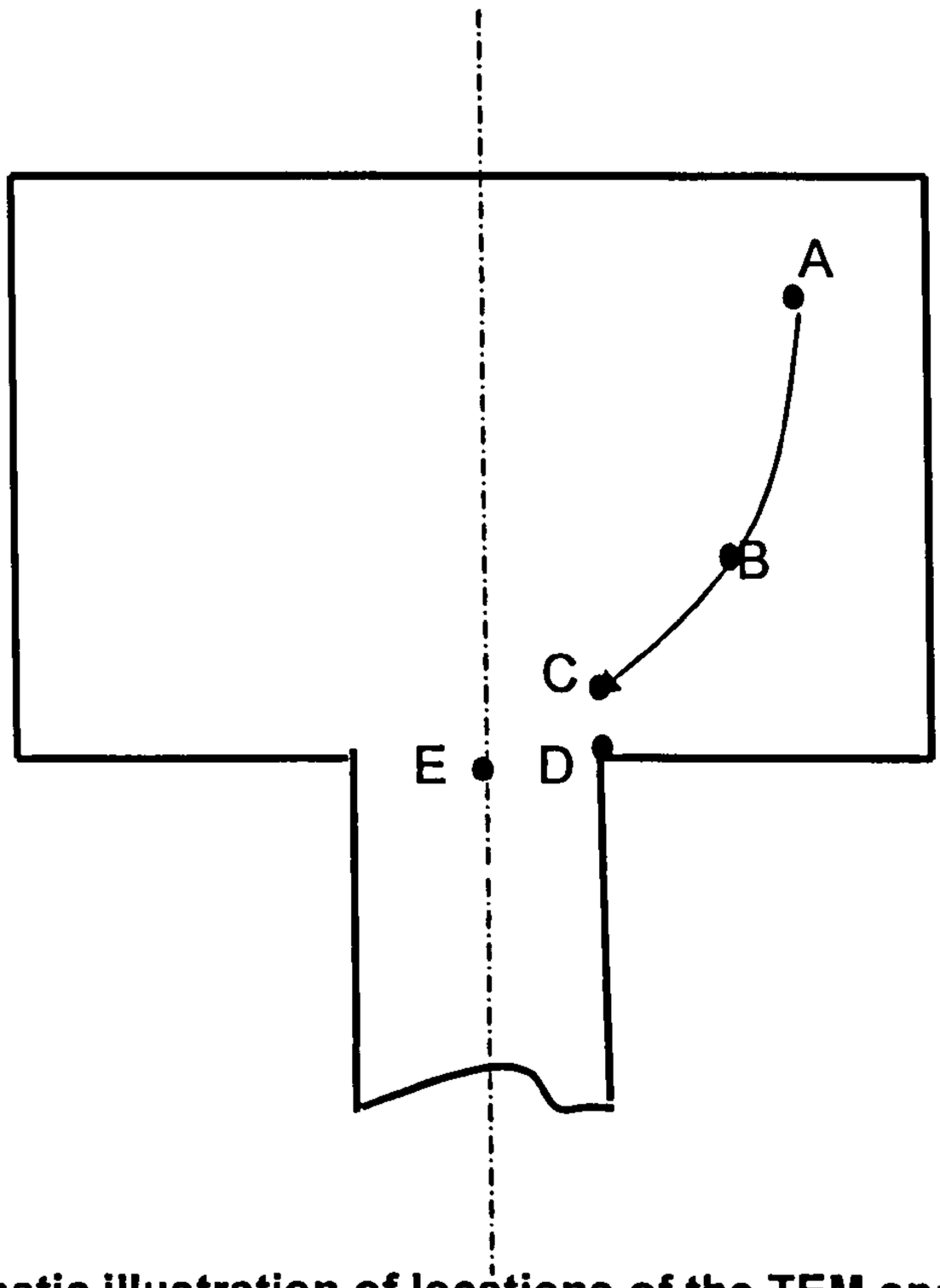

Figure 6.2: Schematic illustration of locations of the TEM specimens

Table 6. 2: Measured subgrain size

Location	Experiments (μm)	Error (±)	Predicted (μm)	Relative Error (%)
A	1.27	0.19	1.31	3.15
B	1.38	0.11	1.43	3.62
C	1.36	0.21	1.46	6.6
D	1.88	0.12	1.84	2.12
E	1.49	0.25	1.52	2.01

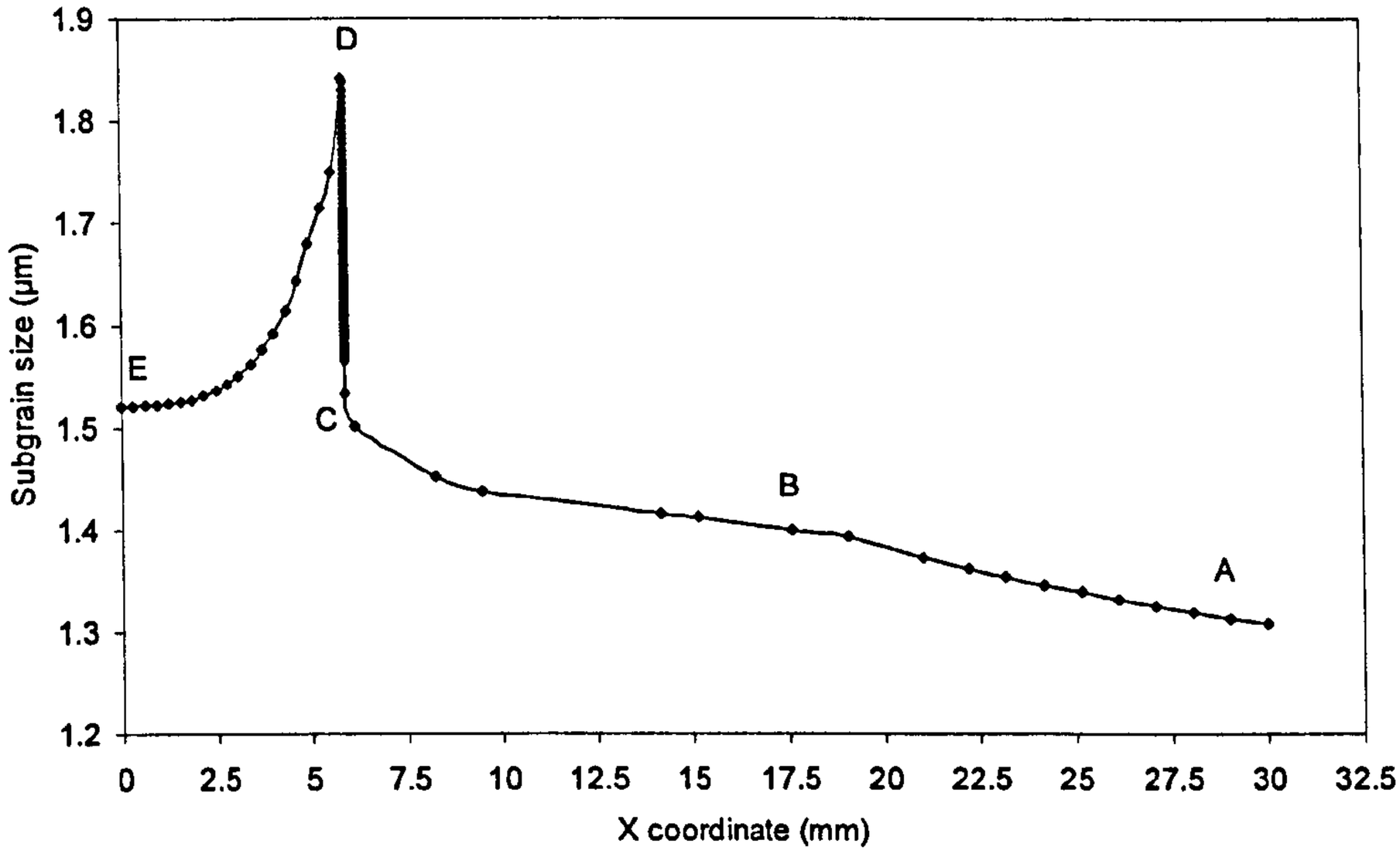

Figure 6. 3: Approximate prediction of the subgrain size along the line ABCDE.

It is clear from Table 6.2 and Figure 6.3 that the predicted subgrain size at the locations shown in Figure 6.2 agreed with the measured data from Vierod's experiment. As expected, the subgrain size increases from position (A) near the rear of the billet adjacent to the shear zone to position (D) at the surface of the extrudate as shown in Table 6.2. The subgrain size decrease in position (A) is attributed to the combined cooling effect of the ram and the container, reducing the subgrain size. The increase in subgrain size from (B) to (C) to (E) is a result of increase in strain gradient and hence strain-rate. This sudden increase in subgrain size is to be expected due to the large increase in strain-rate and the associated temperature rise near the die entrance. The change of subgrain size across the extrudate cross-section as the material flows through the die is shown in Figure 6.4. The predicted subgrain size at position (E) and (D) are 1.52μm and 1.84μm respectively. The relative errors compared with experimental measurement are 2.01% and 2.12% respectively. The predicted

subgrain sizes for the other locations are listed in Table 6.2. The Figures 6.3 and 6.4 also indicate that the subgrain size varies considerably across the billet and the extrudate cross-sections. The variations of subgrain size from the surface (position D) to the centre (position E) of the extrudate are due to the different strains and the different temperatures at the surface and the centre of the extrudate as clearly shown in Figure 6.4 to Figure 6.6. This is expected since the higher the temperature, the larger the subgrain size; the higher the strain-rate, the smaller the subgrain size as denoted by equation 6.1. The Zener Hollomon parameter, (Z) in equation 6.1 indicates that the effect of increasing temperature compensates the effect of increasing strain-rate on the subgrain size, confirming that temperature must play a dominant role on the determination of subgrain size. The location near the edge of the extrudate experiences much more strain and higher temperature than the centre as shown in Figure 6.7. This is consistent with the observation made in Chapter 5 section 5.4.2, that the surface of the extrudate is derived from within heavily-sheared regions of the deformation zone adjacent to the dead metal zone. The strain-rate and temperature at position (D) are significantly greater than at position (E), leading to a larger subgrain size at point (D). The substructures observed at point (D) and (E) are shown in Figure. 6.8 and Figure. 6.9 respectively.

Comparing the experimental and the simulated results, it can be concluded that equation 6.1 is effective in predicting the subgrain size within the billet and the extrudate material during steady-state deformation.

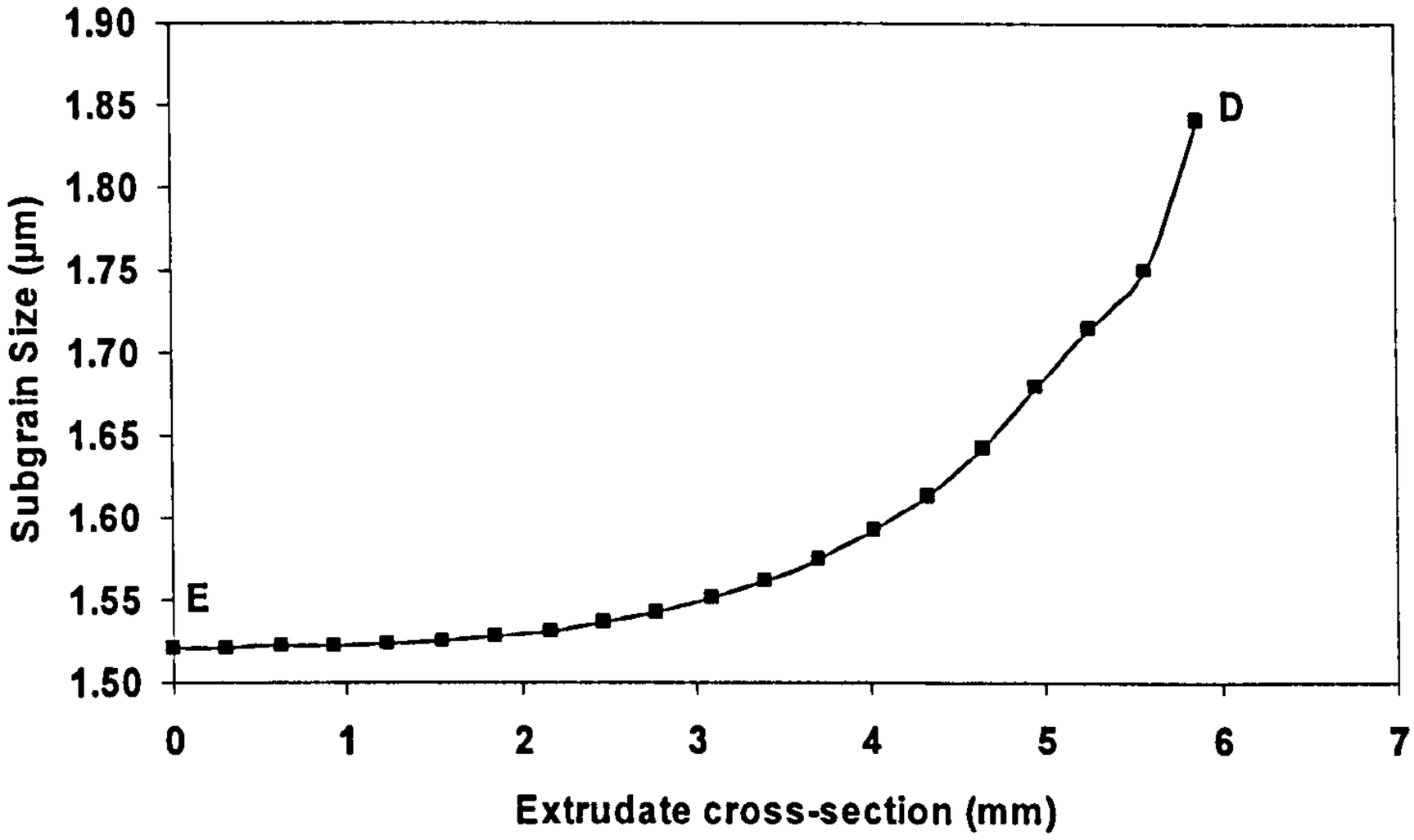

Figure 6.4: Variation of subgrain size along line (ED)

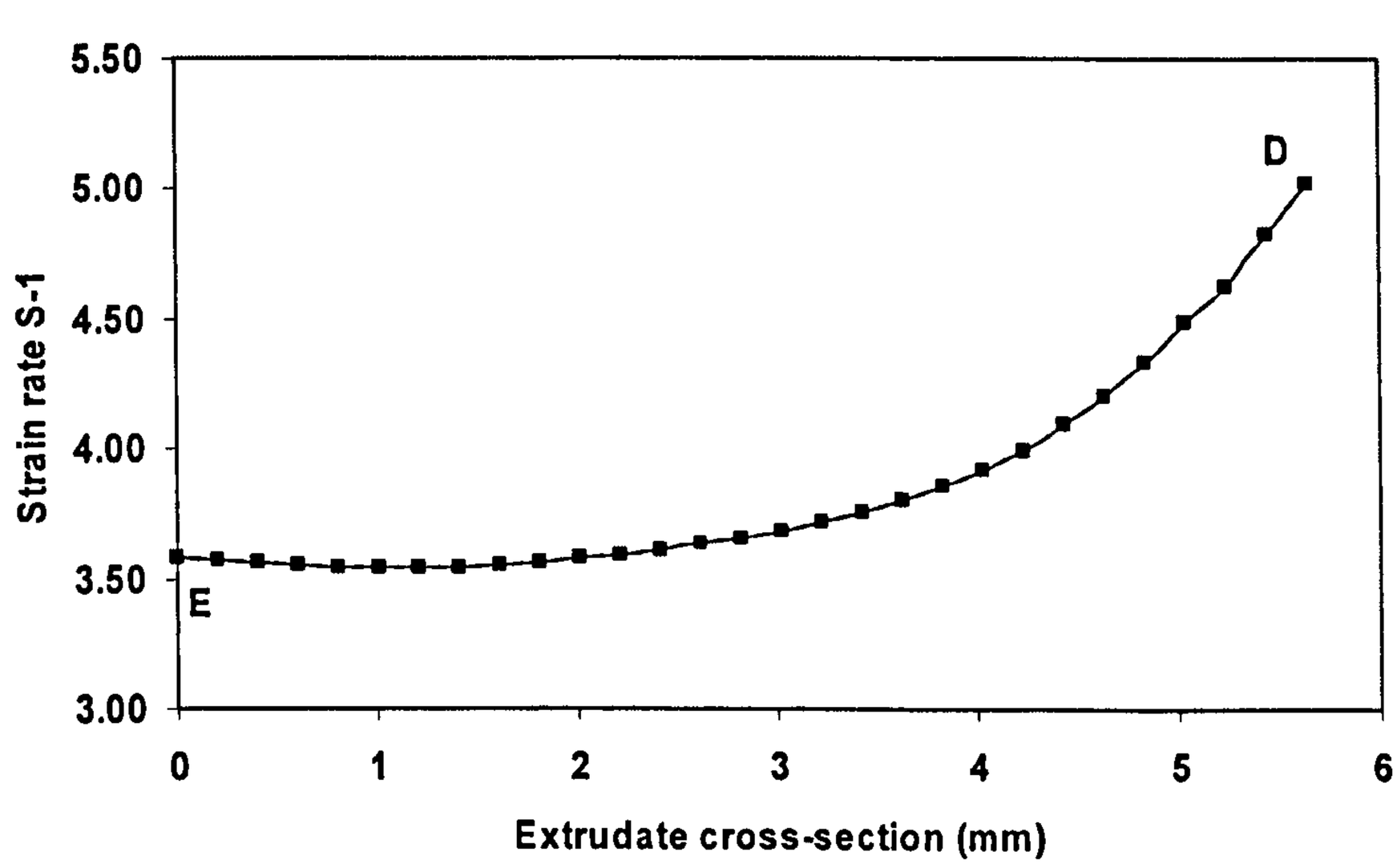

Figure 6.5: Variation of strain-rate along line (ED)

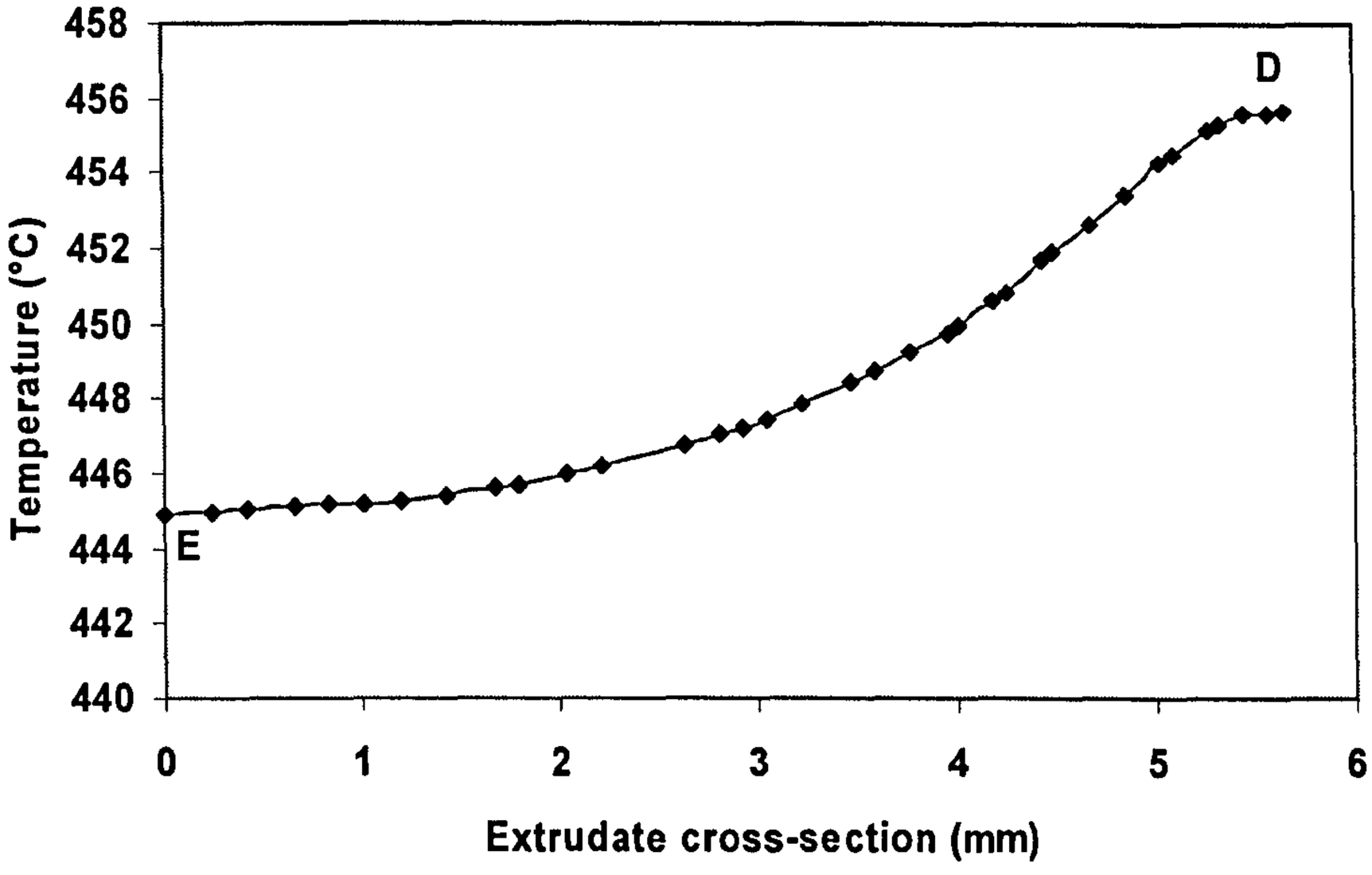

Figure 6.6: Variation of temperature along line (ED)

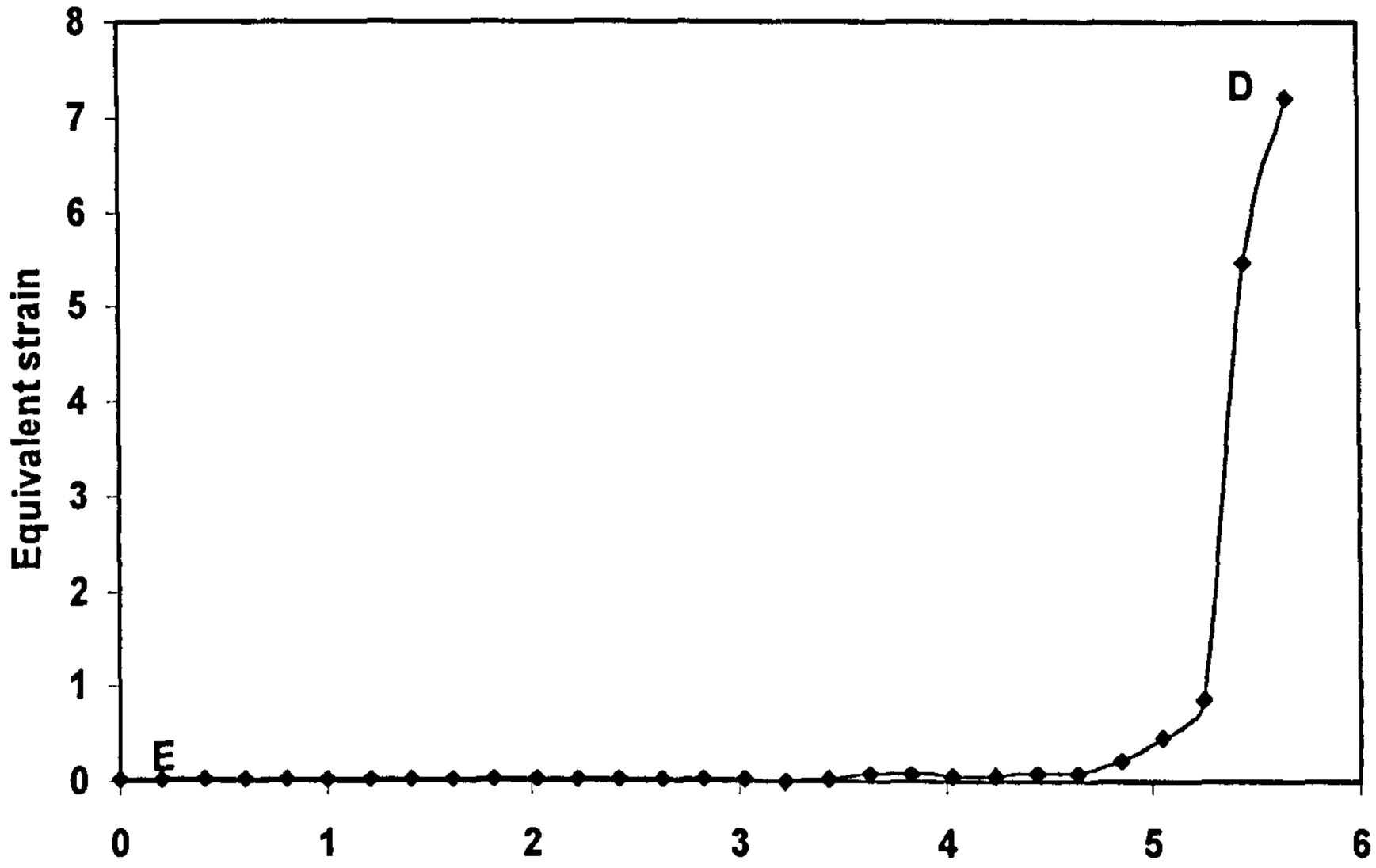

Figure 6.7: Variation of equivalent strain along line (ED)

Figure 6.8: Substructure observed at point (D) (After Vierod [63])

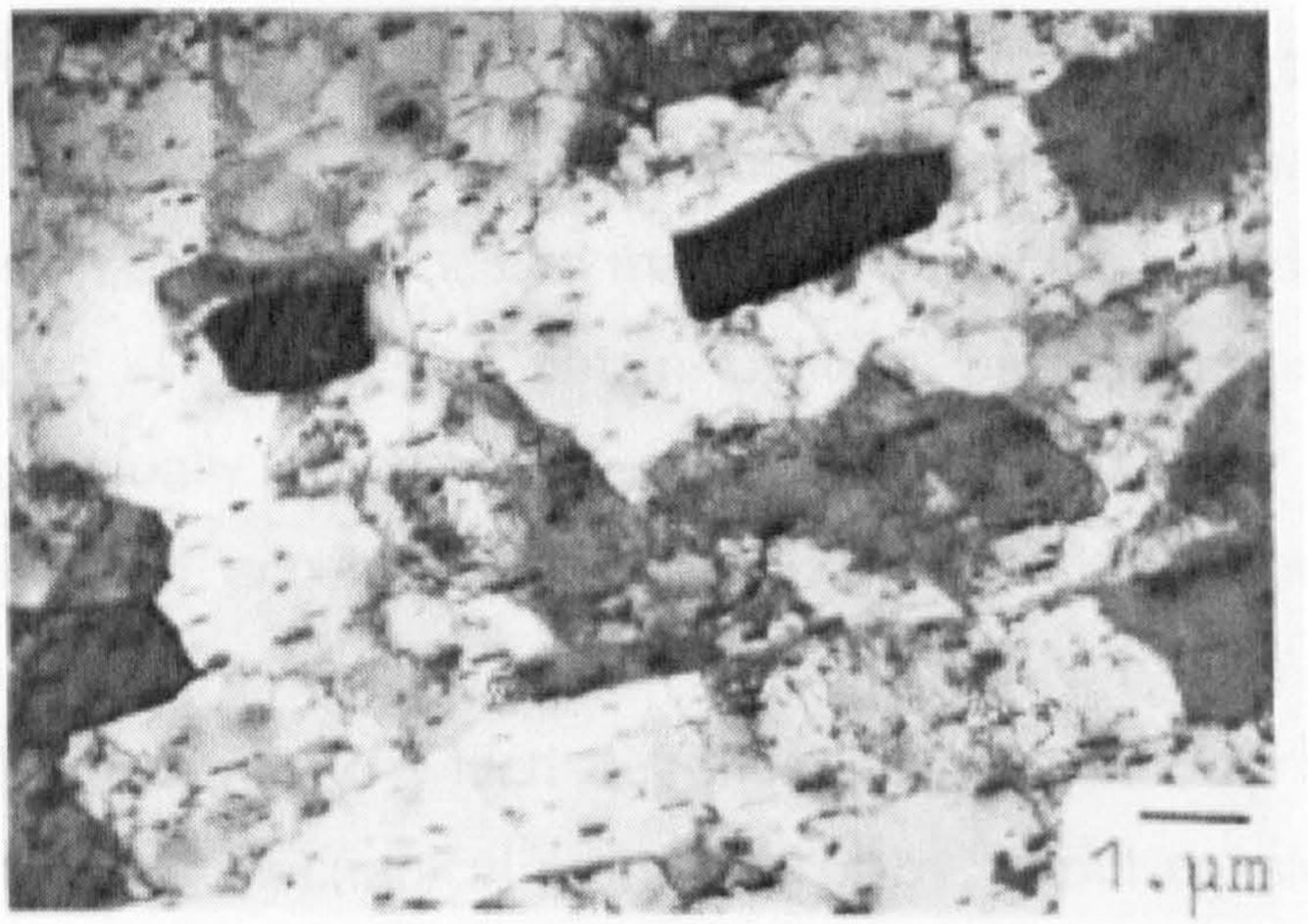

Figure 6.9.: Substructure observed at position (E) (After Vierod [63])

6.3 Control of the extrusion process

The control of the extrudate properties such as exit temperature, subgrain size and the temperature-compensated strain-rate (Z parameter) by FEM is the focus of this section. Thus, the ultimate objective in this section is to present to the extruder velocity-displacement profiles which will produce consistent properties over the length. It would not be necessary for the extruder to measure any output properties as they would already have been simulated.

The changes of temperature and microstructure under normal extrusion conditions were thoroughly discussed in the previous section. The substructure experiences a very complex evolution during the deformation process. The distribution of substructure and the temperature vary considerably across the billet and the extrudate cross-sections under a constant ram speed as shown in Figure 6.3 and Figure 6.6, thus, producing a non-uniform distribution of mechanical properties which, if the material is designed for the aerospace industry may require a post-extrusion operation such as machining away the outside layer of the extrudate. However, to obtain uniform properties, isothermal extrusion is usually adopted. It is possible to monitor the exit temperature to an acceptable accuracy using a closed loop speed control system as shown in Figure 6.10. The exit temperature is the key parameter in Figure 6.10 which depends on the customer's product specification of the mechanical properties or by output considerations. Although the temperature has greater influence on the mechanical properties, there may be other limitations dictated by the structure which is required. Previous studies [97, 101] show that subgrain size has a more direct link with the mechanical properties and furthermore exerts considerable control over subsequent thermal processing.

One way to approach an optimum extrusion condition would be to control the subgrain size instead of exit temperature for the desired

mechanical properties. This can be achieved by controlling the subgrain size through the ram speed and the exit temperature. Another way for an optimum extrusion is to achieve a constant (Z) value over the die mouth during the deformation. The idea behind Iso-Z is generally that the hot deformation of alloys as a thermo-mechanical process depends on temperature, stress and strain-rate as described by Equation (2.2).

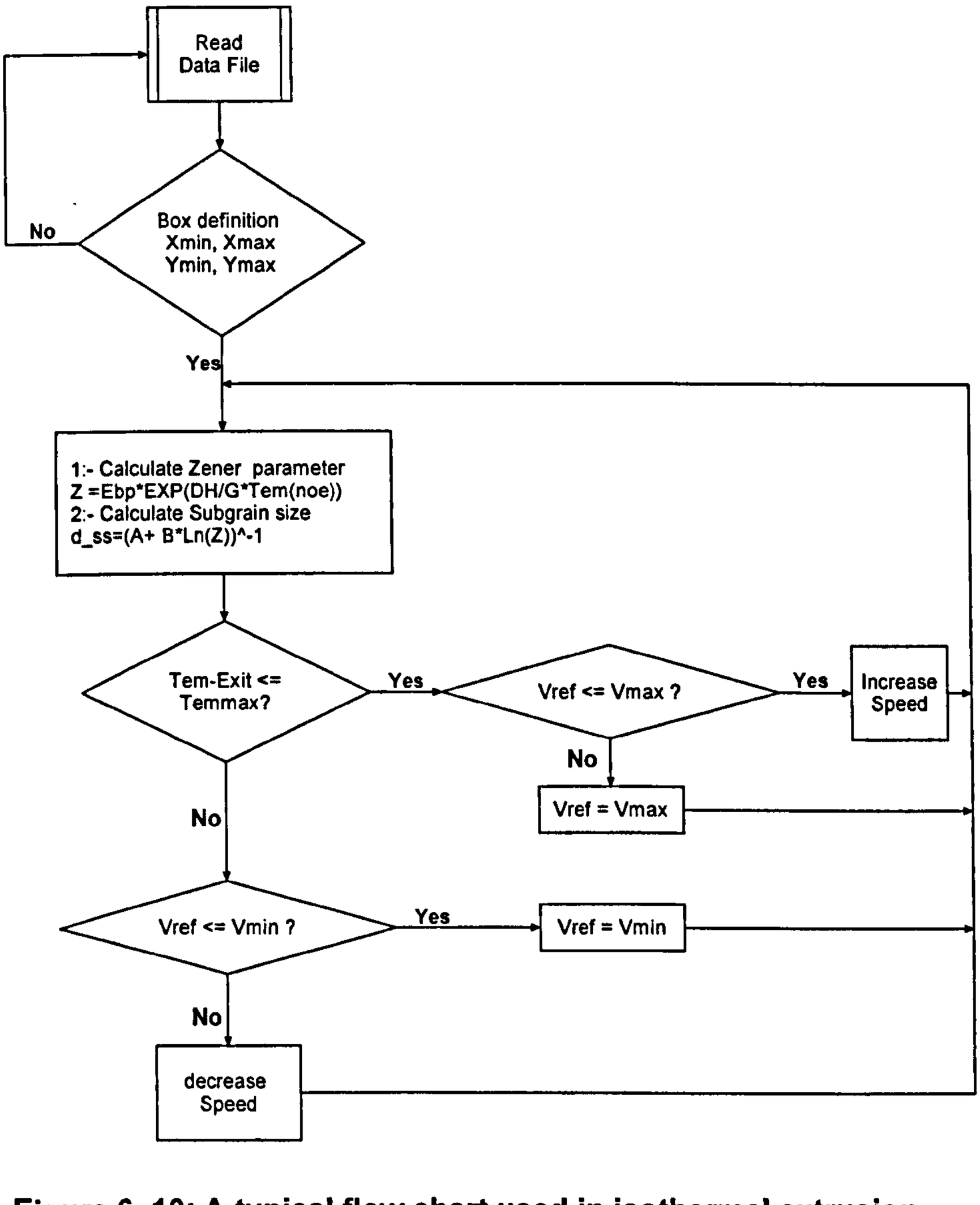

Figure 6. 10: A typical flow chart used in isothermal extrusion

The *box definition* shown in Figure 6.10 and illustrated in Figure 6.11 is used to define the area of control in which the criterion is triggered and measured against the predicted nodal value during deformation.

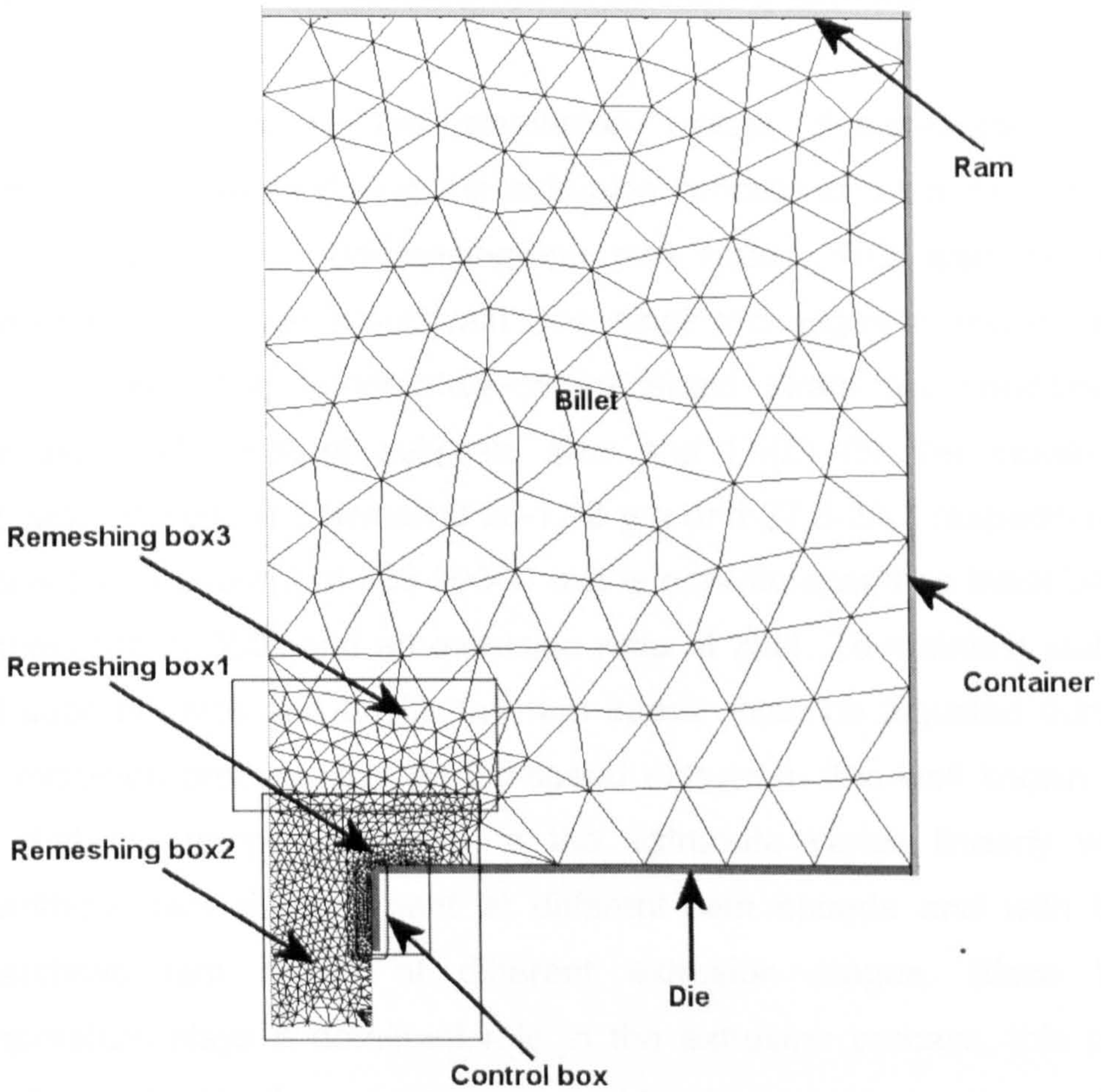

Figure 6.11: Simulation setup and remeshing boxes definition

To the author's knowledge, no model is yet available to control the change in microstructure. Even theoretical studies of the control of microstructure by adjusting the process variables, do not yet exist. This can be achieved by controlling the substructure through the ram speed and the exit temperature. Accordingly, Figure 6.10, the subgrain size and Ln(Z) are used as an alternative criterion to the exit temperature in this study. Thus, attempts to control the change of mechanical properties by adjusting the ram speed according to the prediction of the desired subgrain size, temperature at the die exit and a constant (Z)

have been proposed. These new concepts applied to the extrusion process in this investigation are termed, Iso-Subgrain size and Iso-Z extrusion differing from the usual title of Isothermal extrusion.

As previously shown, the simulation results demonstrated that temperature increase during the extrusion process of aluminium alloy can be assuaged by decreasing the ram speed. This also can be applied to the change in subgrain size, since it changes in accordance with the prevailing temperature-compensated strain-rate conditions. The expected constant subgrain size and Ln(Z) for the modelled extrusion process is between 0.98-1.12 μm and 27.3-28.7 respectively. This is the equivalent of 385-395°C exit temperature with an initial billet temperature of 300° and an extrusion ratio of 20:1. To maintain stable exit subgrain size and Ln(Z), the ram speed must be adjusted during the extrusion process. For an iso-speed extrusion, it is well known [74, 119] that the temperature rise in the extrudate varies linearly with logarithmic ram displacement at different ram speeds and with the logarithmic ram speed at different extrusion stages. Since the temperature plays a dominant role in the extrusion process, this can also be applied to the subgrain size and the temperature-compensated strain-rate parameter (Z). Thus the relationship between the ram speed and the criterion (i.e. Exit temperature, subgrain size or Ln(Z)) can be described with following equations:

For speed decrease: $v_{i+1} = v_{i-1}.Exp[-\Delta C_1.dt.R]$ (6.4)

For speed increase: $v_{i+1} = v_{i-1}.Exp[\Delta C_2.dt.R]$ (6.5)

where ΔC_1 = (Criterion(noe)- Criterion), ΔC_2 = (Criterion – Criterion(noe)) and R is a control factor for the decrease and the increase of the criterion. R = 10 was found to be a suitable value for a smoother change to the ram speed.

At the beginning of the extrusion process, the ram speed was set as a constant 13 mm/s, and then decreased or increased according to an exponential function of the ram displacement as shown in equation 6.4 and 6.5. The maximum speed of 13 mm/s was applied at the start of extrusion in order to obtain the highest constant acceleration rate possible with the retention of an acceptable surface and to shorten the extrusion cycle. The process conditions applied in this investigation are summarised in Table 6.3.

Table 6. 3: Process conditions

Billet Size (mm)	R	V (mm/s)	BT (°C)	CT (°C)	DT (°C)	RT (°C)
ϕ 73.5*95	20:1	13-2	300	250	170	170

R: Extrusion ratio
V: Ram Velocity
BT: Initial Billet Temperature
CT: Initial Container Temperature
DT: Initial Die Temperature
RT: Initial Ram Temperature

The computed histories of temperature and subgrain size obtained by adjusting the ram speed according to the calculated subgrain size at die exit are shown in Figure 6.12. The distribution of microstructure along the length of the extrudate throughout the die bearing length and 1 mm after the die exit, as illustrated in Figure 6.11, is shown in Figure 6.13. The figures show clearly that the subgrain size falls within the range defined (1.1 μm). In Figure 6.13, the subgrain size across the extrudate length exhibited an approximate variation of 0.06 μm from the die entrance to the die exit. Unlike the temperature and subgrain size distribution during an iso-speed extrusion, the exit temperature and the subgrain size using Iso-Subgrain size, almost remained constant throughout the process. The temperature and the subgrain size at the die exit are, not surprisingly; lower than near the die entrance, because the time necessary to change the temperature or reach the desired subgrain size depends on the initial overheating or overcooling of the

extrudate. At the beginning of the extrusion, much of the heat generation occurs at the DMZ/deformation zone shear region and results in a rapid increase in the overall temperature as the material approaches the die land. The temperature of the emerging extrudate is greater at the surface of the extrudate due to the severe shear deformation at this region. As the extrusion continues and the ram speed decreases, heat losses from the billet to the die land become dominant as a result of less work being carried out in this region. It is worth indicating that the initial die temperature was set at 170°C, hence it acts as a heat sink to the billet material adjacent to the die face. The surface temperature of the extrudate thus decreases and consequently so does the subgrain size.

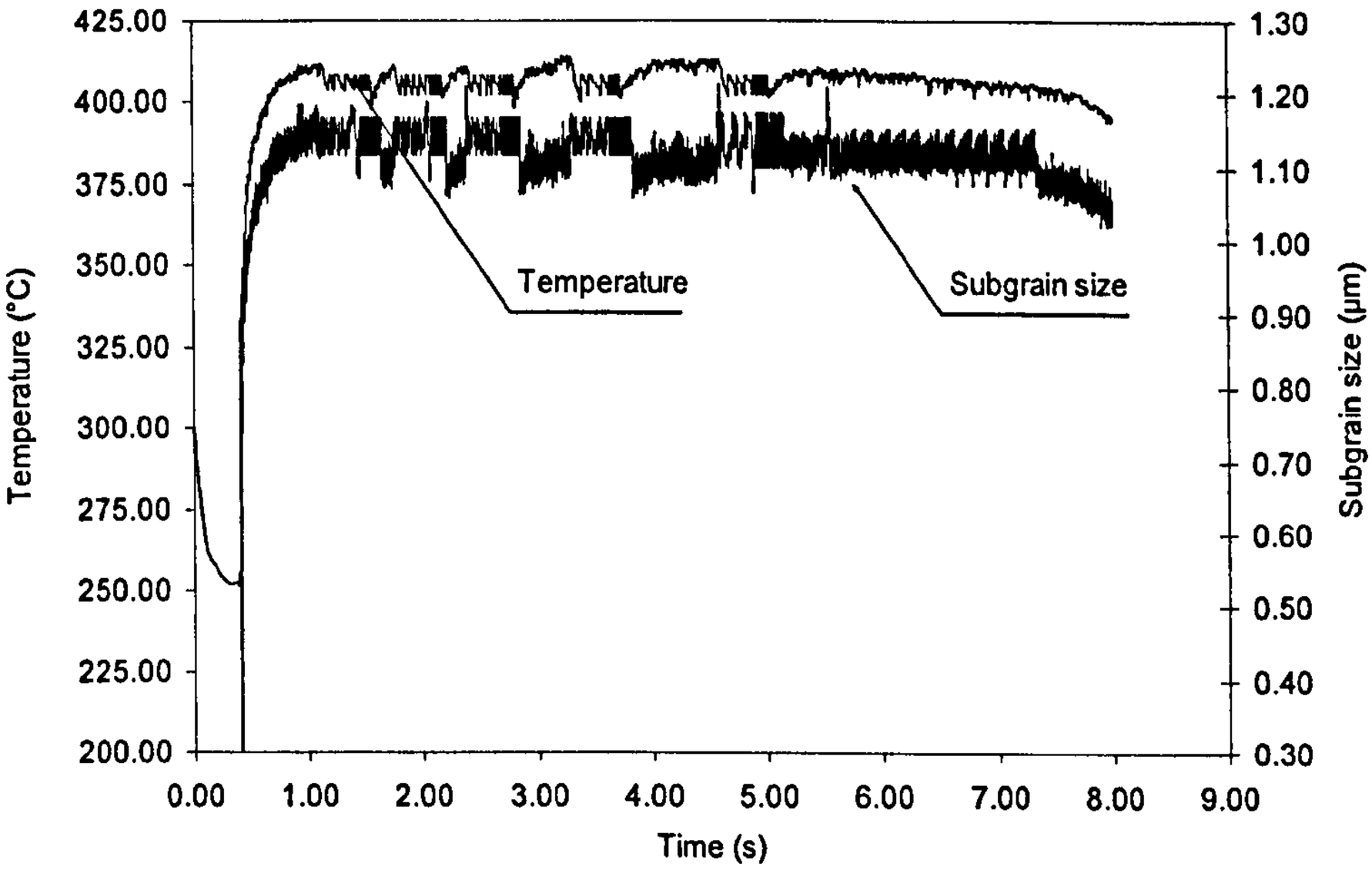

Figure 6.12: Subgrain and temperature evolution under iso-subgrain extrusion

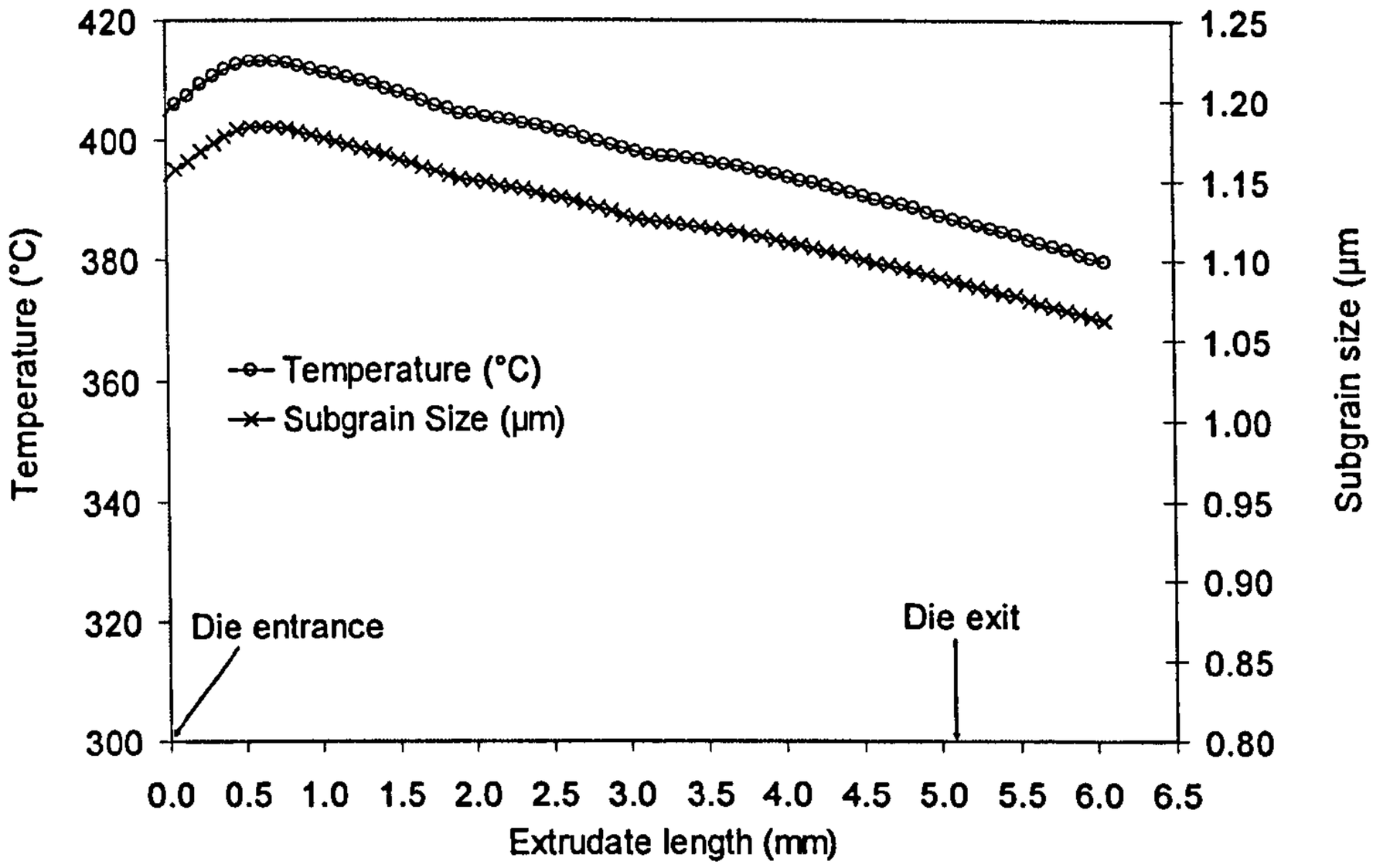

Figure 6. 13: Subgrain size distribution along the length of the extrudate

The computed ram speed profile for the required subgrain size range is shown in Figure 6.14. An initial ram speed of 13 mm/s is predicted over approximately 15 mm of ram travel in order to reach the target subgrain size of 1.1 µm. The ram speed then decreases gradually to 5.4 mm/s over 13mm of ram travel. Once the target subgrain size is reached, the velocity profile changes or maintains a constant ram speed depending on the next predicted value of the subgrain size. This is to allow the heat generated at the higher ram speed to dissipate into the tooling in order to generate a thermal balance which allows a change in subgrain size to the desired size. Similar to the temperature change, the magnitude of the subgrain change of the emerging extrudate is related to time available for heat transfer, which is inversely proportional to the ram speed. The computed ram speed profile in Figure 6.14 changes smoothly and can easily be performed by modern extrusion presses. At the end of the actual extrusion cycle, an average ram speed of 8.4 mm/s is predicted. As the figures illustrate, acceptable results were obtained using iso-subgrain extrusion, except for the fluctuation observed in Figure 6.12. In practice the subgrain size and the

temperature cannot vary in such a short time and could be just the consequence of the simulation. This indicates the complex relationship between the subgrain size and the ram speed. We may therefore conclude that the subgrain size is difficult to control as a criterion for the microstructure when only the ram speed is varied. For isothermal extrusion, if the target temperature is assigned between 400 and 410 °C, the computed histories of subgrain size are shown in Figure 6.15. There is no obvious difference between the curve for subgrain size in Figure 6.12 and the corresponding curve in Figure 6.15 except that the curve in Figure 6.15 is smoother.

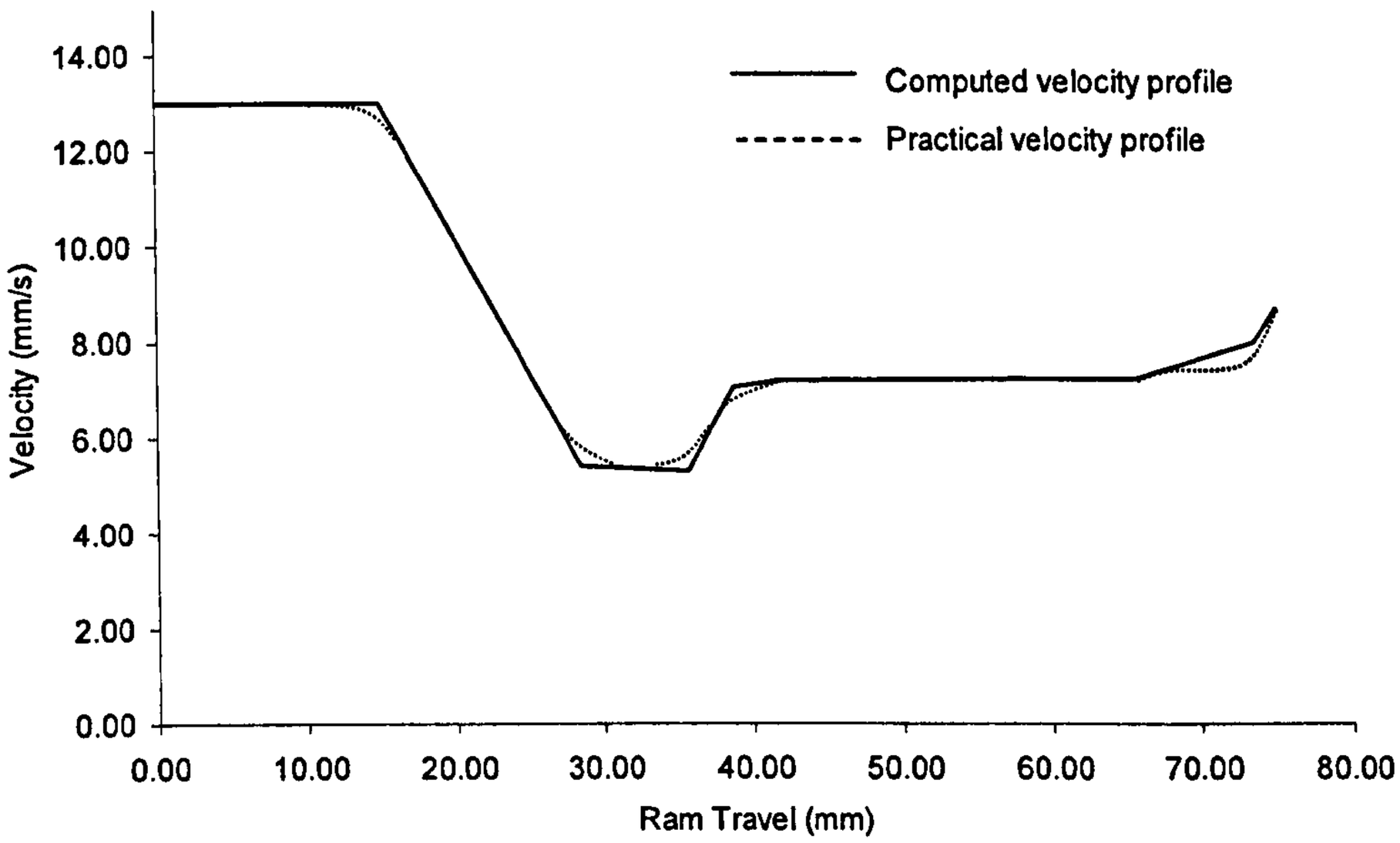

Figure 6.14: Computed ram velocity profile under iso-subgrain extrusion.

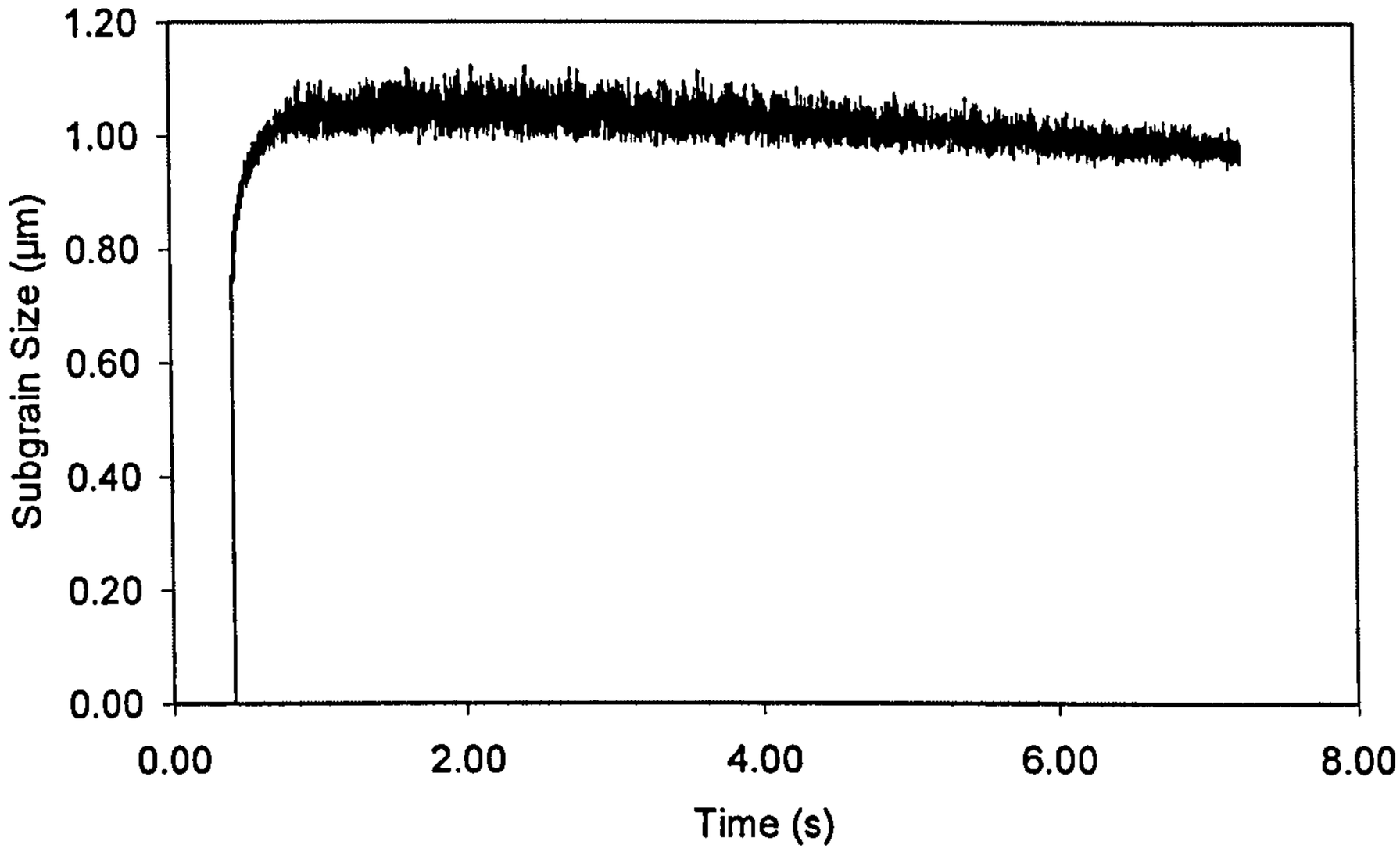

Figure 6. 15: Subgrain size evolution under isothermal conditions

The objective of isothermal or iso-subgrain size is of practical interest for achieving a uniform product quality or making the most efficient use of the maximum speed that the alloy can withstand without poor surface development. It is generally accepted that the subgrain size is dependent on processing conditions, increasing in size with temperature and to a lesser extent, with decreasing strain-rate. Furthermore, the product properties are closely correlated to the microstructure and since the steady-state substructure changes in accordance with the prevailing temperature-compensated strain-rate (Z) conditions as described by equation 6.1, the final product structure and hence its properties are directly linked and dependent on the temperature and strain-rate distribution adjacent to the die mouth. Hence, for a perfect process optimisation one would need to be able to control all process variables affecting the output and quality of the section. These would include section temperature and speed. Combining the speed and temperature gives the Zener-Hollomon parameter (Z), to some extent, control of the properties.

The computed histories of subgrain size and temperature under Iso-Z extrusion are shown in Figure 6.16. One interesting feature in Figure 6.16 is the fluctuation of the temperature and the subgrain size at the start of the extrusion. Figure 6.16 certainly suggests that thermal stability is not immediate at the start of the process. Both the subgrain size and the exit temperature exhibited some fluctuation at the start of the extrusion at approximately 30 mm of ram travel. It is not obvious why such a fluctuation exists, except as a consequence of the simulation. Therefore changes may not be real. Another possible reason is that increase in the ram speed results in a significant change of strain-rate and temperature close to the die entry. The exit temperature increases in proportion to the ram speed and also with increasing strain-rate. The same increase in exit temperature coincided with increasing subgrain size. This is to allow for the heat generated at the higher ram speed to dissipate into the tooling in order to generate a thermal balance which in turn allows a change in the (Z) value.

Similar to the temperature change, the magnitude of the subgrain change of the emerging extrudate is related to time available for heat transfer, which is inversely proportional to the ram speed. In order to achieve a constant (Z), both the strain-rate and the temperature must be held as constants. Usually, the effect of strain-rate on (Z) is lower than the effect of temperature and if the strain-rate increases significantly and temperature changes slowly, the effect of strain-rate could balance the effect of temperature, resulting in little change in subgrain size. However, if both the strain-rate and temperature change considerably, it would significantly affect the change in the subgrain size. This indicates that the relationship between process conditions and subsequent structure is more complex.

However, after extrusion of approximately one-third of the billet, the temperature and subgrain size become more uniform as (Z) approaches a constant value. So for most of the extrusion, Iso-Z

condition is available. Therefore, after the initial extrusion stage, accurate measurement of exit temperature and subgrain size can be relied upon in practice if billet to billet extrusion is adopted. The corresponding computed ram speed profile for the Iso-Z extrusion is shown in Figure 6.17. The ram speed profile for Ln(Z) resulted in a mean extrusion speed of 11.7 mm/s at the end of the extrusion cycle. An increase of approximately 40% over the Iso-subgrain size mean extrusion speed (8.4 mm/s) and hence productivity is increased using Iso-Z extrusion.

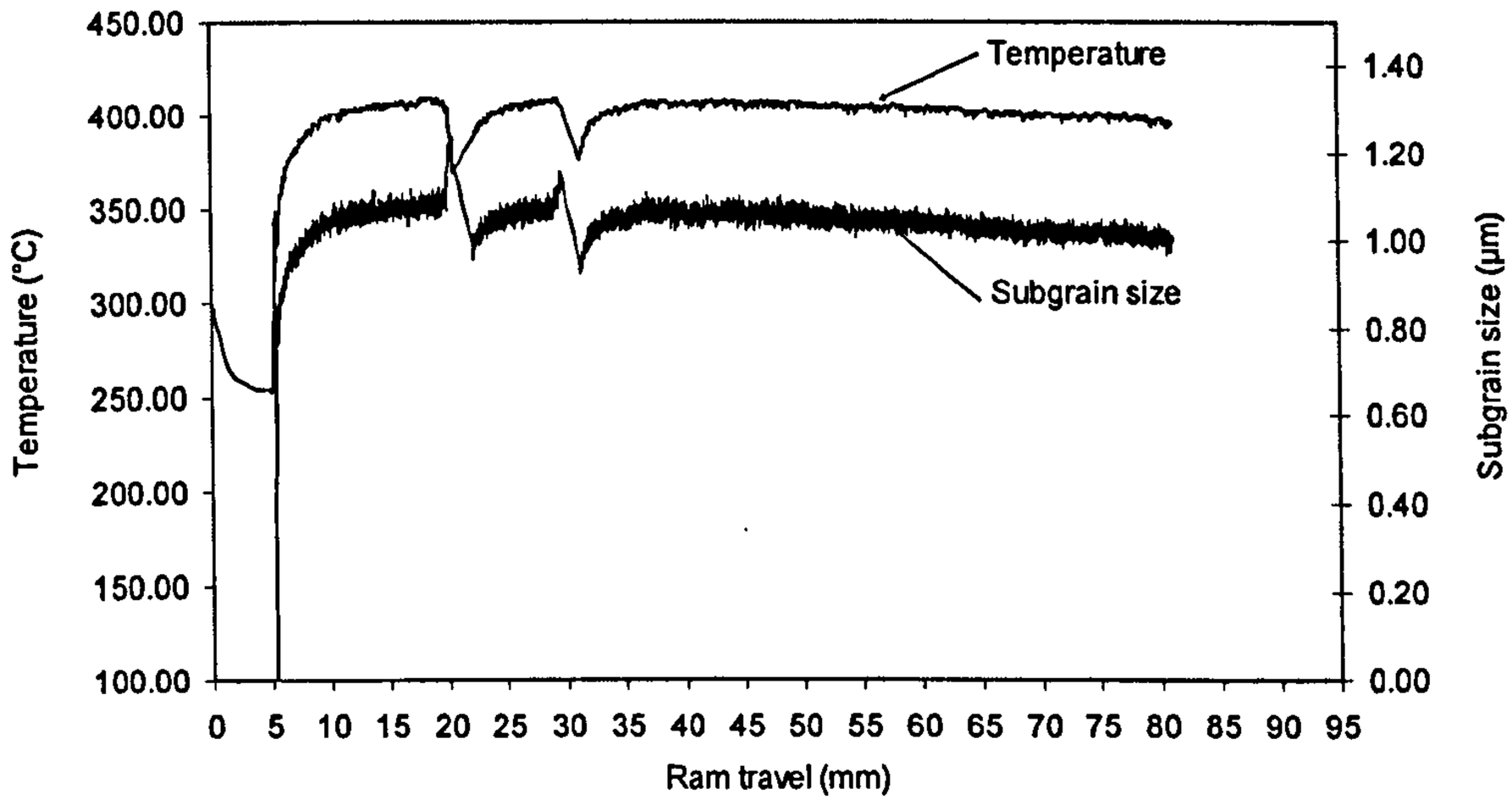

Figure 6.16: Subgrain and temperature evolution under Iso-Z extrusion

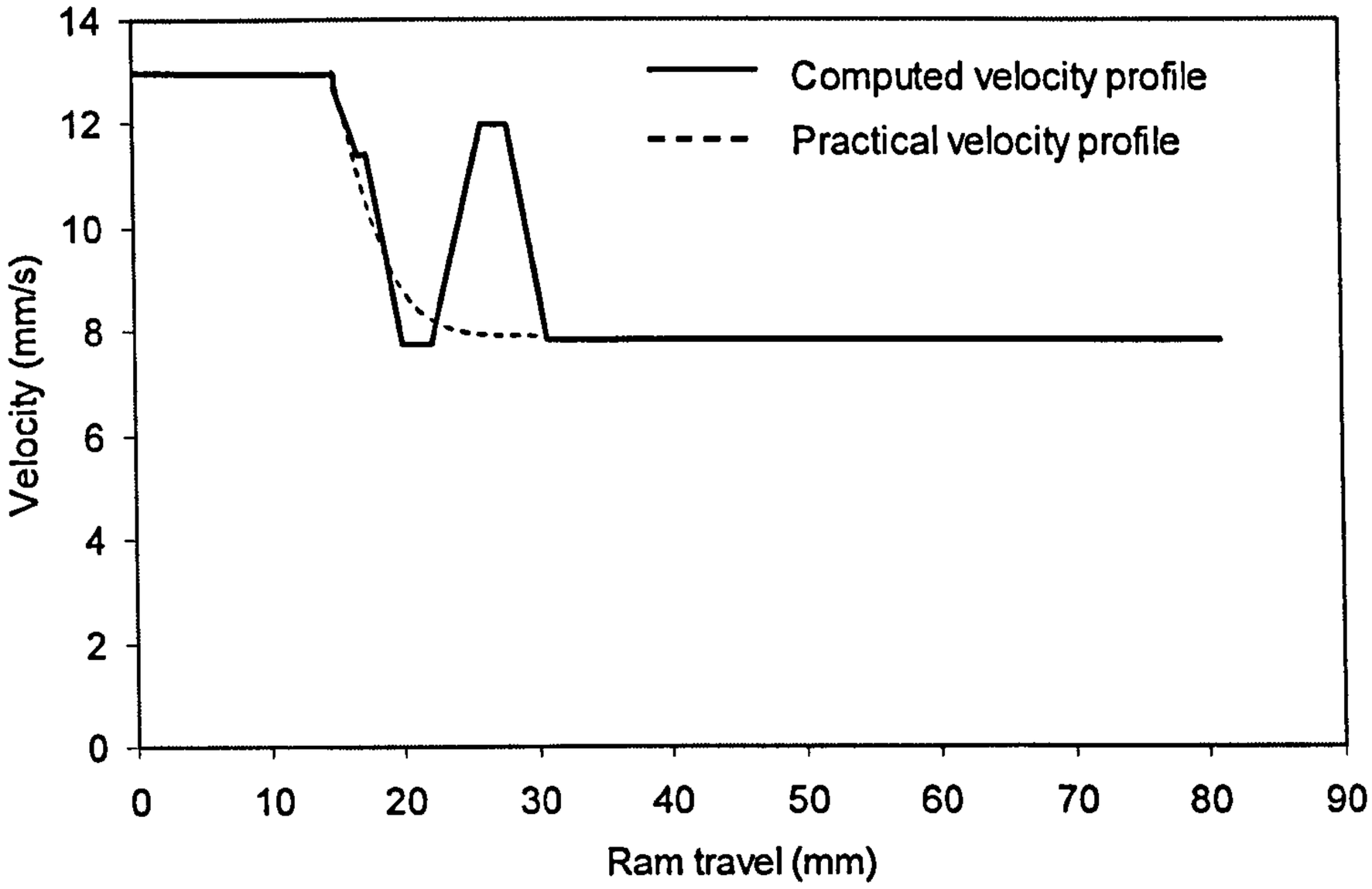

Figure 6.17: Computed ram velocity profile under Iso-Z extrusion

One additional and useful prediction is the variation of subgrain size across the extrudate cross-section for the three iso-extrusion processes (Iso-Subgrain size, Iso-T, and Iso-Z conditions). Figure 6.18 clearly shows the superiority of applying Iso-Z as a control criterion. Under Iso-Z conditions, the subgrain size at the surface of the extrudate was closer (2.7%) to the target value of 1.1 μm, while under Iso-T and Iso-subgrain conditions, a difference of 5.4 and 4.5% respectively was revealed. However, the three criteria in Figure 6.18 exhibited relatively the same variation of 0.07 μm across the extrudate cross-section. Though, due to the non-existence of an on-line model to predict the change in subgrain size or the variation of the (Z) parameter during the process, isothermal extrusion is still valid. Otherwise in terms of which criterion to adopt for an optimum extrusion process, if the speed profile of an extrusion cycle is to be relied upon, then iso-Z indicated superiority in terms of control and productivity.

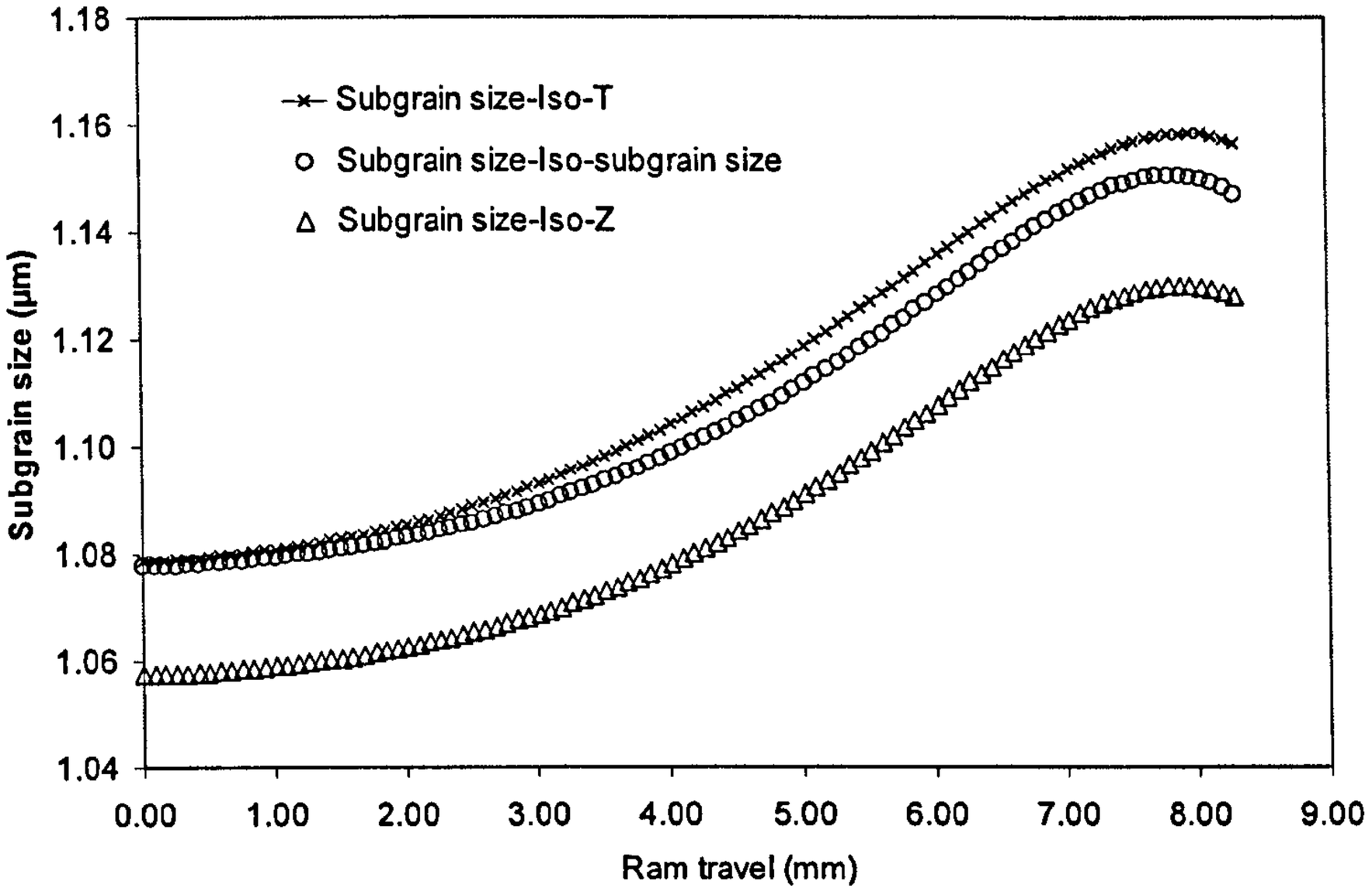

Figure 6.18: Subgrain size variation across the extrudate cross-section.

6.4 Conclusions

1. The predicted variation during the steady-state deformation of the subgrain size within the container and across the extrudate cross-section was found to be in good agreement with the experimental measurements.

2. Under constant ram speed, the temperature and subgrain size increase with increasing ram displacement. The distribution of microstructure along the section and the length of the extrudate as expected, is not uniform.

3. The selected criterion for the control of ram speed in either isothermal or iso-subgrain size extrusion directly determines the quality of the designed ram speed profile.

4. A uniform distribution of microstructure along the length can be achieved by the use of iso-subgrain size, iso-Z conditions and isothermal extrusion processes.

5. FEM is a very effective and efficient way to design the ram speed profile.

6. The ram speed profile for Iso-Z conditions resulted in an improved extrusion speed and hence productivity over iso-subgrain size and Isothermal extrusion.

7. Under Iso-Z conditions, the subgrain size variation resulted in a more uniform distribution across and along the extrudate.

CHAPTER 7: CONCLUSIONS AND RECOMMENDED FUTURE WORK

7.1 Conclusions

1. The FEM Code Forge 2&3 with the programmed hyperbolic-sine function provided a suitable model for simulation and successfully predicted the major extrusion parameters and appeared to predict all the major characteristics of the flow observed macroscopically.

2. For each incremental finite interval the stress is updated by consideration of the derivative of the constitutive equation with respect to strain-rate and stress. It is not possible to quantify this adjustment precisely but if different constitutive equations produce differing derivations, then this will affect the calculated parameters i.e. load, temperature, etc. hence Norton-Hoff and hyperbolic-sine equations.

3. The $\overline{m}$ values do not remain constant throughout the extrusion cycle. The increases in overall temperature of the billet and hence decreases in flow stress, lead to an increase in friction for both alloys and temperatures.

4. For an accurate simulation of extrusion, the friction coefficient must be identified continuously during the process cycle. This is not only required for press capacity, but also the effect on the temperature changes occurring in the material. This subsequently has an effect on the surface quality of the extrudate.

5. In the current investigation it has been shown that the prediction of the metal flow and the dead metal zone formation of the bridge-die extrusion were in good agreement between simulation and experimental findings.

6. Empirical equations, which appear to be adequate to predict pressure requirements, will not predict either metal flow or final temperatures. There is therefore the requirement to refine the FEM approach by further research.

7. The selected criterion for the control of ram speed in either isothermal or iso-subgrain size extrusion directly determines the quality of the designed ram speed profile.

8. A uniform distribution of microstructure along the length can be achieved by the use of iso-subgrain size, iso-Z conditions and isothermal extrusion processes.

9. FEM is a very effective and efficient way to design the ram speed profile.

7.2 Recommended for future work

There are many aspects that can be improved in the future. Some recommendations are given below.

For more complicated shaped extrusion, the prediction of microstructure *has* even greater importance for the guidance of practical die design (such as the determination of die radius, bearing length, port size, bridge height and depth of the welding chamber) and the generation of technological parameters. Of course, a three-dimensional finite element

analysis model is required and it would take a considerable amount of computer time.

Tapered heating or tapered quench is another common method to conduct isothermal extrusion. Designing an appropriate gradient of temperature within the billet is the key element. Another possible way to perform Iso-subgrain size extrusion is to control the container temperature and die temperature. FEM can easily simulate the complicated interactive relationship between the forming parameters and microstructure response of the extrudate. The best way to perform an isothermal extrusion process is to search the optimal combination of tapered billet temperature, ram speed, die temperature, and the container temperature. This requires the use of an advanced optimisation method, such as fuzzy neural network, genetic algorithms or simulated annealing.

APPENDICES

Appendix 1. Constants used in equation (2.10)

Material.	a	b	m	Process of measurement	Reference
AA2014	-1.747	0.096	1	Direct extrusion	63
AA2014	-1.586	0.085	1	Indirect extrusion	63
AA2024	-0.5778	0.0378	1	Direct extrusion	62
AA2024	-0.6457	0.0426	1	Indirect extrusion	62
AA7075	-0.54	0.023	2	Direct extrusion	30
Al-1%Mg	-3.36	0.136	1	Plane strain compression	104

Appendix 2: Constants in the constitutive equation for some Al-alloys (Courtesy of Sheppard 1999) [1].

$$\overline{\sigma} = \frac{1}{\alpha} Ln\left\{\left(\frac{Z}{A}\right)^{\frac{1}{n}} + \sqrt{\left(\frac{Z}{A}\right)^{\frac{2}{n}} + 1}\right\} \quad \text{and} \quad Z = \dot{\bar{\varepsilon}} \cdot \exp\left(\frac{\Delta H}{GT}\right)$$

Alloy	α	n	ΔH	G	lnA	Remarks
1S	0.04	3.84	157000	8.314	26.66	
1050	0.037	3.84	156888	8.314	26.69	
1100	0.045	5.66	158300	8.314	24.67	
2011	0.037	3.712	142000	8.314	19.2	
2014	0.0128	5.13	131309	8.314	22.23	
2014*	0.0152	5.27	144408	8.314	24.41	PH.-SS
2014**	0.0283	3.49	128913	8.314	21.959	4% Cu
2024	0.016	4.27	148880	8.314	19.6	
3003	0.0316	4.45	164800	8.314	26.9	
3004	0.0344	3.6	193850	8.314	28.21	
3005	0.0323	4.96	183100	8.314	29.87	
3105	0.0248	4.83	179300	8.314	29.98	
4047	0.04	2.65	129300	8.314	20.47	
5005	0.029	5.8	183576	8.314	26.65	
M57S	0.02	5.1	155000	8.314	24.20	
5052	0.016	5.24	155167	8.314	24.47	
5054	0.015	5.43	173600	8.314	26.61	
5056	0.015	4.82	166900	8.314	23.05	
5083	0.015	4.99	171400	8.314	23.11	
5182	0.062	1.35	174200	8.314	22.48	
5456	0.0191	3.2	161177	8.314	23.5	
6061	0.045	3.55	145000	8.314	19.3	
6082	0.045	2.976	153000	8.314	19.29	
6063	0.04	5.385	141550	8.314	22.5	
6105	0.045	3.502	145000	8.314	20.51	
7004	0.035	1.28	153000	8.314	20.12	
7050	0.0269	2.86	151500	8.314	22.85	
7075H1	0.0141	5.41	129400	8.314	20.75	24hr.Soak
7075H2	0.01	6.14	158432	8.314	26.32	Sl.Ht.-F.Cool
7075H3	0.012	7.8	155336	8.314	27.54	F.Ht-Sl.Cool
7075H4	0.01	8.5	156325	8.314	27.14	F.Ht-F.Cool
7075H5	0.011	6.32	156837	8.314	26.38	Sl.Ht-Sl.Cool
7150H1	0.01	5.7	161402	8.314	29.8	F.Ht-F.Cool
7150H2	0.013	6.1	158806	8.314	29.2	F.Ht-Sl.Cool
7150H3	0.01	5.5	159832	8.314	30.7	Sl.Ht-F.Cool

Appendix 3: Chemical composition of various aluminium alloys used in the present thesis, in weight% (Courtesy of Sheppard T. [1].

Alloy	Al.	Cu	Mg	Fe	Si	Mn	Ti	Zn
AA2024	Balance	3.8-4.9	1.2-1.8	0.5	0.5	0.3-0.9	0.15	0.25
AA2014	Balance	4	0.47	0.2	0.78	0.78	0.013	0.02
Al-1%Cu	Balance	0.9	0.5	0.2	0.82	0.71	0.15	0.25
AA6063	Balance	0.1	2.0	0.45-0.9	0.2-0.6	0.10	0.10	0.10

Appendix 4: Data structure of FORGE2®

GENERAL DATA FILE FOR FORGE2®:

!================================ FILE Block

1- This module defines the file names for the billet mesh (part.msh) and the tooling which will be used in the simulation

==========

```
.FICHIER

 FMAY   = Billet.may            ! Part Mesh File
 FOUT   = Tools.out             ! Tooling File
 FMAY1  = Def_die.may                   ! Meshed Die File
 FMAY2  = Def_containe.may              ! Meshed Die File
 Delete                         ! overwrite existing output files
.FIN FICHIER
```

!================================ UNITS Block

2- This is the unit system module. It states that we used mm to define lenght, MPa. for stresses and mm.Kg.s for the thermal data. The temperature unit is degrees Celsius(Default).

==========

```
.UNITES
 mm-mpa-mm.kg.s   ! Dimension of Length-Stress-Thermic
.FIN UNITES
```

!================================ RHEOLOGY Block

3- This module defines the part (billet) Rheology and the friction values between the part and dies.

==========

```
.RHEOLOGIE ! Billet
!*************************
!        AA2024          *
!*************************
Thermoecroui : zenerhollomon, ! Flow Curve
        alpha=0.016,
        a=325215956.1,
        dh=148880,
        r=8.314,
        n=4.27
```

The Young modulus and the Poisson coefficient define the elastic behaviour of the Billet material

```
Coeff Poisson = 3.000000e-001  ! Poissons's ration
Module Young  = 30.00000e+003  ! Young Modulus
```

```
Temp Init       = 350.000000  ! Initial Temperature

!Definition of Friction between Billet and Rigid Dies
!-------------------------------------------------------------------

Outil 1 :  Collant,                          !Rigid Die
           Contact bilateral

Outil 2 : Collant,                           !Rigid Container
          Contact bilateral

Outil 3 : tresca,                            !Rigid Ram
          mbarre=0.2500000

!Definition of Friction between Billet and Deformable_Die and
Deformable_Container
!-------------------------------------------------------------------
! Tresca Friction Law
 OutDef 1 : Tresca,              !Deformable Die
 mbarre   = 0.500000

! Tresca Friction Law
 OutDef 2 : Tresca,              !Deformable Container
 mbarre   = 0.7300000

.FIN RHEOLOGIE      !end of the billet rhelogy

!Tooling Properties

.RHEOLOGIE_1                    ! Deformable_Die

 Module Young  = 2.200000e+005
 Coeff Poisson = 3.000000e-001

 Temp init     = 300.000000

!Definition of Friction between Def_Die and Rigid Dies
!-------------------------------------------------------------------
! Sticking Contact
 Outil 0 : Collant,                          !same for all the tools
           Contact bilateral

!Definition of Friction between Def_Die and Def_Container
!-------------------------------------------------------------------
! Sticking Contact
 OutDef 0 : Collant,
            Contact bilateral
.FIN RHEOLOGIE_1            !End of Def_Container rehology

.RHEOLOGIE_2 ! Def_Container
 Module Young  = 2.200000e+005
 Coeff Poisson = 3.000000e-001
 Temp init     = 300.000000

!Definition of Friction between Def_Container and Rigid Dies
```

```
!-----------------------------------------------------------------------
! Sticking Contact
 Outil 0 : Collant,
          Contact bilateral

!Definition of Friction between Def_Container and Def_Die
!-----------------------------------------------------------------------
! Sticking Contact
 OutDef 0 : Collant
.FIN RHEOLOGIE_2
!================================ THERMIC Block
4- This module defines the thermal parameters of the billet material and the thermal boundary conditions between the billet and the dies
==========================================

.THERMIQUE ! Billet   Thermal properties of the billet

!Definition of the Billet thermal data
 MVolumique  = 2.800000e-006  ! Density Rho
 Cmassique   = 9.60000e+008  ! Heat Capacity, c
 Conductmat  = 1.900000e+005  ! Conductivity, k

!Definition of boundary Conditions between Billet and Rigid Dies
!-----------------------------------------------
 Outil 1                                  ! Rigid_Die
  Alphat          = 1.000000e+004         ! Global transfer Coeff with rigid die 1
  tempout         = 300.000000            ! Die 1 Temperature
  effusoutil      = 9.880000e+003         ! Effusivity (SQRT(k.rho.c) )
 Outil 2                                  ! Rigid_Container
  alphat          = 1.000000e+004         ! Global transfer Coeff with rigid die 2
  tempout         = 300.000000            ! Die 2 Temperature
  effusoutil     = 9.880000e+003          ! Effusivity (SQRT(k.rho.c) )
 Outil 3                                  ! Rigid_ram
  alphat          = 1.000000e+004         ! Global transfer Coeff with rigid die 3
  tempout       = 300.000000              ! Die 3 Temperature
  effusoutil     = 9.880000e+003          !Effusivity (SQRT(k.rho.c) )

!Definition of boundary Conditions between Billet and Def_Die and Def_Container
!-----------------------------------------------------------------------
 OutDef 0
   alphat       = 1.000000e+004 ! Global transfer  Coeff with meshed die

!Definition of boundary Conditions between Billet and external
!-----------------------------------------------------
 Face libre
   alphat        = 1.000000e+001 !Global transfer  Coefficient with air
   tempext        = 50.000000 ! External Temperature
   epsilon        = 5.000000e-002 ! Material Emissivite
.FIN THERMIQUE

.THERMIQUE_1 ! Deformable_Die
!Thermal Properties for the Deformable_Die
```

```
MVolumique  = 7.500000e-006
Cmassique   = 6.690000e+008
Conductmat  = 2.758000e+004

!Definition of boundary Conditions between   Defor_Die and Rigid Dies
!-------------------------------------------------
Outil 0
  alphat       = 1.000000e+004
  tempout       = 300.000000
  effusoutil    = 1.176362e+004

!Definition of boundary Conditions between   Def_Die and External
!-------------------------------------------------------------------------
 Face libre
  alphat       = 1.000000e+001
  tempext       = 10.000000
  epsilon       = 8.800000e-001
.FIN THERMIQUE_1

.THERMIQUE_2 ! Meshed Die No 2
!Thermal Properties for the meshed die No 2
 MVolumique  = 7.500000e-006
 Cmassique   = 6.690000e+008
 Conductmat  = 2.758000e+004

!Definition of boundary Conditions between   Meshed Die 2 and Rigid Dies
!-------------------------------------------------
 Outil 0
  alphat       = 1.000000e+004
  tempout       = 300.000000
  effusoutil    = 1.176362e+004

!Definition of boundary Conditions between   Def_Container and External
!-------------------------------------------------------------------------
 Face libre
  alphat       = 1.000000e+001
  tempext       = 10.000000
  epsilon       = 8.800000e-001
.FIN THERMIQUE_2

!================================ INCREMENTS Block
5- This module defines the specific computation of Maximum node
displacement per increment
==========================================================

.INCREMENT
 depmax    = 0.03   !Maximum node displacement per increment - modifies the
time step
.FIN INCREMENT

!================================ EXECUTION Block
6- This module defines the specific computation execution parameters
==========================================================
```

.EXECUTION
dhsto = 1.000000 In order to limit the total storage space for the computation results files, we store only the results every 0.54 mm of ram stroke. In addition to this storage every step before and after each remeshing will be stored.
Sans Visualisation !No dynamic graphic window to save CPU time
facteurdtmin = 0 !minimum time step related to time
facteurdhmin = 0 !minimum time step related to the nodes displacement
.FIN EXECUTION

!========== REMESHING Block
7- This module defines the parameters for the remeshing function during computation.
==========

.MAUTO !The maillage fin keyword defines automatically all the remeshing parameters values for a fine mesh creation (it will take into account the global dimensions of the part to compute a correct mesh element size)
Average mesh !mesh density - average mode
Taille max 4.0 !remeshing parameters active on the !boundary(element size)
fine front !finer size for the front mesh

zone : taille max 0.15, !fixed remeshing box1:value of the maximum !element size associated
Xmin 4.8, !X coordinate of the bottom left corner
Ymin -1.2, !Y coordinate of the bottom left corner
Xmax 8., !X coordinate of the top right corner
Ymax 0.7 !Y coordinate of the top right corner

zone : taille max 0.5, !fixed remeshing box2
Xmin 0.,
Ymin -7.0,
Xmax 12.,
Ymax 4.

zone : taille max 1., !fixed remeshing box3
Xmin 0.,
Ymin 4.0,
Xmax 14.,
Ymax 8.

zone : taille max 1.0, !fixed remeshing box4
Xmin -1.0,
Ymin -50.0,
Xmax 8.0,
Ymax -7.0

autosize 100 !with automatic adaptative remeshing the default local !size will be divided by a maximum ratio of ten.

!This !size ratio can be changed. for example to have a reduction of the size until 1/100th of the local size. !With a negative parameter ratio the size will be only !related to the piece thickness

.FIN MAUTO
!============================== USER ROUTINE Block
8- This module defines the parameters for the user variables for the computation of subgrain size, iso-extrusion conditions, friction variations etc.
==========

.USERVAR
!Nodes Variables
P1ini = 0.000000 ! Initiale value of variable 1 (node): ZENER
P2ini = 0.000000 ! Initiale value of variable 2 (node): LN(Z)
P3ini = 0.000000 ! Initiale value of variable 3 (node): LN(Z/A)
P4ini = 0.000000 ! Initiale value of variable 4 (node): SUBGRAIN SIZE
P5ini = 0.000000 ! Initiale value of variable 5 (node): height
P6ini = 0.000000 ! Initiale value of variable 6 (node): height zone

!Variables for integration points
Pint1ini = 0.000000 ! Initiale value of variable 1 (pt. int.): ZENER
Pint2ini = 0.000000 ! Initiale value of variable 2 (pt. int.): LN(Z)
Pint3ini = 0.000000 ! Initiale value of variable 3 (pt. int.): LN(Z/A)
Pint4ini = 0.00000 ! Initiale value of variable 4 (pt. int.):height
Pint5ini = -1.00000 ! Initiale value of variable 4 (pt. int.): quality

!Real parameters and position used to cut the extrudate

R1 = 3.000000 !used in Oyane damage criterion expression
R2 = -31.500000 !Cutting zone calculation (-31.5<Z<-32.5)
R3 = -32.500000
Rint1 = 3.000000 !used in Oyane damage criterion expression
.FIN USERVAR

!============================== CUTTING Block
9- This module defines the parameters for the user to trigger the cutting of the extrudate.
==========
===

.DAMAGE
!Rupture simulation for the billet
Number = 4 ! law#4
TriggerValue= 33. ! cutting if Z<-33 - opposite value of real Z coordinate
.FIN DAMAGE

!============================== HISTORY Block
10- Before starting the first operation computation, this module is empty After the simulation, this module will contain all the information pertaining to the computation history (all the file names automatically created at each remeshing)
==========
.Histoire
.Fin Histoire

Appendix 5: Experimental data of the flow stress measured by hot torsion for 4% Cu binary 2014 alloy [63]

Strain-rate (s^{-1})	Temperature (^0C)	Actual stress (Mpa)
0.032	300	50.23
2.507	303	93.13
28.768	311	115.85
28.443	312	115.23
0.032	350	32.69
2.633	357	69.46
28.443	360	93.45
28.443	360	93.45
0.032	390	23.37
0.305	391	38.05
2.669	395	55.83
8.567	397	66.65
29.129	400	78.27
0.032	430	17.06
0.305	431	28.67
2.687	433	44.64
8.567	436	54.28
29.472	436	66.4
0.032	475	12.34
0.31	476	21.26
2.76	477	34.64
8.567	478	43.41
29.472	480	54

Appendix 6: Data structure of FORGE3

GENERAL DATA FILE FOR FORGE3:

```
! File Type:              FORGE3V6.2 Data File
! Creator:                GLPre Version 2, 1, 0, 7-Release
! Author:                 Isaac_
! Creation Date:          2003-02-18 08:53:10
! Data File Name:         t-400-3_subgrainaa2024.ref
! Data File Location:     C:\Isaac\T-Shape-19-02-03\T-Shape-400-Die-fine-
mesh-Ghost\ T-400-3_SubgrainAA2024\

!================================ FILE Block
1- This module defines the file names for the billet mesh (part.msh) and the
tooling which will be used in the simulation
==========================================================

.FICHIER
        Fmay=billet.may
        Fout=t-400-3_subgrainaa2024.out
        Fres=t-400-3_subgrainaa2024.res
        Faux=t-400-3_subgrainaa2024.aux
        NomGen=t-400-3_subgrainaa2024_
.FIN FICHIER

!================================ UNITS Block
2- This is the unit system module. It states that we used mm to define lenght,
MPa. for stresses and mm.Kg.s for the thermal data. The temperature unit is
degrees Celsius( Default).
==========================================================


.UNITES
        MM-MPA-MM.KG.S
.FIN UNITES
!================================ RHEOLOGY Block
3- This module defines the part (billet) Rheology and the friction values
between the part and dies.
==========================================================


.RHEOLOGIE
EVP
LOIV SIG0
ZENER-H
PAR DH =146880.d0
PAR R  =8.31d0
PAR alpha =0.016d0
PAR n =4.27d0
```

```
PAR A =325215956.1d0
FIN LOI


!Elasticity Coefficients
Youngmodulus = 7.300000e+04
Poissoncoeff = 0.300000

!Thermal Coefficients
mvolumique = 2.800000e-06 !Density
cmassique  = 1.230000e+09 !Specific Heat
conductmat = 2.500000e+05 !Conductivity
epsilon    = 5.000000e-02 !Emissivity


!----------------------------
OUTIL1                    !Punsh

        !Friction between part and rigid die
        Tresca                              ! Friction Law
        mbarre = 0.2

        !Thermal Exchange between part and rigid die
        ! Unit = si
        alphat     = 1.000000e+04                ! Transfert coefficient
        Effus = 1.176362E+04                          ! tool effusivity

        Temp = 300.000000
FIN OUTIL
!----------------------------

!----------------------------
OUTIL2                    !Container

        !Friction between part and rigid die
        Tresca                              ! Friction Law
        mbarre = 8.000000e-01

        !Thermal Exchange between part and rigid die
        ! Unit = si
        alphat     = 1.000000e+04                ! Transfert coefficient
        Effus = 1.176362E+04                          ! tool effusivity

        Temp = 350.000000
FIN OUTIL
!----------------------------

!----------------------------
OUTIL3                    !Die

        !Friction between part and rigid die
        Coulomb                                     ! Friction Law
        mbarre = 3.000000e-01
        mu     = 1.500000e-01
```

```
        !Thermal Exchange between part and rigid die
        ! Unit = si
        alphat     = 1.000000e+04              ! Transfert coefficient
        Effus = 1.176362E+04                          ! tool effusivity

        Temp = 320.000000
FIN OUTIL
!---------------------------

!---------------------------
OUTIL4                !Ghsot_die

        !Friction between part and rigid die
        Tresca                                ! Friction Law
        mbarre = 0.0

        !Thermal Exchange between part and rigid die
        ! Unit = si
        alphat     = 1.000000e+01              ! Transfert coefficient
        Effus = 1.176362E+00                          ! tool effusivity

        Temp = 45.000000
FIN OUTIL
!---------------------------
        !Thermal Exchange between part and air
        AlphaText = 1.000000e+001          ! Global Transfert Coeff.
        TempExt = 50.000000                       ! Ambient Temperature

        ! Initial temperature already exists in mesh file

!============================== USER ROUTINE Block
4- This module defines the parameters for the user variables for the computation of subgrain size, iso-extrusion conditions, friction variations etc.
==========================================================


LOIV MECA
        Sigma1
        Par STRESSTENSOR(6) = EXIST
        Var SIG1 = 0.
FIN LOI

! USER VARIABLE LAW: Subgrain_size
LOIV UTIL
        SUB_GRAINSIZE
        Par A_ = -1.89  !1
        Par B_ = 0.082          !2
        Par DH_1 = 146880   !3
        Par STRAINRATE= EXIST    !4

        Eta SUBGRAIN_INS = 2.3    ! STEADY STATE SIZE gs_eta(1) = (A_
+ B_*dlog(Zener_I))**(-1.D0)          !SUBGRAIN_INS
```

```
        Eta SUBGRAIN_AVR = 2.3   !STEADY STATE SIZE  gs_eta(2) = (A_
+ B_*dlog(Zener_DXJ_A))**(-1.D0)   !SUBGRAIN_AVR

FIN LOI

        Stock=SIG1
.FIN RHEOLOGIE
==========================================================
===
!============================== TOLERCONV Block
.TOLERCONV
.FIN TOLERCONV

!============================== INCREMENTS Block
4- This module defines the specific computation of Maximum node
displacement per increment
==========================================================
.INCREMENT
        Deformation= 1.000000e-002
.FIN INCREMENT

!============================== EXECUTION Block
5- This module defines the specific computation execution parameters
==========================================================
.EXECUTION
!       Inertia
        dhsto = 8.500000e-001
        Sans Marquage
        Gravite
.FIN EXECUTION

!============================== THERMIC Block
.THERMIQUE
.FIN THERMIQUE

!============================== MESH REFINEMENT Block
6- This module defines the refinement boxes.
==========================================================
.BOITE
   BOX 1
        Type=20                 ! CYLINDER
        Eulerian
        Size= 2
        !Param Info: NbPar, Xcenter, Ycenter, Zcenter, Rext, Rint, H
        Parameters: , 6 , 0 , 0 , 0 , 20 , 0 , 180
        Matrix:, 1, 0, 0, 0,
                 0, 1, 0, 0,
                 0, 0, 1, -170,
                 0, 0, 0, 1
END BOX
BOX 2
        Type=20                 ! CYLINDER
        Eulerian
        Size= 1
```

```
        !Param Info: NbPar, Xcenter, Ycenter, Zcenter, Rext, Rint, H
        Parameters: , 6 , 0 , 0 , 0 , 16 , 0 , 15
        Matrix:, 1, 0, 0, 0,
                 0, 1, 0, 0,
                 0, 0, 1, -10,
                 0, 0, 0, 1
END BOX
BOX 3
        Type=20                 ! CYLINDER
        Eulerian
        Size= 0.4
        !Param Info: NbPar, Xcenter, Ycenter, Zcenter, Rext, Rint, H
        Parameters: , 6 , 0 , 0 , 0 , 14 , 3.5 , 22
        Matrix:, 1, 0, 0, -1.5,
                 0, 1, 0, 1.5,
                 0, 0, 1, -20,
                 0, 0, 0, 1
END BOX
BOX 4
        Type=20                 ! CYLINDER
        Lagrangian
        Size= 2
        !Param Info: NbPar, Xcenter, Ycenter, Zcenter, Rext, Rint, H
        Parameters: , 6 , 0 , 0 , 0 , 40 , 0 , 6
        Matrix:, 1, 0, 0, -2,
                 0, 1, 0, -2,
                 0, 0, 1, 90,
                 0, 0, 0, 1
    END BOX

.FIN BOITE

!================================ SENSORS Block
.CAPTEURS
  Capteur 1
          x = 0
          y = 0
          z = 0
          Eulerien
  Fin Capteur
  Capteur 2
          x = -3.19021
          y = -0.111538
          z = -2.5
          Eulerien
  Fin Capteur
  Capteur 3
          x = -3.15569
          y = -0.142258
          z = -4.5
          Eulerien
  Fin Capteur

.FIN CAPTEURS
```

```
!================================ REMESHING Block
7- This module defines the parameters for the remeshing function during
computation
=================================================================

.MAUTO
        periode= 20
        lbase  = 6
.FIN MAUTO

!================================ KINEMATICS Block
8- This module defines the tool kinematics refinement boxes.
=================================================================

.CINEMAT_OUT
        Outil1          ! Punsh
                maitre
                Axe = 3
                Fin Outil
.FIN CINEMAT_OUT

!.PILOT
        NbPass= 1
        Pass1
        Fin Pass
.FIN PILOT
! ================================================================
```

REFERENCES

1. Sheppard, T. (1999). **Extrusion of Aluminium Alloys.** Kluwer Academic Press, Boston USA. Dordrecht. The Netherlands. 1999, ISBN 041259070 0.

2. Wood, E. P. and T. Sheppard (1975). **Evaluation of shape factors for aluminium alloy extrusions.** *Aluminium*, 51(12), pp.760-764.

3. Sheppard, T.; Wood, E. P. (1976). **On the pressure required for extrusion of shaped aluminium sections.** Proc of Mach Tool Des and Res Conf, 17th, Vol. 3, Sep 20-24, pp. 411-421.

4. Sheppard, T.; Wood, E. P.(1980) **Effect of section geometry on extrudability of Al-Cu-Mn alloy.** *J. Metals Technology*, 7(2), pp. 58-66.

5. Akeret R. (1988). **Control of metal flow in extrusion dies.** Swiss Aluminium Ltd, , *J. Light Metal Age*, Vol. 46, pp. 7-8.

6. Akeret R. (1983). **Extrusion of aluminium: Part I. Process in the deformation zone.** *J. Aluminium* (English Edition) 59(9), pp. 276-280

7. Akeret R. (1983). **Influence of cross-sectional shape and the die design in extrusion of aluminium: Part II friction in the die land.** *J. Aluminium* (English Edition), 59(10), pp. 355-360

8. Sheppard, T. (1993). **Extrusion limit diagrams containing structural and topological information for AA6063 aluminium alloy.** *J. Material Science & Technology.* Vol. 9, pp. 313-318.

9. Hirst, S. and D. H. Ursell (1958). *Metal Treatment,* 25, pp. 401

10. Sheppard, T. and D. Raybould. (1973). **New approach to the constriuction of extrusion-limit diagrams, giving structural information with application to superpure aluminium and Al-Zn-Mg alloys.** *J. Inst Met* (London), Vol. 101, pp. 73-78.

11. Raybould, D. and T. Sheppard (1976). **Structural limit diagrams and the flow stress distribution during the axisymmetric extrusion of aluminium alloys.** Int Conf on the Strength of Metals and Alloys, 4th, Proc, Ed by Lab de Phys du

Solide

12. Sheppard T. and D Raybould (1973). **On load and temperature rise during the extrusion of superpure Al, Al-Zn and Al-Zn-Mg alloys.** J. *Inst. Met.*, Vol. 101, pp. 33-44.

13. Zienkiewick, O. C. Onate, E. Heinrich, JC. (1981). **A General Formulation for Coupled Thermal Flow of Metals using Finite Elements.**_Int. J. I for Numerical Methods in Eng. 17(10), pp. 1497-1514.

14. Zienkiewicz, O.C. and R.L. Taylor. (2000). **Finite Element Method: Vol. 1, The Basis Manufacturer: Butterworth-Heinemann ISBN: 0750650494**

15. Chenot J. L., O. C. Zienkiewicz, and R. D. Wood (1992). : **Numerical Methods in Industrial Forming Processes**. Numiform-92. Ashgate Publishing Company.

16. Gieselberg, K. and K. Lange. (1975). **Elastic deformation of square extrusion dies due to load and temperature**. J. *Ann. CIRP*. 24(1), pp. 167-171.

17. Shabaik, A. H. (1976). **Computer simulation of metal flow during extrusion.** J. Nucl. Metall. 20,2, 752-762. Proc. of the Int. Conf. on Comput. Simul. for Mater. Appl. Apr 19-21. Gaithersburg, MD, USA.

18. Brandal, S A. and H. Valberg (1981) **Analysis of the deformation process during wire drawing by means of the finite element method.** Proceedings of the Annual Convention of the Wire Association International, pp. 110-118.

19. Brandal, S. A. and H. Valberg (1982). **Analysis of the Deformation Process during Wiredrawing by means of the Finite Element Method.** *Wire Journal International*, 15(3), 64-70.

20. Sheppard, T. and A. Jackson. (1997). **Constitutive equations for use in prediction of flow stress during extrusion of aluminium alloys**. *J. Material Science & Technology*. Vol. 13, pp. 203-209.

21. Sheppard, T. and D. Wright (1979). **Determination of Flow Stress: Constitutive equation for Aluminium Alloys at Elevated Temperatures.** J. *Met Tech.*, 6(6), pp. 215-223.

22. Shi, H. A. J. McLaren, C. M. Sellars, R. Shahani and R. Bolingbroke (1997). **Hot plane strain compression testing of**

Aluminum alloys. J. of Testing & Evaluation, 25(1), pp.61-73.

23. Gelin, J. C. and O. Ghouati (1995)**.Inverse approach for the determination of constitutive equations in metal forming.** J. CIRP Annals - *Manufacturing Technology*, 44(1), pp. 189-192.

24. Chenot. J.L.and M. Bellet (1992). **The viscoplastic approach for the finite element modelling of metal-forming processes.** In*: Hartley P., Pillinger I. & Sturgess C.(editors).* Numerical modelling of material deformation processes, Research, development and applications. London. Springer Verlag, pp. 179-224.

25. Gelin, J. C., O. Ghouati, R. Shahani. (1993): **Identification and modelling of flow stress functions for hot rolling of aluminium alloys from plane strain compression test. Proceedings of 1st international conference of metal rolling processes**. 21-23, Sept., Imperial College, London, UK, pp.239-255.

26. Owen D.R.J. (1993). **The Design and Optimisation of Forging Systems by Numerical Simulation**, *Bench Mark,* Dec., pp. 36-41.

27. Norton F.H. (1929): **Creep of Steel at High Temperature_**, McCraw-Hill, New York.

28. Hoff N..J (1954). **Approximate Analysis of Structures in the Presence of Moderately Large Steps Deformation**. *Quart. Appl. Math.*, Vol 2, pp. 49

29. Sellars, C.M. and D. Tegart. (1972), **Hot Workability** . *International Metallurgical reviews* Vol. 17.

30. Dashwood R. J., H. R. McShane, and A. Jackson. (1996). **Computer Prediction of Extrusion Limit Diagrams**. Proc. 6th Int. Seminar on 'Aluminium Extrusion Technology', Chicago, pp. 331-339. Washington, DC. The Aluminium Association.

31. Shi J.H. et al.1997. **Constitutive equations for high temperature flow stress of aluminium alloys**. *J. Material Science & Technology*. Vol. 13, pp. 200-216.

32. Puchi, Eli S. et al. 1998. **Analysis of a hot rolling schedule for commercial aluminium-1%magnesium alloy in terms of dynamic material modelling concepts. Part I: description of the constitutive behavior**. In: Sao T.et al. (editors). Sixth International conference on Aluminium alloys, Toyohashi, Japan, July, pp. 395-400.

33. Flitta I. and T. Sheppard. (2002). **Simulation of bridge die extrusion using the finite element method** *J. Material Science & Technology*. Vol. 18. pp. 987-994.

34. Flitta I. and T. Sheppard, (2003) **On the Nature of Friction in the Extrusion Process and its Effect on Material Flow.** *J. Material Science & Technology*. July. Vol 19. pp. 837-846.

35. Flitta, I and Sheppard, (2002). **Investigation of Friction during the extrusion of Al-alloys using FEM simulation**" Proc. 5th Inter. ESAFORM.. *Krakow, Poland,* pp. 435-438.

36. Saha P .K. (1998). **Thermodynamics and Tribology in Aluminum Extrusion**. *Wear*, Vol 218.

37. Grasmo, G., Holte, K., Stren, S., Valberg, H., Flatval, R., Hanssen, L., Lefstad, M., Lohne, 0., Web, T., ørsund, R., Herberg, J. (1992). **Modelling of two-dimensional extrusion**. Proc. 5th Int. Seminar on 'Aluminium Extrusion Technology', Chicago, pp. 367-376. Washington, DC. The Aluminium Association.

38. Castle A.F. (1992). **Temperature Control in Aluminium Extrusion**. Proc. Fifth International Aluminium Extrusion Technology Seminar, Aluminium Extruders Council and the Aluminium Associations.

39. Akeret, R., and Strehmel W. (1986). **Heat balance and exit temperature control in extrusion of aluminium alloys.** *Proc. Int. Al. Tech.* London. pp. 663-669.

40. Sheppard T. (1981). **Temperature and Speed effects in Hot Extrsuion of Aluminium Alloys.** *J. Met Tech.*, 8(4), 130-141

41. Saha, P. K.; Ghosh, R. K. (1979). **Temperature Distribution During Hot Extrusion of Aluminium: Theoretical Evaluation.** *J. Indian Journal of Technology*, 17(7), pp. 264-268.

42. Castle A. F., and T. Sheppard (1976). **Pressure Required to Initiate Extrusion in Some Aluminium Alloys**. *J. Met Tech.* 3(10), pp. 465-475.

43. Raybould, D. and T. Sheppard, (1973). **Axisymmetric extrusion: The effect of temperature rise and strain rate on the activation enthalpy and material constants of some aluminium alloys and their relation to recrystalisation, substructure and subsequent mechanical properties.**. *J. Inst.*

Met. (London) Vol. 101

44. Bishop J. F. W. (1966). *J. Mech. Appl. Math.*, Vol. 9, pp. 236-256.

45. Velay, X.; X. Duan, X and T. Sheppard. (2003). **Prediction of material flow pattern in the hot extrusion of aluminium alloys by the finite element method.** *Mater Sci Forum.* Vol . 5, pp. 426-432.

46. Duan, X and Sheppard, T. (2003). **The influence of die shape on the behaviour of surface recrystalisation.** *TMS Annual Meeting*, pp. 99-108.

47. Duan, X **and** Sheppard, T. (2003). **Formation of extrudate surface** *TMS Annual Meetin*g, pp. 289

48. Duan, X **and** Sheppard, T. (2003). **Computation of substructural strengthening by the integration of metallurgical models into the finite.** *Computational Materials Science*, 27(3), pp. 250-258.

49. Flitta I. and T. Sheppard: (2000). **On the Mechanics of Friction During the Extrusion Process.** Proc. 7th Int. Seminar on 'Aluminium extrusion technology', Chicago, pp. 197–203; Washington, DC, The Aluminium Association.

50. Chanda T., J. Zhou, L. Kowalsi and J. Duszczyk. (1999). **3D Simulation of the thermal event during AA6061 aluminium extrusion"** *J. Sci. Mat.*, Vol. 41, pp. 195-202..

51. Dean T. A. and Hu Z. M. (1999). **The increase requirements on imperical data for use in metalforming process simulation packages.** Advance Technology of Plasticity. Proceedings of the 6th ICTP, 1(541), pp. 19-24.

52. Van Rens B. J. E. Brelemans W. A. M. and Baajens F. P. T. (2000). **Numerical Simulation of the Extrusion of Complex (Hollow) Profiles.** Proc. 7th Int. Seminar on 'Aluminium Extrusion Technology', Chicago, pp. 99-107. Washington, DC. The Aluminium Association

53. Abtahi S., S. Storen and T. Welo (1996). **Interface Mechanisms on the bearing surface in Extrusion**. Proc. 6th Int. Seminar on 'Aluminium Extrusion Technology', Chicago. Pp. 125-131. Washington, DC. The Aluminium Association

54. Welo T., S. Abtahi and I. Skauvik (1996). **An Experimental and Numerical investigation of the thermo-mechanical**

conditions on the bearing surface of Extrusion dies. Proc. 6th Int. Seminar on 'Aluminium Extrusion Technology', Chicago, pp. 101-106. Washington, DC. The Aluminium Association.

55. Anand, L., (1993). **A Constitutive Model For Interface Friction," Computational Mechanics.** Vol. 12, pp. 197–213.

56. Anand, L., and Tong, W. (1993). **A Constitutive Model For Friction In Forming.** *Annals of CIRP*. Vol. 42 , pp. 361–366.

57. Clode M. P. and T. Sheppard (1990). **Formation of Die Lines During Extrusion of AA6063**. *J. Material Science & Technology*., Vol.6, pp. 755-763.

58. Chanda T., J. Zhou, L. Kowalsi and J. Duszczyk. (2000). **3D FEM Simulation of thermal and Mechanical Events Occuring During Extrusion Through a Channel Shaped Die**. Proc. 7th Int. Seminar on 'Aluminium Extrusion Technology', Chicago, pp. 125-134. Washington, DC. The Aluminium Association.

59. Heege, A., P. Alart, and E. Onate, (1995). **Numerical Modelling and Simulation of Frictional Contact using a Generalised Coulomb Law**. *Engineering Computations*. Vol.12, pp. 41-656.

60. Valberg, H. and T. Malvik. (1994). **An experimental investigation of the material flow inside the bearing channel in aluminium extrusion**. *Int. J. of Mat. & Prod. Tech*. Vol. 9,. Pp. 428-463.

61. Yang, D. Y. (1994). **Investigation into Non-Steady-State Three-Dimensional Extrusion of a Trocoidal Helical Gear by the Rigid-Plastic Finite Element Method**. *Annals of the CIRP*, Vol. 43, pp. 229-233.

62. Subramaniyan J (1989). **Extrusion of 2024 Aluminium Alloy. Sections** PhD Thesis, Imperial College, London.

63. Vierod R. P. (1983). **Effect of copper additions on deformation processing of Aluminium Alloys.** PhD Thesis, Imperial College, London.

64. Sheppard T. and Patterson S.J. *J. Mech. Work. Tech*. Vol. 4, pp. 39-56.

65. Valberg H. (1993). **Metal Flow in the Direct axisymmetric extrusion of Aluminium**. *J. Mat. Proc. Tech*. Vol. 31. pp. 39-55.

66. Valberg H. (1988). **Surface Formation in Al-Extrusion (Direct Extrusion).** Proc. 4th Int. Al. Extr. Techn Sem. Pp. 309-319.

67. Akret R. and W. Strehmel. (1988). **Control of metal flow in extrusion dies**. Proc. 4th Int. Seminar on 'Aluminium Extrusion Technology', Chicago, Vol. 1, pp. 357-397. Washington, DC. The Aluminium Association

68. Clode M. P. and T. Sheppard (1986). **Surface Generation and the Origin of Defects During Extrusion of Aluminium Alloys.** *The Aluminium Technology,* Institute of Metals, London, pp. 230-240.

69. Valberg H. (1986). Title Proc. The Aluminium Technology, London, UK March. pp. 240-251.

70. Valberg H. (1986). **Surface Formation Mechanism in Direct Extrusion of Aluminium Alloys**. Aluminium Technology '86, Proceedings of the International Conference. London, Eng.

71. Hardouin, J. P. (1992). **Bearing length calculation by control of metal flow pressure.** Aluminium association, 5th Extrusion Technology Seminar, Vol. 2, pp. 291-303.

72. Flitta, I. And Sheppard, T (2000). **On the Mechanics of Friction During the Extrusion Process**. Proc. 7th Int. Seminar on 'Aluminium Extrusion Technology', Chicago, Vol. 1, pp. 197-203. Washington, DC. The Aluminium Association.

73. Atzema E. and J. Huetink,(1995). **Finite element analysis of forward–backward extrusion using ALE techniques**. in Proc. 5th Int. Conf. on Numerical Methods in Industrial Forming Processes. NUMIFORM'95, Ithaca, NY, June, pp. 383–388.

74. Chanda T., J. Zhou and J. Duszczyk. (2001). **A Comparative study on iso-speed extrusion and isothermal extrusion of 6061 Al alloy using 3D FEM simulation**. *J. Mat. Proc. Techno.* Vol. 114, pp. 145-153.

75. Lof J. G. Klaseboer and J. Huetink. (2000). **FEM simulations of Aluminium Extrusion using an Elasto-Viscoplastic material model.** Proc. 7th Int. Seminar on 'Aluminium Extrusion Technology', Chicago, pp. 157-168. Washington, DC. The Aluminium Association.

76. Zhang X. and J. Heathcock (2000). **Modeling of Metal flow for bearing design**. Proc. 7th Int. Seminar on 'Aluminium Extrusion Technology', Chicago, pp. 169.176. Washington, DC. The Aluminium Association.

77. Sibilla S. and A. Baron. (2000). **Numerical modeling of three-**

demensional aluminium flow in extrusion dies. Proc. 7th Int. Seminar on 'Aluminium Extrusion Technology', Chicago, pp. 203-210. Washington, DC. The Aluminium Association.

78. Dick A. (1897). UK Patent N°. 99405, March.

79. Sheppard T., E. Nisaratanaporn, and B. H. McShane (1985). **Material Flow and Pressure Prediction when Extruding through Bridge Dies.** Z. Metallkd., 89 (5).

80. Gasiorczyk J. and J. Richet. (2000). **Application of FEM modeling to simulate metal flow through porthole dies**. Proc. 7th Int. Seminar on 'Aluminium Extrusion Technology', Chicago, pp. 195-202. Washington, DC. The Aluminium Association.

81. Akeret, R. (1992). **Extrusion Welds- Quality Aspects are Now Centre Stage**. Proc. 5th Int. Seminar on 'Aluminium Extrusion Technology', Chicago, pp. 319-336. Washington, DC. The Aluminium Association.

82. Duplanic, I. And Prgin, J.(1996). **Determination of Parameters Required for Joining Process in Hollow Dies.**. Proc. 6th Int. Seminar on 'Aluminium Extrusion Technology', Chicago, pp. 225-300. Washington, DC. The Aluminium Association.

83. Valberg, H. (1996). **Extrusion in Welding in Porthole Die Extrusion.** Proc. 6th Int. Seminar on 'Aluminium Extrusion Technology', Chicago, pp. 213-224. Washington, DC. The Aluminium Association.

84. Kusiak, J. et al.(1996). **Application of Finite-Element-Technique to the Simulation of the Aluminium Extrusion Process**. Proc. 6th Int. Seminar on 'Aluminium Extrusion Technology', Chicago, pp. 361-367. Washington, DC. The Aluminium Association.

85. Mooi, H. G. A., et al. (1996). **Simulation of Aluminium extrusion based on a Finite Element Method (FEM).** Proc. 6th Int. Seminar on 'Aluminium Extrusion Technology', Chicago, pp. 359-368. Washington, DC. The Aluminium Association.

86. Welo, T., A. Smabrekke, and H. Valberg. (1995). **Two dimensional Simulation of Porthole Extrusion.,** *Aluminium,* 71(1), pp. 90-94.

87. Devadas C. and O. Celliers.(1992**). Metal flow during the extrusion process**. Proc. 5th Int. Seminar on 'Aluminium Extrusion Technology', Chicago, pp. 359-368. Washington, DC. The Aluminium Association..

88. Macey, G.E. and Salim, M. (1992). **Numerical Simulation of Two-Dimensional Hot Extrusion of Aluminium.** Proc. 5th Int. Seminar on 'Aluminium Extrusion Technology', Chicago, pp. 247. Washington, DC. The Aluminium Association.

89. Mori, K. I., K. Osakada, and H. Yamaguchi. (1992). **FE simulations of 3D extrusion of sections.** In *D. R. J. Owen, editor, 3rd Int. Conf. Comp. Plast.*, pp. 1139-1149. Pineridge Press.

90. Kiuchi, M., J. Yanagimoto, and V. Mendoza.(1995). **Flow of solid metal during extrusion: 3D simulations by FE method.** In *Shen and Dawson, editors, Simulation of Materials Processing: Theory Methods and Applications*, pp. 847-852, Rotterdam, Balkema.

91. Kang, Y. S. and D. Y. Yang. (1996**). Investigation into the thermo-viscoplastic finite element analysis of square die extrusion of square section with Lagrangian description**. *Int. J. Mach. Tools Manufact.*, pp. 36, 907.

92. Yang, D. Y. K. Park and Y. S. Kang. (2001). **Integrated finite element simulation for hot extrusion of complicated Al alloy profiles.** *J. Mat. Proc. Tech.* Vol. 111, pp. 25-30.

93. Kang, B. S., B. M. Kim, and J. C. Choi. (1994). **Preform design in extrusion by FEM and its experimental confirmation.** *J. Mater. Proc. Tech.*, Vol. 41, pp. 237-248.

94. Plata, M and Piwnik, J. (2000). **Theoretical and Experimental analysis of Seam Weld Formation in Hot Extrusion of Aluminium Alloys.** Proc. 7th Int. Seminar on 'Aluminium Extrusion Technology', Chicago, pp. 205-211. Washington, DC. The Aluminium Association.

95. Sheppard, T. (1993). **Extrusion of AA2024 alloy**. Materials Science &Technology. Vol. 9, pp. 430-440.

96. Sheppard, T. M. G. Tutcher and H. M. Flower. (1979). Development **of recovered dislocation substructures during plastic flow. W**. *J. Met Sci*, 13(8), pp. 473-481.

97. Zaidi, M.A. and Sheppard, T. (1982). **Development of microstructure throughout roll gap during rolling of aluminium alloys**. *Metals technology*. Vol. 16, pp. 229-238.

98. Raghunathan, N. and Sheppard, T. (1989). **Microstructural development during annealing of hot rolled Al-Mg alloys.**

Materials Science and Technology. Vol. 5, pp. 542-547.

99. McQueen, H.J. and W. Blum. (1998). **Recovery and recrystallization in AL alloys fundamentals and practical applications**. In: Sao T.et al. (editors). 6th International conference on Aluminium alloys, Toyohashi, Japan, pp. 99-112.

100. Sellars, C.M. and Zhu, Q. (2000). **Microstructure modelling of aluminium alloys during thermomechanical processing**. *Materials Science and Engineering* A: Structural Materials: Properties, Microstructure and Processing. 280(1), pp. 1-7.

101. Jonas, J.J. et al. (1969). **Strength and structure under hot-working conditions. Metallurgical reviews.** Vol. 14, pp. 1-24.

102. Zhu, Q. and C. M. Sellars (2000). **Microstructural evolution of aluminium-magnesium alloys during thermomechanical processing**. *Materials Science Forum*, 331 (I), pp. 409-420.

103. Sellars, C.M. and Q. Zhu. (2000). **Microstructure modelling of aluminium alloys during thermomechanical processing**. *Materials Science and Engineering* A: Structural Materials: Properties, Microstructure and Processing. 280(1), pp. 1-7.

104. Furu, T. et al. (1999). **The influence of transient deformation condition on recrystallization during thermomechanical processing of an Al-1%Mg alloy. Acta material.** 47(5), pp. 2377-2389.

105. Zhu, Q. et al. (1997). **Modelling hot deformation behaviour based on evolution of dislocation substructures**. In: Chandra T. and Sakai T. (editors). Proc. Intern. Conf. On Thermomechanical Processing of Steels and Other Materials (THERMEC'97). The Minerals, Metals and Materials Society, pp. 2039-2045.

106. Nes, E. et al. (1994). **Physical modelling of microstructural evolution during thermomechanical processing of aluminium alloys**. In: Sanders, T. and Starke, E.A. (eds). Aluminium alloys physical and mechanical properties (ICCA4), Altanta, pp. 250-257.

107. Lange G. (1971). **Heat balance of the extrusion process 1-** Z Metallk, 62(8), pp. 571-7.

108. Pinkham, M. (2002). *Aluminium Today*, 14(7), pp. 31-32.

109. Kialka J (1996). **Isothermal Extrusion of Aluminium Alloys by Employing Force-Ram Speed Feedback.** Proc. 6th Int.

Seminar on 'Aluminium Extrusion Technology', Chicago, pp. 73-78. Washington, DC. The Aluminium Association.

110. Venas I. , J. Herberg, and I. Skauvik (1992). **Isothermal Extrsuion principles on Extrusion Speed**. Proc. 5th Int. Seminar on 'Aluminium Extrusion Technology', Chicago, pp. 229-233. Washington, DC. The Aluminium Association.

111. Akeret, R., and W. Strehmel W. (1986). **Heat balance and exit temperature control in extrusion of aluminium alloys**. *Proc. Int. Al. Tech.* London. pp. 663-669.

112. Ruppin, D. and W. Strehmel. (1983). **Automation of the extrusion process in the direct extrusion of aluminium alloys (I)** *Aluminium* (English Edition), 59 (9), pp. 285-289

113. Ruppin, D. and W. Strehmel (1981). **Conditions for the Automation of the press process in the direct extrusion of Al Alloys** In: *Extrsuion, Sci. and Tech. Dev.*. ED.G. Lang et al., DGM Oberursel.

114. Chenot, J.-L. et al. (1999). **Practical simulation of forging sequence of complex 3-D parts in industry.** In: Geiger, M. (editor). Advanced technology of plasticity 99: Proceedings of the 6th ICTP, 19-24 Sept. Springer-Verlag, New York, pp. 1597-1612.

115. Wagoner R. H. and J. L. Chenot (1997). **Fundamentals of metal forming**. John wiley & sons, Inc. NY.

116. Transvalor S. A. 2000. **FORGE3 V5.3 user guide & reference guide**. Transvalor S. A.

117. Laroussi, M. and L. Fourment. (2002). **The adjoint state method for sensitivity analysis of non-steady-state problems Applications to 3D forging**. 5th Inter. EESAFORM Conf. on Mater. Forming Krakow. pp. 19-21.

118. Williams A. J., T. N. Croft and M. Cross. (2002). **Computation Modelling of Metal Forming Processes**. 5th Inter. EESAFORM Conf. on Mater. Forming Krakow April, pp. 67-70.

119. Zhou L. Li, J., J. Duszczyk. Date **Prediction of Temperature Evolution during the Extrusion of 7075 Aluminium Alloy at Various Ram Speed by Means of 3D FEM Simulation"**, *J. Mater. Process. Tech.*

120. Clode M. P. (1987). **The origin of defects during Al-Mg-Si extrusion.** PhD Thesis, Imperial College, London.

121. Sheppard T. and M. G. Tutcher (1980). **Development of duplex deformation substructure during extrusion of a commercial Al-5Mg. alloy.** : *Metals Science*, 14(12), pp. 579-589.

122. Tutcher M. G. (1979). **Deformation processing applied to the Al-Mg alloy system.** PhD Thesis, Imperial College, London.

123. Nisaratanaporn E. (1995). **Microstructure development and Pressure requirements in 6063 Aluminium alloy tube extrusion.** PhD Thesis, Imperial College, London.

Nature of friction in extrusion process and its effect on material flow

I. Flitta and T. Sheppard

This investigation focuses on simulation of the extrusion process and in particular the effect of the initial billet temperature on friction and its consequences on material flow. The simulation is compared with data obtained from an experimental extrusion press. All the simulations are performed with the implicit finite element codes FORGE2 and FORGE3. The effect of the initial billet temperature on the deformation zone pattern and its consequent effect on friction using both numerical simulation and experimental work are presented. A comparison with experiments is made to assess the relative importance of some extrusion parameters in the extrusion process and to ensure that the numerical discretisation provided a true simulation of the process. A specific functional relationship to directly measure interfacial friction under conditions approaching those encountered in the quasi-static deformation process is described. The results revealed that the friction factor increases with increase in initial billet temperature and varies from 0·65 at 300°C to a 0·91 at 450°C after reaching the peak pressure. The dead metal zone is observed to vary in form and has a greater volume at high temperatures. The increase in friction results in an increase of initial extrusion load. The finite element program appears to predict all the major characteristics of the flow observed macroscopically.

MST/5520

The authors are in Bournemouth University, 12 Christchurch Road, Studland House Bournemouth, Dorset BH1 3NA, UK (Iflitta@bournemouth.ac.uk; tsheppard@bournemouth.ac.uk). *Manuscript received 15 May 2002; accepted 16 December 2002.*

Introduction

The basic process of extrusion is well described as a thermomechanical event in a quite recent text,[1] which indicates that the mathematical description of the process is still largely semiempirical. The extrusion process is complex, involving interaction between the process variables and the material's high temperature properties. Theoretically, the process variables that can be controlled are the extrusion ratio R, the ram speed V, and the initial extrusion temperature T. However, events on the micromechanical scale are still not adequately described. The most important of these is possibly the mechanics at the interface between tooling and material. This influences the analyses of the temperature changes occurring during the process, the final temperature and the temperature history determining the structure of the extrudate and hence, to a large extent, its properties.

Most authors agree that one of the most significant parameters to define when modelling extrusion processes is the friction coefficient.[1–6] The mechanism of interfacial friction in aluminium extrusion is very complex and is not a well understood phenomenon. Owing to the high pressures and temperatures that are necessary features of the process, experimentation is difficult and this combined with only a rough estimation of the relevant parameters, indicates that an accurate simulation might be of some use.

In the industrial context, assumptions are made that sticking friction prevails at the interface between the billet and the tools, and its value is a constant for all extrusion temperatures. Various studies and analytical methods have been used to establish the complex relationship between the extrusion parameters, friction, temperature, stress, strain, strain rate, etc. Some of these studies[7–11] provided some understanding into the mechanisms that govern friction but fall short in supplying sufficient information to identify the mechanisms that can be applied quantitatively to model friction for the extrusion process.

Other workers[1,9,10,12–17] have expressed the friction coefficient to be a constant and to range between 0·8 and 1 based on experimental observations, using either varying billet lengths or by measurement of the slope of the pressure–displacement locus. Variations of pressure with billet lengths have been investigated for 1100 and 2014 aluminium alloys,[1,18] by extruding billets of varying lengths under identical extrusion conditions. It was observed that the peak pressure–billet length relationship in each case was linear, and the friction coefficient value determined from the data was 0·88 for AA 1100 and 0·8 for AA 2014. The work indicated that the friction coefficient has an approximately constant value during the extrusion process regardless of the initial extrusion temperature.

Clearly neither of these methods of establishing the value of friction is satisfactory and for design purposes, the friction is usually assumed to be 0·85. However, such measurements fail to take into account the differences in temperature at differing locations during the ram stroke and the consequent deviation in the flow stress. The extrusion pressure is significantly influenced by the temperature gradients modified in the billet during transfer to the container, and after upsetting in the container. Metal flow in the extrusion process is an important factor controlling the mechanical and structural properties of the extruded product.

The modelling of aluminium extrusion must be based on a fundamental understanding of the thermomechanical phenomena occurring during the process. While the problem is thus one of broader complexity, the derivation of systematic data from which it can be studied is rendered very difficult under industrial conditions. It is also difficult to quantify by experimental techniques. Accurate thermal and microstructural data of materials and in particular the interface data such as friction and heat transfer properties must be available. The accuracy of the results are not only sensitive to the geometric definition of the tooling and the input of the material rheological data under investigation, but they are also highly sensitive to the data input for the boundary conditions between the billet and the tooling. These parameters are clearly extremely sensitive when attempting to simulate the extrusion process. In early software development, requirements were only confined to a graphical illustration of the change in geometrical shape of the workpiece and an approximate value of pressure to

DOI 10.1179/026708303225004422

undertake the process. In such cases, the accuracy of the data input, i.e. friction, heat transfer etc., were not necessarily high and consisted of an approximation to the yield stress and a global, averaged friction factor. With the ever increasing use of finite element method (FEM) techniques in the last few years to the extrusion process, the necessity for accurate input data becomes increasingly crucial. The analytical ability of current finite element codes enable the continuum parameters of the extrusion process, stress and strain histories and metal flow to be predicted in detail as deformation continues. In order to enable full advantage to be taken of the use of finite element programs available to simulate manufacturing processes to be exploited, not only are detailed mechanical, thermal and microstructural constitutive descriptions of materials required but mechanical and thermal properties of workpiece/tool interfaces and the tools also must be available. However, the definition of the interfacial friction in most of the current programs is one of the boundary conditions required for a solution to the problem. To overcome this problem a coupled experiment with inverted analytical solutions would inevitably obtain reliable data describing the friction phenomena of the process.

Friction

The coefficient of friction at the metal/billet interface contributes significantly to the complexity of extruding, and it is a point where the friction resistance approaches the shear resistance of the hot material during deformation. Furthermore, it is a point where a fraction or all of the displacement of the billet at the interface occurs by shear in its surface layers leaving a fragment of the billet deposited on the wall of the container. In practice, aluminium alloys are extruded without any lubricant or with only, a small amount of graphite applied to the die face. Finding a suitable lubricant would be a difficult task and in any case unlubricated aluminium extrusion is desirable in order to prevent impurity pick up from the tools and to ensure that all the material making up the extrudate surfaces originates from virgin material within the billet. Hence, the interfacial conditions at the billet/container interface during extrusion has a direct effect on metal flow, the stresses acting upon both the tools and within the material, and hence load and energy requirements and extrudate temperature.

During the extrusion process, the force necessary to overcome the friction between the billet and the container results in an increase in overall pressure to extrude. At the extreme condition between the billet and the container, friction at the interface cannot exceed the shear strength of the material. This extreme condition is termed sticking friction and can be represented generally as

$$\tau_F = \tau_{max} \quad . \quad . \quad . \quad . \quad . \quad . \quad . \quad . \quad . \quad . \quad . \quad . \quad . \quad . \quad . \quad (1)$$

where τ_F is the interfacial friction and τ_{max} is the shear yield stress of the billet material. The shear stress can be defined either by the Tresca yield criterion

$$\tau_{max} = \bar{\sigma}/2 \quad . \quad . \quad . \quad . \quad . \quad . \quad . \quad . \quad . \quad . \quad . \quad . \quad . \quad . \quad . \quad (2)$$

where $\bar{\sigma}$ is the mean equivalent yield stress, or by a Von Mises material when the shear strength can be expressed as

$$\tau_{max} = \bar{\sigma}/\sqrt{3} \quad . \quad . \quad . \quad . \quad . \quad . \quad . \quad . \quad . \quad . \quad . \quad . \quad . \quad . \quad . \quad (3)$$

where $\bar{\sigma}/\sqrt{3}$ is the mean equivalent shear flow stress. A modification to sticking friction is often introduced to account for the fact that friction forces are seldom as high as the shear strength of a material. The friction can be defined using what is sometimes referred to as the Tresca friction law, which assumes proportionality between the friction and the current shear flow stress of the material and can be written

$$\tau_F = \bar{m}\tau_{max} \quad . \quad . \quad . \quad . \quad . \quad . \quad . \quad . \quad . \quad . \quad . \quad . \quad . \quad . \quad . \quad (4)$$

$\bar{m}$ is the factor of proportionality and is commonly referred to as a friction factor and varies between $\bar{m}=0$ for perfect lubrication and $\bar{m}=1$ for sticking friction. The Tresca law treats the interface friction as pressure independent and relates the friction stress directly to the shear flow stress of the deformed material. The value of τ_{max} can be determined from either Tresca or Von Mises yield functions, or from other descriptions of the plastic flow stress in shear.

The FEM used in metal forming can be generally categorised into viscoplastic plastic FEM and elastic viscoplastic plastic FEM, depending on which material constitutive equations are used. For extrusion of hot aluminium alloys, viscoplastic FEM is adopted to simulate the process because plastic strain dominates the process. For the convenience of simulation and modelling purposes, friction is considered in terms of the relative velocity between two surfaces, i.e. billet and the tooling. The friction law may be considered by assuming the Tresca friction law criteria described in equation (4) and is written as follows

$$\tau = -m\bar{\sigma}_i/\sqrt{3} \quad . \quad . \quad . \quad . \quad . \quad . \quad . \quad . \quad . \quad . \quad . \quad . \quad . \quad . \quad . \quad (5)$$

At the limit when $\bar{m}$ is of unit value, all deformation will be in the form of shear in the subcutaneous regions of the billet rather than sliding against the tools. However, this simple representation is not able to include the contribution of local conditions such as temperature, pressure, surface quality and geometry. Otherwise, with the description and the inclusion of heat transfer, the value of $\bar{m}$ is defined with the same value as a constant, and it would be more realistic to specify this constant as a function of process variables. Although $\bar{m}$ should be assumed as a constant value, this formulation can be more useful and more sophisticated by allowing the friction coefficient or the friction factor to be functions of several variables.

Finite element models and source of experimental data

GOVERNING EQUATIONS

In this investigation, a commercial finite element package FORGE2 and FORGE3* (Refs. 19 and 20) developed by Transvalor (France) was used to simulate the extrusion of aluminium alloys. The data structure of the program includes the governing equations, the finite element of the workpiece, the rheology of the material, the tooling description, the frictional interface, and the numerical parameters to be defined in the iterative solution. The program uses implicit FEM to calculate the hot working parameters: load, strain rate, temperature rise, and deformation.

The temperature evolution is governed by internal heat conduction and internal heat dissipation under the constraints defined on the area boundary in terms of interchange (radiation, conduction and convection) and in terms of imposed temperature. This evolution is represented by the following heat equation

$$\rho c \frac{\partial T}{\partial t} = \mathrm{div}(k \ \mathrm{grad} \ T) + Q \quad . \quad . \quad . \quad . \quad . \quad . \quad . \quad . \quad . \quad (6)$$

where ρ is the density, c the specific heat, T is the temperature, Q is the internal heat dissipation generated by plastic deformation and k is the conductivity. The temperature field in the billet or in the die is computed using equation (6). The work generated by the plastic deformation is largely dissipated in terms of heat inside the body leading to some energy being retained within the material.

*FORGE2 and FORGE3 are registered trademarks.

In addition to the above governing equation, boundary conditions to describe geometry and friction are required. Friction can be dealt with by using equation (5).

In the FORGE2 and FORGE3 programs, the Norton–Hoff law describes the default rheology of the material. However, in order to obtain reliable results with a high degree of confidence, it is important to reduce the errors owing to approximate data used to describe the material behaviour. Experience shows that some differences can appear between the numerical predictions and experimental results. Part of these variations result from discretisation of the problem (FEM), however, inaccuracy often occurs from using data not calculated for the specific alloy over the complete working range. The most widely used equation to describe the deformation of aluminium alloys, is that proposed by Sellars and Tegart[21] and subsequently modified by Sheppard and Wright[22] to yield the steady state flow stress from the equation

$$Z = A[\sinh(\alpha\bar{\sigma})]^n = \dot{\bar{\varepsilon}} \exp\left(\frac{\Delta H}{GT}\right) \quad \ldots\ldots\ldots \quad (7)$$

from which

$$\bar{\sigma} = \alpha^{-1} \ln\{(Z/A)^{1/n} + [(Z/A)^{2/n} + 1]^{1/2}\} \quad \ldots\ldots \quad (8)$$

where Z is termed the temperature compensated strain rate (s^{-1}); ΔH is the activation energy for deformation (kJ mol^{-1}); G is the universal gas constant (8·314 J mol^{-1} K^{-1}); $\dot{\bar{\varepsilon}}$ is the mean equivalent strain rate (s^{-1}); $A(s^{-1})$ and n are constants; α is a constant (m^2 MN^{-1}); and T is the initial billet temperature (K).

PROCESS CONDITIONS

The chemical compositions of the alloys used in this investigation are given in Table 1. All the experimental data are extracted from the literature.[16,17] Experiments were performed on a 5 MN press vertically mounted with a heated container. The main ram was driven by a hydraulic pump during the extrusion cycle. The load was measured by Mayes load cell situated directly above the ram, the output from the cell being recorded on a Labmaster data recorder. Ram displacement and speeds were measured by a rectilinear potentiometer fixed between the moving crossheads and the press bolster.

Constant ram speeds of $v = 3$ and 8 mm s^{-1} were imposed with an extrusion ratio of 30:1 for AA 2024 and Al–1 wt-%Cu respectively. In FORGE2 program, only half of the cross-section requires modelling due to symmetry. A flat faced die with a 5 mm die bearing length was used for all simulations. The boundary conditions at the billet/container interface were evaluated by the Tresca friction type mechanism. The coefficient of friction was varied from 0·5 to 0·99 in order to simulate conditions ranging from low stick-slip to fully sticking conditions. The container and die temperatures were 50 K below the initial billet temperature for all the analyses in an attempt to reduce the temperature of the extrudate and hence, to simulate industrial conditions.

The data describing the material behaviour available to the authors were obtained using Torque Twist data from torsion tests and optimised to obtain the form of equation (8). The input data for the simulation is summarised in Table 2. Consequently, in the simulations conducted in this paper, the modified Sheppard–Wright law was programmed and used to describe the material behaviour. In the extrusion process, the areas in which small strains occur can be ignored because they do not affect either the pressure or the properties. Equation (8) is therefore adequate to describe the rheology of the material.

During the simulation of extrusion, large deformations are predominant which require a Lagrangian mesh to be defined. The elements become severely distorted during the process and consequently, the need for remeshing is necessary to continue the simulation. The frequency of remeshing is controlled by the degree of deformation and is a user variable. To improve the accuracy of the results, it is critical to control the degree of remeshing in the areas where high deformation is expected. Refinement mesh boxes of Eulerien type (but maintaining Lagrangian flow) were applied to the billet at re-entrant corners to the die where high deformation is expected to occur. A coarser mesh is used for the remainder of the billet. The mesh for the FEM simulations was generated automatically for a space domain that included billet, container and the ram. Simulations were conducted on a Dell dual processor workstation.

METHOD OF IDENTIFYING FRICTION FACTOR

The extrusion process requires large compressive loads and involves a minimal displacement when first upsetting the ram to fill the container. The simulation output ensures that given the correct data, FEM is able to predict the real material behaviour, which is determined in such a way that conditions are identical to these encountered in industrial practice.

The basic experimental principle of the extrusion process consists of applying a velocity v to a billet heated at an initial temperature $T°$ while recording the values of experimental pressure P^{ex} as a function of the displacement of the ram. The data is obtained from the experimental pressure displacement trace curves obtained for different initial temperatures.

The method consists of changing the friction coefficient $\bar{m}$ in the simulation in order to build the corresponding computed loads P^C, for each extrusion temperature. The goal is to determine the friction coefficient that allows the prediction of the experimental data when the computed

Table 1 Chemical compositions of aluminium alloy 2024 and Al–1 wt-%Cu (Refs. 16 and 17), wt-%

Alloy	Al	Cu	Si	Mn	Mg	Fe	Ti	Zn
AA 2024	Balance	3·7–4·5	0·15	0·15–0·8	1·2–1·5	0·2	0·15	0·25
Al–1 wt-%Cu	Balance	0·9	0·82	0·71	0·5	0·2	0·014	0·02

Table 2 Rheology data input used for computer simulation[16,17]

	Flow stress data*				
Alloy	α, m^2 MN^{-1}	n	ΔH, kJ mol^{-1}	ln$A$	Temperature, °C
2024	0·016	4·25	148880	19·6	300–350–400–450
Al–1 wt-%Cu	0·0167	5·65	147950	26·7	300–450

*α, n, and A are constants; ΔH activation energy for deformation.

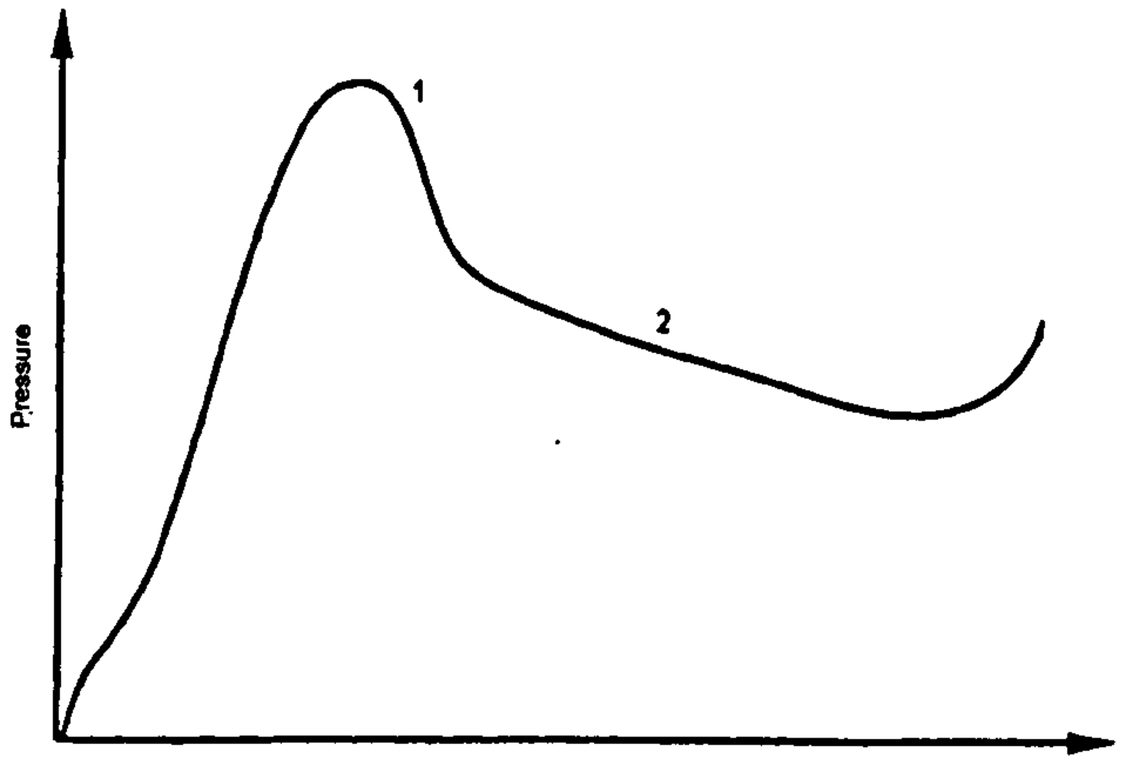

1 Locations where friction was examined

results are close or agree with experiment measurements for a specific material and conditions.

Since various factors during the extrusion process require experimental procedures, there are many points at which a direct comparison between the experimental work and its analytical counterpart can be compared and the accuracy of the output assessed. To investigate in greater detail the friction phenomena during the extrusion cycle, two locations of interest were selected for examination and are shown in Fig. 1. The first location identifies the friction at the start of the extrusion after the peak pressure has been established and the second location where the pressure is influenced to a greater extent by the associated temperature rise.

Results and discussion

EFFECT OF INITIAL BILLET TEMPERATURE ON FRICTION

Friction conditions at the billet/tool interface are known to affect the flow paths of the material at the container and through the die by changing the extrusion parameters, loads, stresses, and surface quality. Using different friction conditions and various input temperatures permits the experimental pressure to be predicted from the simulation. The predicted loads $P_{\bar{m}}^{c}$ of the corresponding friction coefficients for each extrusion temperature are given in Table 3. By comparing the predicted loads $P_{\bar{m}}^{c}$ with the experimental loads P^{ex}, the results gave a clear indication that the coefficient of friction varies with the initial billet temperature for both aluminium alloys investigated.

The computed results for the variation of the coefficient of friction $\bar{m}$ with temperature are illustrated in Fig. 2. The figure indicates a linear relationship with a good correlation of the form

$$\bar{m} = A + B.T \quad . \quad . \quad . \quad . \quad . \quad . \quad . \quad . \quad . \quad . \quad . \quad . \quad . \quad (9)$$

The figure also illustrates that the difference in friction

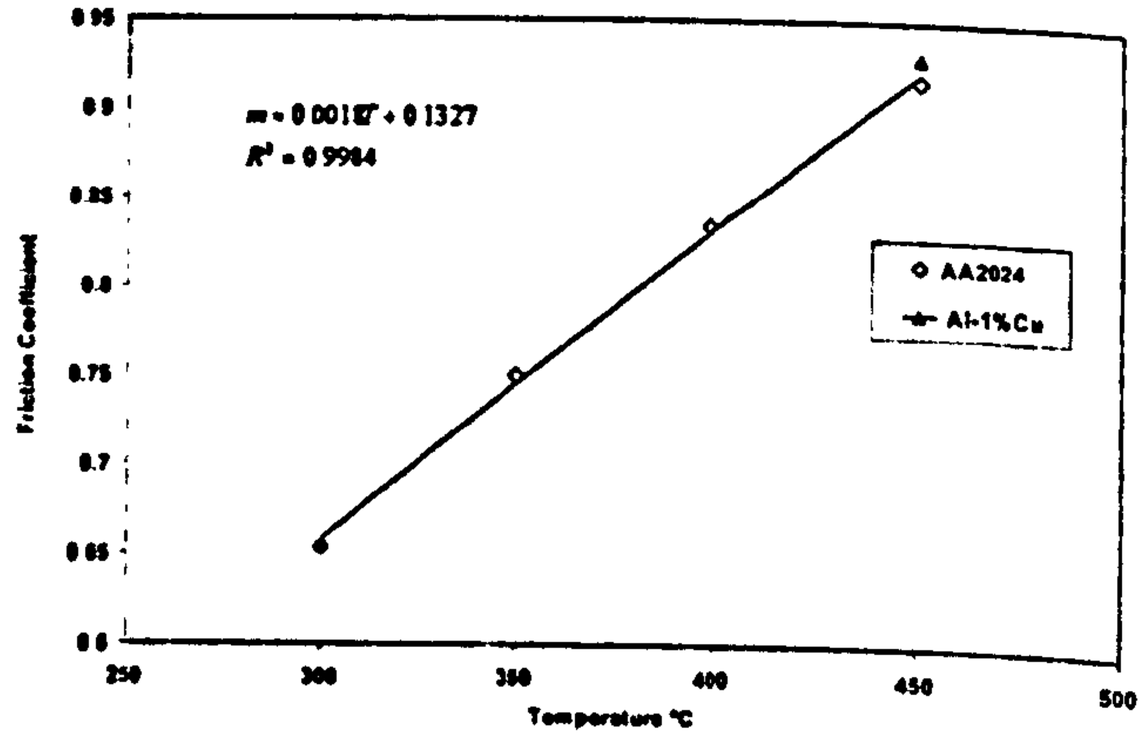

2 Variation of friction coefficient $\bar{m}$ with initial billet temperature

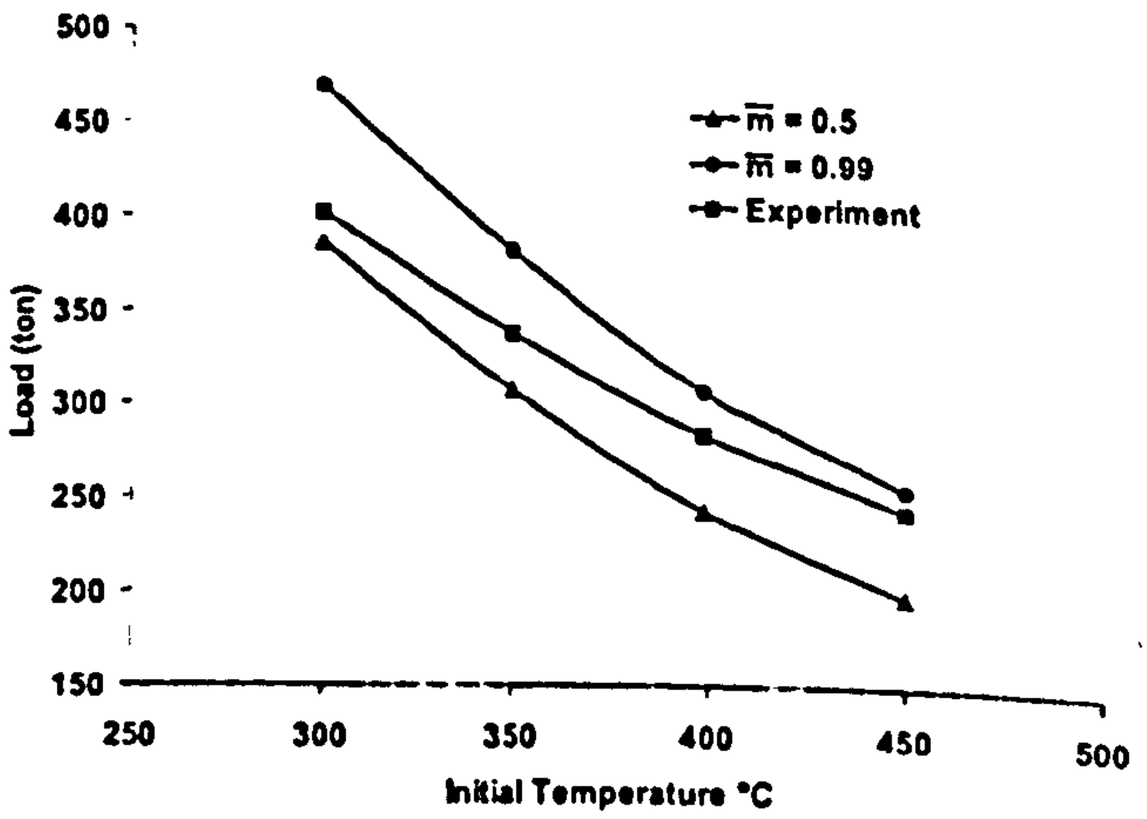

3 Predicted and experimental load variation with initial billet temperature for aluminium alloy 2024: $\bar{m}$ friction coefficient; 1 ton = 1·016 t

coefficient between low and high temperature extrusion increases with increasing temperature. The predicted pressures for input temperatures correspond to the extremes of frictional conditions, denoted by $\bar{m}=0{\cdot}5$ and 0·99, are shown in Fig. 3. As expected, a general trend of increasing extrusion pressure with decreasing initial billet temperature was found. The experimental points shown in the figure support the thesis that the friction coefficient varies with temperature. Hence, it can be concluded that it will also vary during the ram stroke. The figure also illustrates a greater difference between the experimental and predicted pressure at low and high friction for all extrusion temperatures. The results show that at 300°C using sticking friction overestimates the peak pressure significantly. Hence, the assumption that the friction is a constant value for all extrusion temperatures is incorrect. Moreover, the friction coefficient was found to vary from 0·654 for 300°C to 0·92 for 450°C as given in Table 3 at location (1) (just after the peak pressure has been established).

Table 3 Comparison of predicted loads P^{c} and experimental loads P^{ex} with initial billet temperature for both alloys at location (1)

	$P_{0\cdot5}^{c}$		$P_{0\cdot6}^{c}$		$P_{0\cdot7}^{c}$		$P_{0\cdot8}^{c}$		$P_{0\cdot9}^{c}$		$P_{0\cdot99}^{c}$		P^{ex}		$\bar{m}$	
Temperature, °C	2024	Al–1 wt-%Cu	2024	Al–1 wt-%Cu	2024	Al–1 wt-%Cu	2024	Al–1 wt-%Cu	2024	Al–1 wt-%Cu	2024	Al–1 wt-%Cu	2024	Al–1 wt-%Cu	2024	Al–1 wt-%Cu
300	385	456	396	470	414	488	432	510	448	536	469	569	401	458	0·654	0·655
350	NA	NA	NA	NA	332	NA	346	NA	362	NA	381	NA	338	NA	0·75	NA
400	NA	NA	NA	NA	NA	NA	268	NA	279	NA	306	NA	284	NA	0·835	NA
450	NA	NA	NA	NA	NA	NA	NA	NA	242	275	256	284	244	280	0·917	0·93

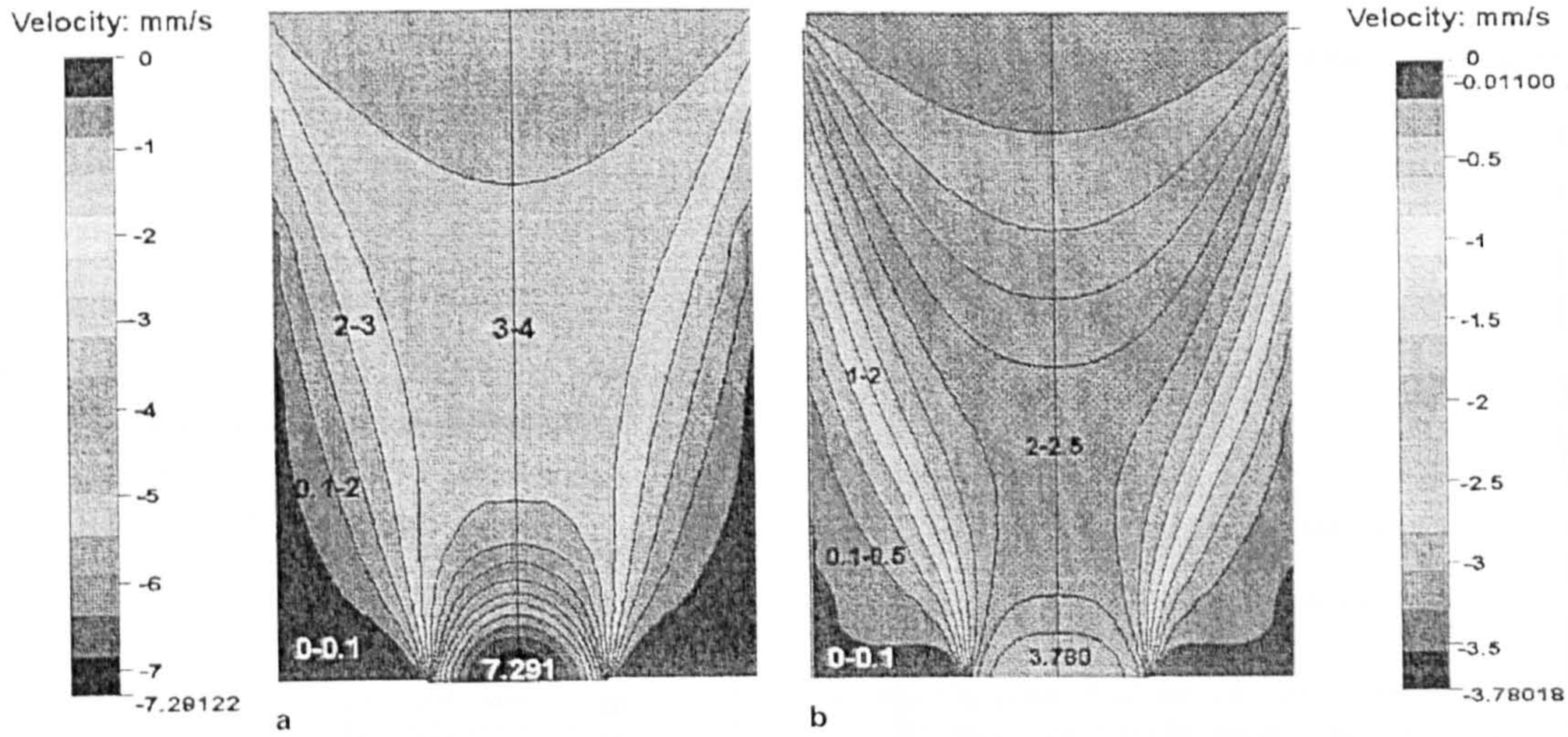

a 450°C; *b* 300°C

4 Initial contact area at 450 and 300°C extrusion

Before extrusion can proceed, the billet must be inserted into the container and to facilitate entry there is generally appreciable clearance between the two. At this initial setup, the only contact of the billet with the tools is at the die face where the boundary conditions including friction have no direct effect on the deformation. The necessary force needed to be applied to cause the billet to fill the clearance is affected predominantly by the nature of the material and the manner in which its properties are affected by the temperature, i.e. material flow stress and the rate at which the work is carried out. The first effect of pressure at this stage is thus to compress or upset the billet into firm contact with the cylinder wall. The upsetting stages, before location (1) has been reached for the billet at high and low temperature extrusions are shown in Fig. 4 represented by the prevailing velocity profiles. The pressure at this stage rises sharply while the billet is being compressed to fill the container. As the figures illustrate, at higher temperature extrusion, the deformation is characterised by more rapid flow. The velocity at which the material flows to fill the space of the container and a move towards the die opening is significantly greater compared with that at lower temperature. This is evident since the resistance to deformation of the billet material decreases as the temperature increases and reaches its lowest permissible value when the material is close to the melting point of the alloy's lowest melting phase (i.e. 511°C for 2024). However, there are significant differences in the rate as a result of which this change occurs and in the ultimate degree of ductility, which is reached. Consequently at higher temperature extrusion, the billet is more ductile and tends, under deformation, to spread more easily to fill the container. The deformation of the billet at this initial stage is characterised by nearly half of its length sticking along the container wall as illustrated in Fig. 4*a*. On the other hand, at lower temperature extrusion, the billet is less ductile and acts in a relatively stiffer manner. The upsetting stage at this temperature extrusion is initiated by sliding along most of the container wall and only one fifth of the billet length is sticking as shown in Fig. 4*b*. The shapes of the dead metal zones (DMZs) are also quite different at these varying temperatures. This initial contact and the extent of this contact area along the container wall have a significant effect on the commencement of the deformation path which occurs in localised regions in the billet where the interface results in a stick, slip or fully sticking friction situations before the quasi-static DMZ formation. Moreover, when the billet has been fully compressed to fill the container, the elastic properties of the container and plastic properties of the materials in contact, have a significant effect on the difficulty of the two materials to slide relative to each other. Similarly, the plastic work dissipated depends on the local temperature at the contact area and the thermal conductivity for the two materials in contact, i.e. billet/container. As a result of the extent of the area of contact, at higher temperature and lower flow stress, the force to deform the material increases as the contact pressure at the container increases. In addition, at lower temperature extrusion (i.e. 300°C), the surfaces in contact would produce a greater elastic deformation in the container owing to the higher flow stress.

After further ram travel, the billet is further compressed and a very small amount of extrusion takes place. The DMZ is fully established by this time. However, the deformation zone is not clearly defined at this stage until the peak pressure reaches its maximum. The deformation zone is not stationary, the billet is deforming plastically while the shearing forces are operating which promotes the burnishing effect at the DMZ/billet interface. It is at this stage, after the peak pressure has been established, that the friction is of great interest. Not only because of press capacity requirement, but also because of its contribution to the temperature changes occurring in the material whilst reaching the peak pressure.

In order to relate the friction factor through a relationship applicable for all extrusion variables and to overcome the separate relationships generated for the variation of friction coefficient with temperatures as stated in equation (1), it would therefore be more instructive to incorporate the friction factor into a sinh relationship by using the ln$Z$ parameter. The parameter Z defined in equation (8) contains the data describing the alloy behaviour (Table 2), ram speed and temperature. The temperature compensated strain rate just after the peak pressure is established, Z_d at location (1), incorporating both strain rate and temperature should enable the friction variation to be related by one relationship. The strain rate varies from point to point throughout the deformation zone during the extrusion process. It is thus necessary to use an average value for this parameter. The mean equivalent strain rate used in this investigation is calculated from an average area over the deformation zone where the maximum deformation is expected to occur. The parameter Z_d was programmed and incorporated into FORGE2 and FORGE3 by the authors as one of the outputs of the simulation. The parameter Z_d

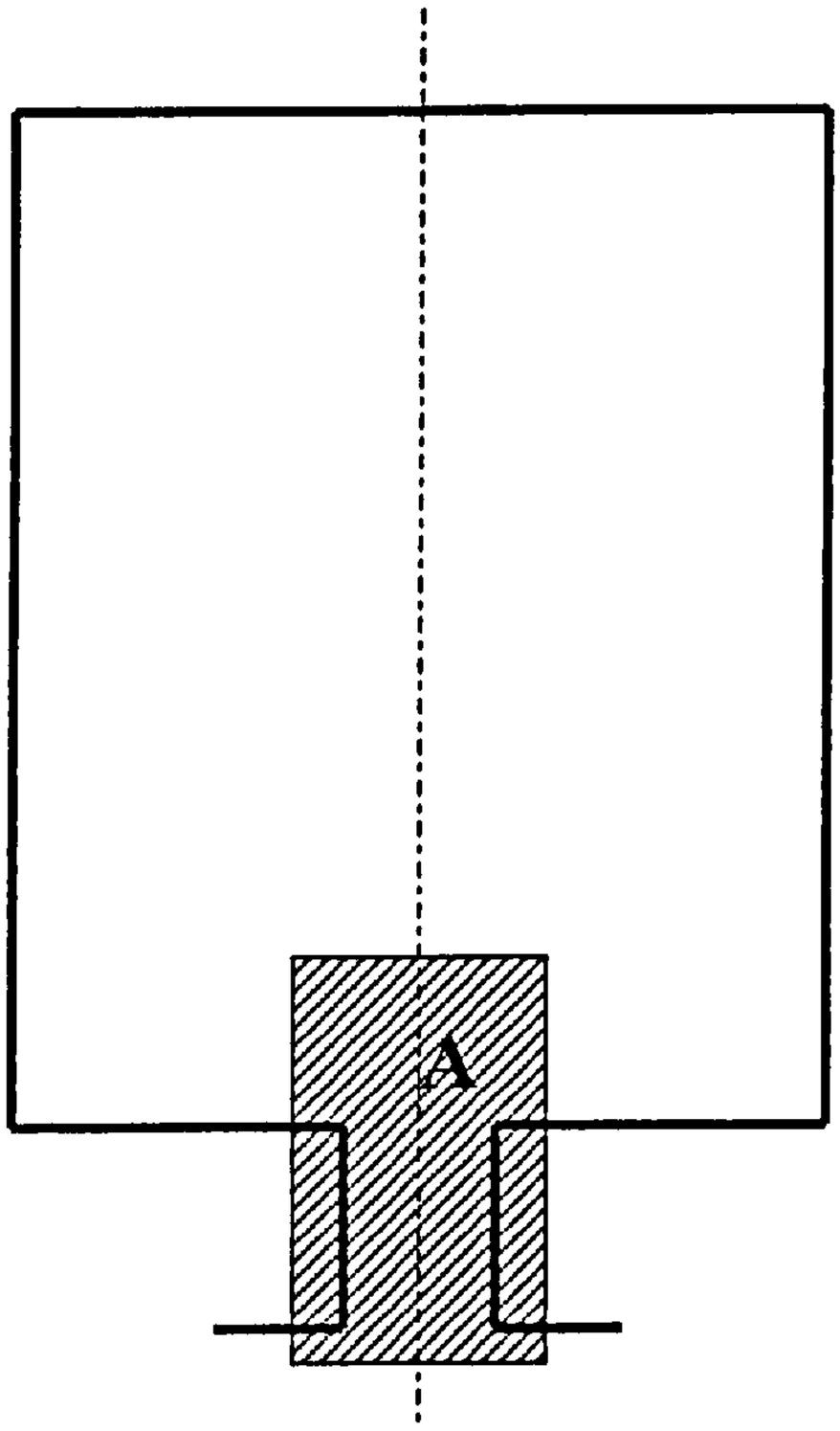

5 Boundary area where values of Z_d were averaged: Z_d temperature compensated strain rate just after peak pressure is established

used in this investigation is calculated in the same manner as the mean equivalent strain rate at an instantaneous maximum temperature as illustrated in Fig. 5. To ensure different alloys to be represented by the same mathematical expression and to account for the effect of chemical composition of the materials, $\ln(Z_d/A)$ together with the function αn was used[1] as proposed by Sheppard for pressure calculations. The constant α is a reciprocal flow stress, and its value has been interpreted as the position where the dependence of flow stress upon strain rate changes from, a power relationship to an exponential one, and is a function of material chemistry. The constant n can be termed the inverse of the temperature compensated strain rate sensitivity. The actual value of this constant is strongly dependent upon the value of α. Both are intimately related to the chemical composition of the material.

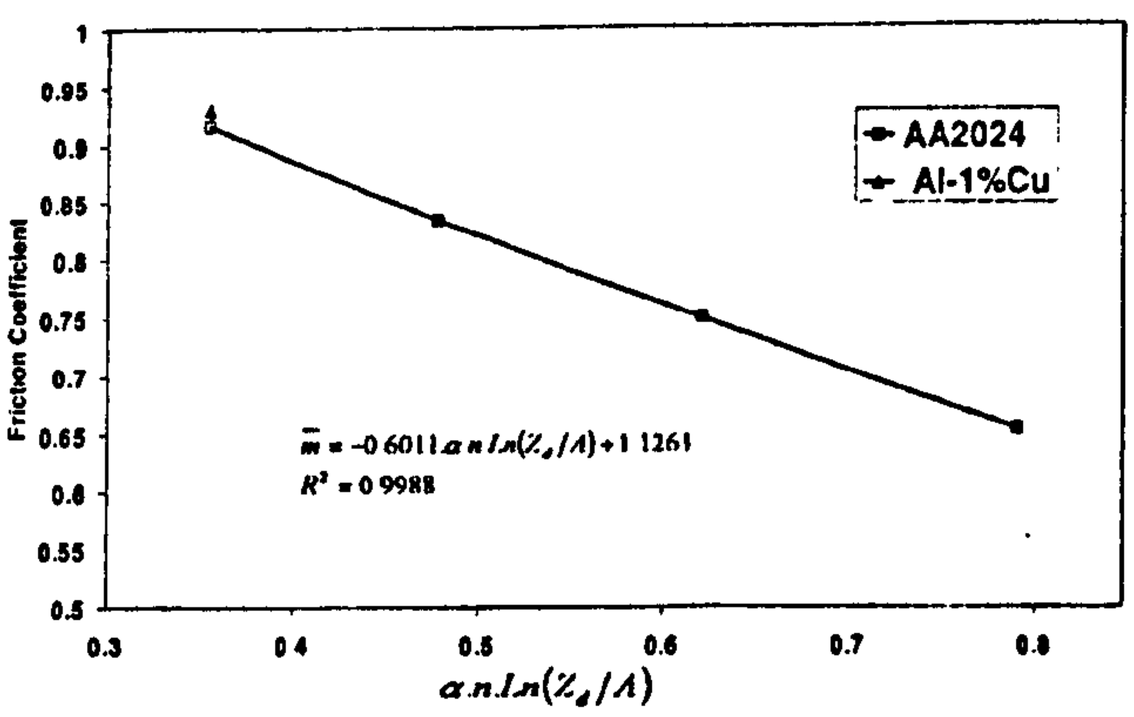

6 Friction variation with αn $\ln(Z_d/A)$ at location (1): $\bar{m}$ friction coefficient; Z_d temperature compensated strain rate just after peak pressure is established; A, α, and n are constants

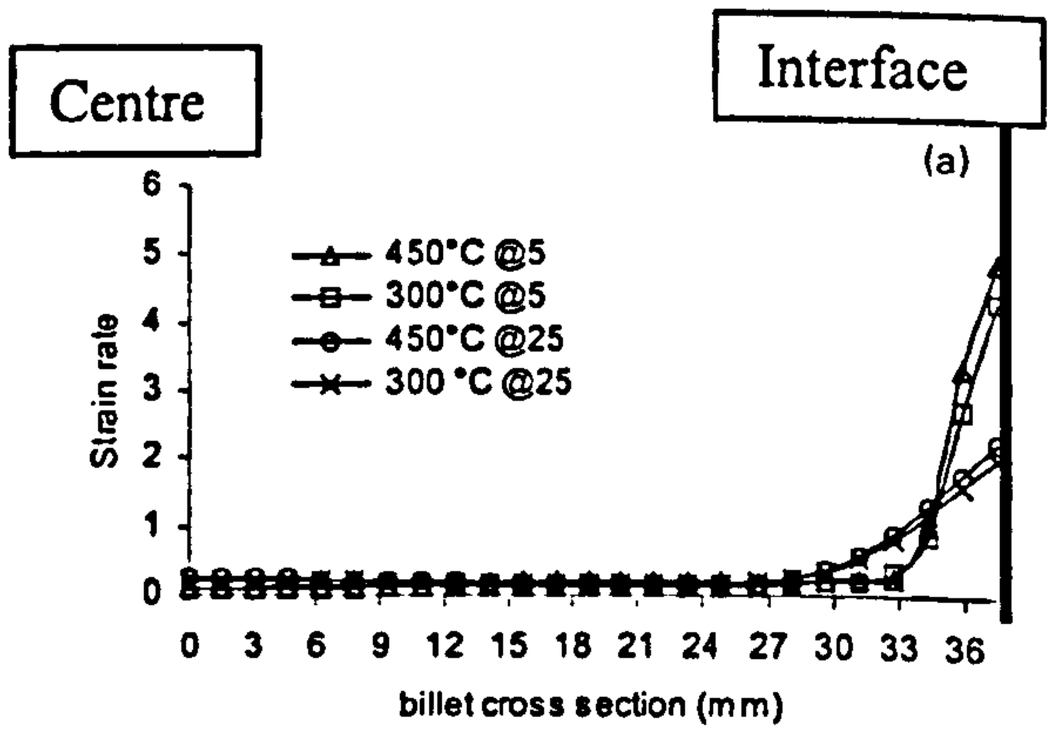

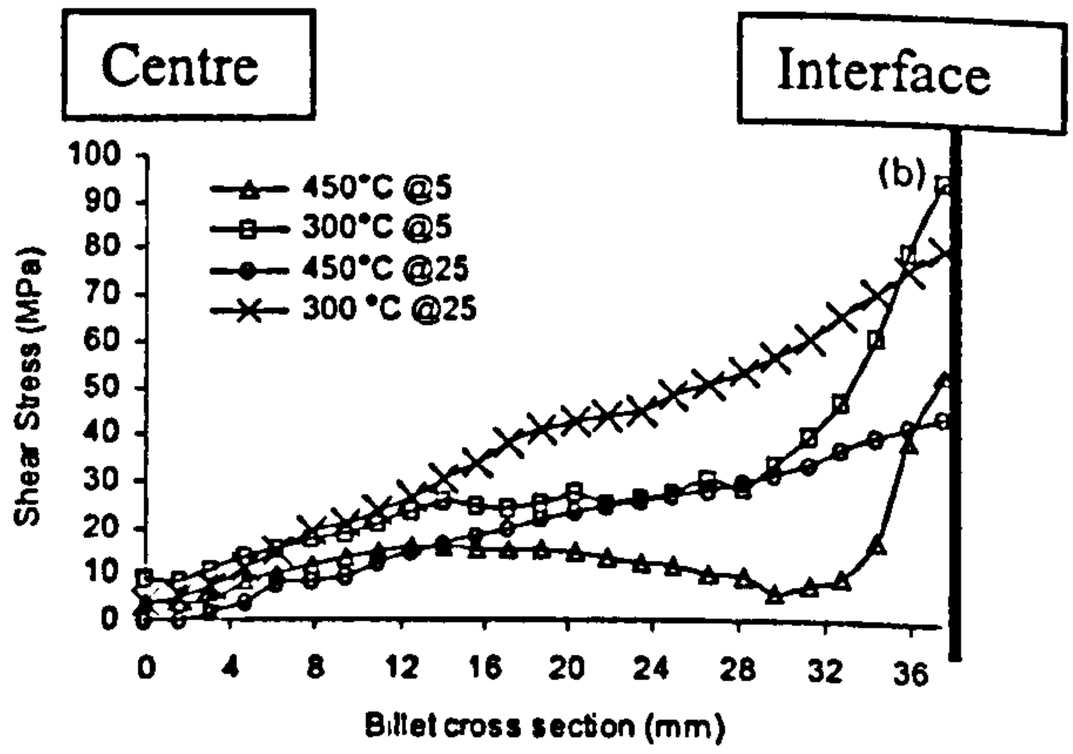

a strain rate, 5 and 25 mm are distances from ram position after peak pressure had been achieved; *b* shear stress, at 5 mm from ram

7 Strain rate and shear stress variations across billet cross-section

When friction coefficients are plotted against $\alpha n \ln(Z_d/A)$ a linear relationship of the form

$$\bar{m} = -0{\cdot}6011 \alpha n \ln(Z_d/A) + 1{\cdot}1261 \quad . \quad . \quad . \quad . \quad . \quad . \quad (10)$$

is apparent and is shown in Fig. 6. The resistance of the material to withstand the imposed strain gradients at low Z_d conditions, i.e. low flow stress, results in a larger deformation zone extending to the rear of the billet whilst at high Z_d conditions, the high flow stress restricts the deformation zone to the die mouth region. As shown in Fig. 7*a* and *b*, at 5 mm from the ram face, high deformation occurs such that there is a shear zone at the billet/container interface in which the strain rate and the shear stress vary from a higher value to zero for the strain rate and to a minimum value for the shear stress at the centre of the billet. At 25 mm distance from the ram, the decay of both the shear stress and the strain rate when moving from interface to billet centre is much more gradual. This is clearly owing to the absence of deformation at the rear of the billet in the first case and the interaction with the DMZ and the position of greater deformation as the material approaches the die. When approaching the die, the zone of intense shear increases toward the die opening, separating the deformation zone from the DMZ. In this case, the frictional stress is identical to the flow stress of the billet material in pure shear, whereas the relative speed increases from the ram speed at the rear end of the billet to approach the exit speed of the extrudate when approaching the die opening.

Another factor that must be considered is the strain rate. Although the total strain is the same for each case, i.e. in terms of the reduction, the time in which the heavy deformation zones form is different. Since the deformation is initiated nearer the rear of the billet in the high temperature case, over a longer contact area, there will be an

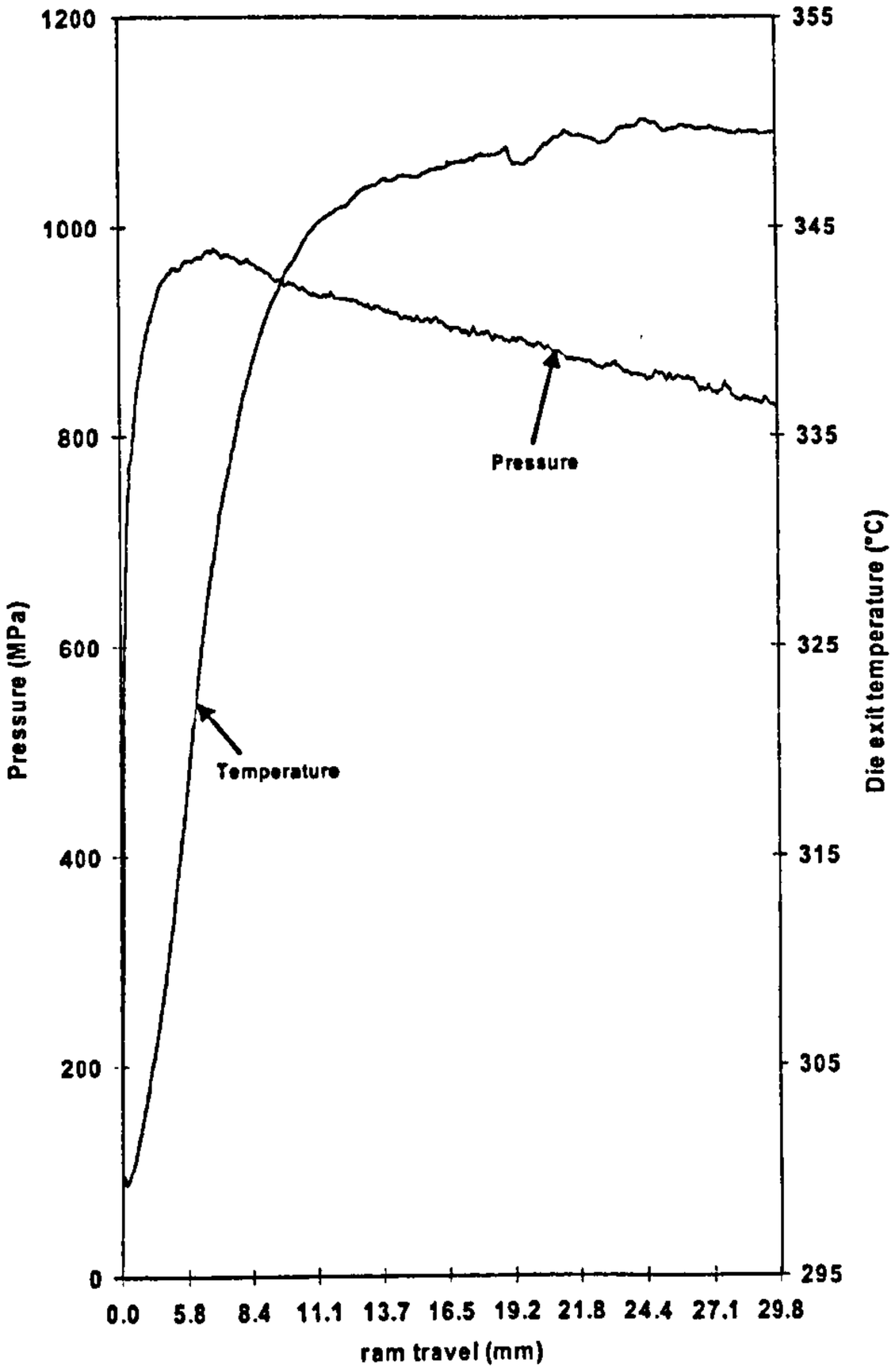

8 Variation of billet temperature with pressure

associated greater time available for the major deformation to be completed resulting in a lower strain rate. Thus the friction coefficient is raised and approaches a unit value. In terms of the material plastic flow behaviour, the observations are not unrealistic.

However these values of friction do not remain constant through the extrusion process. These changes are the consequences of an increase in the overall billet temperature within the deformation zone and the decrease of the area of contact with further ram travel. Complex thermal changes begin as soon as the extrusion commences. The most critical temperature is clearly the die exit temperature of the extrudate, which is related to the heat balance history commencing at the upsetting stage of the operation. It increases if the heat produced by deformation and friction exceeds the heat losses and decreases if the reverse is true. The exit temperature increases as the peak pressure is reached and appears to remain approximately constant after ~30 mm ram travel (*see* Fig. 8). The figure illustrates the variation of pressure displacement with the exit die temperature. For the initial temperature of 300°C, the temperature of the billet increased sharply by 27 K in reaching the peak pressure. This temperature rise would be expected as a result of the work done in upsetting the billet, and the work done against friction between the material and the tooling. This is caused by the work done as the material is forced to commence flow through the die orifice owing to the production of heat by deformation being transferred to material at the inlet of the die from the deformation zone. This heat is generated in the deformation zone and influenced by the friction coefficient. Clearly this would produce an increase in the extrusion temperature. Since the work done in overcoming friction is a function of the shear

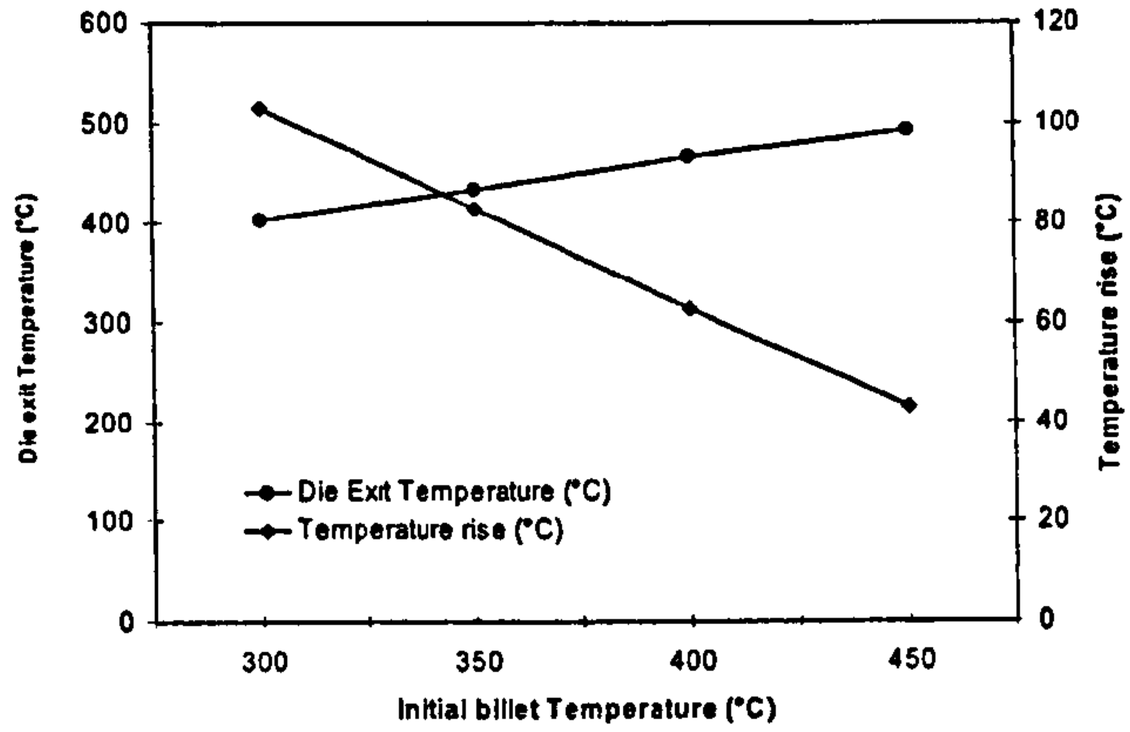

9 Predicted die exit temperature rise

stress within the deformation zone, then the pressure needed to overcome the friction must also be a function of the temperature differential ΔT between the initial and actual billet temperature, which produces a decrease in flow stress. However, the value of ΔT depends on the initial billet temperature of the material as shown in Fig. 9. The exit temperature increases with increasing initial billet temperature and the temperature rise ΔT decreases as the billet temperature increases, resulting in a decrease in the material flow stress. Taking into account the temperature rise ΔT within the deformation zone at location (2), it was found that the friction coefficient increases from 0·65 to 0·89 for the initial billet temperature of 300°C and from 0·91 to 0·98 for 450°C as shown in Fig. 10. Similar to location (1), an

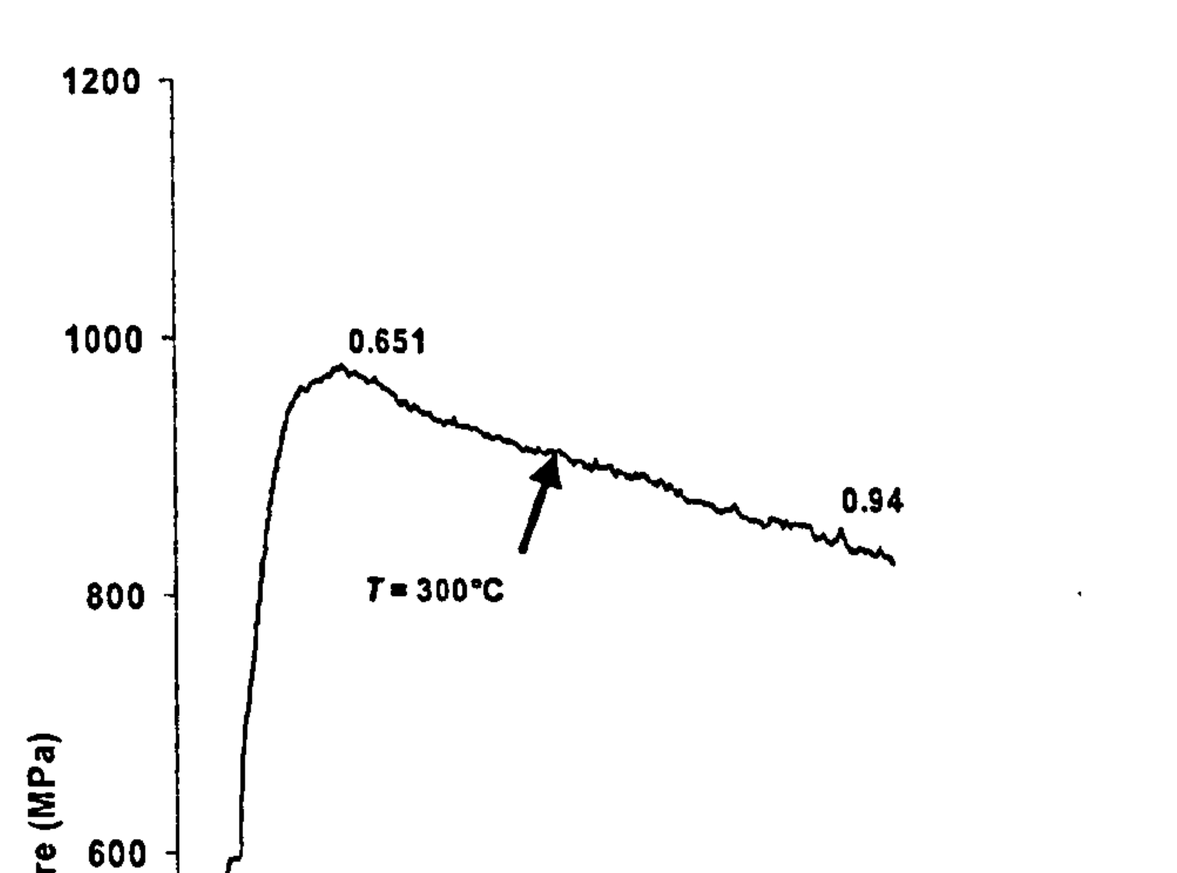

10 Friction variation during extrusion process for aluminium alloy 2024 at locations (1) and (2); temperatures given are initial billet temperatures

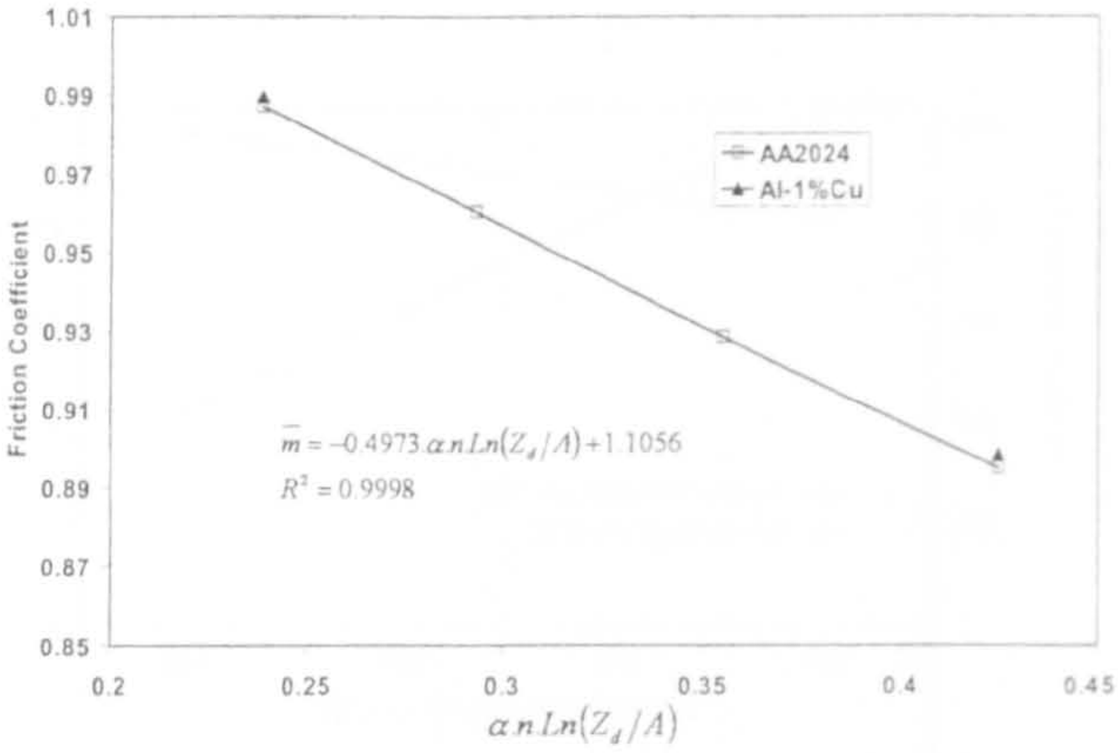

11 Friction variation with $\alpha n \ln(Z_d/A)$ at location (2): $\bar{m}$ friction coefficient; Z_d temperature compensated strain rate just after peak pressure is established; A, α, and n are constants

apparent linear relationship of the form

$$\bar{m} = -0{\cdot}4973\alpha n \ln(Z_d/A) + 1{\cdot}1056 \quad \ldots\ldots\ldots \quad (11)$$

was found when the coefficient of frictions were plotted against $\alpha n \ln(Z_d/A)$ and is shown in Fig. 11. Figures 6 and 11 indicate that over the range of $\ln(Z_d/A)$ considered, the function relating $\bar{m}$ and $\alpha n \ln(Z_d/A)$ are of similar form. The high correlation obtained throughout the analysis indicates that the relationship is applicable to all temperatures. The results show that the use of the Z_d parameter is justified, since for a given value of Z_d, the pressure necessary to carry out extrusion increases with reduction ratio as predicted by previous workers.[1,16] At the initial stages of the process, the main parameters affecting the friction are the increase in the temperature and the contact length. However, near the end of the process, the contact length has diminished as the length of the billet shortens. It was not feasible to predict the coefficient of friction after location (2) because of computer time considerations. However, there is no indication that such an operation would alter the interpretation of the data already collected. At all locations, the total friction force is significantly influenced by the billet length remaining in the container, and thus falls as extrusion proceeds.

Hence, the only method of predicting friction could be to program the FEM code to define friction as

$$\bar{m}_{\Delta L_n} = [A + \alpha n \ln(Z_d/A) + B]_{\Delta L_{n-1}} \quad \ldots\ldots\ldots \quad (12)$$

where ΔL_n is incremental ram travel (i.e. each 2·5 mm of ram displacement).

The authors realise that programming a boundary condition in this way would not be a trivial task and would increase computer time considerably. Nevertheless, if friction is to be addressed in a scientific manner such an approach will be necessary.

EFFECT OF INITIAL BILLET TEMPERATURE ON MATERIAL FLOW

To evaluate the effects of material flow at both high and low temperature extrusion i.e. 450 and 300°C respectively, two billets were sectioned along a meridian plane with square grid lines. Similar grid lines were simulated in order to compare with the experimental results.[23]

The effects of the initial billet temperature on material flow for high and low temperature extrusion are illustrated in Fig. 12. The figure shows a comparison between the simulated gridded billets at the end of the extrusion (Fig. 12*a* and *b*) and the macrographs taken from experiments (Fig. 12*c* and *d*).[23] A good agreement between the experiments and the simulation is obvious. As these figures illustrate, it is clearly evident in both cases that there is a significant change in deformation zone geometry. For high temperature extrusion (i.e. 450°C), the deformation zone gradually spreads from above the die mouth to the

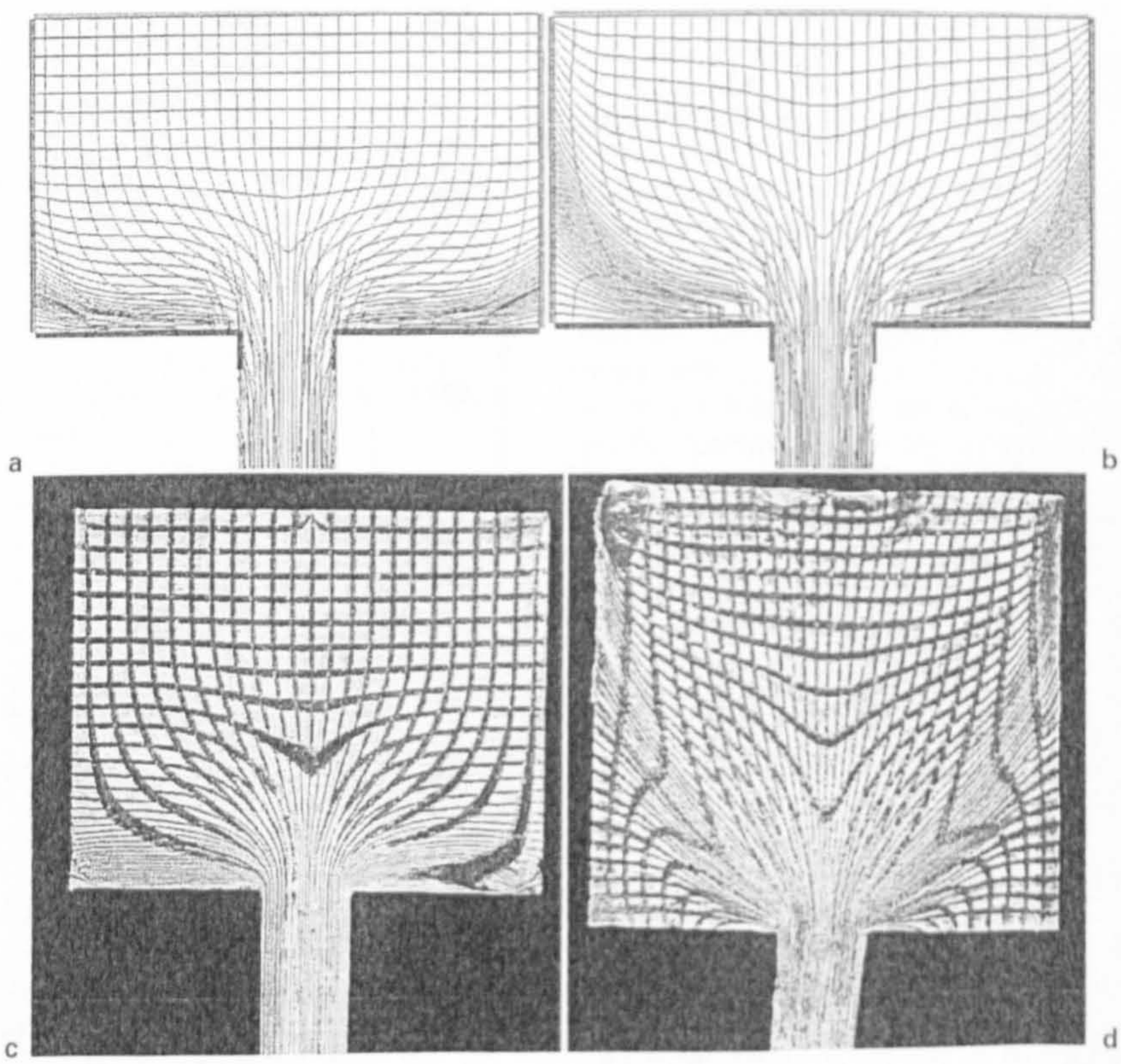

a flow at 300°C; *b* flow at 450°C; *c* and *d* are corresponding experimental[23] flow patterns at 300 and 450°C respectively

12 Simulated flow patterns at end of extrusion

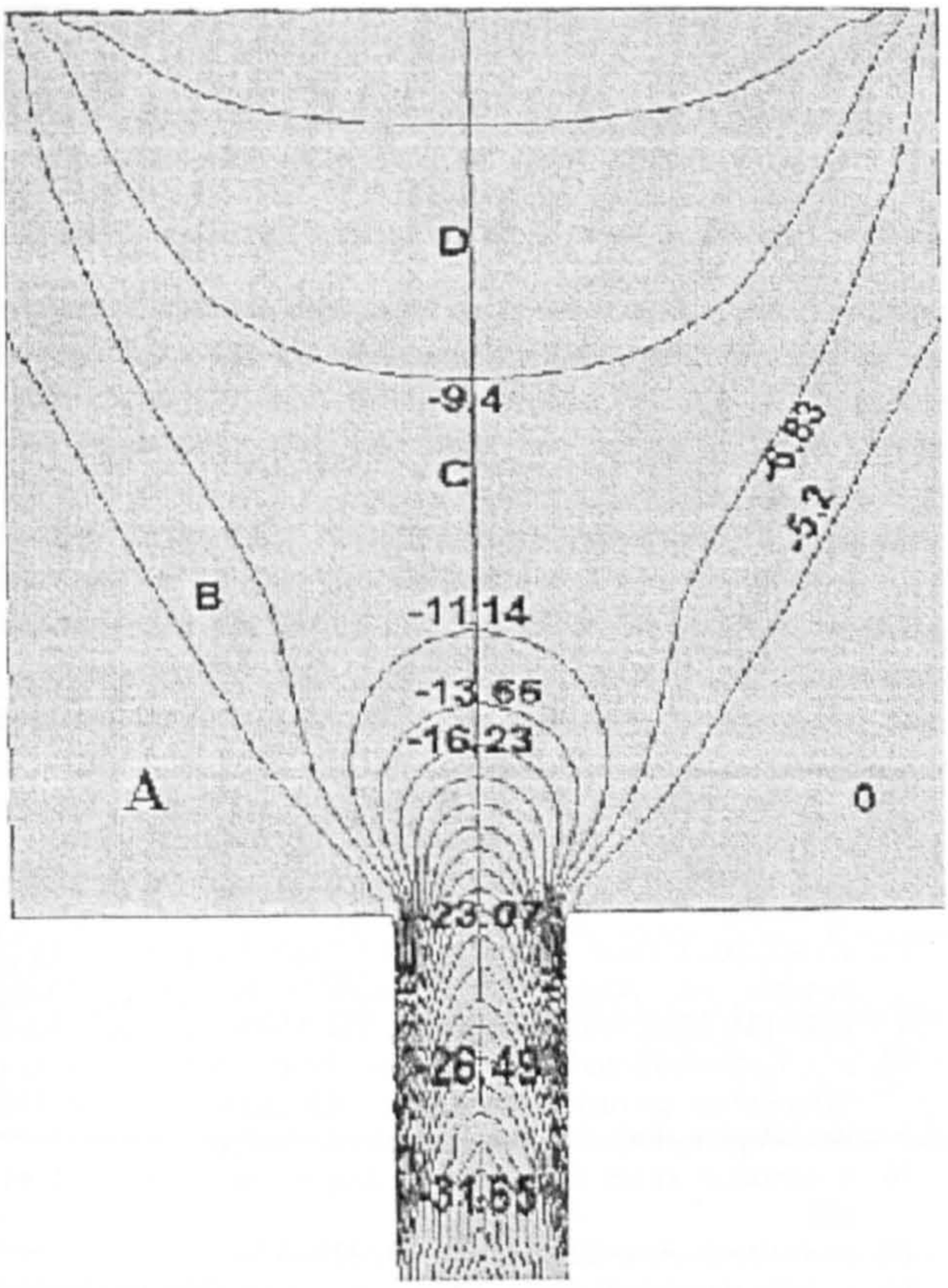

(A) dead metal zone; (B) surface generation zone; (C) main deformation zone; (D) central deformation zone

13 Flow velocity of material during extrusion at 450°C

container walls by progressive thickening of the zones of heavy shear. The shearing zone occurs in the subcutaneous regions of the billet in preference to sliding at the container wall interface. On the other hand for lower temperature conditions (i.e. 300°C), the extent of this zone is volumetrically less than that observed with higher temperature conditions, the most severe deformation is limited to a small volume close to the die mouth. The formation of the DMZs is evident and over at least 50% of the volume shown there is no evidence of deformation, the grid is regular across the entire width. Comparing this with the result of the high temperature extrusion shows a considerable difference. In this case, the effects of the deformation can be found over the entire surface shown. Considerable amounts of cylinder wall shear can be seen stretching from the rear of the billet up to the DMZ boundary and progressing further back into the billet, leaving the die mouth flow at a more obtuse angle to the DMZ than the one observed at lower temperatures. The zone of shear produced by friction at a temperature of 450°C is greater in depth than the one formed at 300°C. The shearing at the DMZ boundary can be regarded as a measure of the work required to provide the force needed to produce a satisfactory surface. This work increases with an enlarged DMZ as a result of the increase of the initial billet temperature and consequent increase in the friction factor at the billet/container interface.

Therefore, the extent of the DMZ provides some understanding of the influence of temperature on the friction and can be visualised by assessing the velocity profiles. As illustrated by Fig. 13, in the regions of the deformation zone close to the die, the central velocity is greater. The boundaries of the deformation zones illustrated in Fig. 12 shows a smaller volume for the lower temperature extrusion. In addition there is a greater amount of material from the billet subcutaneous layers appearing to reach the extrudate in the high temperature case than the low temperature. This would tend to imply greater diffusion of internal energy dissipation. The temperature gradient between the centre and the container wall will also cause the shearing layer between the billet and the container to occur at a greater depth below the surface, and so leave a thicker rim of metal at the billet/container interface. In this connection, the strong adherence of aluminium at lower flow stress to the wall of the container would eventually lead to a very high value of $\bar{m}$.

Thus, the evidence confirms that a lower temperature extrusion increases the resistance to deformation, reduces the volume of DMZ and decreases the proportion of the work required to produce the desired surface. Therefore, the friction factor is associated with the thermally activated events involved. The results found in Figs. 6 and 11 of a decreasing $\bar{m}$ with increasing $\alpha n \ln(Z_d/A)$ term can therefore be attributed to a change in deformation zone geometry caused by a variation in the plastic flow behaviour of the material.

In order to achieve a sound quality surface during the extrusion process, the surface of the extrudate must be generated from within the billet. The generation of this surface involves the production of a virgin surface by shearing of the DMZ. The nature of shear involves production of continuous virgin surfaces at the entrance to the die throat. However, the boundary conditions at the billet/container interface, i.e. friction, heat transfer etc., have a significant effect on the material which constructs the surface of the extrudate.

The quasi-static flow of material during extrusion is shown in Fig. 13. The conditions at the billet interface wall have promoted the formation of a DMZ at the front of the billet. This static volume of material (A) extends from the die throat, back towards the container wall at an angle, which depends on the initial billet temperature and the boundary conditions at the interface. Outlining this zone is a region of intense shear. The zone resembles the frustum of a cone in shape and extends from the die throat to the container wall. It can be seen from the figure that the extrudate material originates from various locations in the deforming billet that can be represented by three zones. The surface generation zone (B) outlining the DMZ, the main deformations zone (C) and the central deformation zone (D). The outer surface of the extrudate originates from the surface generation zone (B) as illustrated by Fig. 13. It is material from this zone moving along the DMZ boundary that forms the extrudate surface. The figure also suggests that the outside surface of the extrudate originates from the material which is located on the edge of the DMZ and moving more slowly into the extrudate surface promoting a continuous formation of a virgin surface. The material forming the core of the extrudate originates from the central deformation zone (D) of heavy shear feeding into the bulk of the extrudate. This central deformation zone supplements the material feeding the body of the extrudate from within the main deformation zone (C).

Conclusions

1. The initial stages of the deformation, where the billet is primarily affected by the flow stress of the material and the rate, at which the work is carried out, proved to be of some significance in dictating the material flow distribution during the extrusion process.
2. The assumption that the friction conditions are a constant value for all extrusion temperatures is incorrect. The apparent friction coefficient was found to vary from 0·654 for 300°C to 0·92 for 450°C.
3. The $\bar{m}$ values do not remain constant throughout the extrusion cycle. The increases in overall temperature of the billet and hence decreases in flow stress, lead to an increase in friction for both alloys and temperatures.

4. The variation of friction conditions during the extrusion cycle for both alloys relating the process conditions, resulted by relationships of the form $\bar{m} = -0{\cdot}6011\alpha n \ln(Z_d/A) + 1{\cdot}1261$ at location (1) and $\bar{m} = -0{\cdot}4973\alpha n \ln(Z_d/A) + 1{\cdot}1056$ at location (2). This implies that friction should be introduced into the computer program in the form of

$$\bar{m}_{\Delta L_n} = [A + \alpha n \ln(Z_d/A) + B]_{\Delta L_{n-1}}$$

5. For an accurate simulation of extrusion, the friction coefficient must be identified continuously during the process cycle. This is not only required for press capacity, but also the effect on the temperature changes occurring in the material. This subsequently has an effect on the surface quality of the extrudate.

6. During the extrusion process, the billet surface adheres to the container and affects the possibility of surface layer incorporation into the extrudate. Using a constant value for friction for all extrusion temperatures, as many workers have indicated, would affect the incorporation of the surface layers into the extrudate. This would directly affect the predicted minimum discard.

7. The accuracy of the friction factor $\bar{m}$ is largely dependent upon the flow stress of the material at the billet/container interface.

8. A good agreement between the experimental and simulated results was found for high and low temperature extrusion flow. An enlarged dead metal zone was observed as a result of the increase in the initial billet temperature and in turn yielded an increase in friction factor.

Acknowledgements

The authors wish to thank and recognise excellent contributions to the experimental work by Dr M. G. Tutcher, Dr R. P. Vierod, and Dr J. Subramaniyan.

References

1. T. SHEPPARD: 'Extrusion of aluminium alloys'; 1999, Dordrecht, Kluwer Academic Press.
2. I. FLITTA and T. SHEPPARD: Proc. 7th Int. Seminar on 'Aluminium extrusion technology', Chicago, 197–203; 2000, Washington, DC, The Aluminium Association.
3. I. FLITTA and T. SHEPPARD: Proc. 5th Int. ESAFORM Conf., Krakow, Poland, April 2002, European Scientific Association for Material Forming, 435–438.
4. T. CHANDA, J. ZHOU, L. KOWALSI and J. DUSZCZYK: *Sci. Mater.*, 1999, 41, 195–202.
5. B. J. E. VAN RENS, W. A. M. BRELEMANS and F. P. T. BAAJENS: Proc. 7th Int. Seminar on 'Aluminium extrusion technology', Chicago, 99–107; 2000, Washington, DC, The Aluminium Association.
6. T. A. DEAN and Z. M. HU: Proc. 6th Int. Conf. on 'Technology of plasticity', Nuremburg, Germany, September 1999, Vol. 1, 541–550; Springer – Verlag.
7. S. ABTAHI, T. WELO and S. STOREN: Proc. 6th Int. Seminar on 'Aluminium extrusion technology', Chicago, 125–131; 1996, Washington, DC, The Aluminium Association.
8. T. WELO, T. S. ABTAHI and I. SKAUVIK: Proc. 6th Int. Seminar on 'Aluminium extrusion technology', Chicago, 101–106; 1996, Washington, DC, The Aluminium Association.
9. L. ANAND: *Comput. Mech.*, 1993, 12, 197–213.
10. L. ANAND and W. TONG: *Ann. CIRP*, 1993, 42, 361–366.
11. M. P. CLODE and T. SHEPPARD: *Mater. Sci. Technol.*, 1990, 6, 755–763.
12. T. CHANDA, J. ZHOU, L. KOWALSI and J. DUSZCZYK: Proc. 7th Int. Seminar on 'Aluminium extrusion technology', Chicago, 125–134; 2000, Washington, DC, The Aluminium Association.
13. R. J. DASHWOOD and H. B. MCSHANE: Proc. 6th Int. Seminar on 'Aluminium extrusion technology', Chicago, 331–339; 1996, Washington, DC, The Aluminium Association.
14. A. HEEGE, P. ALART and E. ONATE: *Eng. Comput.*, 1995, 12, 41–656.
15. D. Y. YANG: *Ann. CIRP*, 1994, 43, 229–233.
16. J. SUBRAMANIYAN: PhD Thesis, Imperial College, London, 1989.
17. R. P. VIEROD: PhD Thesis, Imperial College, London, 1983.
18. T. SHEPPARD and S. J. J. PATTERSON: *Mech. Work. Technol.*, 1982, 4, 39–56.
19. J.-L. CHENOT *et al.*: Int. Conf. on 'Forging and related technology' (ICFT 98), 113–122; 1998, Suffolk, Professional Engineering.
20. 'Software manual,' FORGE3 Version 5.3 Transvalor SA, Sophia Antipolis, France, 2001.
21. C. M. SELLARS and D. TEGART: *Int. Met. Rev.*, 1972, 1, 17.
22. T. SHEPPARD and D. WRIGHT: *Met. Technol.*, 1979, 13, 215–223.
23. M. G. TUTCHER: PhD Thesis, Imperial College, London, 1979.

Simulation of bridge die extrusion using the finite element method

I. Flitta and T. Sheppard

This communication reviews previous work on the extrusion of hollow shapes and uses a three-dimensional (FEM) solution to predict load-required, temperature of the extrudate and material flow during the process. A comparison with experiments is made to assess the relative importance of some extrusion parameters in the extrusion process and to ensure that the numerical discretisation yields a realistic simulation of the process. The usefulness and limitations of FEM when modelling complex shapes is also discussed. Methods to assess the difficulty of extrusion of hollow extrusions in general are presented. The paper also illustrates the essentials of numerical analysis to assist the reader in the comprehension of the thermomechanical events occurring during extrusion through bridge dies. Results are presented for velocity distribution in the extrusion chamber, iso-temperature contours and pressure/displacement traces. These are compared with experiments conducted using a 5 MN press. It is shown that the finite element program predicts the pressure requirement: the pressure/displacement trace showing a double peak which is discussed in some detail. The finite element program appears to predict all the major characteristics of the flow observed macroscopically.

MST/5236

Mr Flitta (iflitta@bournemouth.ac.uk) and Professor Sheppard (tsheppar@bournemouth.ac.uk) are at Bournemouth University, Studland House, 12 Christchurch Road, Bournemouth BH1 3NA, Dorset, UK. *Manuscript received 6 September 2001; accepted 1 November 2001.*

Introduction

Aluminium extrusion is the most common method used to produce solid and hollow shapes. Solid profiles are generally produced with a die that consists of only one part, while hollow profiles are produced with at least two parts, a die and a mandrel. The production of tubes represents an important activity in commercial extrusion. In order to extrude hollow sections, the billet has to be pressed through a die that determines the outside diameter, and over a centrally located mandrel that determines the inside diameter. The metal must, therefore, flow through an annular gap. For the extrusion of hollow aluminium profiles this is achieved by the use of the dies following the principles laid down by Dick.[1] There are three types of hollow die: bridge, porthole, and spider dies, which substantially increase the market for aluminium sections. The dies contain a weld chamber in which the stream of flowing metal is first divided into distinct streams and consequently rejoined by a pressure weld before passing through the die. Therefore, extruded sections produced on such dies have one or more seams or longitudinal weld lines. Because the separate metal streams are joined within the die without atmospheric contamination, a perfectly sound weld is usually obtained.

Extrusion of the 6000 alloy series through bridge dies producing hollow shapes is common in the aluminium industry. One of the largest problems in tube extrusion is tube eccentricity reported by Sheppard *et al.*[2] which affects the quality of the product and is generally due to poor design of the welding die. There are a number of experimental investigations conducted in to the study and prediction of conditions occurring during the extrusion process in the welding chamber.[3–5] Few of them, however, attempt to quantify the process. The complexity of metal flow calls for simulation of the complete process in three-dimensions. The finite element method (FEM) also gives new and important information, since local values for temperature, stress, and velocity within the deformation zone are not readily accessible by experiments. The research related to metal forming processes during the last few decades has widely used FEM in their investigations. However, it is only during the last decade that useful numerical simulations of aluminium extrusion have been reported. This is partially due to the nature of the process demands and the excessive time required for computation. Early work was mainly involved with 2D extrusion problems[2,6–11] or simple 3D geometry with low extrusion ratio.[12–15] Some have been experimentally verified.[16–21] Despite the fact that temperature evolution and distribution are of paramount importance in the extrusion process, very few publications pay attention to this aspect.[18,20–22] During bridge die extrusion this is an important factor because the quality of the joints along the entire length of the final product are primarily determined by the conditions in the welding chamber.[23]

Finite element modelling formulation

GOVERNING EQUATIONS

A commercial finite element package FORGE3 (Refs 24 and 25) developed by Transvalor (France) was used to simulate the extrusion of aluminium 6063 alloy through a bridge die. The model used for this simulation is described by Chenot.[26,27] The data structure of the program include, the governing equations, the finite element of the workpiece, the rheology of the material, the tooling description, the frictional interface, and the numerical parameters to be included in the calculation code. The program uses implicit FEM to calculate the hot working parameters: load, strain rate, temperature rise and deformation. A Lagrangian method is adopted for the program which can thus accurately define the material properties, state variables and boundary conditions.

The temperature evolution in the deformation zone is governed by internal heat conduction and internal heat dissipation under the constraints defined on the area boundary in terms of interchange (radiation, conduction, and convection) or in terms of imposed temperature. This evolution is represented by the following heat equation

$$\rho c \frac{\partial T}{\partial t} = div(k\ grad\ T) + Q \quad . \quad . \quad . \quad . \quad . \quad . \quad . \quad . \quad . \quad (1)$$

where ρ is the density, c the specific heat, T the temperature,

Q the internal heat dissipation generated by plastic deformation, and k the thermal conductivity.

The temperature field in the billet or in the die is computed using equation (1). The work generated by the plastic deformation is largely dissipated in terms of heat inside the body, an insignificantly small amount being retained within the material.

In addition to the above governing equation, boundary conditions to describe geometry and friction are required. Friction can be dealt with by assuming the Tresca yield criterion and is written as follows

$$\tau = -m \frac{\sigma_s}{\sqrt{3}} \quad \ldots\ldots\ldots\ldots\ldots\ldots \quad (2)$$

where τ is the shear stress at the interface, σ_s represents the yield stress, $\sigma_s/\sqrt{3}$ is usually termed the shear flow stress, and m is commonly referred to as a friction factor and varies between $m=0$ for perfect lubrication and $m=1$ for sticking friction. The Tresca law treats the interface friction as pressure independent and relates the friction stress directly to the shear flow stress of the deformed material.

In the FORGE2 and FORGE3 programs, the Norton–Hoff law describes the default rheology of the material. However, in order to obtain reliable results with a high degree of confidence, it is important to reduce the errors due to approximate data used to describe the material behaviour. Experience shows that some differences can appear between the numerical predictions and experimental results. Part of these variations results from discretisation of the problem (finite element method); however, inaccuracy often occurs from using data not calculated for the specific alloy over the complete working range. The most widely used equation to describe the deformation of aluminium alloys, is that proposed by Sellars and Tegart[28] and subsequently modified by Sheppard and Wright[29] to yield the steady state flow stress $\bar{\sigma}$ from the equation

$$Z = A[\sinh(\alpha\bar{\sigma})]^n = \dot{\bar{\varepsilon}} \exp\left(\frac{\Delta H}{GT}\right)$$

from which

$$\bar{\sigma} = \frac{1}{\alpha} \ln\left\{\left(\frac{Z}{A}\right)^{1/n} + \left[\left(\frac{Z}{A}\right)^{2/n} + 1\right]^{1/2}\right\} \quad \ldots\ldots \quad (3)$$

where Z is termed the temperature compensated strain rate; ΔH is the activation energy for deformation; G is the universal gas constant (8·314 J mol^{-1} K^{-1}); $\dot{\bar{\varepsilon}}$ is the mean equivalent strain rate; A, α, and n are constants; and T is the initial billet temperature

SIMULATION CONSIDERATIONS

The simulation approach is based on a viscoplastic constitutive model. This type of model neglects the elastic behaviour of the material, because of the fact that hot aluminium has rate dependent behaviour and that the elastic deformations are small when compared to the large plastic deformations that occur during the process.[23]

The definition of the tooling is one of the essential data inputs that have to be integrated into the simulation calculation. Consequently, both for the geometry (the precision of the boundary) and the kinematics (to follow the mechanical deformation), simulation must be designed accurately. The accuracy of the results is closely related to the meshing quality. In FORGE3, the meshing is based on two concepts: the quality of the elements and shape preservation (geometry). These two concepts are quantified and controlled by the user. The strategy to obtain the 'best' mesh is based on node addition, suppression, and regularisation to improve an existing given surface or to rebuild a new surface from an intial one. These should be done without modifying the domain

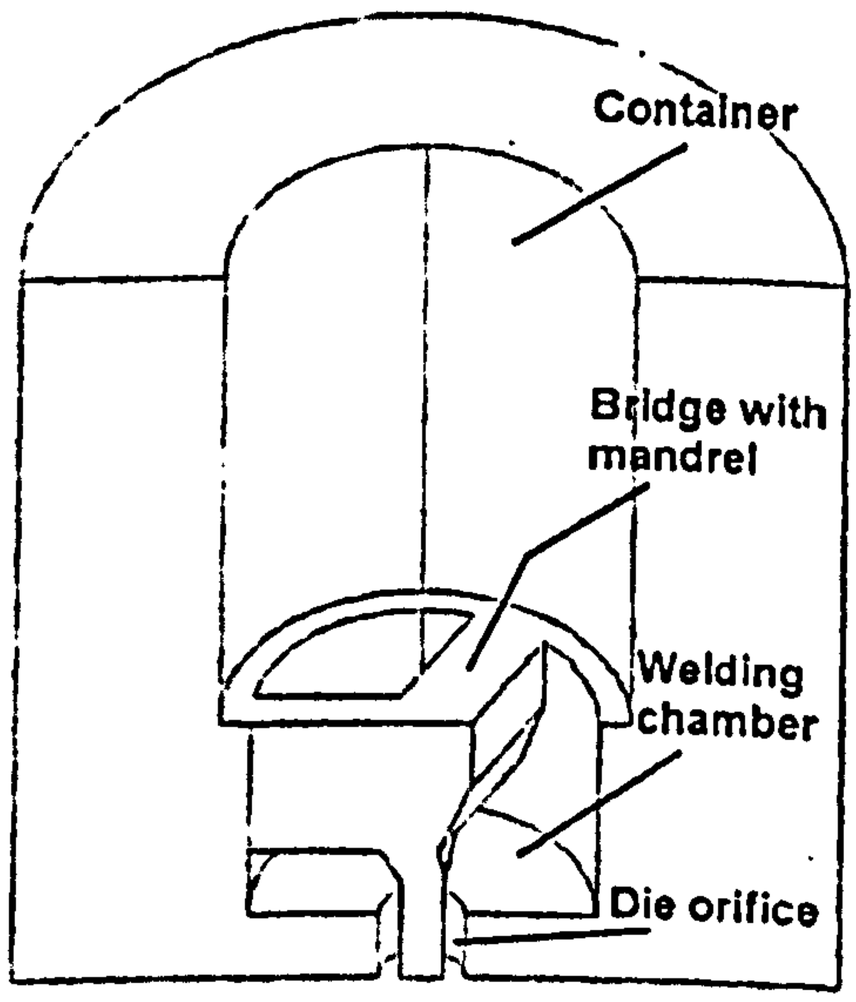

1 Half model of bridge die mandrel assembly

geometry (shape preservation). In order to generate a volume mesh, the program requires an initial triangular surface mesh with three node linear triangles. The quality of this volume mesh depends on surface mesh quality of the part (billet) imported from a CAD system.

During the simulation of extrusion, large deformations are predominant which require a Lagrangian mesh to be defined. Thus, complete remeshing which is mandatory in areas of excessive deformation is a source of loss/gain of volume. The elements become severely distorted during the process and consequently, remeshing is needed to continue the simulation. The frequency of remeshing is controlled by the degree of deformation and is a user variable. Therefore, careful judgement for the mesh refinement is required and the user must be able to identify the locations that need remeshing and call for local remeshing. This is crucial to minimise the computation volume.

PRE-PROCESSING

In the present investigation a bridge die having three legs was used, thus producing three welded seams in the tube extrudate. The die had two parts; the upper portion which acted as a sleeve for the bridge and the lower portion which formed a welding chamber and the die orifice (Fig. 1).

The tooling geometry of the bridge die and the billet were modelled using the I-DEAS Master-Series software. Taking advantage of the symmetry planes in the design and in order to reduce computation time, 1/6 of the models were constructed (Fig. 2). A surface mesh (two-dimensional) was then generated using three node linear triangles corresponding to the outer surface of the tooling and the billet as shown in Fig. 2. Once these models were built and meshed in 2D, the finite element model information was imported using the FORGE3 program algorithm in order to check the surface quality of the tools and to generate the three-dimensional volume mesh for the billet using four node tetrahedral elements.

To control the degree of remeshing in the areas where high deformation is expected, fine refinement mesh boxes of the Eulerian type (but maintaining Lagrangian flow) were applied to the billet. The remeshing values are controlled by the average target size of an element and the distribution is specified by 'mesh-boxes', i.e. boxes that define regions of the mesh on which a mesh size is imposed during the computation. In this investigation, three boxes were defined in what are considered the most important areas in the billet during the deformation. The first refinement was applied

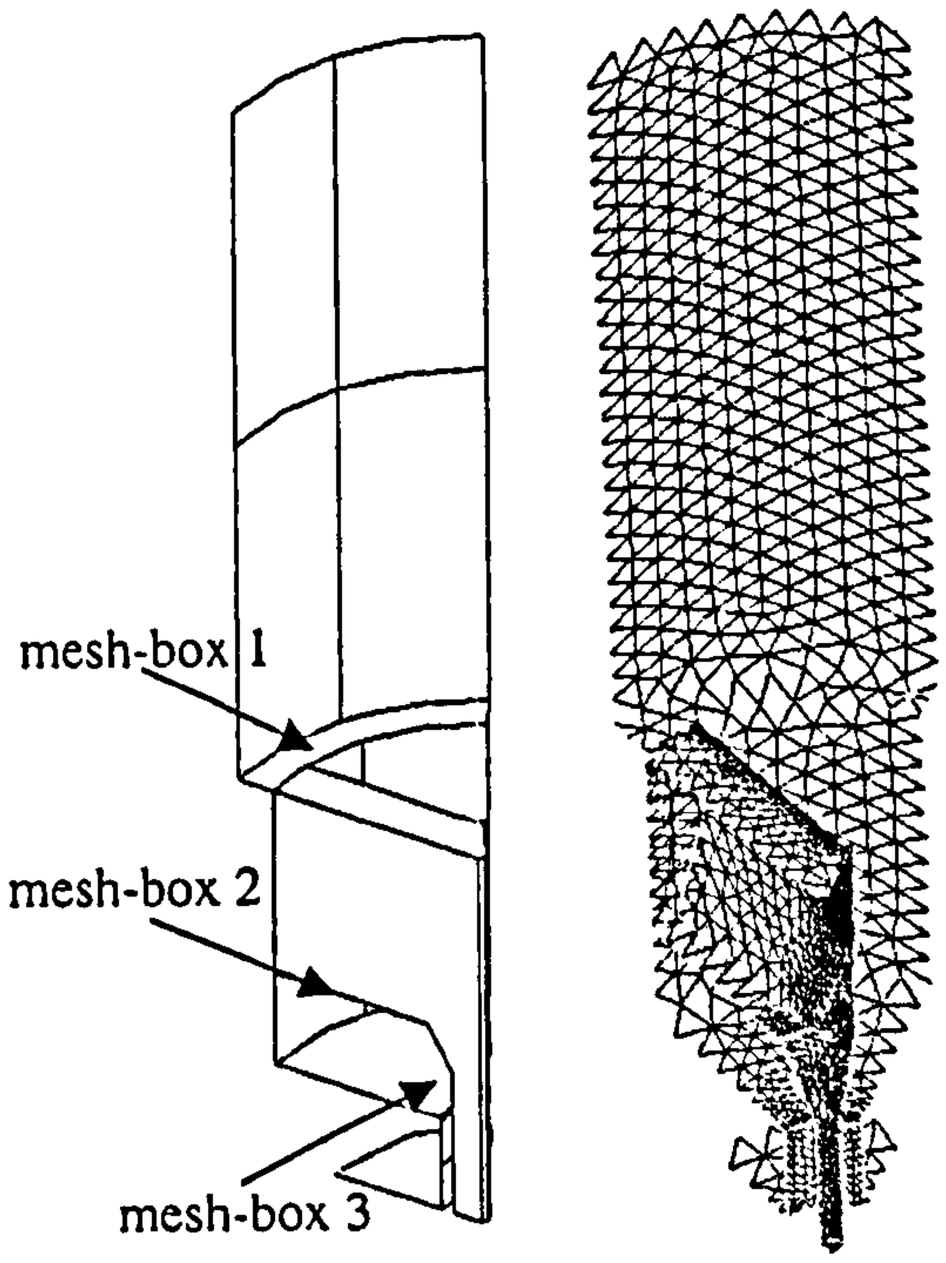

2 Computer aided design model and mesh of outer surface of bridge die mandrel assembly

just before the material started to flow around the core support (mesh-box1). The second refinement was applied just before the material commenced to weld in the welding chamber (mesh-box2). The final refinement was applied just before the material started to flow through the die orifice (mesh-box3). The aimed mesh size refinement value of 1·5 mm was imposed for mesh-box 1 and 2 and a value of 1 mm for mesh-box3. The average initial mesh size in the billet was 4 mm.

FEM models and source of experimental data

The chemical compositions of the alloys used in this investigation are given in Table 1. All the experimental data are extracted from the literature.[30,31] Experiments were performed on a 5 MN vertically mounted extrusion press with a heated container. The main ram was driven by a hydraulic pump during the extrusion cycle. The load was measured by Mayes load cell situated directly above the ram, the output from the cell being recorded on a Labmaster data recorder.

Table 1 Chemical composition of aluminium alloys, wt-%[23]

Alloy	Cu	Mg	Fe	Si	Mn	Ti	Zn	Al
2024	3·8–4·9	1·2–1·8	0·5	0·5	0·3–0·9	0·15	0·25	Bal.
6063	0·1	2·0	0·45–0·9	0·2–0·6	0·10	0·10	0·10	Bal.

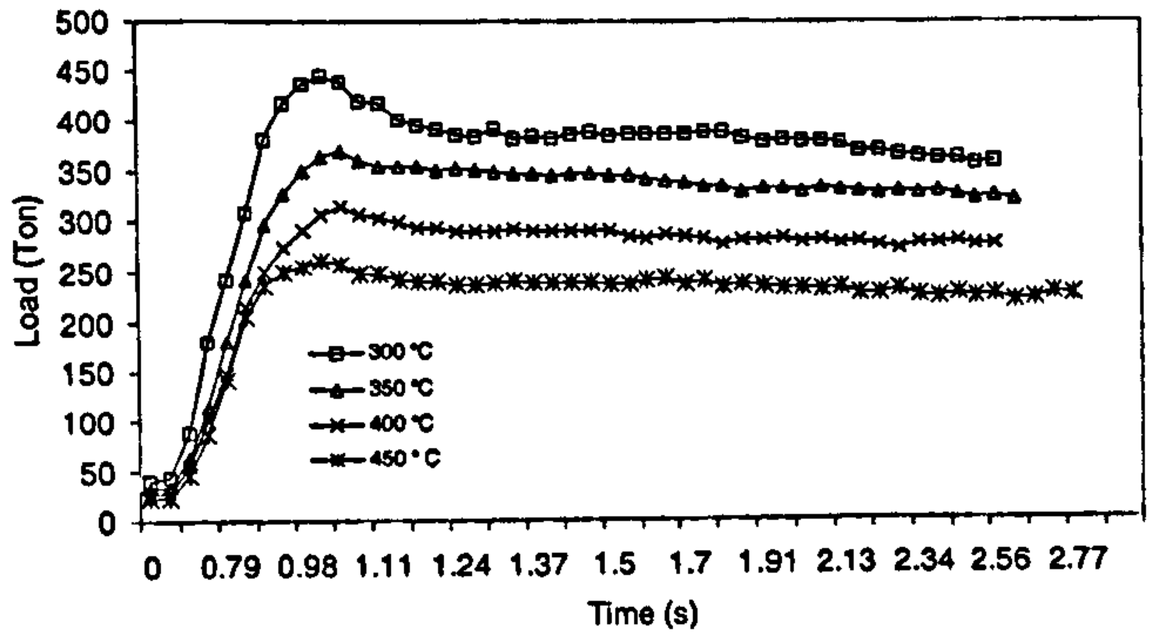

3 Rod extrusion: computed load *v.* time for direct extrusion

Ram displacement and speeds were measured by a rectilinear potentiometer fixed between the moving crossheads and the press bolster.

The input data for the bridge die simulation is summarised in Table 2. The dimensions of the billet are 75 mm dia. and 100 mm length. The dimensions of the extruded tubes are given in Table 2. The initial container temperature was 50°C below that of the initial billet temperature (450°C) to simulate industrial conditions.[23] The billet was extruded at a constant ram speed of 3 mm s^{-1}. The mathematical models were analysed using the viscoplastic solution algorithm of FORGE3.

The data describing the material behaviour available to the authors were obtained using torque–twist data from torsion tests and optimising to obtain the form of equation (3). Alloys reported in this communication were 6063 and 2024 aluminium alloys.[23] As a result, in the simulations conducted in this paper, the modified Sheppard–Wright law was programmed and used to describe the material behaviour. In the extrusion process the areas in which small strains occur can be ignored because they do not affect either the pressure or the properties. Equation (3) is adequate to describe the rheology of the material. Simulations were conducted on a Dell dual processor workstation.

MODEL VALIDATION

Simulations of rods for which experimental results were available were utilised to validate the numerical models used by FORGE3 software. This ensured that numerical discretisation functioned satisfactorily. The experimental results were for 2024 alloy extruded in a temperature range between 300 and 450°C, identical strain rate, and extrusion ratio of 30:1. The comparisons of major interest are the extrusion load and die exit temperature since if these are coincident then a valid numerical simulation model of the process may be assumed. The input data for the simulation of rod extrusion is summarised in Table 2.

Typical load *v.* time curves for rod extrusion are shown in Fig. 3. All the curves show the initial stages of extrusion to be characterised by a rapid increase in load as the billet is upset to fill the container. During this stage a very small amount of extrusion takes place. The curves also show a

Table 2 Rheology data input and dimensions used for computer simulation[23]

	Flow stress data						Dimensions (mm)		
Alloy	α	n	ΔH, kJ mol^{-1}	ln A	T (°C)	Product	ER*	o.d.*	i.d.*	WT*
2024	0·016	4·25	148880	19·6	300–450	Rod	30	...	0	...
6063	0·04	5·385	141550	22·5	450	Tube	29·2	16	8	4
							70	12	8	2

*ER extrusion ratio; o.d. outside diameter; i.d. inside diameter; WT wall thickness.

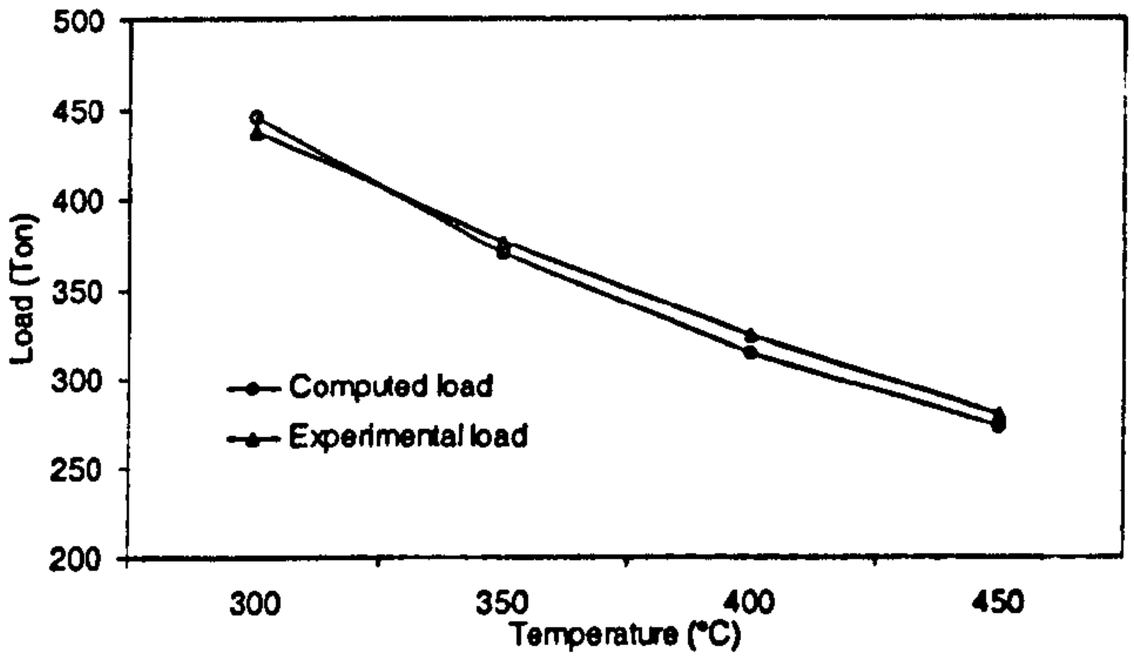

4 Comparison of experimental and computed peak extrusion load as function of initial billet temperature

'peak pressure region' which agrees with observations first reported by Castle and Sheppard.[32] The authors show in a previous communication that this 'peak' pressure is connected with the formation of the dead metal zone. After the end of this region, there is an abrupt fall in load which also agrees with the observations reported by Castle and Sheppard[32] followed by a more gradual decrease as the billet length decreases. This gradual decrease in the load results from the temperature rise generated during the extrusion cycle and the reduction in friction as the billet is extruded. The effect of the initial temperature on the peak pressure for the predicted and experimental loads is shown in Fig. 4. The figure shows a good correlation indicating that the discretisation of the FEM method is more than efficient in producing the necessary simulation.

Results and discussion

Although some of the figures presented show illustration of greater than 1/6 of symmetry, the analyses, in all cases, were conducted only for 1/6 of the model.

Most of the figures are more or less carefully defined in the discussion. In order to assist the reader some of the terminology used more frequently to describe the features of the figures are;

(i) 'step' is used to describe the succession of metal flow in Fig. 5.
(ii) DMZ is used to describe the location of dead metal zones in Fig. 6.
(iii) 'zone' is used to describe the heavy shear zones in Fig. 6
(iv) 'region' is used to describe the pressure–displacement curve in Fig. 7.

METAL FLOW IN TUBE EXTRUSION

When extruding with a bridge die, there are many surfaces in contact with the material. The die has two parts, the upper portion which forms a welding chamber and the lower portion which consists of the die orifice. The metal during the process undergoes severe deformation to adapt to the new shapes following a streamline course of flow determined in accordance with the geometrical conditions of the die. Therefore, the flow pattern during the extrusion process is very complex compared with a normal extrusion. There are three material flow streams of which each stream flows around the central axis. Hence, metal flow through a bridge die can be described as a succession of four steps: division of the metal, circumferential extrusion, joining of the metal, and formation of the tube.

Successive steps occurring during the extrusion of tubes using bridge die and the corresponding flow vectors at each step are shown in Fig. 5. During the first step (Fig. 5*a*), the billet is upset to fill the container, the material divides into three sections after encountering the bridge and the surface of the upper die portion. This produces the three metal streams which initially show only a vertical component of the flow vectors. At this stage the metal is not in contact with the welding chamber. In the second step of the process, each part of the material then flows along the bridge before entering the lower portion of the die. Subsequently, each stream approaches and contacts the lower surface of the die, i.e. the welding chamber, and flows tangentially into the space beneath the bridge as shown in Fig. 5*b*. This leads to circumferential flow of the extrusion. These streams of material are then brought into intimate contact and bonded to one another as shown in Fig. 5*c* (third step). Excessive shear is induced causing a large component of the velocity vector to become circumferential, thus, permitting individual streams to bond and produce a seam weld in the extrudate. Formation of the weld lines is the result of solid state welding involving circumferential extrusion in which metal flow has been distorted severely beneath the bridge legs. The final stage is shown in Fig. 5*d* (fourth step), the material in the welding chamber is extruded to form the tube effected by the mandrel attached beneath the centre of the bridge and suspended in the centre of the die orifice. It is clear that the flow through the bridge and over the mandrel is in very close agreement with experimental findings.[2,30]

The remaining dead metal zones (DMZs) in the die during extrusion are shown in Fig. 6 and represented by those zones in which the profile velocity is zero. The figure shows the dead metal zones in the die during extrusion. As the extrusion proceeds, there is a tendency for relative motion between the billet and the interfaces (container/bridge/welding chamber). Because of the high shearing forces generated at these interfaces, DMZs are formed during extrusion. This material remains sensibly stationary through the process. It can be seen that the DMZs form at the container adjacent to the surface of the upper portion of the bridge die (DMZ1) and the area above the bridge (DMZ2). These two locations are established just after the material passes through the bridge. The centre part of the billet travels forward more rapidly than the sides, which are held back above the shoulders of the die. In the welding chamber the front of each extruded stream encounters the die face and sticks; first at the circumference of the die and then spreading almost to the inner die corner. This causes circumferential extrusion as shown in Fig. 5*b*, leaving a DMZ in the chamber (DMZ3). The deformation is more severely distorted in the welding chamber than the container. Beneath the bridge (DMZ4) and near the mandrel and mandrel base (DMZ5) where small DMZs are formed. DMZ3 and 4 were established after the material started to extrude. DMZ4 would be expected to increase the peak pressure.

The deformation zones which form the inner and outer surface of the extrudate are termed surface generation zones and are shown in Fig. 6 as Zone1 and Zone2. The metal forming the outer surface of the tube originates from the metal bounding the DMZ3 and the surface generation Zone1, the metal forming the inner surfaces, from the metal bounding the DMZ4 and the surface generation zones adjacent to the mandrel Zone2. At these locations, the metal is forced into contact with the DMZs formed by the complex shape of the die and the bridge. The metal forming the centre of the tube originates from the metal which undergoes heavy shear in Zone3. Reference to Fig. 6 also indicates that these zones originate from the interior of the billet in the intense shear zones. This is due to the interaction of DMZ3 and 4 with the Zones 1 and 2 respectively and the position of greater deformation as the material approaches the die in Zone3.

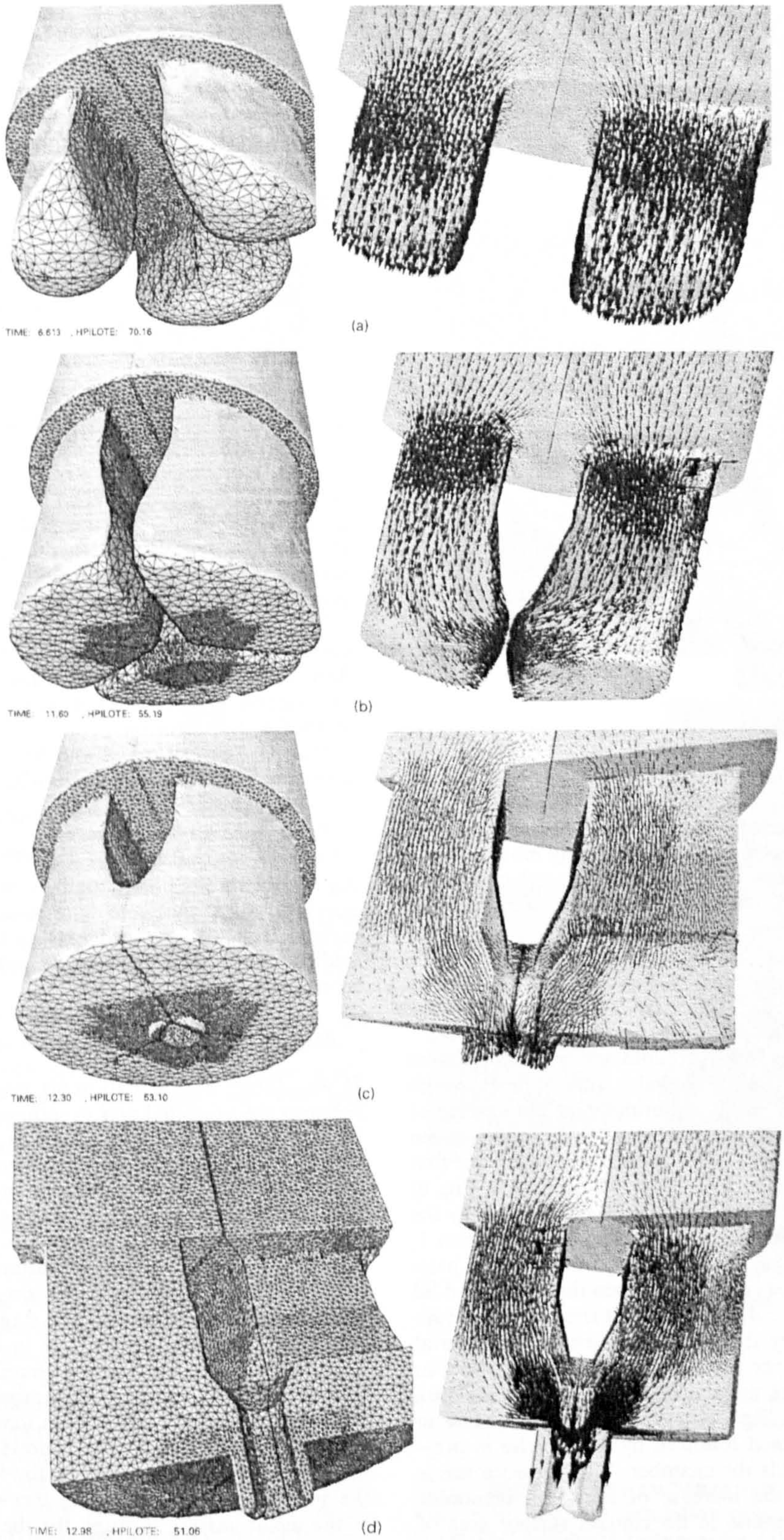

5 *a* metal passing the bridge; *b* flowing sideways beneath the bridge; *c* filling weld chamber and formation of weld line; *d* passing through die

PRESSURE PREDICTION CURVE AND TEMPERATURE PROFILE FOR TUBE EXTRUSION

There is little in the literature concerning the pressure required for the extrusion of multi-holes or extrusion using bridge or porthole dies. The prediction of peak pressure is critical because it determines the pressure capacity required to extrude the billet under extrusion conditions. An estimate of the pressure required to extrude through a bridge die may be produced by considering the operation as two separate extrusions: the pressure required to force the metal into the weld die and the pressure required to extrude the tube from the weld chamber.

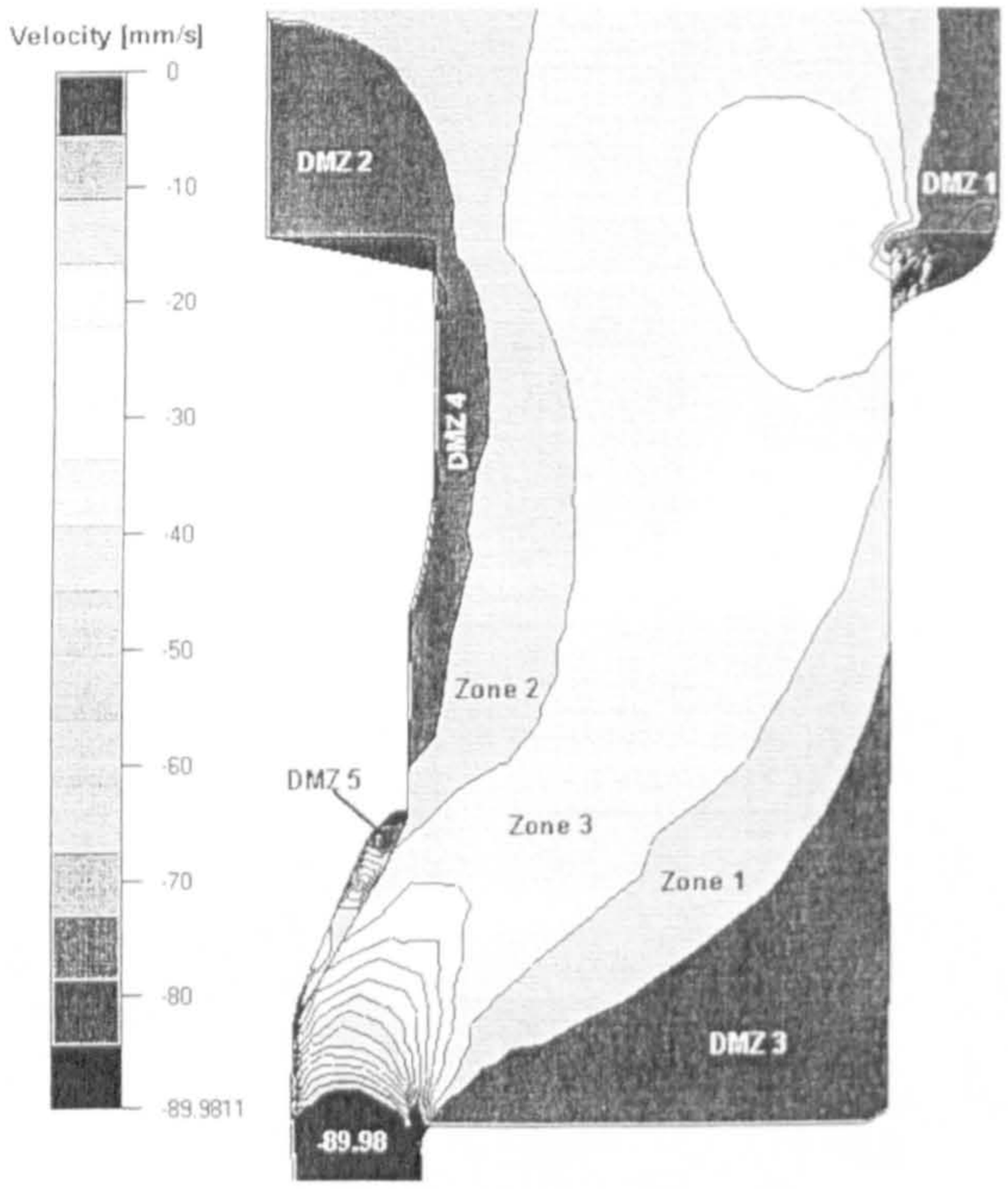

6 Dead metal zone formation represented by velocity field

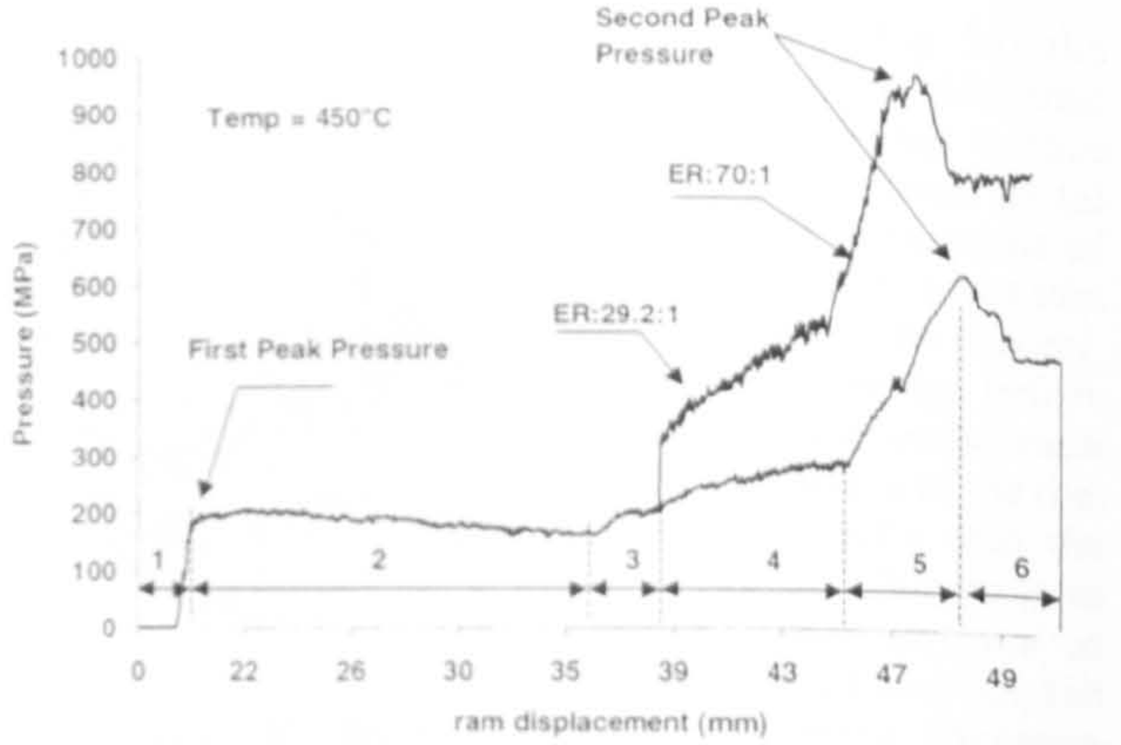

7 Predicted pressure–displacement curves

The pressure–displacement curve is shown in Fig. 7. The locus for the bridge extrusion is considerably more complex than normal rod extrusion, this is logical since there are four separate extrusion stages (*see* Fig. 5) compared with the almost single operation required for rod extrusion. Flow through the bridge die results in the pressure curve being similar to the curve for normal rod extrusion after the peak pressure has occurred. The curve can conveniently be divided into six regions.

The billet is upset to fill the container and the pressure rises rapidly to the first peak value (first breakthrough pressure) after encountering the bridge and the surface of the upper die portion. Some material has already been extruded past the bridge. When the pressure reaches the first peak value, the DMZs in the billet (DMZ1 and 2 in Fig. 6) have been established where the material is held back by the shoulders of the container and above the bridge (region 1, Fig. 7). Pressure then decreases slightly from the first peak pressure as the material continues to pass the bridge and fill the die chamber. This is due to the slight rise in temperature in the billet caused by the work done when the material passes through the upper portion of the bridge (region 2 in Fig. 7). As soon as the metal streams contact the welding chamber as shown in Fig. 5*b*, a small incremental rise in pressure can be discerned followed by a steep rise in pressure when the metal fills the chamber. This pressure rise is needed to overcome the increase of frictional resistance associated with the increase in the contact surface area of the welding die to produce sufficient energy for the bonding process (regions 3 and 4 in Fig. 7). Subsequently, the pressure rapidly rises to the second peak value allowing extrusion to commence and to force the material through the mandrel/die gap. Some material has already been extruded through the die orifice and when the pressure reaches its peak value, DMZ3, 4 and 5 are completely formed in the die chamber (region 5 in Fig. 7). The pressure falls from the second peak value and so called steady state extrusion will be established. A gradual fall in pressure can be seen in this region which can be attributed to the decreasing billet length, and hence decreasing friction, and the decrease in flow stress due to the temperature rise. When the back of the billet approaches the bridge apex the metal ideally is cropped, allowing the introduction of a further billet. Therefore very little scrap is formed. This concurred with experimental observations observed by Sheppard *et al.*[2]

The occurrence of the peak in the pressure displacement curve is a result of the combined effect of the 'three maxima' flow formed from the three streams in the die chamber and the friction of the mandrel which produces the effective strain for the extrusion.

Sheppard and Wood[33] and Sheppard *et al.*[23] presented formulae for pressure prediction as given below

$$P = \bar{\sigma}\left[0{\cdot}17 + 1{\cdot}86\ln(\lambda^2 R) + \left(\frac{4L_B}{D_B\sqrt{3}}\right)\right] + \Delta p \quad \ldots \quad (4)$$

L_B represents the billet length, Z is the Zener–Hollomon constant and is the same as in equation (3), λ is the shape factor, R is the modified extrusion ratio, and Δp is the additional pressure to initiate extrusion and for 6063 aluminium alloy is equal to

$$\Delta p = 6{\cdot}62 + 0{\cdot}921\ \frac{\ln(Z/A)}{\alpha n} \quad \ldots \quad (5)$$

It was found that equation (4) gives a good correlation between the predicted and experimental extrusion pressure data in aluminium alloys. However, this has been proved true only over a limited range of extrusion conditions. There is no evidence to show the equation (4) can deal with, for example, tube incorporating thin fins at internal or external surfaces. The pressure required for stages 1, 2, and 3 in Fig. 7 is dependent on the extrusion temperature and the extrusion ratio of the metal passing the bridge. Furthermore, the pressure required for stages 4, 5, and 6 also in Fig. 7, is dependent on the rise in temperature from the previous stages in the welding chamber and the extrusion ratio of the metal leaving the chamber and passing through the mandrel–die gap. The rise in temperature is due to the heat generated from the work done in the metal passing the upper portion of the bridge, the friction in overcoming the surface contact area inside the welding chamber, and in the metal passing through the die to produce the tube. Consequently, the variation in the pressure for the first three steps at different temperatures affects the total pressure required to extrude the tube. Equation (4) does not take into account the temperature rise during the first three stages and is based on initial billet temperature. Equation (4) is derived from an axisymmetric upper bound solution and thus cannot be as accurate as the FEM solution (which is a refined upper bound). Furthermore, in equation (4) and in general in all empirical formulae, it may not be possible to account for the geometrical complexity of the dies other than simple tubes and the intricacy of the consequent flow could present a problem. Hence, FEM

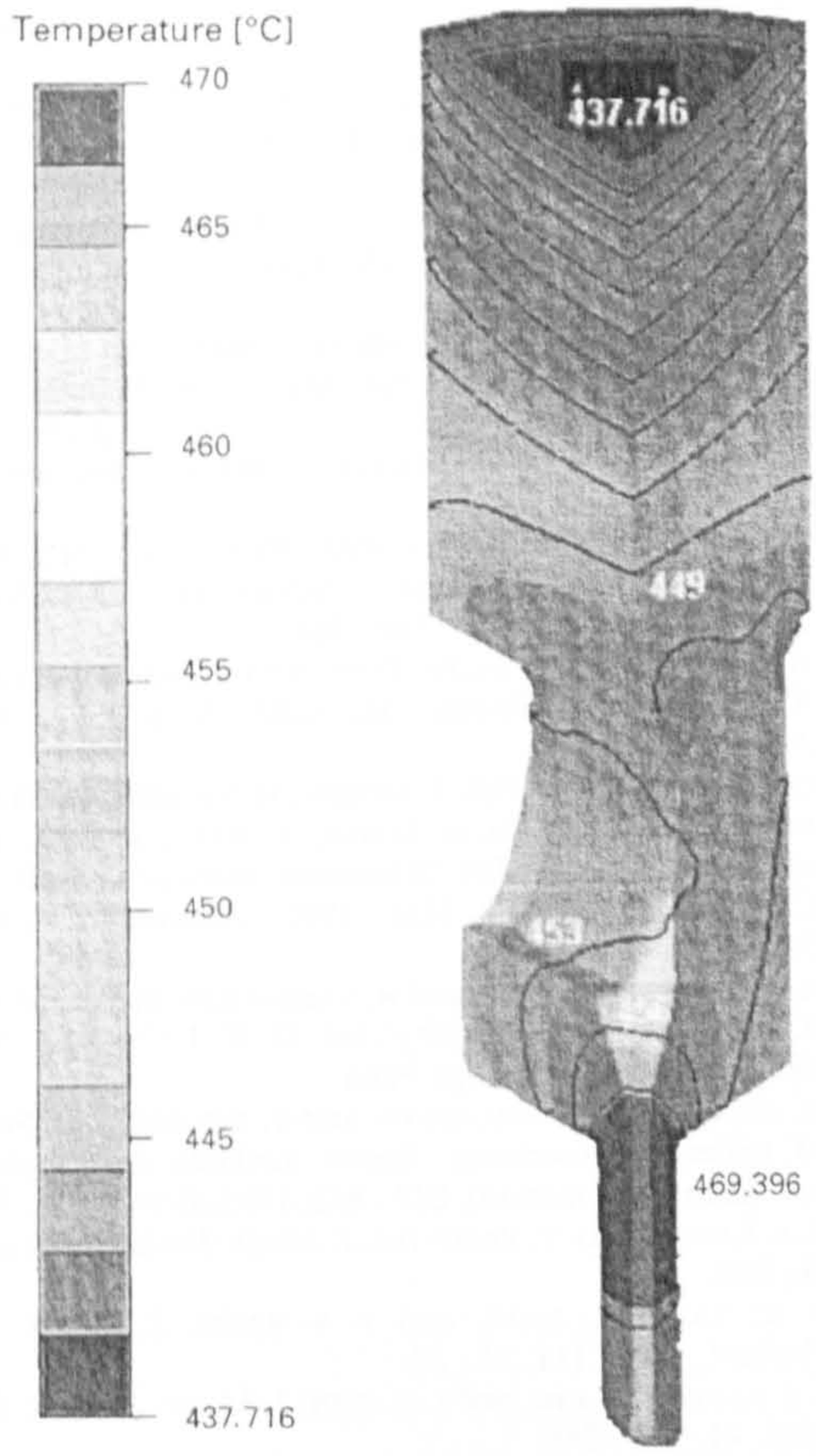

8 Temperature evolution for an extrusion ratio of 29·2 : 1

codes which by definition are analytical have a great advantage over semi-empirical formulae in predicting the main parameters before and after the so called steady state is achieved.

In this investigation, the value of the peak pressures, 623 and 975 MPa for the two extrusion ratios 29·2 : 1 and 70 : 1 respectively agreed with those observed experimentally predicting a 5 and 4% difference respectively (593 and 937 MPa).[30] The multi-step extrusion distorts the metal flow more severely and increases the friction due to an increase in the area of billet/tool interface. Therefore the complex shear leads to an increase in the pressure; particularly for the high extrusion ratio.

Complex thermal exchanges begin as soon as the extrusion commences. The most critical temperature is clearly the die exit temperature of the extrudate, which depends on heat balance history commencing at the upsetting stage of the operation. The temperature evolution simulated in the tube extrusion is shown in Fig. 8. The figure shows that there is a small increase in temperature of the billet after encountering the bridge and the upper die (453°C for both extrusion ratios). The maximum temperature occurs at the die exit and it is 470 and 493°C for the two extrusion ratios 29·2 : 1 and 70 : 1 respectively. This is caused by the work done as the material flows through the die orifice and by the friction which is converted into heat at the die exit during extrusion and consequently results in an increase in the extrusion temperature. The heat generated near the die exit increases the local temperature. However, the temperature in the billet at the container surface thus appears lower than the actual temperature (449°C). Unlike the FORGE2 program, where the meshing of the tooling through the thickness is possible for thermocouple analysis as illustrated in Fig. 9, in the FORGE3 program, the tooling can only be surface meshed (rigid die). This results in the contour appearing to be of infinite thickness and hence promotes a slightly

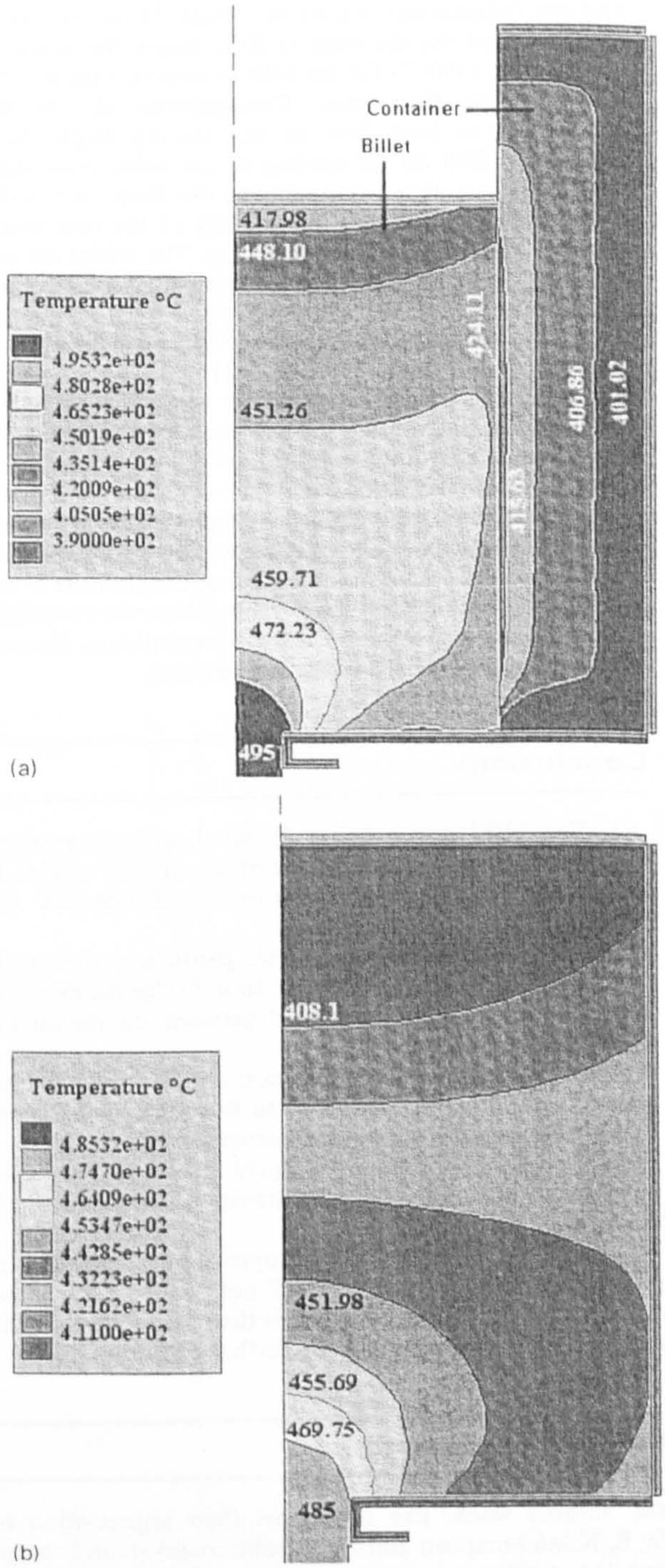

a meshed tools; *b* rigid tools

9 Temperature evolution for rod extrusion (450°C initial billet temperature, extrusion ratio 30 : 1)

slower apparent heat exchange rate. It can be seen from Fig. 9*a* for the 2-D simulation using FORGE2, that there is thermal exchange between the billet and the container wall. It also demonstrates there is a temperature increase at the billet surface caused by friction at the container wall (initial tooling temperatures are 50°C below the billet temperature). Ignoring the meshing of the tools as shown in Fig. 9*b* gives a differing distribution of the temperature at the interface and an exit temperature of 485°C compared with 495°C in Fig. 9*a* when we are able to mesh the tools. Hence, the 10°C difference in the exit temperature probably accounts for the difference observed between the experimental and predicted pressure in 3-D tube extrusion. The critical role of tool meshing on the temperature evolution

and exit temperature is thus very clear. However, since the container and the die were at 50°C below the initial billet temperature (450°C) for the tube extrusion, they acted as a heat sink to the metal. Consequently the boundary conditions for heat flow in the tooling might have a significant effect on the cooling of the billet. Although we might expect a higher temperature rise than observed, the reader should recall that the velocity of the ram was just 3 mm s^{-1}, which is slow for this alloy. The bridge die would however be better modelled by assigning to it a higher temperature than 50°C below the initial billet temperature. There is, however no doubt that the assumed temperature of the tooling resulted in a lower final material temperature. Hence, a slightly greater force was needed to extrude the material. The temperature rise was expected as a result of the work done in upsetting the billet, and the work done against friction between the material and the tooling during extrusion. These contribute only relatively slightly to small changes in the mean temperature due to the heat flow to the container, but the effect of friction on the surface temperature is more significant. Despite these minor errors in boundary conditions the results are very close to the experimental data. However, this might be the subject of further research.

Conclusions

1. The FEM codes Forge 2 and 3 with programmed hyperbolic sine function provided a suitable model for simulation for simple rod extrusion and complex tube profile.

2. In the current investigation the prediction of the metal flow and dead metal zone formation in bridge die extrusion is seen to be in good agreement between simulation and experimental findings.[30,31]

3. Finite element simulation successfully predicted the origin of differing sections of the extrudate which flows from varying portions of the deformation zones.

4. The pressure prediction curve produces two peak pressures as well as a small pressure rise when the metal fills the welding die.

5. Empirical equations, which appear to be adequate to predict pressure requirements, will not predict either metal flow or final temperatures. There is therefore a requirement to refine the FEM approach by further research.

Acknowledgements

The authors would like to express their appreciation to Dr E. Nisatatanaporn and Dr J. Subramaniyan and recognise the excellent contribution from their experimental work. The provision of facilities by Bournemouth University is also gratefully recognised.

References

1. A. DICK: GB Pat. 99405, UK Patent Office, London, March 1897.
2. T. SHEPPARD, E. NISATATANAPORN, and B. H. MCSHANE: *Z. Metallkd.*, 1998, 89, 5.
3. R. AKERET: Proc. 5th Int. 'Aluminum extrusion' Tech. Seminar, Chicago, IL, USA, May 1992, Aluminum Association, 319–336.
4. H. VALBERG: Proc. 6th Int. 'Aluminum extrusion' Tech. Seminar, Chicago, IL, USA, May 1996, Aluminum Association, 213–224.
5. I. DUPLANČIĆ and J. PRGIN: Proc. 6th Int. 'Aluminum extrusion' Tech. Seminar, Chicago, IL, USA, May 1996, Aluminum Association, 225–300.
6. J. KUSIAK *et al.*: Proc. 6th Int. 'Aluminum extrusion' Tech. Seminar, Chicago, IL, USA, May 1996, Aluminum Association, 361–367.
7. H. G. A. MOOI *et al.*: Proc. 6th Int. 'Aluminum extrusion' Tech. Seminar, Chicago, IL, USA, May 1996, Aluminum Association, 359–368.
8. T. WELO, A. SMABREKKE, and H. VALBERG: *Aluminium*, 1995, 71, (1), 90–94.
9. C. DEVADAS and O. CELLIERS: Proc. 5th Int. 'Aluminum extrusion' Tech. Seminar, Chicago, IL, USA, May 1992, Aluminum Association, 359–368.
10. G. E. MACEY and M. SALIM: Proc. 5th Int. 'Aluminum extrusion' Tech. Seminar, Chicago, IL, USA, May 1992, Aluminum Association, 247.
11. G. GRASMO, K. HOLTHE, S. STOREN, H. VALBERG, R. FLATVAL, L. HANSSEN, M. LEFSTAD, O. LOHNE, T. WELO, R. ORSUND, and J. HERBERG: Proc. 5th Int. 'Aluminum extrusion' Tech. Seminar, Chicago, IL, USA, May 1992, Aluminum Association, 367–376.
12. K. I. MORI, K. OSAKADA, and H. YAMAGUCHI: in 3rd Int. Conf. on 'Computational plastisticity', (ed. D. R. J. Owen), 1139–1149; 1992, Swansea, Pineridge Press.
13. M. KIUCHI, M. J. YANAGIMOTO, and V. MENDOZA: in 'Simulation of materials processing: theory methods and applications', (ed. Shen and Dawson), 847–852; 1995, Rotterdam, Balkema.
14. Y. S. KANG and D. Y. YANG: *Int. J. Mach. Tools Manufact.*, 1996, 36, 907.
15. D. Y. YANG, K. PARK, and Y. S. KANG: *J. Mater. Process. Technol.*, 2001, 111, 25–30.
16. B. S. KANG, B. M. KIM, and J. C. CHOI: *J. Mater. Process. Technol.*, 1994, 41, 237–248.
17. H. VALBERG and T. MALVIK: *Int. J. Mater. Prod. Technol.*, 1994, 9, 428–463.
18. R. J. DASHWOOD and H. B. MCSHANE: Proc. 6th Int. 'Aluminum extrusion' Tech. Seminar, Chicago, IL, USA, May 1996, Aluminum Association, 331–339.
19. M. PLATA and J. PIWNIK: Proc. 7th Int. 'Aluminum extrusion' Tech. Seminar, Chicago, IL, USA, May 2000, Aluminum Association, 205–211.
20. I. FLITTA and T. SHEPPARD: Proc. 7th Int. 'Aluminum extrusion' Tech. Seminar, Chicago, IL, USA, May 2000, Aluminum Association, 197–203.
21. I. FLITTA and T. SHEPPARD: Proc. 7th Int. 'Aluminum extrusion' Tech. Seminar, Chicago, IL, USA, May 2000, Aluminum Association, 141–147.
22. T. CHANDA, J. ZHOU, L. KOWALSI, and J. DUSZCZYK: *Scr. Mater.*, 1999, 41, 195–202.
23. T. SHEPPARD: 'Extrusion of aluminium alloys' 1999, Boston, MA, Dordrecht, Kluwer Academic Press.
24. J.-L. CHENOT *et al.*: 'Internationl conference on forging and related technology', ICFT'98, April 1998, 113–122; Bury St Edmunds, Professional Engineering Publishing.
25. FORGE3, Version 5·3, 'Software manual', Transvalor SA, Sophia Antipolis, France, 2001.
26. J.-L. CHENOT and M. BELLET: in 'Numerical modelling of material deformation processes: Research, development and applications' (ed. P. Hartley *et al.*), 179–224; 1992, London, Springer Verlag.
27. J.-L. CHENOT: *J. Mater. Process. Technol.*, 1992, 24, 9.
28. C. M. SELLARS and D. TEGART: *Int. Met. Rev.*, 1972, 17, 1.
29. T. SHEPPARD and D. WRIGHT: *Met. Technol.*, 1979, 6, 215–223.
30. E. NISATATANAPORN: PhD Thesis, London University (Imperial College), UK, 1995.
31. J. SUBRAMANIYAN: PhD Thesis, London University (Imperial College), UK, 1989.
32. A. P. CASTLE and T. SHEPPARD: *Met. Technol.*, 1976, 3, 465–475.
33. T. SHEPPARD and E. P. WOOD: Proc. 17th Machine Tool Design and Research Conf., Birmingham, UK, September 1976, 411–421; 1976, London, McMillan.